SHEAR STRENGTH CHARACTERISTICS OF A CRUSHED QUARTZ SAND

BY

MOHAMMED HASNAIN

B.Sc.Engg. (Civil), Dacca University, 1959

A thesis submitted in partial fulfillment
of the requirement for the degree of
Master of Applied Science
in
Civil Engineering
in the Graduate School of the
University of Ottawa
Ottawa, Canada
1974

© Mohammed Hasnain, Ottawa, Canada, 1974.

ABSTRACT

An investigation has been carried out on the shear strength properties of crushed quartz sand in the laboratory using drained triaxial compression tests and conventional direct shear box tests. The tests have been carried out at different relative densities and normal stresses. K_o tests have been performed for various densities.

Relationships between shear displacements and shear stresses have been established for very dense to medium dense sand and normal stresses varying from 8 psi to 120 psi.

Variations in the value of the angle of internal friction with normal stresses and relative densities are presented.

The results of the triaxial tests have been given in the form of stress paths for various densities of the sand and stress ranges.

Strain contours have been drawn to predict strains for given densities and stress conditions.

For K_o tests, comparisons have been made with solutions presented by Jaky and Hendron as reported by Bauer (1969).

ACKNOWLEDGEMENT

This thesis was prepared under the direction and guidance of Dr. G. E. A. Bauer, Assistant Professor, Department of Civil Engineering, to whom the author wishes to express his most sincere and heartfelt gratitude for his continued advice, assistance and constructive criticism during the course of this investigation.

The author is extremely grateful to Dr. J. D. Scott and Dr. D. H. Shields, Professors, Department of Civil Engineering, University of Ottawa for their continued guidance during various stages of this investigation.

Thanks are also due to Dr. R. Kretz, Department of Geology for carrying out the mineralogical analysis of the sand.

Acknowledgement is extended to Mrs. Wanda Storto who has ably and patiently typed the manuscript.

The author must also acknowledge his indebtness to the National Research Council for the financial assistance under Grant No. A-5105 which made this study possible.

Finally, the writer extends his most sincere appreciation to his wife for her patience and continued encouragement throughout his entire education. To his beloved wife Sufaira this thesis is dedicated.

TABLE OF CONTENTS

LIST OF TABLES

LIST OF FIGURES

LIST OF PLATES

PRINCIPAL SYMBOLS

A_o	Original area of sample in direct shear.
A_c	Contact area of the particles.
dx	Increment of shear deformation in direct shear.
dh	Corresponding increment in the thickness of the sample.
dv	Incremental increase in volume.
dv^p	Plastic component of the volumetric strain.
$d\varepsilon_1^p$	Plastic component of axial strain.
D_r	Relative density.
e	Void ratio.
E_s	Secant modulus.
f	Coefficient of friction.
n	Porosity.
N	Normal force.
P	Shear force as used by Rowe (1962) in sliding wedge model.
Q	Force normal to the direction of P.
q_u	Normal stress to cause yielding.
S	Shear strength of the adhered junction in sand.
T_{max}	Maximum shear force.
V_o	Original volume of the sample in direct shear.
V	Volume of the sample.
α	Packing property of the spheres.
β	Direction of the interparticle sliding relative to the major principal.

σ_1	Major principal stress.
σ_2	Intermediate principal stress.
σ_3	Minor principal.
σ_n	Normal stress in direct shear.
τ_e	Shear stress required to provide energy for expansion.
ε_f	Axial strain at failure.
ε_1	Axial strain in major principal direction.
ε_{1s}	Major principal compressive strain ε_1 due to inter-particle slip.
δ_{ε_1}	Strain increment in major principal direction.
δ_{ε_3}	Strain increment in minor principal direction.
δ_v	Volumetric strain in direct shear.
δ_x	Transverse displacement in direct shear.
δ_γ	Shear strain.
ϕ	Angle of internal friction.
ϕ_μ	Angle of friction of the particles.
ϕ_f	Corrected angle of friction (Rowe)
ϕ_{cv}	Value of Coulomb ϕ, ϕ_f or ϕ_r at critical void ratio state.
ϕ_r	Corrected angle of friction (Bishop).
ϕ_d	Angle of friction determined from drained tests.
ϕ_{dr}	Angle of friction after dilatancy effect is deducted.
ϕ_{ds}	Angle of friction in direct shear.
ϕ_{ps}	Angle of friction in plane strain.
$(\Delta v/v)f$	Volumetric strain at failure.
μ	Poisson's ratio.

CHAPTER 1

INTRODUCTION

1.1 Preamble

A programme of study concerning the ultimate bearing capacity of model footings on sand has been started at the University of Ottawa.

The footing tests will be carried out in a rigid steel box measuring about 48 ft x 6 ft x 7 ft high. The sand box is divided into two equal components of 24 ft each.

Each component, alternately can be used as test bin. After the test has been carried out, the sand will be deposited in the other compartment at the required uniform density for the next test. Sixty tons of sand will have to be redeposited for each test.

A spreading device for depositing the sand at a predetermined density is mounted on a pair of rails, independent from the sand box. The sand spreading device is similar in principle to the one described and used by Walker and Whitaker (1967).

The density of the deposited sand is controlled by adjusting the speed of rotation of the drum, the gap, the angle of the deflector blade and the speed of translation of the raining device itself.

In situ densities in the sand box will be measured by using calibrated cylinders, Menard Pressuremeter and static cone penetrometers.

As shown in Fig. 1.1 (after Meyerhof, 1963), it is evident that the bearing capacity factors increase rapidly at higher densities or higher ϕ values.

The study reported in this thesis pertains to the measurement of the physical properties of the sand, that will be used in the sand box; particularly the determination of the shear strength parameters of the sand by laboratory tests, simulating the conditions of placement, density and confining pressure, etc., existing in the sand box.

Tests in the sand box will be carried out under plane strain conditions; ideally the laboratory tests should be performed under the same conditions.

Since shear strength parameters in the laboratory are generally determined by triaxial compression and/or direct shear box tests, these tests were used. It has been shown (Cornforth, 1964) that the ϕ values obtained from triaxial compression tests can differ by several degrees as compared to tests run on a plane strain device. Therefore, a comparison of ϕ values obtained from triaxial test and plane strain tests are made based on studies by Lee (1970).

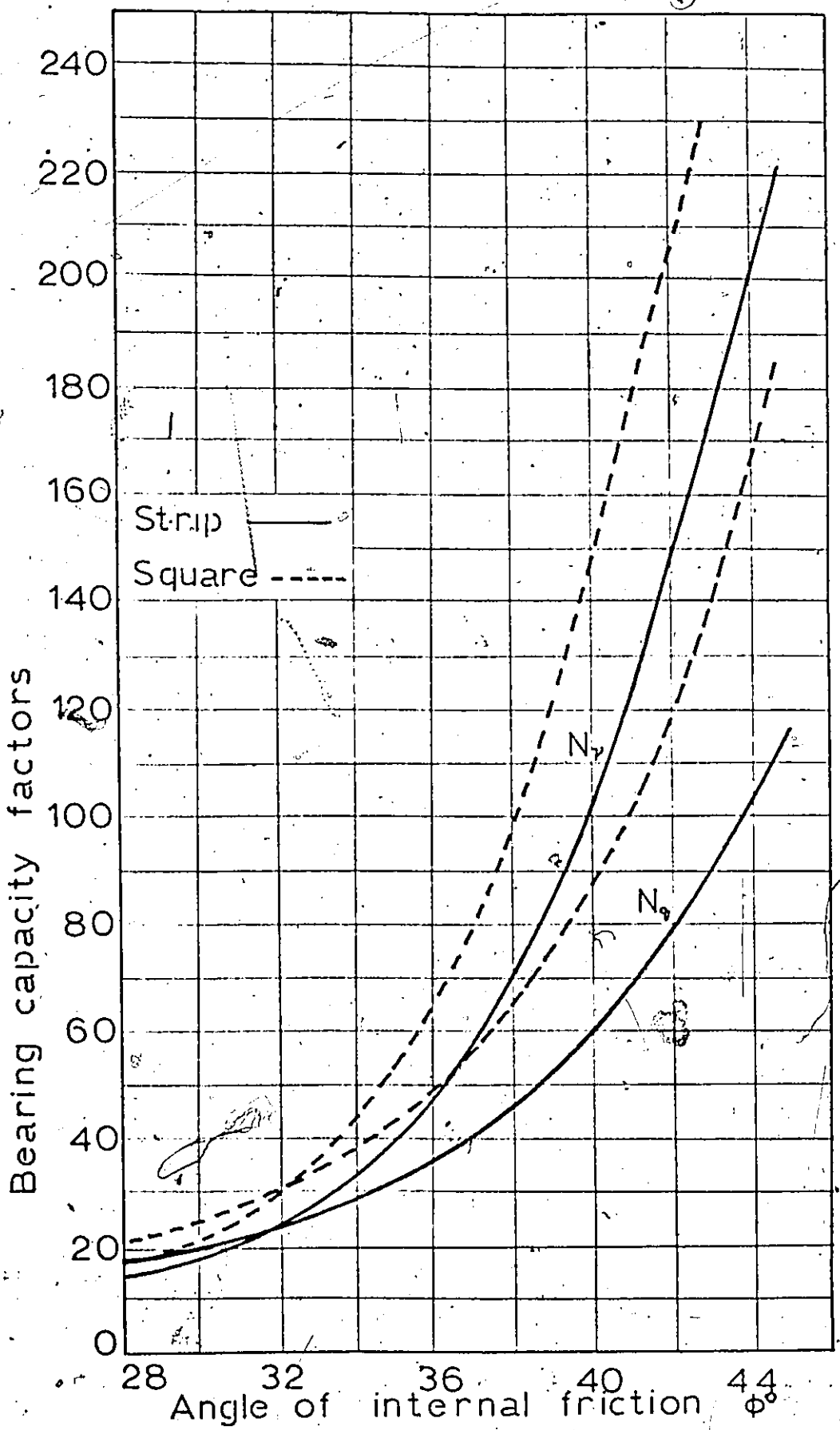

FIG. 1.1 BEARING CAPACITY FACTORS VERSUS ANGLE OF INTERNAL

1.2 Statement of the Problem

The problem involved was the determination of strength parameters of the sand at densities, placement conditions and confining pressures as would be encountered in the prototype sand box.

The basic consideration in this test programme was to use common laboratory techniques such as triaxial compression, and direct shear box tests. Elimination of sources of errors and repeatability of tests were also considered.

The main testing programme consisted of consolidated drained triaxial compression tests.

These studies were conducted prior to model footing tests, hence it was considered advisable to encompass as wide a field of stresses and densities as possible in order to cover the possible densities and pressure ranges eventually encountered in the sand box[1]. It was decided to run drained triaxial compression tests at relative densities of 90, 75 and 60 per cent and at confining pressure of 5, 25, 50 and 80 psi.

Some researchers believe that direct-shear test results are closer to footing failure conditions than triaxial test results. Hence, it was decided to run direct shear box tests under comparable normal stresses and densities, in order to compare the results from direct shear tests with triaxial compression tests.

---

[1] With a footing 2 ft wide at a depth of 2 ft and a $\emptyset'$ of 42° it is estimated that σ_3 will be of the order of 40 psi.

In order to find Poisson's ratio for different relative densities, Ko-tests had to be performed.

1.3 Objectives and Scope of Study

The main objective of this study was to determine accurately the value of ϕ for different relative densities under various normal stresses in order to cover a fairly wide range of conditions that could be encountered in the sand box. However, the study was concentrated on very dense, dense and medium dense samples, since these densities were of primary interest for the proposed footing tests.

The effect of soil structure on the strength of sand was also evaluated. This was accomplished by compacting samples by different methods; as for example by hand compaction and by using the special sand raining device. The two values for the same density and confining pressure were compared. That the soil structure has an effect on the strength of sand has been established, by Feda (1969) for example.

Values of ϕ were obtained from triaxial compression tests, and direct shear box tests and were compared with one another.

Kolbuszewski (1958) recommends the determination of sphericity and roundness to define the physical properties of a sand. Hence these were determined by the methods

proposed by Rittenhouse (1943) and Krumbein (1941).

1.4 Outline of the Thesis

In Chapter 1, a general introduction to the present work is given. Chapter 2 presents a general treatment of the theoretical behavior of sand in drained shear.

Chapter 3 deals with the laboratory tests and procedures. It describes the experimental set up for the triaxial compression tests. It also discusses the factors which influence the test results and the steps taken to remedy the sources of errors. Properties of the sand particles used in the test like grain size distribution, maximum and minimum densities, sphericity and roundness, etc., are also presented in Chapter 3.

In Chapter 4, the experimental test results have been presented for drained triaxial compression tests, and direct shear tests. Ko-test results are also presented.

Chapter 5 discusses and compares the results of the triaxial compression tests and direct shear tests. Comparisons between experimental test results and theoretical behavior as discussed in Chapter 2 are made. The findings of this study are also compared to the results of other researchers.

Summary and conclusions are given in Chapter 6. In the appendices a list of references, the structural

details of the frictionless end platens, a diagram of the sample former, details of the piston load transducer and factors affecting direct shear box tests are presented.

CHAPTER 2

THEORETICAL BEHAVIOUR OF SAND IN DRAINED SHEAR

2.1 Cohesionless Soil

Cohesionless soil is a granular medium consisting of discrete particles. They are not bonded together in the way crystals of a metal are; and hence the particles are relatively free to move with respect to each other. Their relative movements also are not as free as those of the elements in a fluid. Thus cohesionless soils are inherently a particulate system. Sand is a cohesionless soil with no cementation and is made up of solid particles and voids. These voids may be filled by a liquid and/or a gas.

The state of density of the sand is expressed in terms of the void ratio, dry density or relative density.

In this work the cohesionless soil is an air dried sand. Complete drainage was allowed by allowing air to enter or leave the sample during the tests. The properties of the sand will be discussed in detail in Chapter 3.

2.2 Nature of Soil Deformation

Consider a box filled with dry sand, and a rigid plate through which load could be applied to the sand; as shown in Fig. 2.1. The sand is compressed and contact forces would develop between adjacent sand particles. The forces can be resolved in directions normal and tangential to the

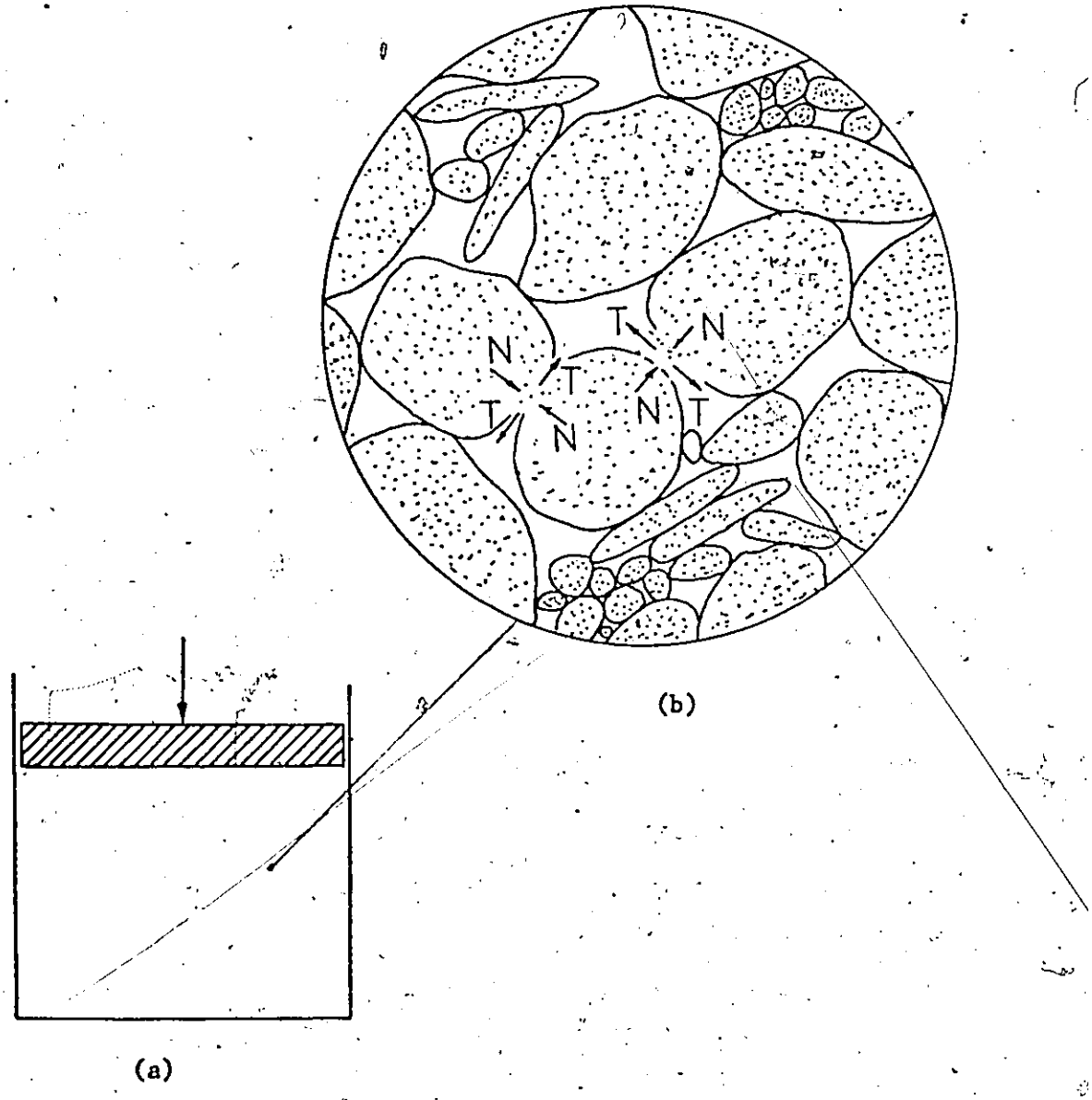

FIG. 2.1 SCHEMATIC REPRESENTATION OF FORCE TRANSMISSION THROUGH SOIL. (a) Cross section of box filled with soil. (b) Enlargement through portions of cross section showing forces at two of the contact points (after Lambe and Whitman, 1969).

contact surfaces. The individual particles will deform elastically as a result of these contact forces. Particle crushing can take place thus enlarging the contact area and bringing the particles closer to one another as shown in Fig. 2.2(a). If platelike particles are present, these will bend, allowing relative movements between particles; as seen in Fig. 2.2(b). In addition once the shear forces at the contact points become larger than the shear resistance at the contacts, there will be relative sliding, rolling or a combination of the two between the particles (Fig. 2.2(c)). The overall deformation will thus consist of elastic deformation of the individual particles and relative translocation. However, it will be seen later that the largest contribution to soil deformation comes from interparticle movement.

If the box in Fig. 2.1 has rigid sides, the soil will decrease in volume, as the load is increased. The voids in the soil will also decrease. The volume decreases because the particles are packed closer and closer together. There will be shear failures at many contact points, but there will be no overall shear failure. The load could be increased without limit.

If the applied load is now removed the soil would increase in volume but will not regain its original volume. The elastic deformation of the particles is considered to be a reversible process. The translocation of the individual

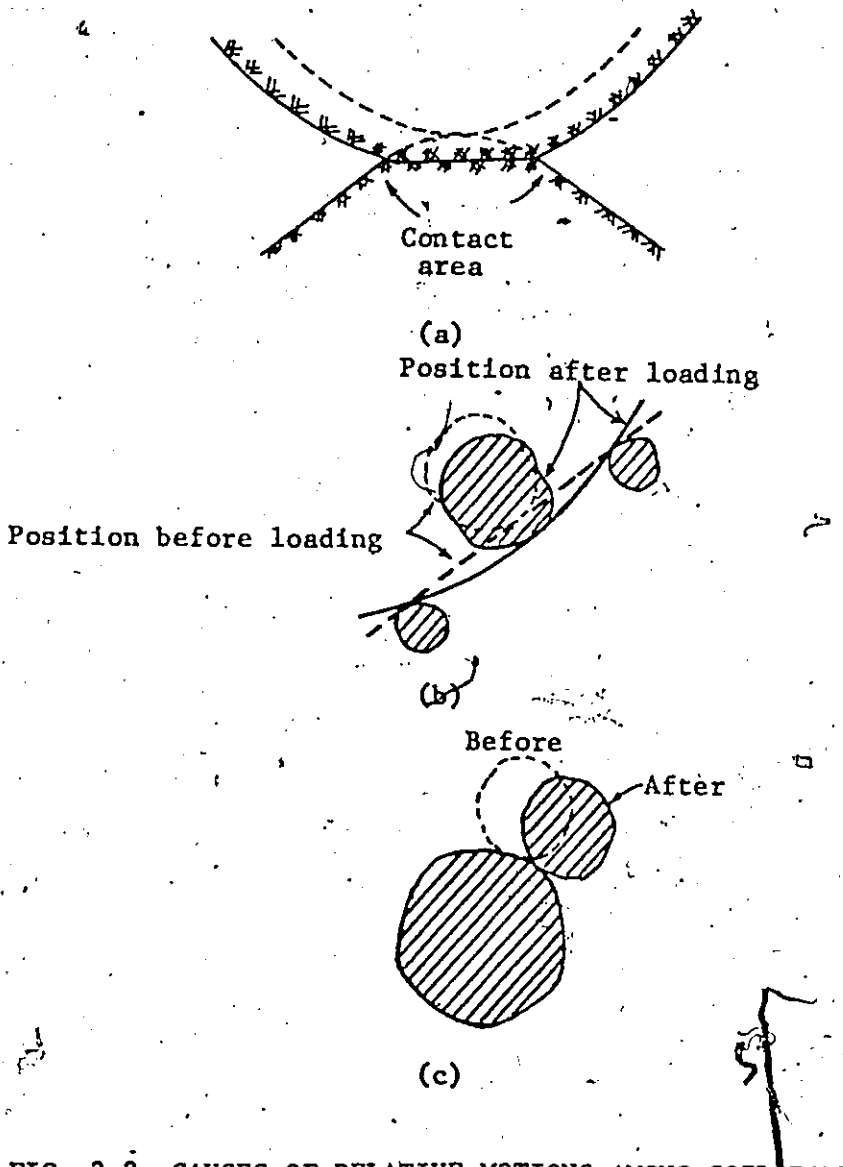

FIG. 2.2 CAUSES OF RELATIVE MOTIONS AMONG SOIL PARTICLES. (a) Motions of particles due to deformation of contacts. Solid lines show surfaces of particles after loading (the lower particle was assumed not to move); dashed lines show surfaces before loading. (b) Relative motions of particles due to bending of platelike particles. (c) Relative motions of particles due to inter-particle sliding (from Lambe and Whitman, 1969).

particles is irreversible. This results in overall deformation of the soil.

On the other hand if the box had flexible side walls; an overall shear failure could take place. The vertical load at which the failure could occur is related to the shear strength of the soil.

2.3 Mechanism of Shear Resistance

The shear resistance between particles is the force that must be applied to cause a relative movement between the particles. This shear resistance between particles is made up of at least two components:

(a) One whose magnitude is controlled by the frictional nature of the particles, namely ϕ_μ; and

(b) a second component whose magnitude is related to the degree of interlocking.

Two alternate ways of expressing frictional resistance are in common use. One is to use the coefficient of friction f. Thus if N is the normal force across a surface the maximum shear force is $T_{max} = N.f$ (Lambe and Whitman, 1969).

The other is to use a friction angle ϕ_μ defined such that

$$\tan \phi_\mu = f \qquad (2.1)$$

The following statements offer an explanation of the frictional behaviour of materials.

On a submicroscopic scale most surfaces, even carefully polished ones, are actually rough. Hence two solids will be in contact only where the high points (asperites) touch one another. That is, the actual contact area is a small fraction of the apparent contact area. The actual contact area Ac, is given by the expression

$$Ac = N/qu \qquad (2.2)$$

where N is the normal load and qu is the normal stress to cause yielding (plastic flow). Since qu is fixed in magnitude, an increase in total normal load must mean an increase in the actual area of contact. This increase results from the plastic flow of the asperites. The high contact stresses cause the two surfaces to adhere at the points of actual contact. Shear strength is provided by the adhesive strength of these points. Thus the maximum shear force is given as

$$T_{max} = S.Ac \qquad (2.3)$$

where S = shear strength of the adhered junction. Combining Equation (2.2) and (2.3) one gets, $T_{max} = N.S/qu = N.f$. The term S/qu is the property of the material and is denoted by $\tan \phi_\mu$ given by Equation (2.1).

This friction factor ϕ_μ is found to be independent of normal load. Rowe (1962) showed that the friction angle ϕ_μ is affected by the size of the particles involved in the test as shown in Fig. 2.3.

From the foregoing it would appear that ϕ_μ would apply to cases where the soil particles are sliding over a smooth surface.

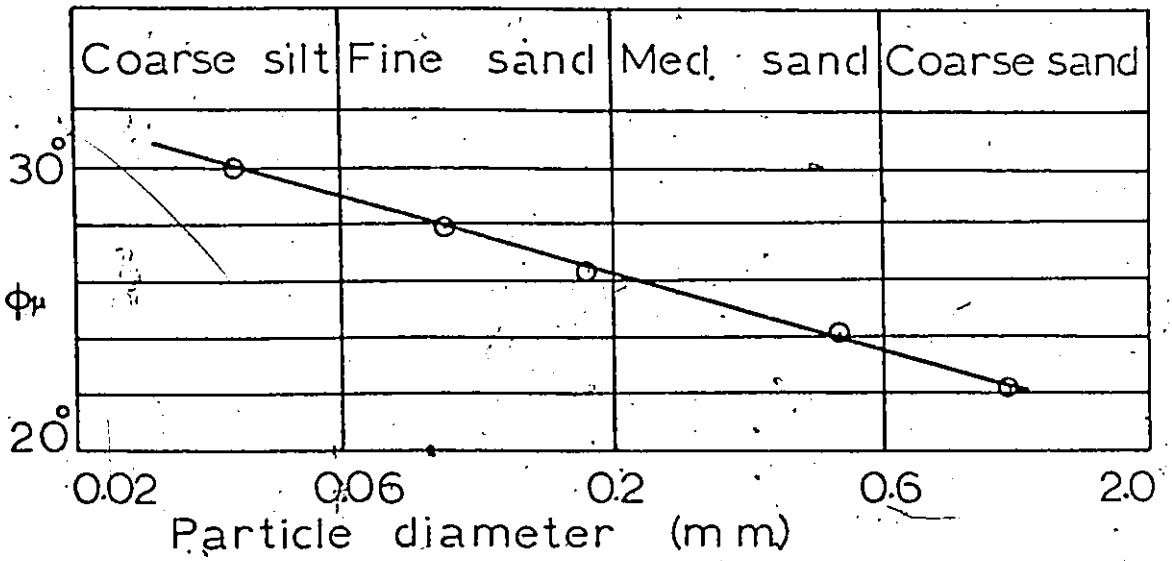

FIG. 2.3 FRICTION ANGLE OF QUARTZ SAND AS A FUNCTION OF GRAIN SIZE (AFTER ROWE, 1962).

However in actual soil this is not the case. Soil particles are in contact with other soil particles and planes through the contact points are inclined to the horizontal. In order to bring about a shear failure between particles, it is not only necessary to overcome the mineral to mineral frictional resistance, ϕ_μ of the soil particles, it is, in addition necessary to make particles move up and over one another.

The energy required by the particles to ride one over the other will be the greatest in cases where the degree of interlocking between the particles would be the greatest. This is another factor contributing to the strength of the soil. It may be visualized that the interlocking between particles would be the greatest when they are densely packed and when they are angular. The number of contact points will be highest for angular and densely packed particles for the same mineral composition and grain size. Hence in order for the soil to fail in shear the amount of energy required will be the greatest for the greatest degree of interlocking. The soil will thus exhibit high strength in this case. However, if the packing of the particles is loose and the number of contact points small, the soil will exhibit a low strength. Rolling is not considered an important factor for strength in cohesionless soils.

2.4 Mobilization of Shear Resistance

In a mass of soil, the shear resistance is not mobilized all at once, but is a function of displacement and level of stress.

In a cohesionless soil which is made up of discrete solid particles there exists a stability of the individual particles and a stability of the soil element as a whole. The stability of the soil sample as a whole is governed by the average property of the soil.

Although the soil sample as a whole can be in a stable equilibrium, all the individual particles in the soil may not necessarily be in a stable equilibrium. At any stress level there may be a few particles in critical equilibrium but that does not violate the overall stability of the material. The number of particles at limiting equilibrium increases as the stress level is increased. At the maximum stress the majority of the particles is at critical equilibrium and the system will become unstable upon further increase of stress so the system fails.

Thus it can be seen that mobilization of shear is a progressive process and is associated with increase in strain. Any typical stress-strain curve for cohesionless soil makes this apparent. For any mass of sand this stress-strain curve is dependent on the void ratio or the density of the sand; and to a smaller extent on the angularity of

the grains, the grain size and the mineral content of the sample.

2.5 Brief Review of Previous Work

The shear strength of sand appears to have been first defined by Coulomb by the equation $S = \sigma_n \tan \phi$, where S = shear strength of sand, psf.

σ_n = normal stress, psf.

ϕ = angle of internal friction.

This equation has formed the basis for most of the work done on the subject since it was first proposed.

However, the drained and undrained behaviour of sand has necessitated a more fundamental understanding of the factors contributing to the strength of sand.

As reported by Lee et al (1967); the earliest demonstration of volume changes was made by Reynolds in 1885, who showed experimentally that dense sands dilate when sheared.

Casagrande (1940) demonstrated the full extent of the dependence of the angle of friction ϕ_{max} of a sand on the void ratio and the associated volume changes during shear. Casagrande showed that whereas dense sand dilated during shear and exhibited a high angle of friction, loose sand compressed during shear and developed a much lower angle of friction. He defined a critical void ratio to describe the particular state of density at which a sand will shear with no volume changes. He further demonstrated that the critical void ratio decreases as the confining pressure acting on the

sand was increased. Similar observations were made by Holubec (1966).

In order to explain the influence of the void ratio on the angle of friction of sand, Taylor (1948) suggested that part of the shear stress required to cause failure of a dense sand was used up in providing the energy required to permit the sand to expand against the confining pressure. The shearing strength was therefore the combined result of two factors - friction and a volume change component (which he called interlocking).

In order to determine the volume change component in a direct shear test he derived the expression

$$\tau_e = \sigma_n \, dh/dx \qquad (2.4)$$

where τ_e = shear stress required to provide energy for expansion

σ_n = applied normal stress

dx = increment of shear deformation

dh = corresponding increment in thickness of the sample.

In order to determine the portion of applied deviator stress in a triaxial compression test which must be applied to provide the energy for sample expansion, Bishop (1954) derived a corresponding expression

$$\sigma_e = \sigma_3 \frac{dV}{V \varepsilon_1} \qquad (2.5)$$

where σ_e = shear stress required to provide the energy for expansion, in psi.

σ_3 = confining pressure in psi.

dV = incremental increase in volume in cc.

V = volume of sample in cc.

ε_1 = incremental increase in axial strain.

By deducting the dilatancy or the volume change component of shear resistance from the total stresses, the shear resistance due to other strength mobilizing factors could thereby be determined.

If the angle of friction of a sand determined from the total applied stresses at failure in a drained test is designated as ϕ_d, and the angle of friction computed after the dilatancy component is deducted is termed ϕ_{dr}, then

$$\tan^2(45 + \phi d/2) = \left(\frac{\sigma_1}{\sigma_3}\right)_f \qquad (2.6)$$

and

$$\tan^2\left(45 + \frac{\phi dr}{2}\right) = \left(\frac{\sigma_1}{\sigma_3} - \frac{dV}{V\varepsilon_1}\right)_f \qquad (2.7)$$

for triaxial test conditions,

But Rowe (1962) has shown in his stress-dilatancy theory that even this is not quite correct. The value of ϕ_{dr} after applying the Taylor-Bishop correction still exceeded ϕ_μ, the angle of friction of the particles comprising a granular medium.

He therefore derived an alternate expression for

after dilatancy effects were deducted, ϕ_f as follows

$$\tan^2(45 + \phi_f/2) = \frac{\sigma_1}{\sigma_3} \frac{1}{1 + \frac{dV}{V\varepsilon}} \qquad (2.8)$$

obtained from a knowledge of the stress, strain and the volume change conditions at failure.

Stress-dilatancy theory as proposed by Rowe in 1962 is fundamental to the understanding of shear behaviour of sand; it would therefore be preferable to deal with certain aspects of the theory in greater detail in the following section.

Many researchers, such as Lee (1966) have confirmed the applicability of the above theory to the stress-strain behaviour of cohesionless soils.

2.6 Stress-Dilatancy Theory

Stress-dilatancy theory as proposed by Rowe in 1962 gives a relationship between stress ratio and dilatancy expressed as $1-dV/d\varepsilon$, where dV is the unit volumetric strain, positive when decreasing, and $d\varepsilon$ is the axial strain.

Rowe neglected the elastic strains and examined the statics and geometry of an ideal system of spheres and rods, in which a mechanism of deformation was assumed.

Figure 2.4 shows an idealized element of a cohesionless soil. Iterparticle sliding occurs in a direction β from the direction of the applied shear force P. Resolving forces in the horizontal direction we have

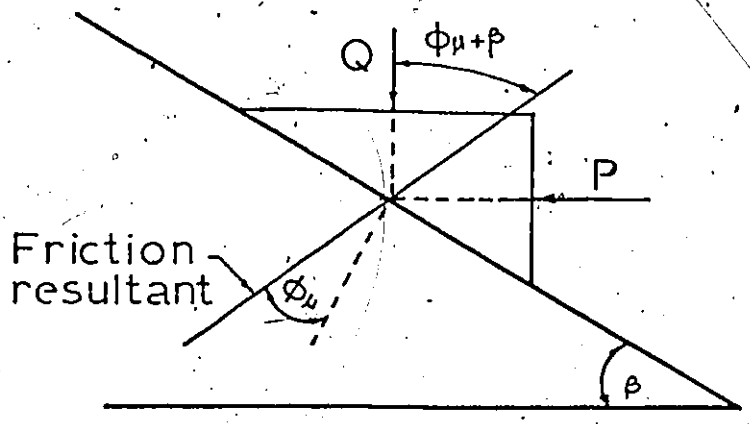

FIG. 2.4. SLIDING WEDGE MODEL (AFTER ROWE, 1962).

$$P = Q.\tan(\phi_\mu+\beta) \qquad (2.9)$$

where Q is the force normal to the direction of P.

Consider, for example, the case of uniform spheres in rhombic packing under triaxial compression, Fig. 2.5. In this packing the side of a sphere has three contact points in direction 1 and two contact points in direction 3. Using Equation (2.9)

$$L_1/L_3 = \frac{3}{2} \tan(\phi_\mu+\beta) \qquad (2.10)$$

where L_1 and L_3 = loads per sphere

ϕ_μ = angle of friction

β = direction of movement of the particles at the sliding contact relative to the major principal direction.

If N_1 is the number of spheres per unit area in plan and N_3 the number of alternate rows per unit area in elevation, then from the packing geometry of spheres

$$\frac{N_1}{N_3} = \frac{2ad}{bc} = \frac{2ad}{3cd} = \frac{2}{3}\tan\alpha \qquad (2.11)$$

α can be seen to be the packing property of the spheres.

From Equations (2.10) and (2.11) we can write

$$\frac{\sigma_1}{\sigma_3} = \frac{3}{2}\frac{N_1}{N_3}\tan(\phi_\mu+\beta) = \tan\alpha\tan(\phi_\mu+\beta) \qquad (2.12)$$

The strain increment, $\delta\varepsilon_1$ and $\delta\varepsilon_3$ are related by the deformation mechanism and this is expressed as

$$\frac{\delta\varepsilon_3}{\delta\varepsilon_1} = \frac{1}{2}\tan\alpha\tan\beta = \frac{1}{2}\left(1 - \frac{dv^p}{d\varepsilon_1^p}\right) \qquad (2.13)$$

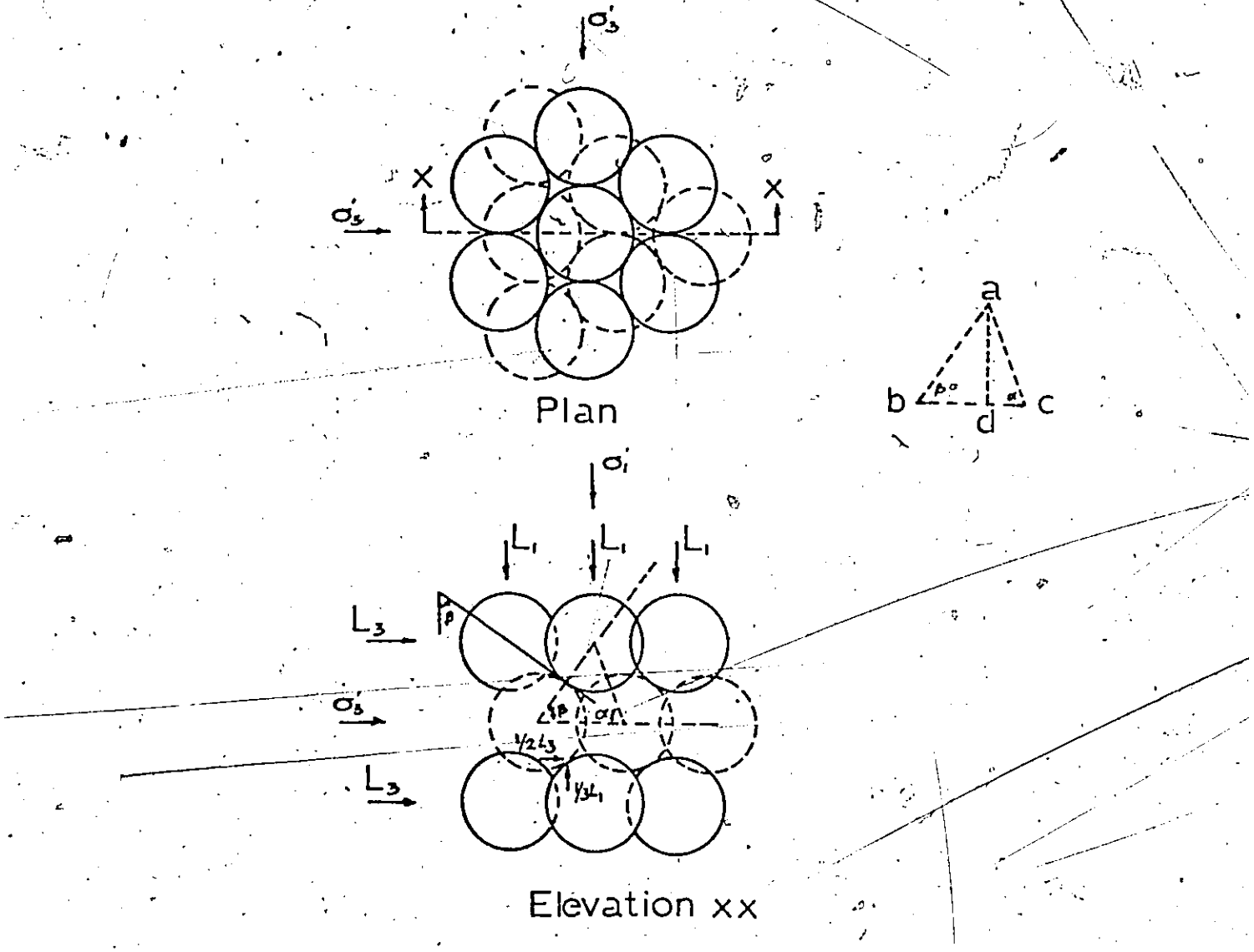

FIG. 2.5 UNIFORM RIGID SPHERES; RHOMBIC PACKING; DEFORMATION MODE (AFTER ROWE, 1962).

The energy ratio is the 'ratio of work done per unit volume on the assembly by the major principal stress to the work done on the minor principal stress by the assembly during an increment of expansion', is expressed as

$$\frac{\sigma_1 \delta\varepsilon_1}{2\sigma_3 \delta\varepsilon_3} = \frac{\tan(\phi_\mu+\beta)}{\tan\beta} = \frac{\sigma_1}{\sigma_3[1-(dv^p)/(d\varepsilon_1^p)]} \qquad (2.14)$$

Noting that this expression is free of the packing parameter α, Rowe suggested that in a real soil a minimum energy ratio state will be developed at each stage of the deformation history. Minimizing Equation (2.14) with respect to β leads to a β value of $(45-\phi_\mu/2)$ and substitution in Equation (2.14) leads to

$$\frac{\sigma_1}{\sigma_3[1-(dv^p)/(d\varepsilon_1)^p]} = \tan^2(45^o+\phi_\mu/2) \qquad (2.15)$$

referred to as the stress-dilatancy equation for compression.

The same results as in Equation (2.15) are obtained with different types of packings; such as uniform spheres in face centred cubic packings and for any regular packings.

In the light of experimental observations it was considered inevitable to substitute ϕ_μ with ϕ_f in Equation (2.15) so that Equation (2.15) now becomes

$$\frac{\sigma_1}{\sigma_3[1-(dv^p)/(d\varepsilon_1)^p]} = \tan^2(45^o+\phi_f/2) \qquad (2.16)$$

where ϕ_f varied from ϕ_μ to ϕ_{cv}.

The reasons for substituting ϕ_μ with ϕ_f will be explained in section 2.8.

2.7 Components of Shear Strength

Application of the expression given by Equation (2.16) to a series of strength tests conducted at different void ratios led Rowe to the following observations.

For dense sands the dilatancy effects reduced the angle of friction ϕ_f to a value equal to that for sliding of the mineral grains. For higher void ratios, the angle of friction after deduction of dilatancy effects still exceeded that of the mineral grains. Accordingly Rowe concluded that throughout most of the range of void ratios there were three components of strengths of granular materials.

1. The strength mobilized by frictional resistance.

2. The strength developed by energy required to rearrange and reorient soil particles; and

3. The strength developed by energy required to cause expansion or dilation of the material.

In a detailed analysis of the factors contributing to the strength of granular soils, Rowe, Barden and Lee (1964) proposed that the energy required to cause dilation can be further subdivided into

1. Energy required to do external work during volume changes.

2. Energy absorbed in friction as the mass dilates.

The Taylor-Bishop expression takes into account the former component only. Hence the component of shear strength due to dilation will be somewhat underestimated by their expressions. Hence Taylor-Bishop's ϕ_r will always be greater than Rowe's ϕ_f.

In the next section appropriate expressions for various strength components for shear strength parameters for direct shear, triaxial and plane strain test will be presented.

2.8 Direct Shear Tests

Referring again to Fig. 2.4 where the particle moves through an incremental distance δx in the direction of the shearing force P, Lee (1968) has given the expression

$$\tan\phi_r = \tan\phi_d + \frac{Vo}{Ao}\frac{\delta v}{\delta x} \qquad (2.17)$$

where ϕ_r = corrected angle of shearing resistance in the drained test taking into account external work done due to dilatancy.

ϕ_d = measured drained ϕ

Vo = original volume of the sample.

δv = the change in volume per unit volume which is positive for all decreasing volumetric strain.

δx = transverse displacement.

In order to relate ϕ_r with ϕ_μ one would use the expression

$$\tan\phi_r = \tan\phi_\mu + \tan\phi_d \frac{Vo}{Ao}\frac{\delta v}{\delta x}\tan\phi_\mu \qquad (2.18)$$

Equation (2.18) does not take into account the additional energy component absorbed within the sample because slides in a natural soil do not necessarily occur in directions associated with the minimum energy state. This condition could be numerically expressed by replacing ϕ_μ with ϕ_f in Equation (2.18) such that

$$\tan\phi_r' = \tan\phi_f + \tan\phi_d \cdot \frac{Vo}{Ao} \frac{\delta v}{\delta x} \tan\phi_f \qquad (2.19)$$

where $$\tan\phi f = \frac{\frac{S}{N} - \frac{\delta v}{\delta \gamma}}{1 - \frac{S}{N}\frac{\delta v}{\delta \gamma}} \qquad (2.20)$$

and s = shear force

N = normal force

δv = volumetric strain

$\delta \gamma$ = shear strain

The difference between ϕ_r' and ϕ_r gives the component of strength absorbed by the sample.

2.9 Triaxial Compression Tests

The Taylor-Bishop expression for the angle of shearing resistance corrected for dilatancy as given by Lee (1968) may be written as

$$\tan^2(45+\phi_r/2) = \frac{\sigma_1}{\sigma_3} + \frac{\delta v}{\delta \varepsilon_1} \qquad (2.21)$$

where δv and $\delta \varepsilon_1$ are volumetric and axial strain; δv is positive if there is a decrease in volume.

The corresponding expression by Rowe is given as

$$\tan^2(45+\phi_f/2) = \frac{\sigma_1}{\sigma_3(1 - \delta v/\delta\varepsilon_1)} \qquad (2.22)$$

Here the difference between Equation (2.21) and Equation (2.22) is nothing but the energy absorbed within the sample as a result of reorientation of the particles.

2.10 Relationship Between the Shear Strength Parameters of Sand from Triaxial Compression, Plane Strain and Direct Shear Box Tests

Rowe (1969) expressed the stress-dilatancy equation as

$$R = Dk \qquad (2.23)$$

where $R = \sigma_1/\sigma_3$

$D = 1 - dv_s/d\varepsilon_{1s}$

v_s = volume decrease per unit volume

ε_{1s} = major principal compressive strain ε_1 in a compression test, due to interparticle slip (denoted by subscript s)

$K = \tan^2(45^o+\phi_f/2)$.

The value of ϕ_f depends on the relative density, the pressure range and stress path. It varies between a lower value ϕ_μ, the angle of friction between mineral particles and an upper value ϕ_{cv} at the critical state.

In the case of plane strain compression writing $d\varepsilon_2 = d\varepsilon_2 s = 0$, Equation (2.23) applies, although boundary strain conditions will influence the value of ϕ_f.

Rowe (1969) quoting works by Horne said, that in a triaxial compression test the maximum value of D = 2. Hence

$$1 < D < 2 \tag{2.24}$$

It may be noted that Equation (2.23) is derived from the equation

$$\frac{\sigma_1}{\sigma_3} = \tan\alpha \tan(\phi_\mu + \beta) \tag{2.12}$$

where α is the packing parameter given by the expression

$$\tan\alpha = \left|\frac{\sigma_1}{\sigma_3}\left(1 - \frac{dv}{d\varepsilon_1}\right)\right|^{1/2} \tag{2.25}$$

The Equation (2.12) was also independently derived by Leussink and Wittke (1963).

Rowe further reported that $\tan\alpha$ was not independent of ϕ_μ; whereas the dilatancy rate D was independent of ϕ_μ and k.

The experimental relation between ϕ_μ and ϕ_{cv} as shown in Fig. 2.6 was in agreement with the theoretical prediction by Horne as shown by Rowe (1969).

2.10.1 Strength Limits in Triaxial Compression Tests

Based on the works of Wightman, Horne and others, Rowe (1969) suggests taking the upper dilatancy rate of D = 2 and using Equation (2.23); and the relationship $\phi_\mu < \phi_f < \phi_{cv}$ the stress ratio of a sand in the densest state is given by

$$\sigma_1/\sigma_3 = 2\tan^2(45^\circ + \phi_\mu/2) \tag{2.26}$$

Taking D = 1 and the relationship $\phi_f = \phi_{cv}$ for the loosest state

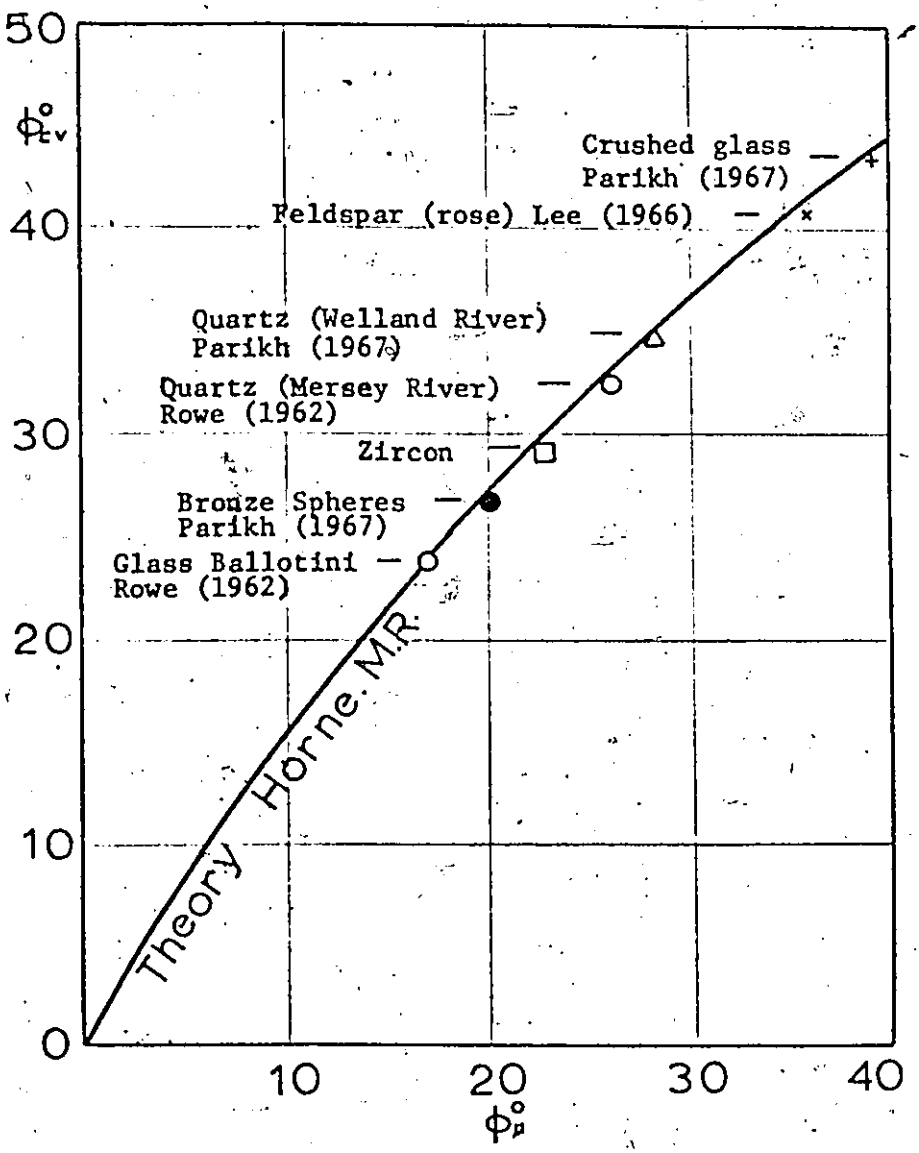

FIG. 2.6 RELATIONSHIP BETWEEN ϕ_μ AND ϕ_{cv} (AFTER ROWE, 1969)

$$\sigma_1/\sigma_3 = \tan^2(45^\circ+\phi_{cv}/2) \qquad (2.27)$$

2.10.2. Strength Limits in Plane Strain Compression Test

In plane strain compression for any packing $\phi_f = \phi_{cv}$.

Therefore, for the dense state

$$\sigma_1/\sigma_3 = 2\tan^2(45+\phi_{cv}/2) \qquad (2.28)$$

and for the loose state

$$\sigma_1/\sigma_3 = \tan^2(45+\phi_{cv}/2) \qquad (2.29)$$

The maximum dilatancy rate of 2 is not necessarily reached by dense packings. An increase of mean principal stress for example leads to crushing and a reduction of the dilatancy rate to such an extent that at very high pressure the dilatancy rate is unity.

In order to relate a measured value of ϕ_{max} for one sand in one state (loosest or densest) and the mean principal stress at failure in the triaxial test, the corresponding value of ϕ_{max} in plane strain may be deduced from a plot of the limiting values of ϕ_μ and ϕ_{cv}. For this purpose ϕ_μ may be determined during a reloading stress path in the triaxial test using free ends and large strains or as suggested by Lee and Seed (1967) for ϕ_{cv} using the relationship

$$\sin\phi_{cv} = \frac{15\tan\phi_\mu}{10+3\tan\phi_\mu} \qquad (2.30)$$

where ϕ_μ is the value suggested by Bishop (1954).

2.10.3 Relationship between Direct Shear and Plane Strain Tes

As reported by Rowe (1969) several researchers have reported direct measurements of normal and shear stresses on the boundary of an element of sand in the centre of the Cambridge Simple Shear apparatus MK6. Assuming uniformity of strain throughout the element; it has been shown that the direction of principal stress and principal strain coincide during small incremental stress relations.

Based on the above observation Rowe derived the following expression

$$\tan\phi_{ds} = \tan\phi_{ps} \text{ Cos } \phi_{cv} \qquad (2.31)$$

relating ϕ_{ds} with ϕ_{ps} where ϕ_{ds} is the value of ϕ for direct shear tests and ϕ_{ps} is the value of ϕ for the plane strain tests.

Figure 2.7 shows the relation of ϕ_{ds} with ϕ_{ps}.

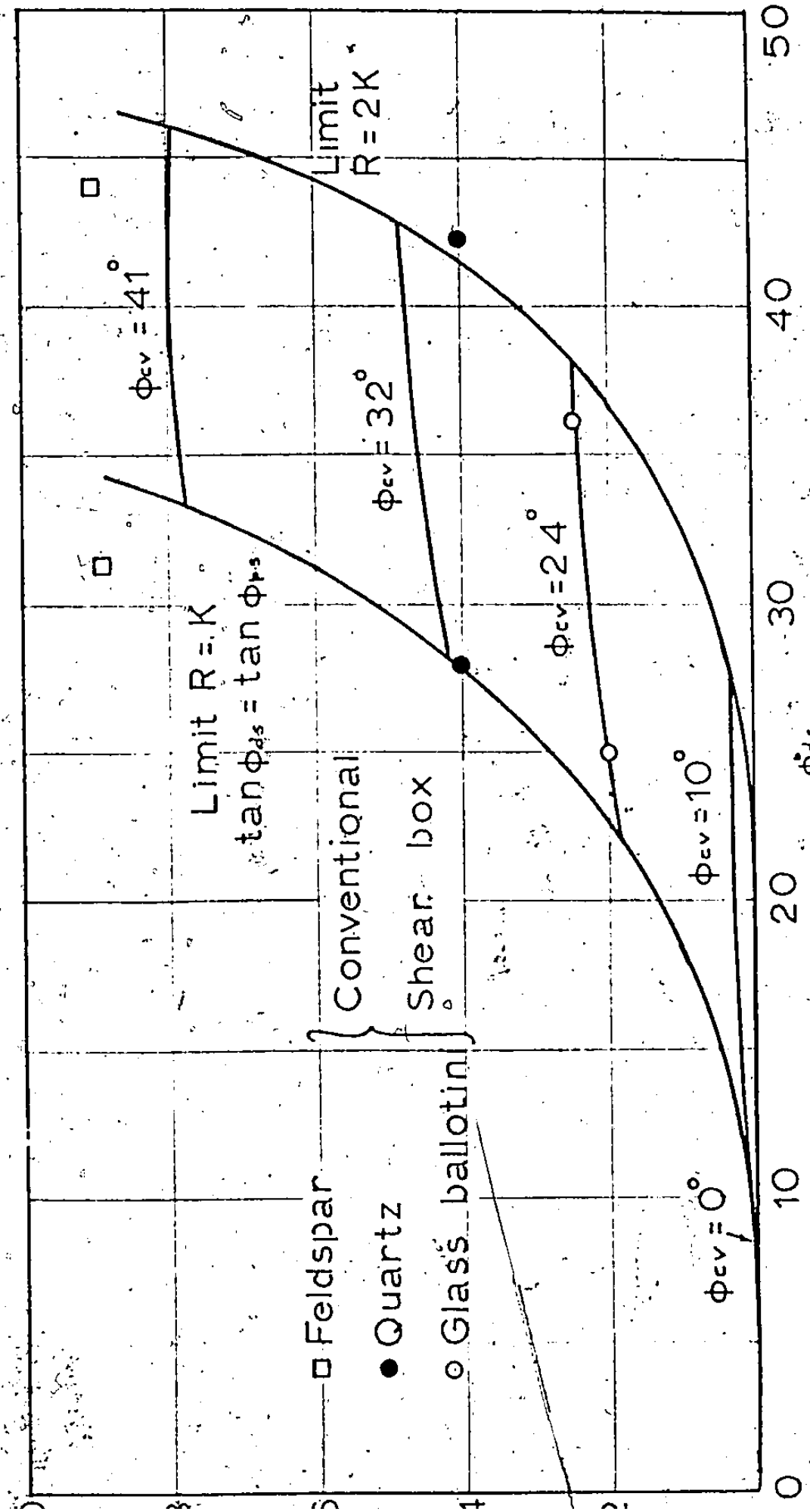

FIG. 2.7 DIFFERENCE BETWEEN ϕ_{max} IN PLANE STRAIN AND DIRECT SHEAR FOR VARIOUS VALUES OF ϕ_{cv} (AFTER ROWE, 1969).

CHAPTER 3

LABORATORY TESTS AND PROCEDURES

3.1 Description of the Sand Tested

The sand used was factory crushed quartz designated as Silica-24. It was sharp and angular with an uniformity coefficient of about 2.1. Hence it can be classified as uniform sand. From the grain size distribution curves, Fig. 3.1 it would appear that it was a fine to medium sand. Four tests were conducted for grain size determination. Only the coarsest and finest gradation curves are shown.

The maximum and minimum densities using A.S.T.M. procedures were 103.3 and 77.9 lbs/cft. These values were the average of two maximum densities of 103.6 and 103.1 lbs/cft and two minimum densities of 78.1 and 77.7 lbs/cft. The specific gravity of the particles was found to be 2.66. The minimum and maximum void ratios were 0.61 and 1.13, and the corresponding porosities were 0.38 and 0.53 respectively.

In order to describe the sand fully; procedures outlined by Krumbein (1941) and Rittenhouse (1943) were used to determine the sphericity of the grains. This procedure had been used by several other investigators; for instance, Walker and Whitaker (1967) and Kolbuszewski (1958). A new roundness scale was used to determine the roundness of the particles as described by Powers (1953).

Figure 3.2 shows the shape of the particles as viewed under a microscope and drawn on paper. The particles were picked up in a random way. Based on charts, values of

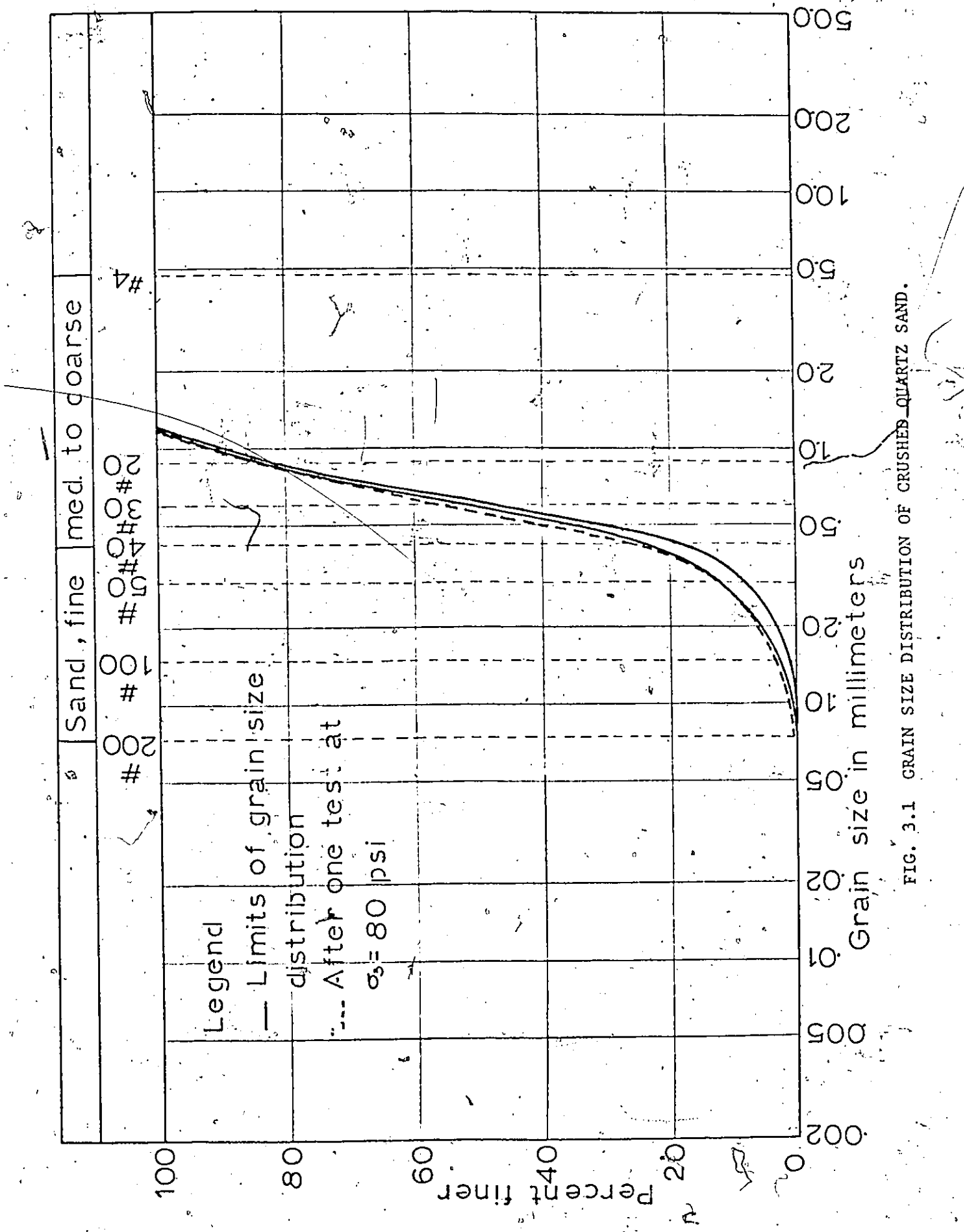

FIG. 3.1 GRAIN SIZE DISTRIBUTION OF CRUSHED QUARTZ SAND.

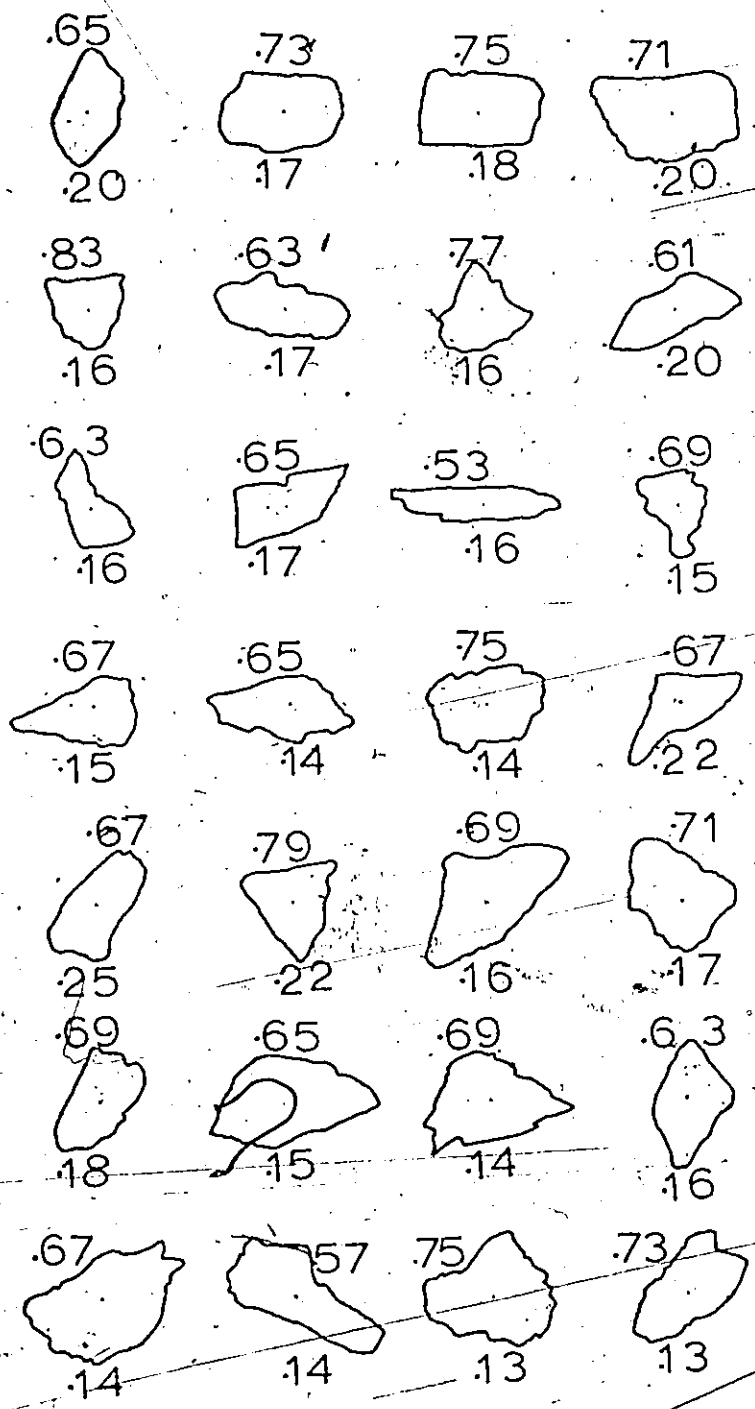

Mean sphericity: 0.68
roundness: 0.17

FIG. 3.2 TYPICAL EXAMPLE OF MEAN SPHERICITY AND ROUNDNESS ESTIMATED FOR CRUSHED QUARTZ SAND (MAGNIFIED 15 TIMES) BY MEANS OF STANDARD CHARTS.

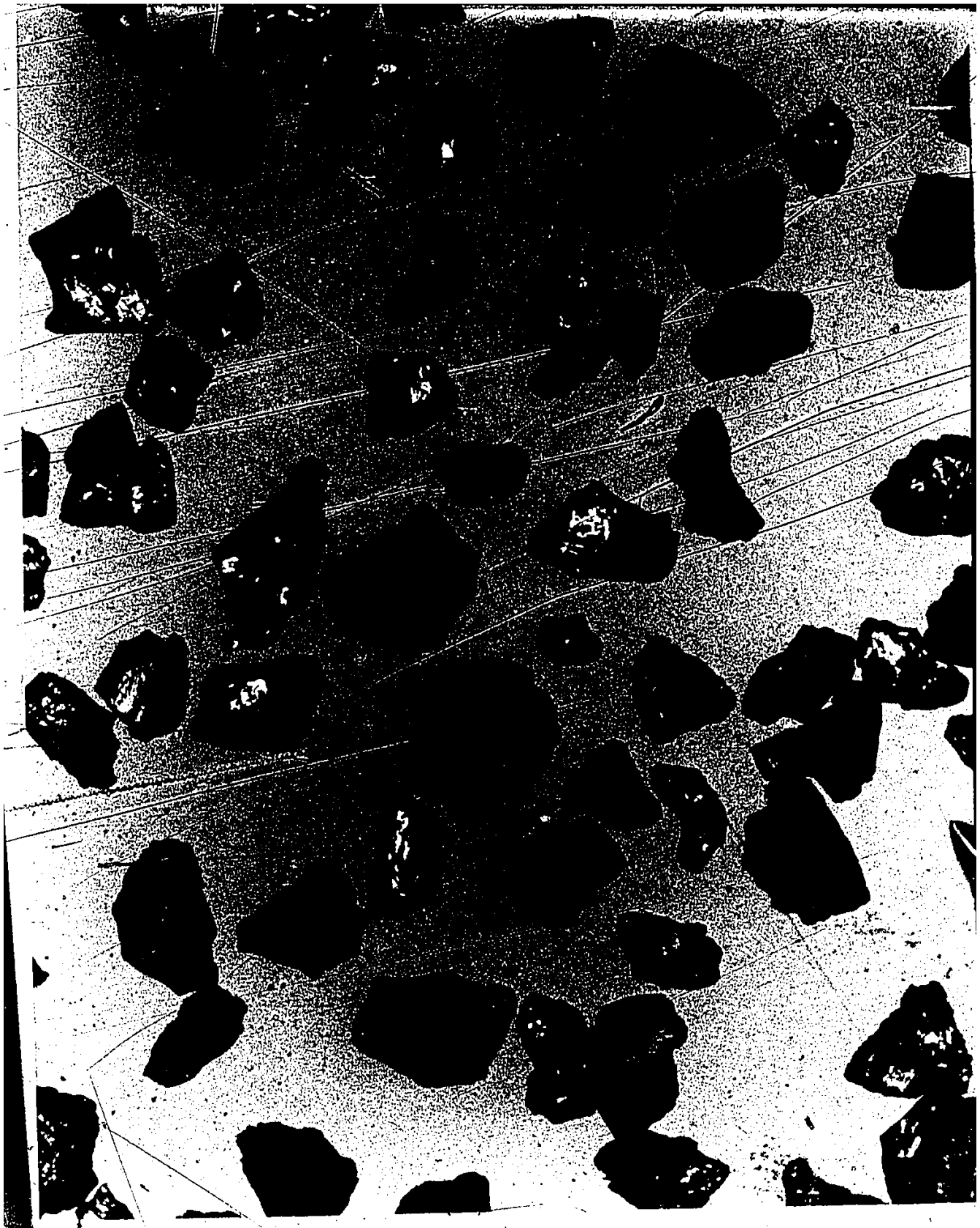

PLATE 3.1 PHOTOGRAPH OF CRUSHED QUARTZ PARTICLES (MAGNIFIED 30 TIMES) USED IN THE TEST.

roundness and sphericity were then assigned to them. Plate 3.1 shows a photograph of the particles magnified 30 times.

According to Krumbein (1941), the shape of the particles is its form, "entirely independently of whether the edges or corners are sharp or round. Fundamentally the shape is the measure of the ratio of the surface area of a particle to its volume. For a sphere this ratio is a minimum, and for all other forms it is larger. Hence the ratio of surface area to volume indicates how closely or remotely the particle approaches a sphere in form. For practical purposes this ratio is difficult to measure, and the actual measurement is expressed in terms of the ratio of the volume of the particle to the volume of its circumscribing sphere. The cube root of this ratio is called the sphericity of the particles.

"The roundness of a particle is a measure of the curvature of the corners and edges expressed as a ratio to the average curvature of the particle as a whole, independent of its form. For practical purposes the average curvature is expressed in terms of the inscribed circle drawn on a projection of the particle in a plane."

Thus roundness depends upon the sharpness of the edges and corners and is independent of shape.

From Fig. 3.2 it can be inferred that basically the grains were oblong and that the particles were angular to very angular.

3.2 Some Triaxial Testing Techniques

The importance of free ends in triaxial testing has been pointed out by many investigators, like Rowe

and Barden (1964), Lee and Seed (1964) and Lee (1968).

Figure 3.3 shows the importance of using free ends in triaxial testing. In using frictionless end platens the distribution of axial strain becomes more or less uniform throughout the sample. As a result the shear strength is mobilized throughout the whole sample, and is not restricted to the central portion only as would be the case with fixed end platens.

In this work frictionless end platens similar to those described by Barden and Mcdermot (1965) have been used. The details of the platens are given in Appendix C.

Bishop and Green (1965) have compared the effects of using a length to diameter ratio of 1 to 2 and the influence of using one or more than one membrane in between the sample and the top and the bottom frictionless platens.

Their findings indicate that with a length to diameter ratio of 2 of the sample and using one lubricated rubber membrane, the results became very consistent as can be seen from the Fig. 3.4.

Hence in this work 8-inch high by 4-in. diameter samples were used. One lubricated membrane at each platen was employed. Silicone grease was used as the lubricating medium. Its effectiveness has also been pointed out by several investigators.

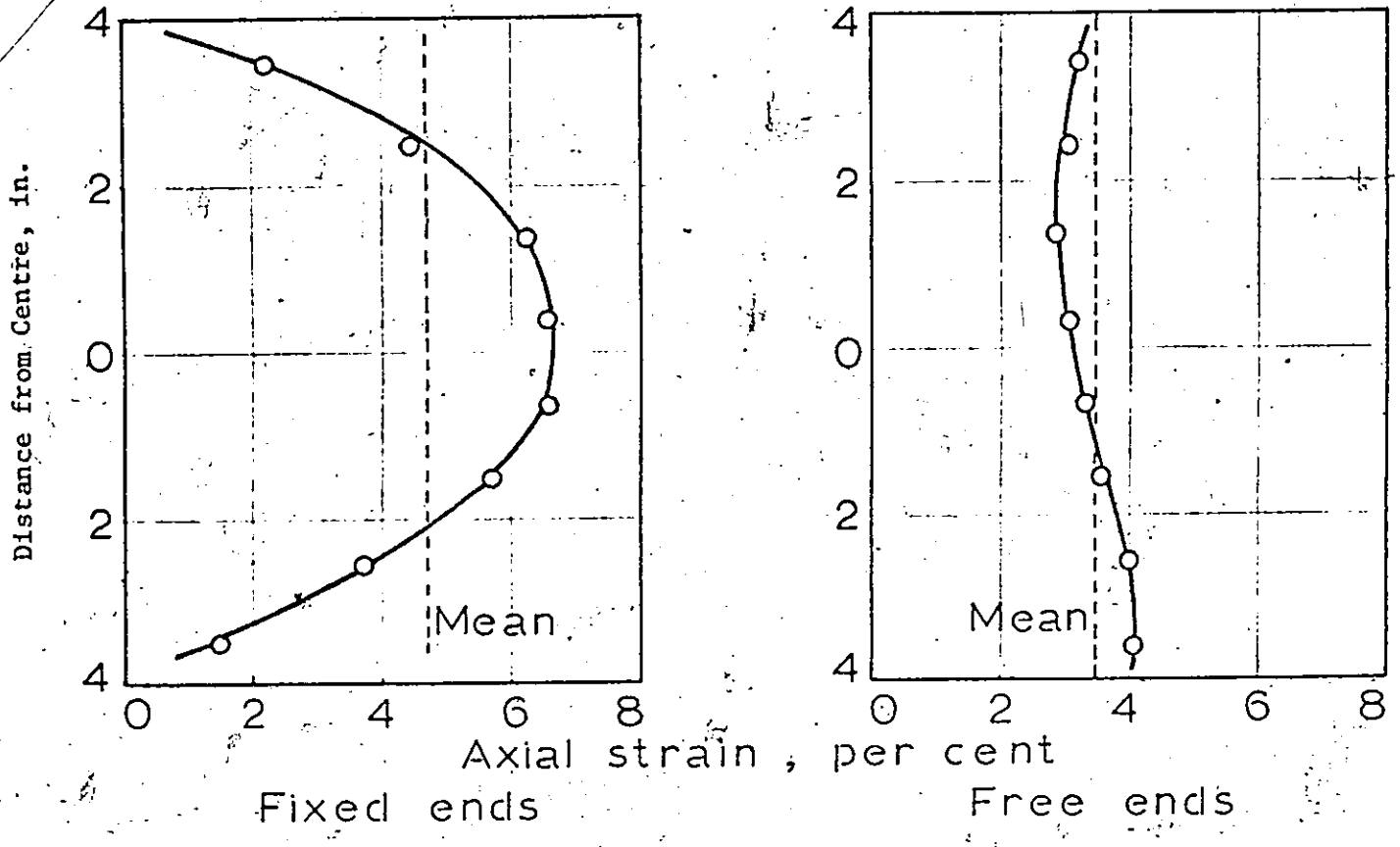

FIG. 3.3 AXIAL STRAIN DISTRIBUTION FOR 8 in x 4 in SAMPLES (AFTER LEE, 1968).

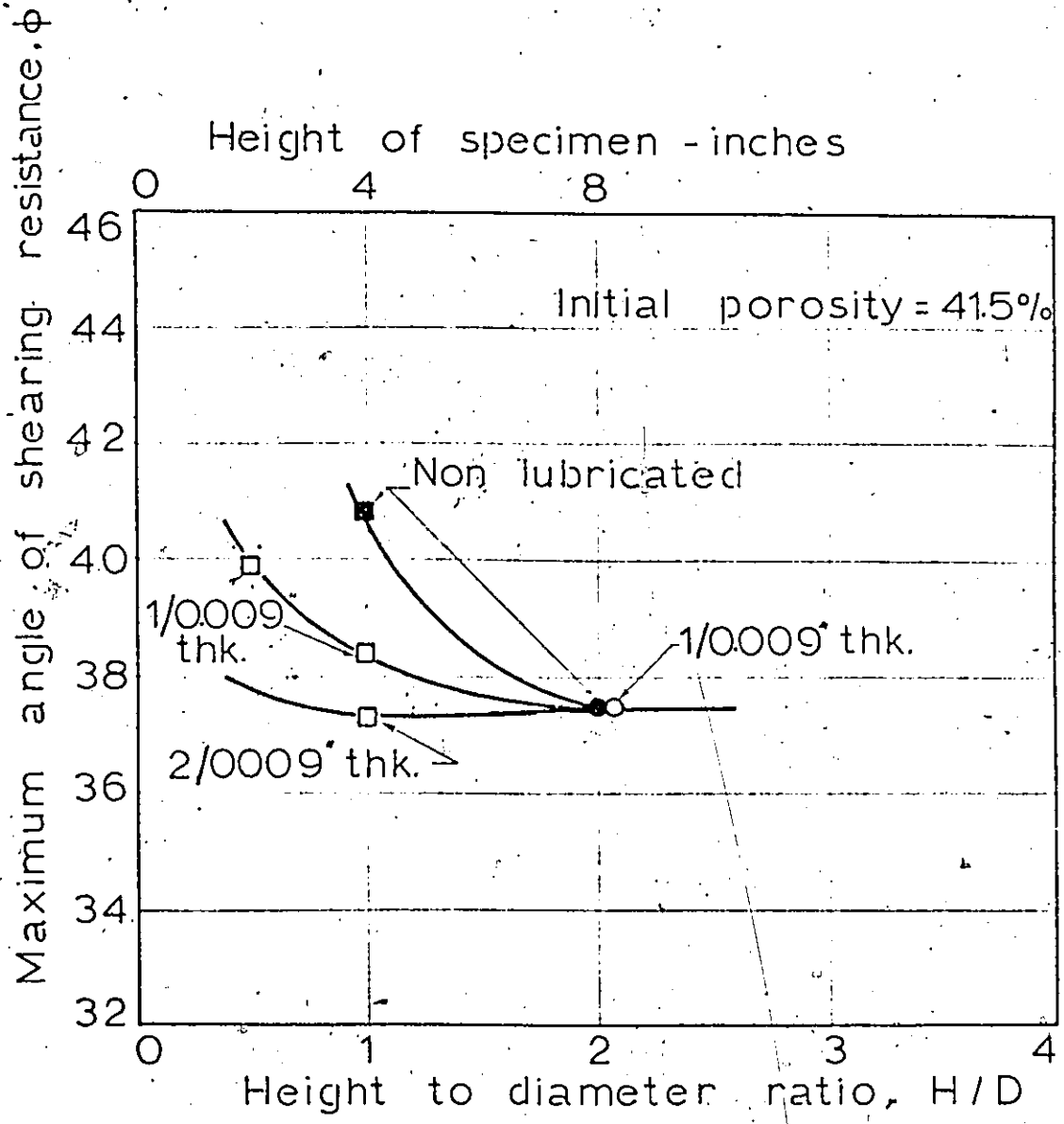

FIG. 3.4 INFLUENCE OF HEIGHT TO DIAMETER ON THE STRENGTH OF SAMPLES HAVING VARIOUS DEGREES OF END RESTRAINT (AFTER BISHOP AND GREEN, 1965).

3.3 Sources of Error in Triaxial Testing

Since it is easier to eliminate sources of errors in triaxial testing, drained triaxial compression tests were chosen as the major testing programme. Considerations were given to the elimination of errors that could have a bearing on the test results. Some of the factors as pointed out by Bishop and Henkel (1962) are summarized as follows.

1. The friction on the loading ram.

2. The expansion of the cell on application of the cell pressure and the effects of creep on the measurement of volume changes.

3. Deformation of the sample during testing and determination of effective area during each stage of deformation.

4. Calibration of the pressure gauge.

5. Calibration of the proving ring.

6. Measurement of volume changes.

7. Corrections to the volume changes due to movement of the ram.

8. Corrections due to penetration of membrane into the sample on application of σ_3.

These corrections will be discussed in some detail in section 3.5.

3.4 Preparation of Samples

3.4.1 General

As pointed out earlier the factors governing the strength of sand are the state of density of the sand and the packing factor or the structure; other factors such as grain size, mineral composition, angularity of the grains, confining pressure, etc., remaining constant.

Feda (1969) defined the structure of a sample of cohesionless soils as the variation of local porosities compared to the overall porosity of the sample.

The preparation of a sample may be considered to consist of stages when a sample of sand passes from a random collection of particles to a shape when it is ready to be sheared in a particular test set up.

Regardless of the extent of care exercised in the deposition of sand into the sample former using a spoon or dropping it through a funnel keeping the height of fall constant, tamping and vibration, etc.; there is no guarantee that the structure of the sand will be the same throughout the body of the sample. The behaviour of the sand during shear would thus tend to be erratic.

Further; in order to get worthwhile results from laboratory tests it would appear imperative to use techniques that would produce specimens for test having the same densities and structures as are likely to be encountered in the sand box.

The problems of reproducing densities and structure were overcome by using a miniature type of sand deposition device. The design of this apparatus was similar to that described by Walker and Whitaker (1967) and has been successfully used by a number of other researchers. This device was to simulate the deposition of sand in the sand box.

The bed of sand in the sand box and the samples for triaxial compression and direct shear box tests in the laboratory are prepared in a series of thin layers by a rain of sand falling from a hopper. Sand is drawn out of the hopper as the drum rotates. The whole assembly passes forwards and backwards, building a bed of sand. The details of the hopper are shown in Plate 3.2. The hopper has the dimensions of 11 ins. by 9 ins. and a height of 11 ins. with a capacity of 40 lbs of sand. It is made of plexiglass and is mounted on wheels so that it can be moved on rails (2). The intensity of flow of sand is regulated by the size of the opening of the hopper, and the speed of the revolving drum (4). The size of the opening can be adjusted by a plate (3). The drum is rotated by a unit consisting of a motor (D.C., H.P. 1/50, 1,725 r.p.m.), a variac (1 Amp. Max.) and a reduction gear. This system was designed to produce speeds from 5 to 200 r.p.m. by choosing suitable gears.

The curtain of sand, flowing over the drum, is regulated by a deflection plate (6). For uniform deposition of sand the curtain of sand that flows down should have a

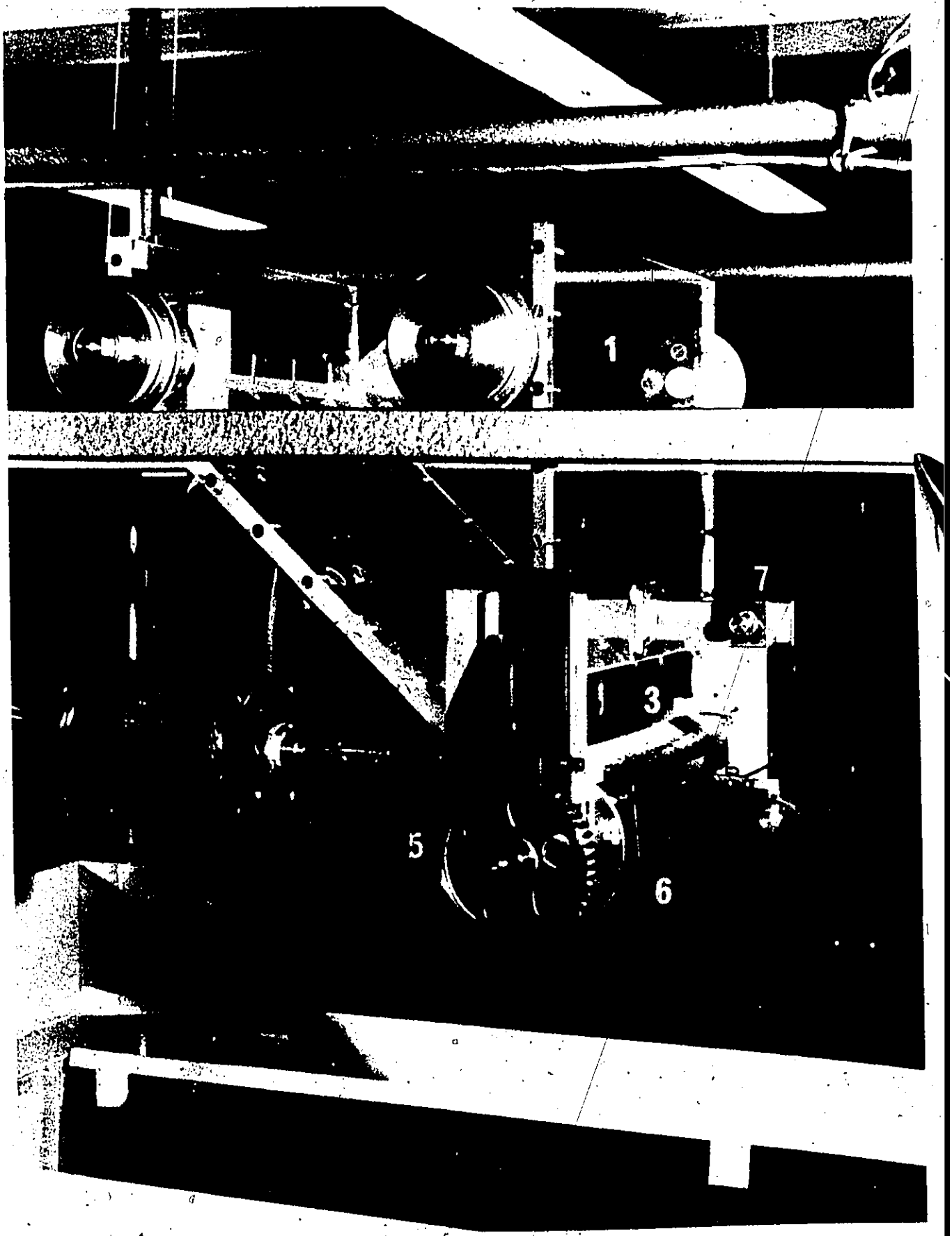

PLATE 3.2 SAND SPREADING DEVICE (FROM ASHTAKALA, 1968)

uniform thickness. The deflection plate can be rotated to any angle and it can be moved in vertical or horizontal directions for proper setting. This arrangement is shown by the unit indicated as item 7 in Plate 3.2. The hopper can be moved back and forth manually, maintaining a constant speed of movement. By varying the drum speed and the gap opening the desired density can be obtained.

During the preparation of the sample in the laboratory a height of fall of about 3 ft. from the centre of the sample former to the centre of the rotating drum was maintained. It was noted that an increase in height beyond 2.5 ft. did not materially influence the density of the deposited sand.

Initially the sand was deposited in a calibrated perspex cylinder with knife edges measuring 4 ins. in diameter and having an inside height of 4.6 ins. The volume of the cylinder was 57.25 in.^{3} when struck even with the top. The density in pounds per cubic feet could then be obtained.

From the relationship

$$D_r = \frac{\gamma_{d\ max}}{\gamma_d} \times \frac{\gamma_d - \gamma_{d\ min}}{\gamma_{d\ max} - \gamma_{d\ min}} \qquad (3.1)$$

the relative density was calculated.

For the sake of quick reference a plot of relative density versus unit weight was made as given in Fig. 3.5.

A difference of about 4 ins. in the height of fall of the sand did not have any significant difference on the density of the sample. Similar observations were made by Walker and Whitaker (1967).

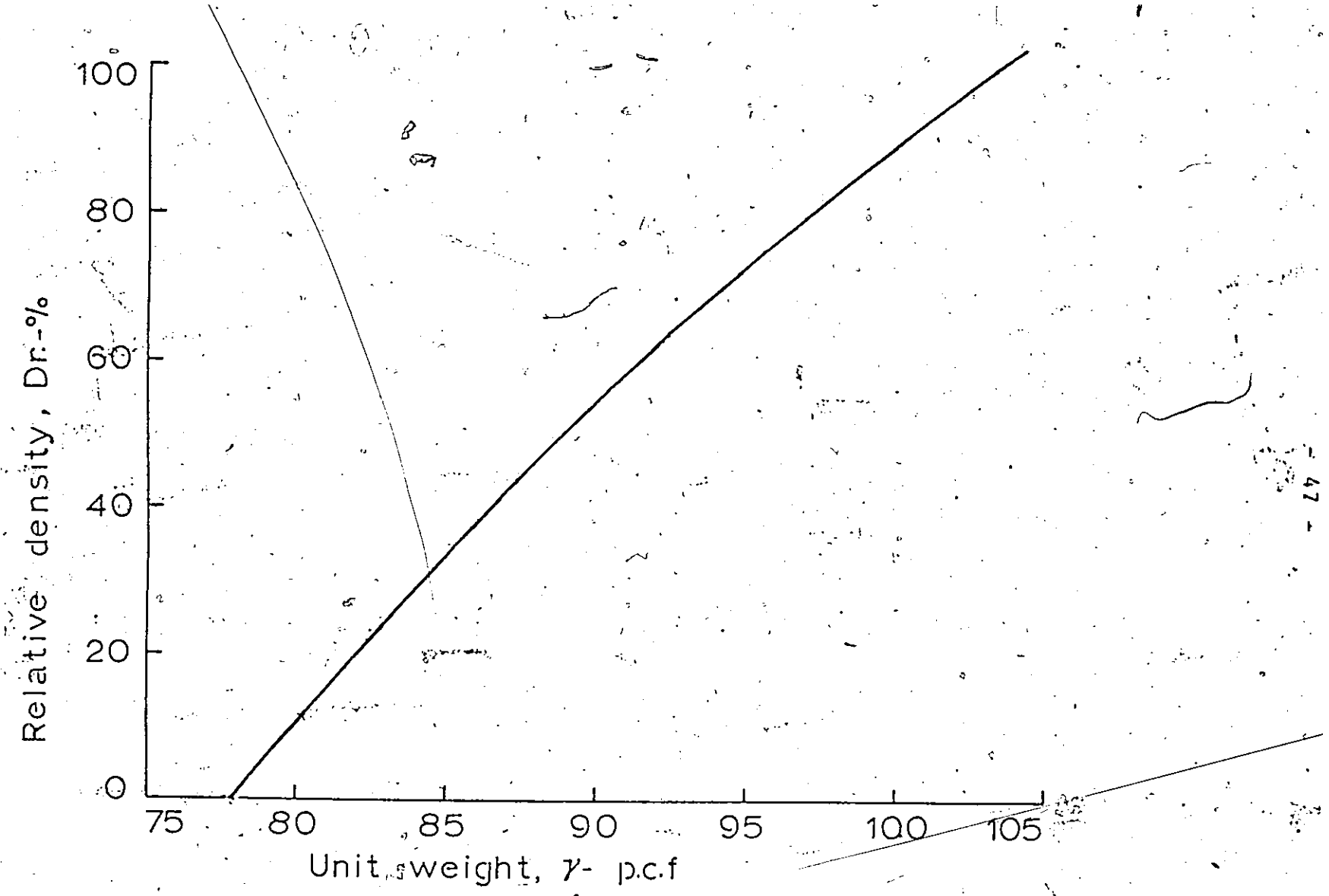

FIG. 3.5 RELATIONSHIP BETWEEN THE UNIT WEIGHT AND RELATIVE DENSITY OF THE SAND.

The sand depositing device used for the preparation of the samples has been previously used and was described by Ashtakala (1968).

From 4 repetitive tests on 3 different densities it was found that for a given quantity of sand falling per unit of time per unit of area, the variation in relative density was in the order of 2 percent, which could be considered acceptable. Hence it might be said that the disturbance due to air current was negligible.

3.4.2 Preparation of Triaxial Test Samples

Four inch diameter and eight inch high samples were used. The air drainage from the base of the frictionless platen was provided by using a 1/2 inch diameter porous disc recessed in the bottom platen. A small circular right cylinder with bevelled top, as described in Appendix B, was provided to prevent the eccentric loading of the sample during testing. The sample was then prepared by depositing a curtain of sand into the former having a collar with a knife edge. Suction between the membrane and former was provided to make the sample diameter uniform. After the former was full of sand, the raining of the sand was stopped; the sides and the top of the former were cleaned and any excess sand was removed slowly and gently with the help of a small hair brush. The top platen along with a greased rubber membrane was placed in position. It was then given a small rotation in either direction to ensure a perfect seating. Two rubber O-rings were used to seal the sample. Suction was then applied

by mouth and the "Klinger" valve was closed.

The former was then removed. The sample stayed upright. This suction was removed only after a confining pressure was applied to the sample as detailed in section 3.6.

The diameter of the sample was measured by a micrometer screw gauge at a total of six different places located at mid height of the sample and one inch below the top and one inch above the bottom of the sample.

A set of three diameter readings were taken in one position. The sample was then turned through 90 degrees and another set of three diameter readings were taken.

3.4.3 Direct Shear Box Test Sample Preparation

Two inch by two inch samples with a height of about 1.5 inch were used in the Direct Shear Box tests run in the conventional way using serrated plates at top and bottom of the sample.[1] The samples were prepared by directly depositing the sand from the sand raining device into the shear box. Care was taken to see that the thickness of the bed produced was uniform throughout and that the thickness of the sample was sufficient and adequate. The top of the sample was then lightly pressed with a wooden block before placing the top serrated plate into place. The total compression beyond the ten pound hangar load was considered in calculating the initial volume of the sample.

[1] The tests were run with the lifting screws in the lowered position. The influence of these on the test results is discussed in Appendix D.

3.5 Triaxial Compression Test Procedures

After the sample was prepared, sealed and a vacuum applied to it, the cell was assembled and transferred on to the triaxial machine. The cell was filled nearly to the top with distilled water. The top 1/4 inch was filled with paraffin oil to prevent leakage during the test taking care not to entrap any air bubbles. The loading ram was lowered and brought into snug contact with the top of the platen. The cell pressure was then applied and the drainage valve opened. This cell pressure was maintained for about half an hour before starting shearing of the sample. The initial volume change of the sample on application of the cell pressure was measured with the help of the volume measuring device only. This volume change was a maximum for the maximum cell pressure which was applied.

A strain rate of 0.015 inches per minute was adopted. According to Bishop and Henkel (1962) a shearing time of one hour is considered adequate for drained test on sand. In the present case about 100 minutes would be required for an axial compression of 1.5 inches.

Rotating bushings were used to eliminate friction in the loading ram in all triaxial tests.

Volume change measurements in the sample were made with the help of a volume measuring device, described by Bishop and Henkel (1962), by noting the quantity of water entering and leaving the cell. The volume was corrected for cell expansion and the movement of the loading ram.

Volume change was also noted by measuring the amount of air entering or leaving the sample. The two volume changes were compared and the average was taken. The maximum difference in the value of the two readings was 2 cc, or about 4%. 10,000 and 3,000 lbs proving rings were used which were calibrated against other proving rings for their reliability.

Plate 3.3 shows the details of the experimental set up for the drained triaxial compression test on sand. The numbers in Plate 3.3 refer to the different components and are explained below.

No. 1. The 5 ton triaxial machine

2. The triaxial cell with rotating bushing arrangement

3. Proving ring with dial gauges

4. Motor for running the rotating bushing device

5. Volume measuring device; measures the amount of water entering or leaving the cell

6. Burettes measuring the amount of air expelled or absorbed into the samples

7. Mercury pressure pot system.

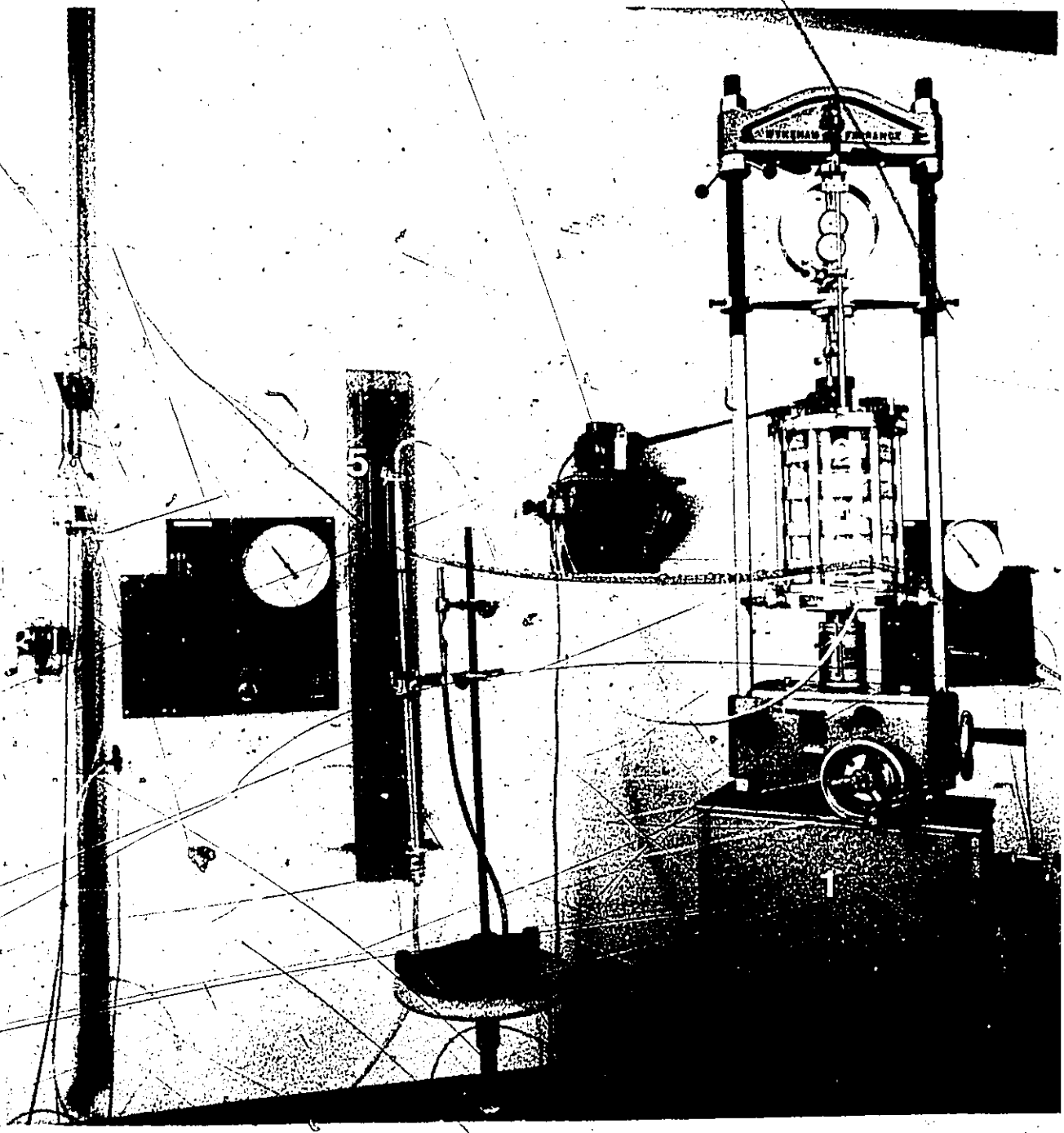

PLATE 3.3 TRIAXIAL TEST SET UP

Figure 3.6 gives a diagrammatic layout of the triaxial compression test set up.

3.5.1 Calibration of Pressure Gauges

The pressure gauges were calibrated by measuring the actual height of columns of water and mercury as suggested by Bishop and Henkel (1962), pages 45-47. A curve showing gauge pressure correction versus gauge pressure was plotted based on results of the calibration test as shown in Fig. 3.7.

The spring constant for the self compensating mercury pot system was found to be 0.56 inches/lb.

For low pressure range a mercury manometer was used for reading the pressure; 5.2 cms of Hg being equal to 1.0 p.s.i.

3.5.2 Calibration of Cell for Expansion

Figure 3.8 gives the calibration for cell expansion, including the volume change of the pressure line. The cell expansion almost ceased entirely after thirty minutes of application of the cell pressure.

The points on the curve denote expansion of the cell after thirty minutes.

Volume change measurements in the triaxial tests were corrected for cell expansion. The ram correction was found to be 7.2 cm^3 per inch of movement of the ram.

3.5.3 Membrane Correction

The amount of correction to be applied to the

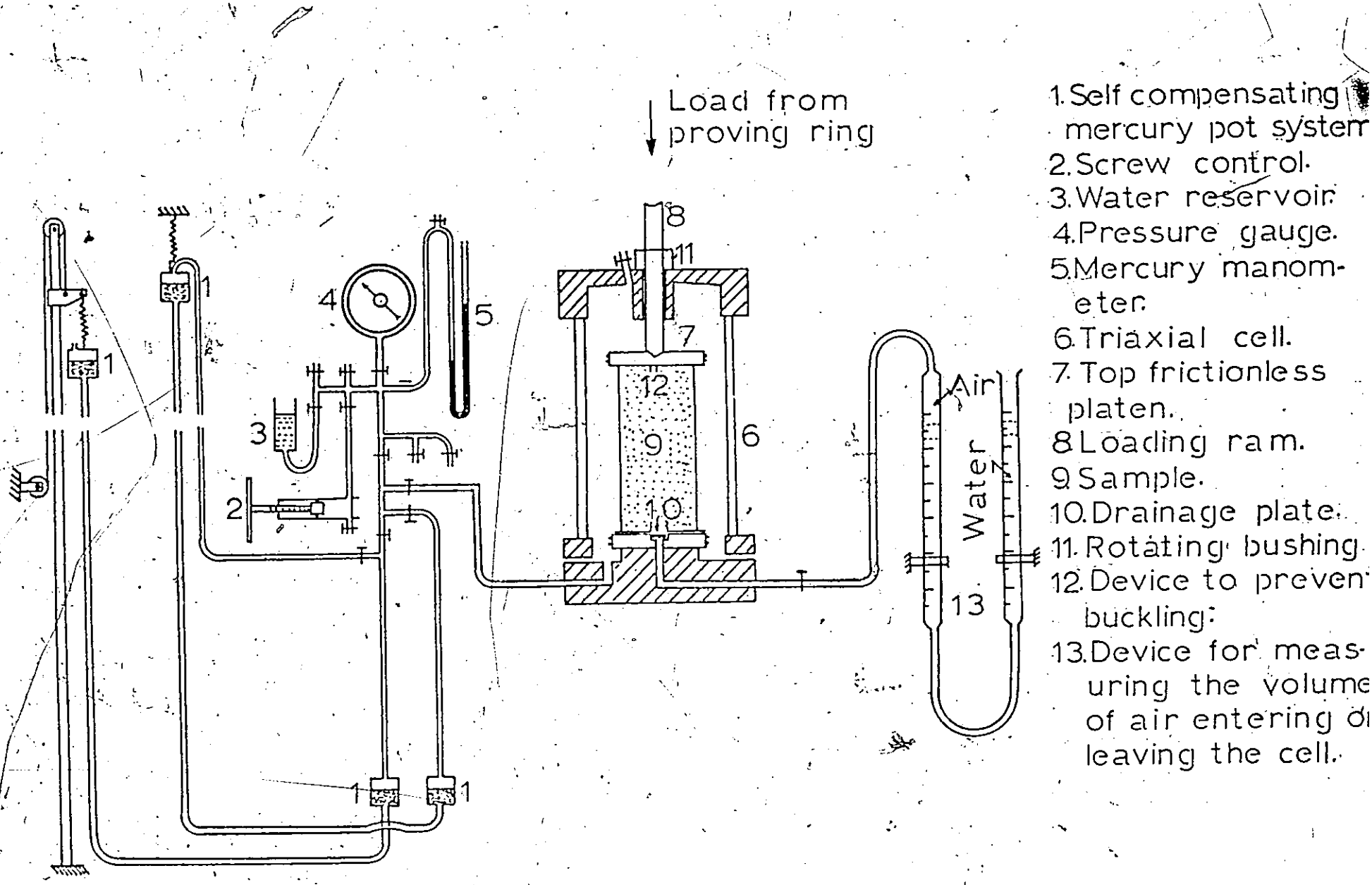

FIG. 3.6 DIAGRAMMATIC LAYOUT OF THE TRIAXIAL TEST SET UP.

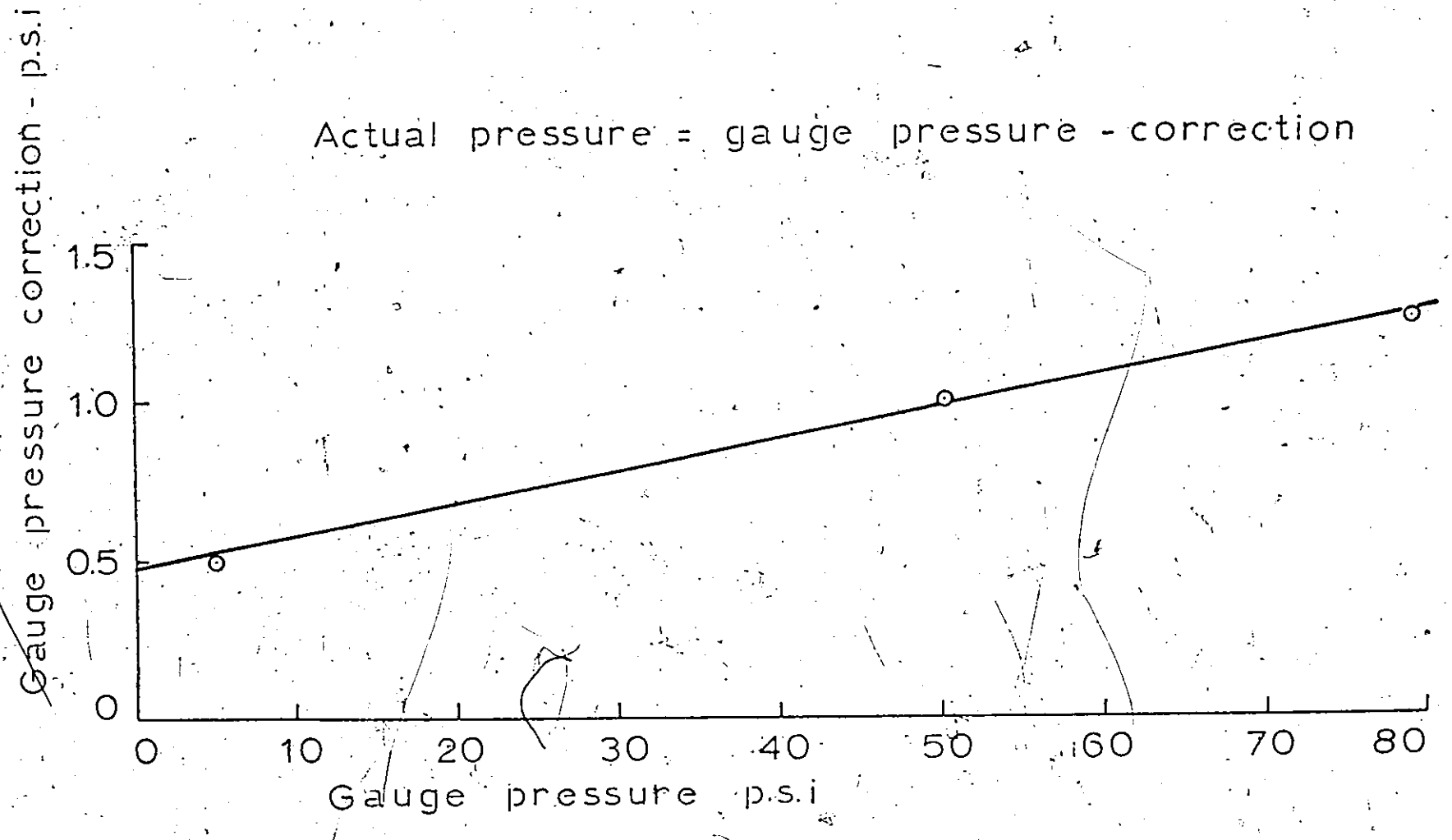

FIG. 3.7 CALIBRATION OF PRESSURE GAUGE.

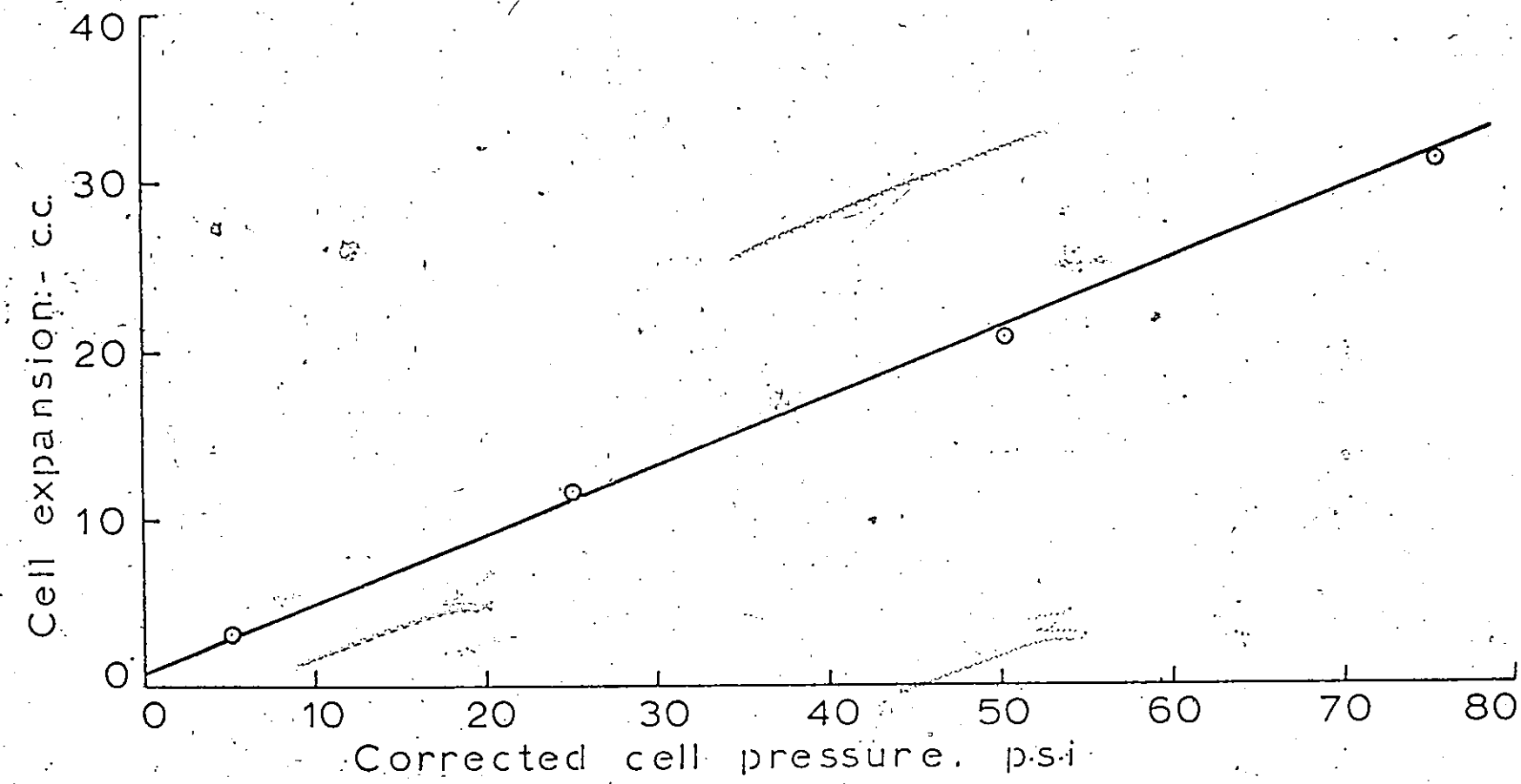

FIG. 3.8 CALIBRATION OF TRIAXIAL CELL FOR EXPANSION.

deviator stress for the 4-inch diameter sample was found to be small and about 0.35 lbs/in.^{2} for a membrane thickness of about 0.012 in.; as determined experimentally using the method suggested by Bishop and Henkel (1962) at 10 percent axial strain.

3.5.4 Correction due to Penetration of Membrane into the Sample

Using the methods suggested by Frydman, Zeitlen and Alpan (1973), the volume changes due to penetration of the membrane into the sample was found to be around 5 cm^3 at a confining pressure of 50 p.s.i. Considering the volume of the sample which was about 1,600 cm^3. This volume change effect was considered negligible and was not taken into account in the analysis.

3.5.5 Elimination of Piston Friction

Piston friction has a pronounced effect on the results of triaxial testing wherever conventional proving rings are used to determine the loads. According to Bishop and Henkel (1962) the simplest satisfactory way of reducing piston friction is provided by a rotating bushing built into the triaxial cell. This was eventually used in this test series.

Efforts were made to read the loads by designing a load transducer fixed on the loading ram and placed inside the cell. Details of this transducer are given in Appendix C.

The load transducer was not used in the long run because the reasons for improper functioning of the load cell could not be ascertained.

Other researchers like Bishop and Green (1965) have measured loads by placing the proving ring inside the cell and therefore eliminated the piston friction entirely.

3.6 Direct Shear Box Test Procedures

Direct shear box tests were performed on 2 in. by 2 in. by 1.5 in. high samples prepared by sand raining device as described in section 3.4.3. These tests were carried out at a strain rate of 0.016 in. per minute. The normal stresses used in these tests were 8, 40, 80 and 120 p.s.i., which roughly corresponded to 5, 25, 50 and 80 p.s.i. of confining pressure in triaxial test as evidenced by Table 4.2-1. Relative densities of 60, 75 and 90% were generally used for these tests.

The type of tests carried out were conventional in nature with the exception that the lifting screws were left in the lowered position (see Appendix D). A 400 lbs capacity proving ring was used to read the shear force.

The value of ϕ for particular tests were determined from the maximum ratio of τ/σ_n expressed as

$$\tan\phi = \tau/\sigma_n$$

where ϕ is the angle of shearing resistance, τ is the shear stress and σ_n is the normal stress.

3.7 Ko Test Procedures

Ko tests were performed on 4 in. diameter and 8 in. high dry samples at relative densities of 90.0, 73.3, 62.4 and 58 percent. The samples were prepared exactly in the same way as in the case of samples for the triaxial compression tests. The initial suction given to the sample was released at about 5 p.s.i. of σ_3.

The rate of axial strain was chosen to be 0.004 in/minute. As the load was applied to the sample, the cell pressure was continuously adjusted to give a zero lateral yield as indicated on the lateral strain indicator. At the start of the test the gauge pressure was set at about 0.5 p.s.i.

The lateral strain indicator used was exactly the same as detailed by Bishop and Henkel (1962) in Part II and Section 4. Plate 3.4 shows the sample with lateral strain indicator.

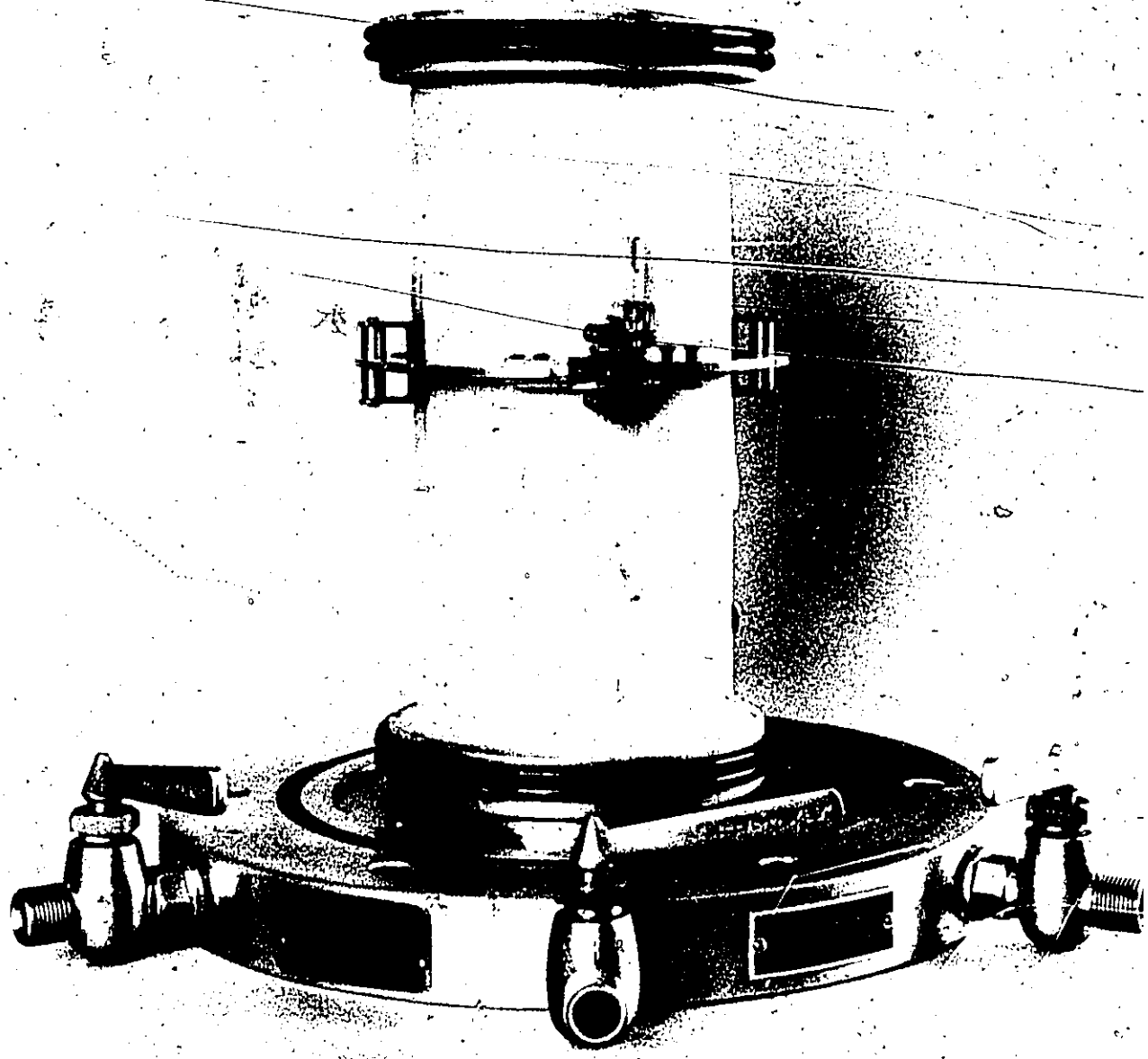

PLATE 3.4 (4 inch x 8 inch) SAMPLE WITH LATERAL STRAIN INDICATOR

CHAPTER 4

EXPERIMENTAL TEST RESULTS

4.1 General

The test results for consolidated drained tri-axial compression tests on sand conducted on 4 inch diameter by 8 inch high samples having free ends are presented in the form of customary stress-strain curves. The results are also presented in tabular form. The table includes the pertinent information like method of preparation of the samples, relative-density, confining pressure, deviator stress, major principal stress, the stress ratio, the strain at failure, the void ratio, the porosity, the volumetric strain at failure, the angle of internal friction, the normal stress and the shear stress at failure.

For the direct shear box tests, shear stress and ratio of shear stress to normal stress versus shear displacement plots were drawn. The variation of volumetric strain was also shown on the plots. The results were also presented in the tabular form. The tabulated results included information on the relative density, the void ratio, the porosity, the normal stress, the corrected normal stress at failure, the maximum shear force, the shear stress, the ratio of shear stress to normal stress, the shear displacement, the volumetric strain at failure, the angle of shearing resistance, etc.

The Ko-tests were also presented in the conventional form that is the major principal stress was plotted against the minor principal stress. Individual tests are presented.

4.2 Consolidated-Drained Triaxial Compression Tests

These tests were conducted on samples isotropically consolidated at the required confining pressure. The initial relative densities and void ratios of the sample are the relative densities and void ratios at the end of the consolidation on application of the confining pressure. The deviator stress was applied to the sample half an hour after the application of the confining pressure so as to allow time for the cell to expand and reach a state where further expansion of the cell with time was negligible. A strain rate of 0.015 inch per minute was adopted as explained in Chapter 3 under Section 3.5.

All the tests conducted were drained tests. Either the maximum deviator stress or the maximum stress ratio could be considered as the failure criterion because they yielded the same results for drained tests on sand. The maximum deviator stress was used as the failure criterion because this yielded a more pronounced peak value and is also the most common approach adopted by other researchers and therefore simplified the comparison with other works.

In Fig. 4.2.1 to 4.2.4, typical results are shown of the consolidated-drained triaxial compression tests, subsequently referred to as triaxial tests only, for very dense sand samples. In Fig. 4.2.1 the sand sample had an initial relative density of 92.4 per cent and a corresponding initial void ratio of 0.65. The samples, the results of which are shown in Figs. 4.2.2 to 4.2.4, had relative densities of 92.6 per cent, 92.9 per cent and 94.7 per cent, respectively. The corresponding void ratios were 0.65, 0.65 and 0.64. The confining pressures for the tests shown in Figs. 4.2.1 to 4.2.4 were 5, 25, 50 and 80 psi respectively.

Figures 4.2.5 to 4.2.8 show the stress-strain curves for the dense sand samples. The relative density was 70.7 per cent, 70.4 per cent, 73.3 per cent and 75.3 per cent, respectively. The corresponding void ratios were 0.77, 0.77, 0.75 and 0.74. The tests were run at confining pressures of 5, 25, 50 and 80 psi, respectively.

Figures 4.2.9 to 4.2.12 have been drawn for the medium dense sand samples.

Figure 4.2.13 shows the variation of deviator stress with strain for various confining pressure and exhibits the general nature of the stress-strain curves for triaxial tests.

Table 4.2.1 summarizes the results of all triaxial tests on the sand.

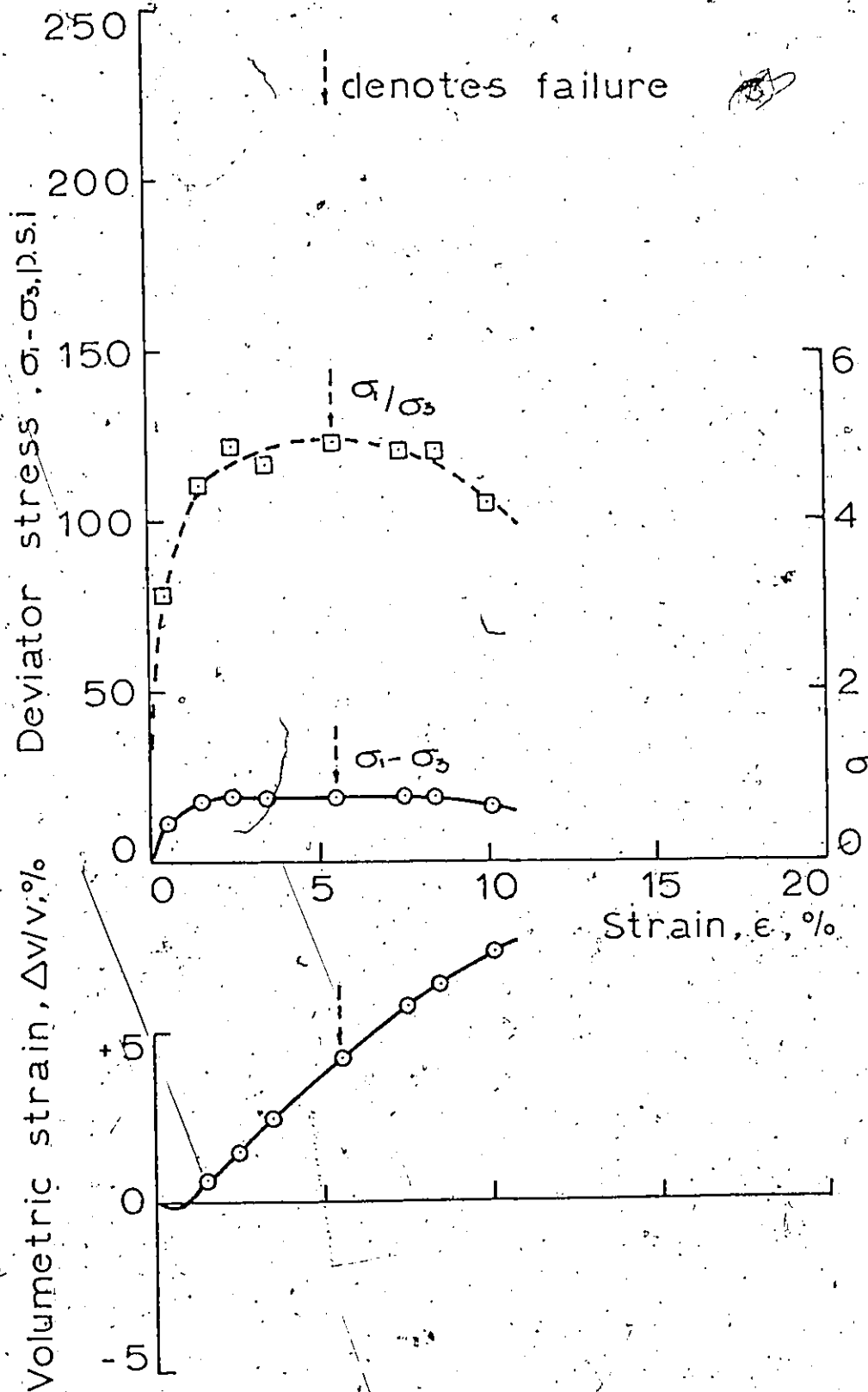

FIG. 4.2.1 STRESS-STRAIN RELATIONSHIP FOR VERY DENSE SAND IN DRAINED TRIAXIAL COMPRESSION AT A CONFINING PRESSURE OF 5 p.s.i.

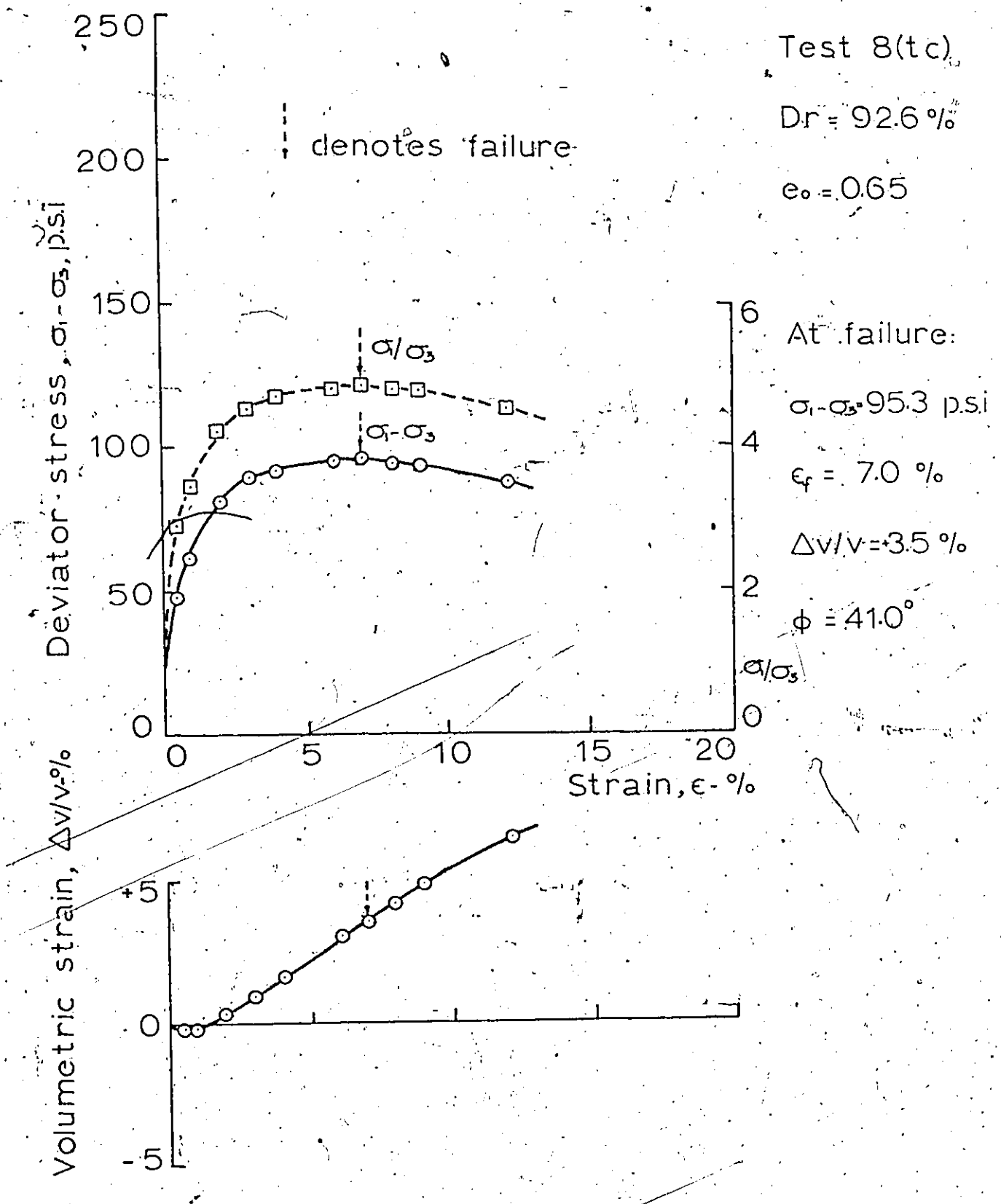

FIG. 4.2.2 STRESS-STRAIN RELATIONSHIP FOR VERY DENSE SAND IN TRIAXIAL COMPRESSION AT A CONFINING PRESSURE OF 25 p.s.i.

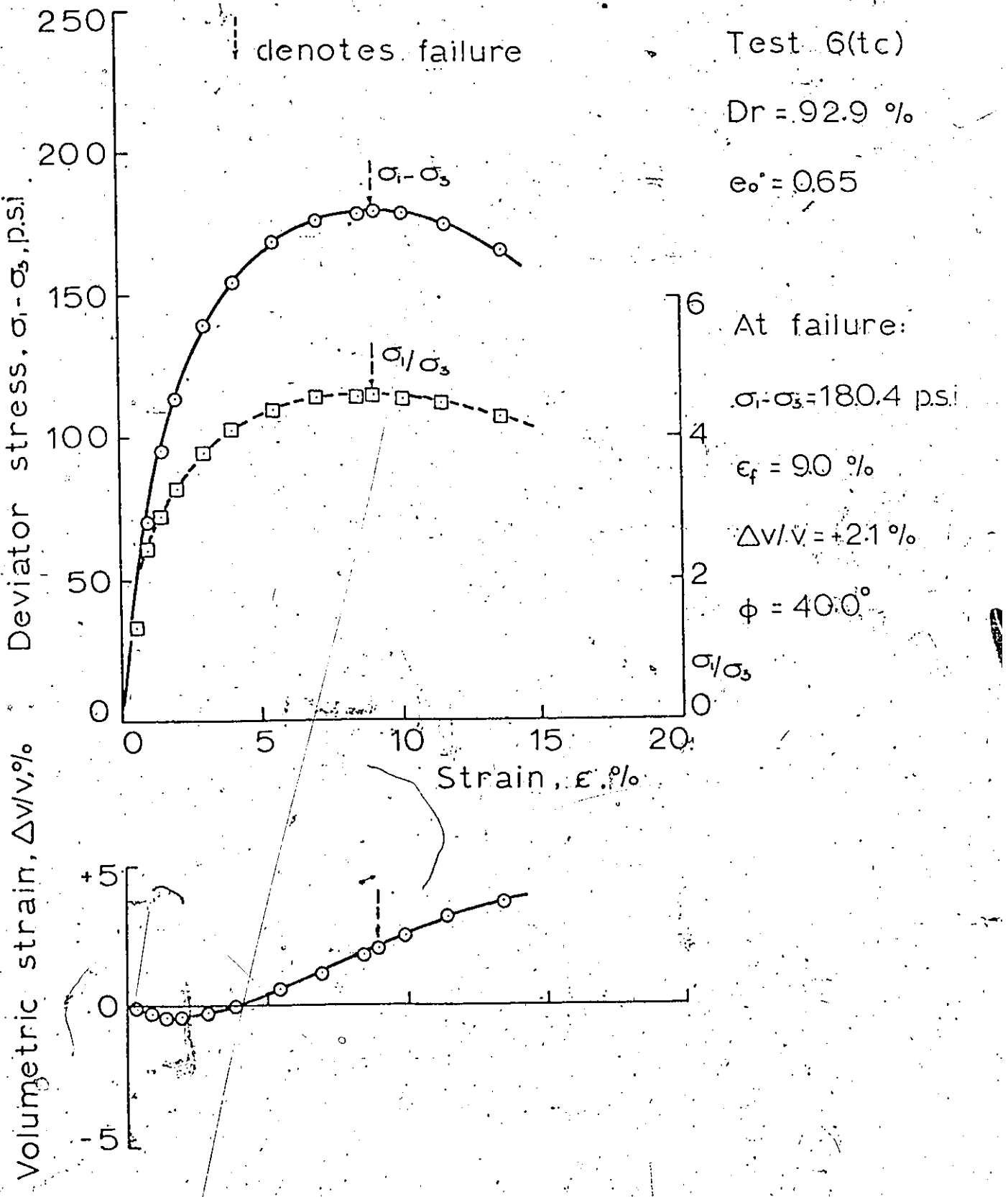

FIG. 4.2.3 STRESS-STRAIN RELATIONSHIP FOR VERY DENSE SAND IN TRIAXIAL COMPRESSION AT A CONFINING PRESSURE OF 50 p.s.i.

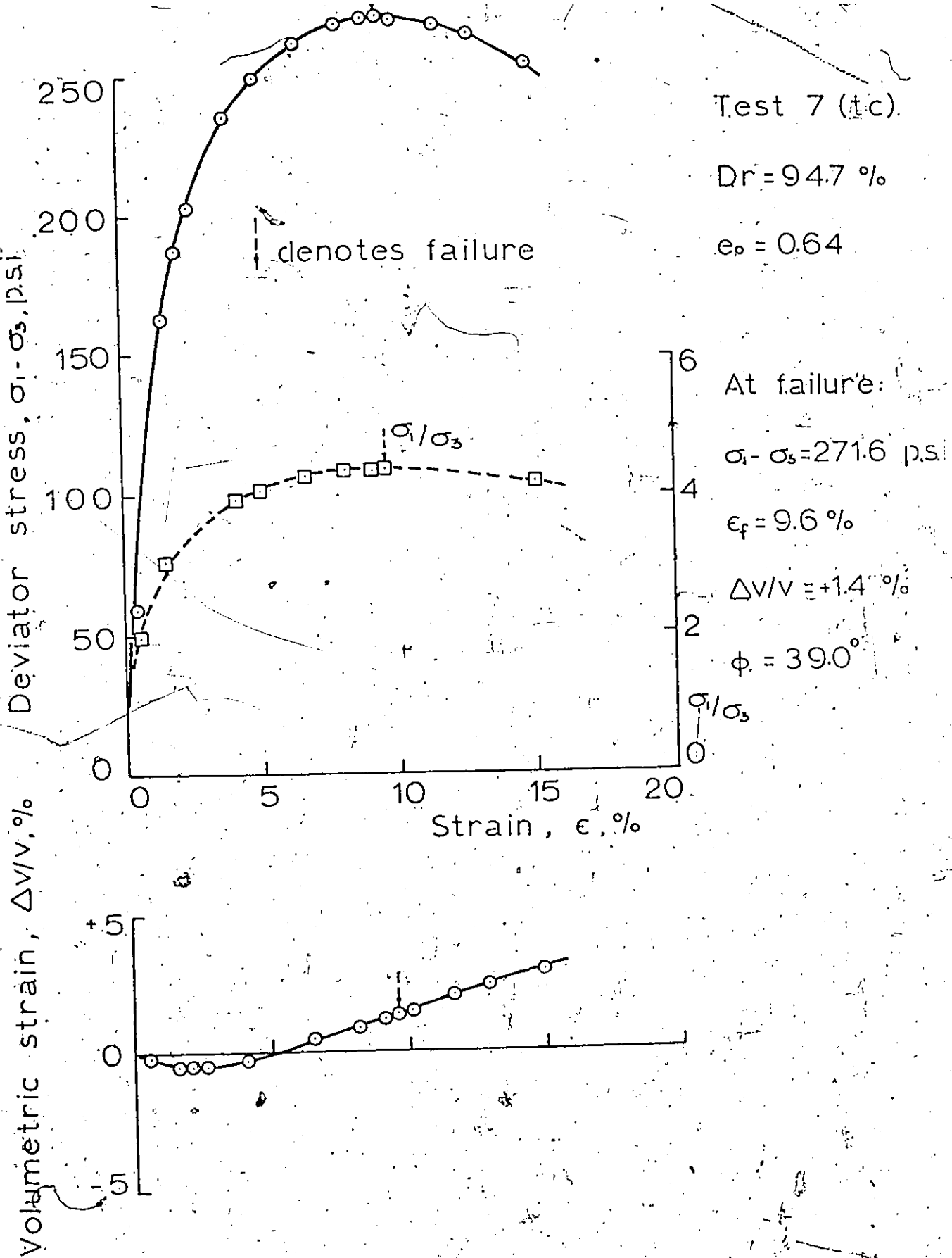

FIG. 4.2.4 STRESS-STRAIN RELATIONSHIP FOR VERY DENSE SAND IN TRIAXIAL COMPRESSION AT A CONFINING PRESSURE OF 80 p.s.i.

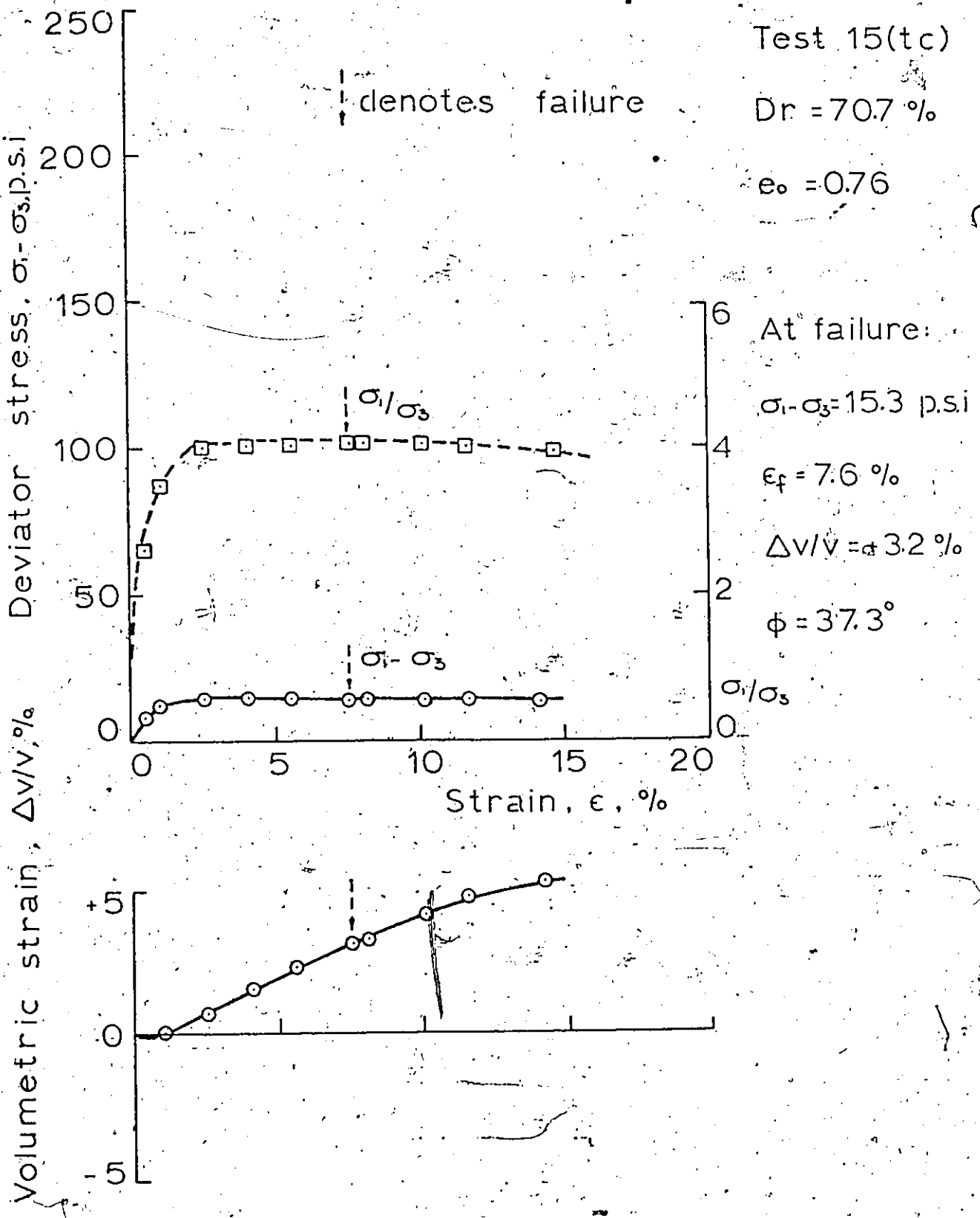

FIG. 4.2.5 STRESS-STRAIN RELATIONSHIP FOR DENSE SAND IN TRIAXIAL COMPRESSION AT A CONFINING PRESSURE OF 5 p.s.i.

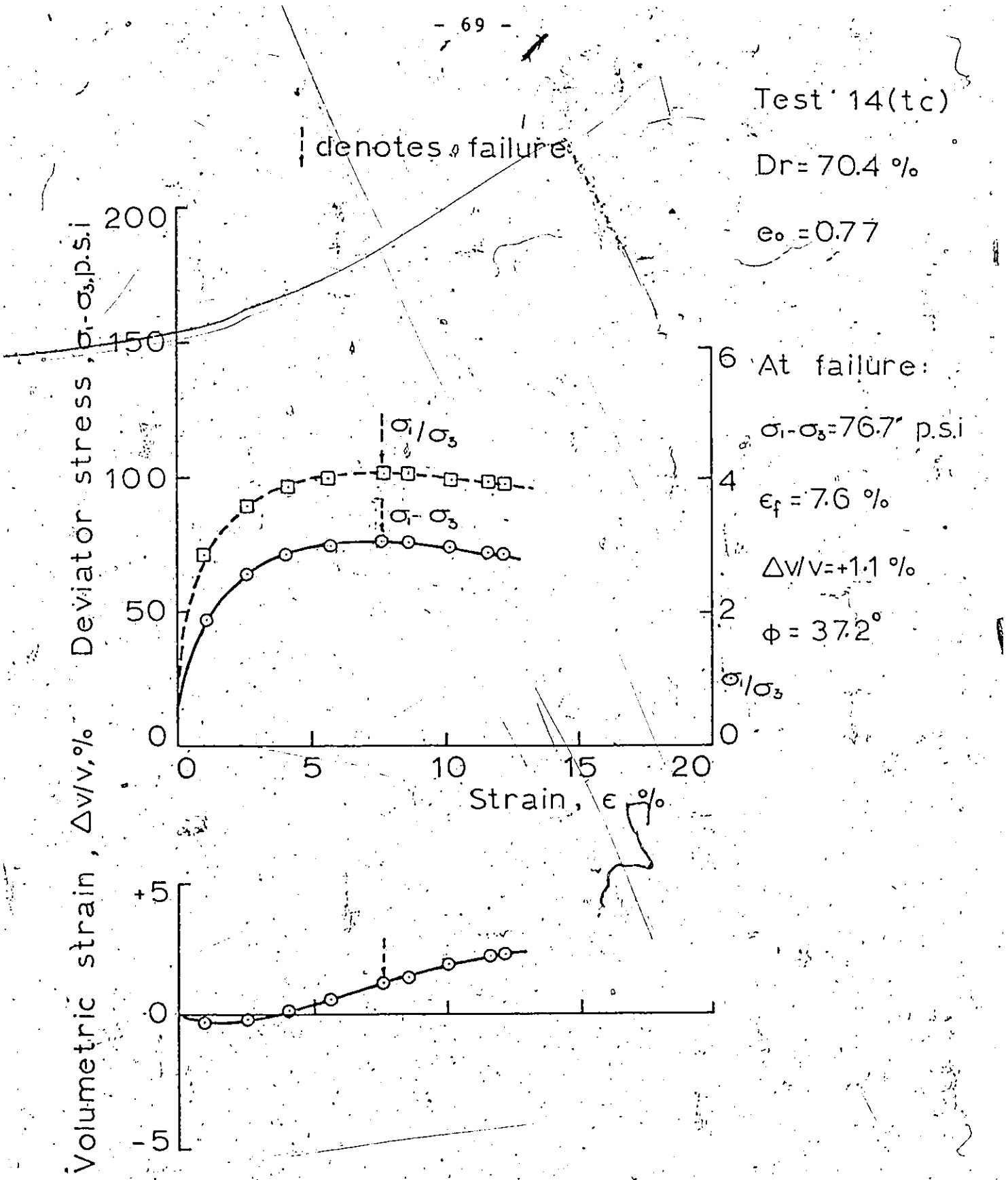

FIG. 4.2.6 STRESS-STRAIN RELATIONSHIP FOR DENSE SAND IN TRIAXIAL COMPRESSION AT A CONFINING PRESSURE OF 25 p.s.i.

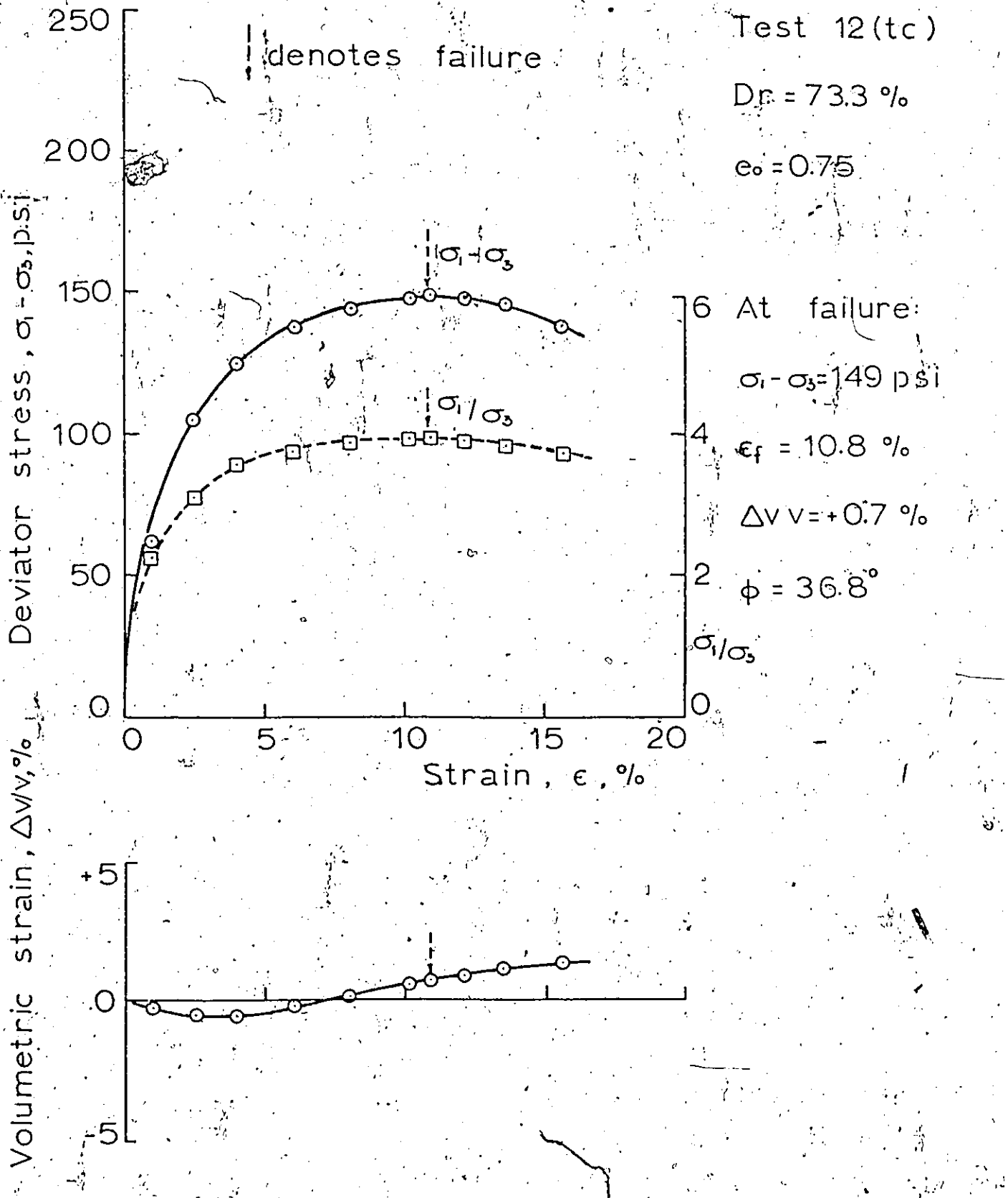

FIG. 4.2.7 STRESS-STRAIN RELATIONSHIP FOR DENSE SAND IN TRIAXIAL COMPRESSION AT A CONFINING PRESSURE OF 50 p.s.i.

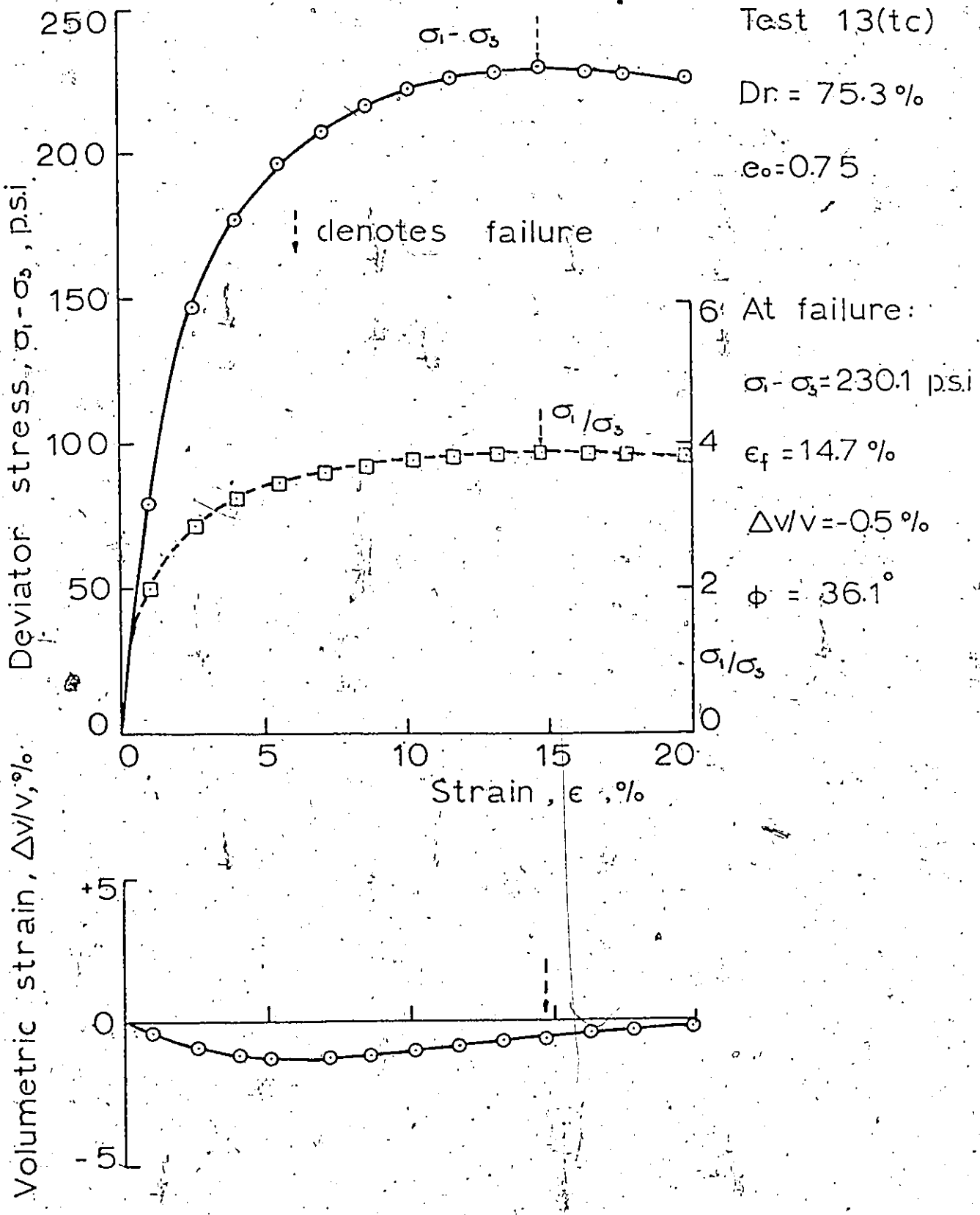

FIG. 4.2.8 STRESS-STRAIN RELATIONSHIP FOR DENSE SAND IN TRIAXIAL COMPRESSION AT A CONFINING PRESSURE OF 80 p.s.i.

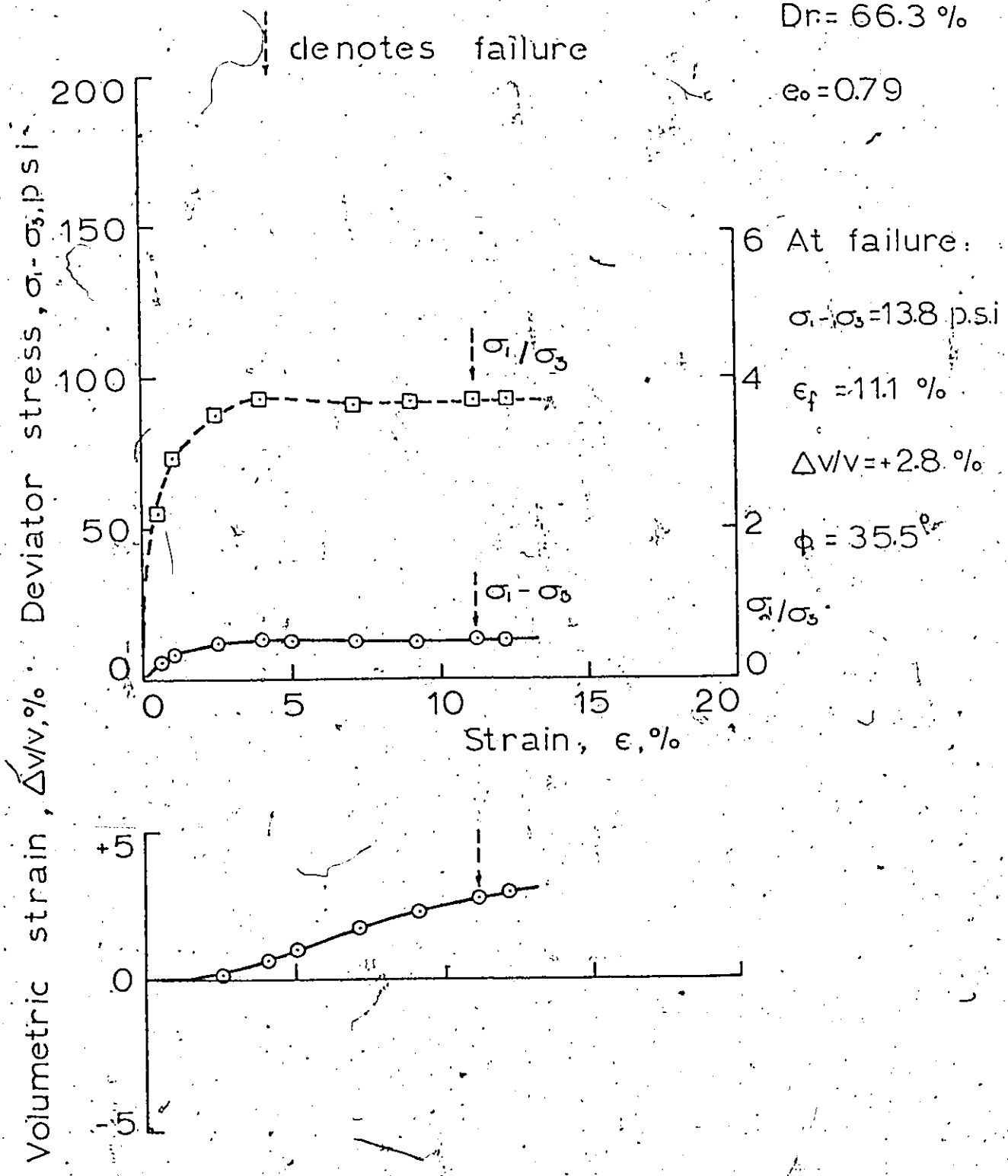

FIG. 4.2.9 STRESS-STRAIN RELATIONSHIP FOR MEDIUM DENSE SAND IN TRIAXIAL COMPRESSION AT A CONFINING PRESSURE OF 5 p.s.i.

Test 21(tc)

Dr. = 57.0 %

e_o = 0.84

At failure:

$\sigma_1 - \sigma_3$ = 67.9 p.s.i

ϵ_f = 13.2 %

$\Delta v.v$ = +0.4 %

ϕ = 35.2°

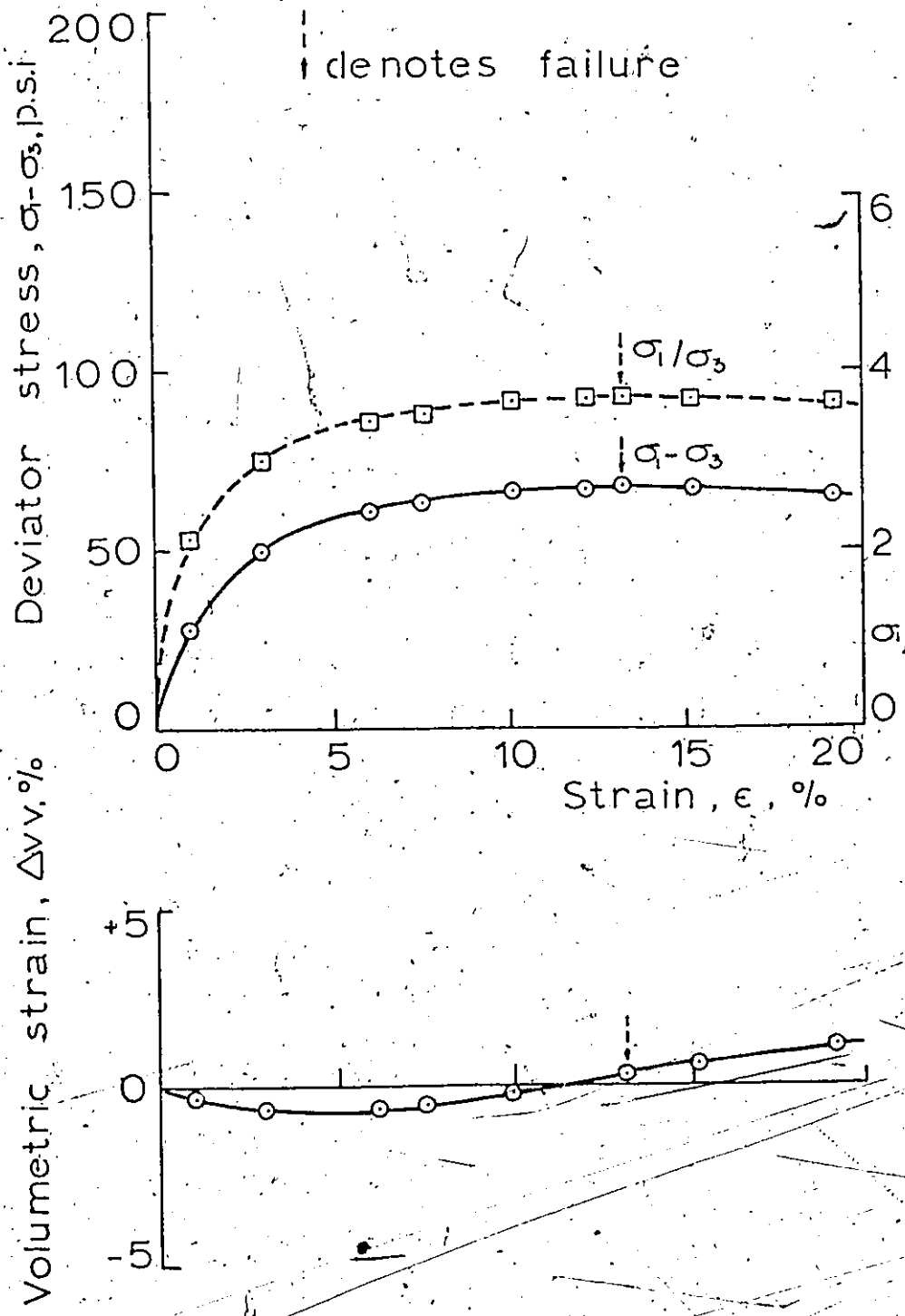

FIG. 4.2.10 STRESS-STRAIN RELATIONSHIP FOR MEDIUM DENSE SAND IN TRIAXIAL COMPRESSION AT A CONFINING PRESSURE OF 25 p.s.i.

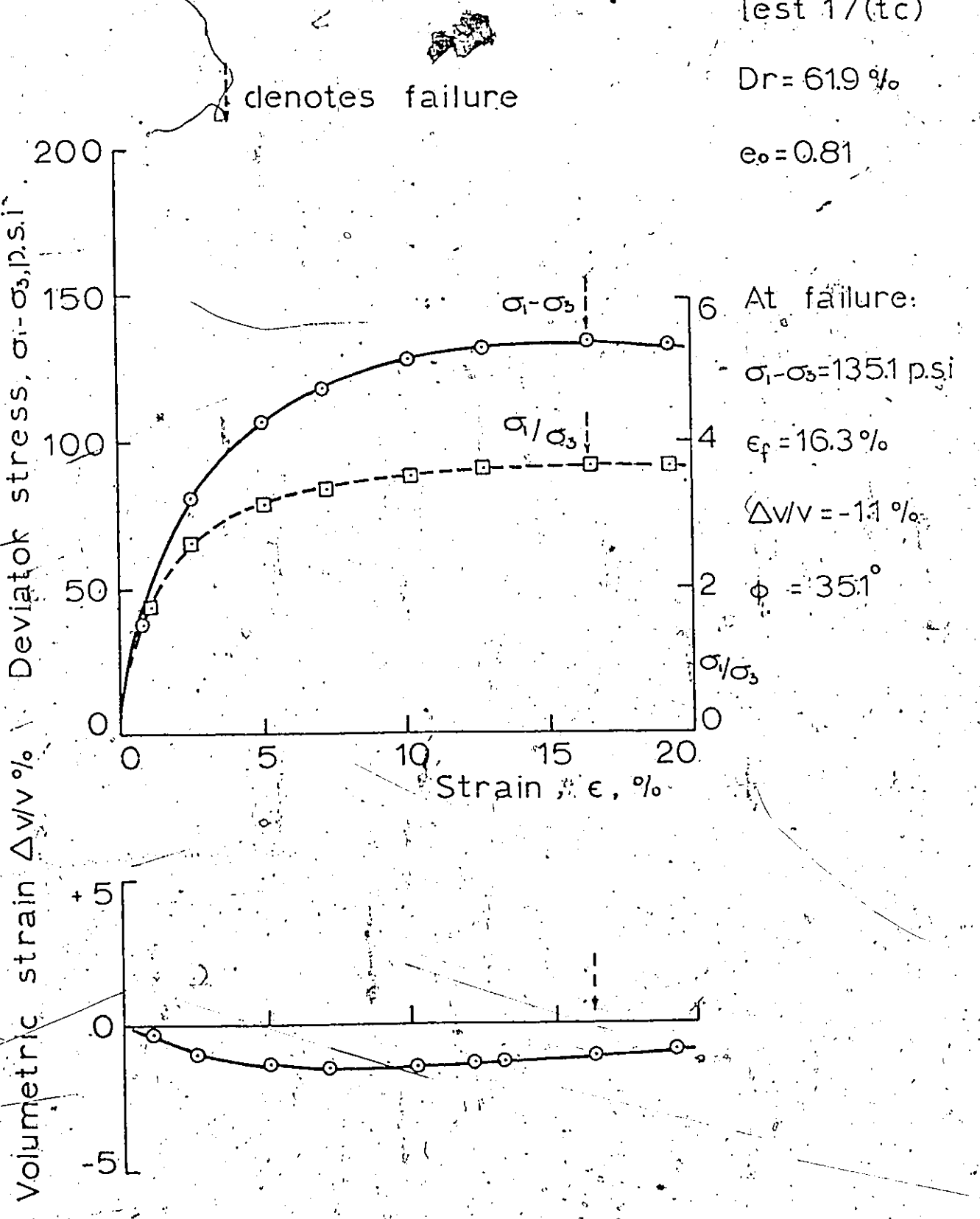

FIG. 4.2.11 STRESS-STRAIN RELATIONSHIP FOR MEDIUM DENSE SAND IN TRIAXIAL COMPRESSION AT A CONFINING PRESSURE OF 50 p.s.i.

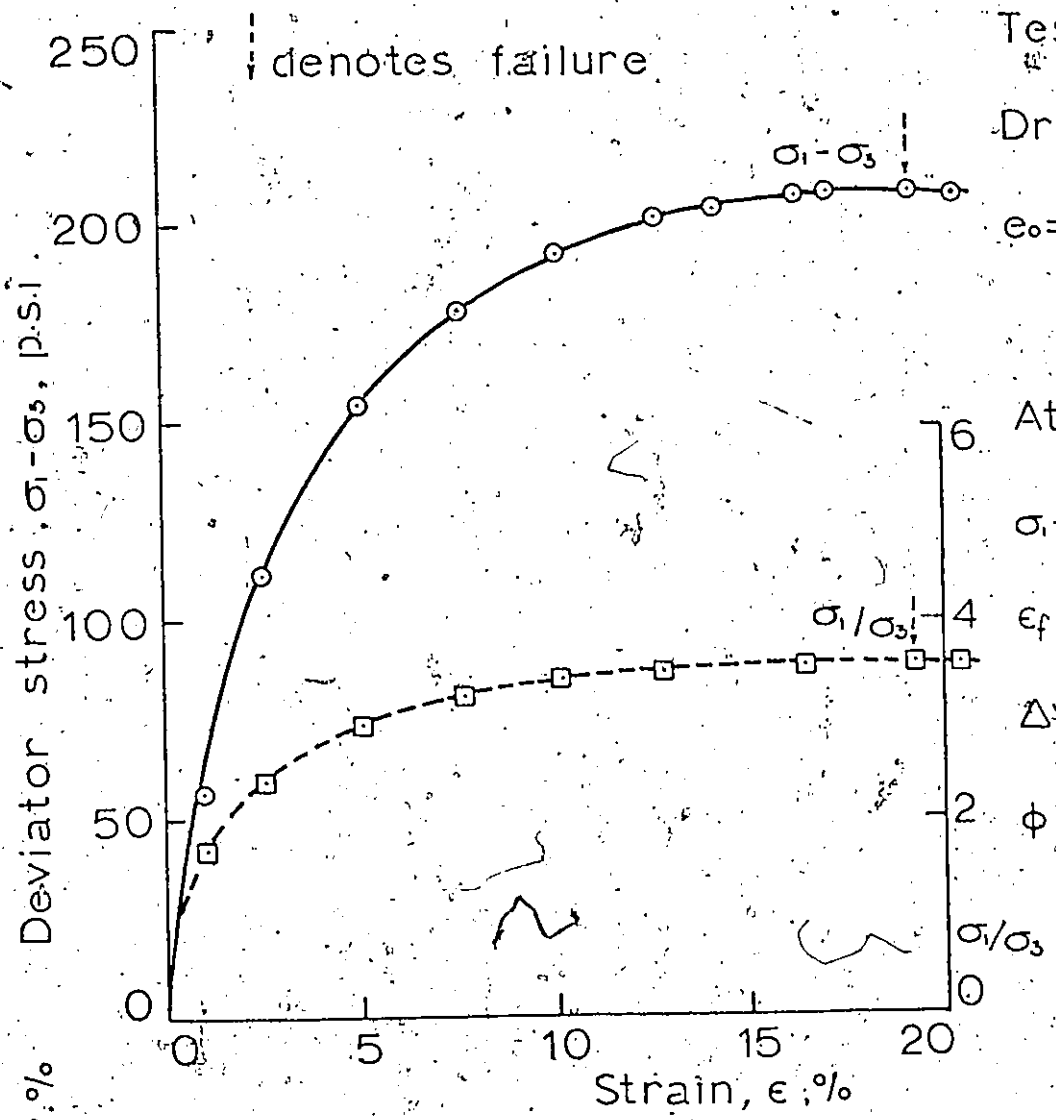

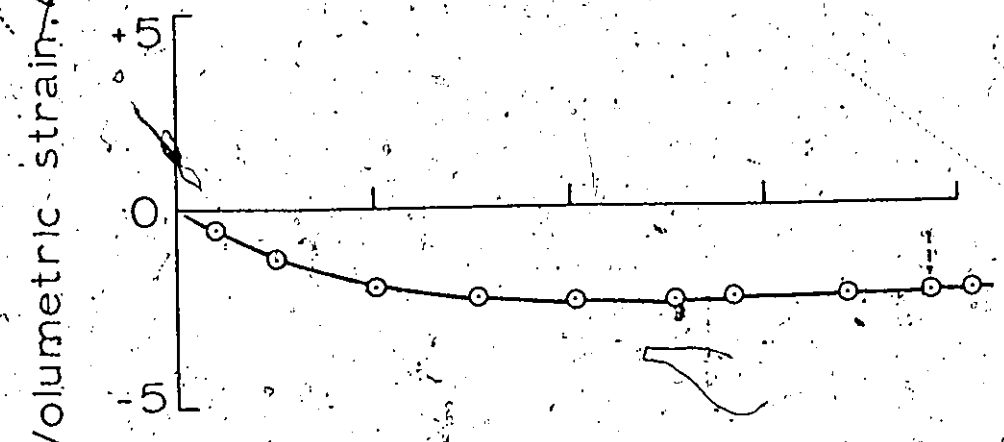

FIG. 4.2.12 STRESS-STRAIN RELATIONSHIP FOR MEDIUM DENSE SAND IN TRIAXIAL COMPRESSION AT A CONFINING PRESSURE OF 80 p.s.i.

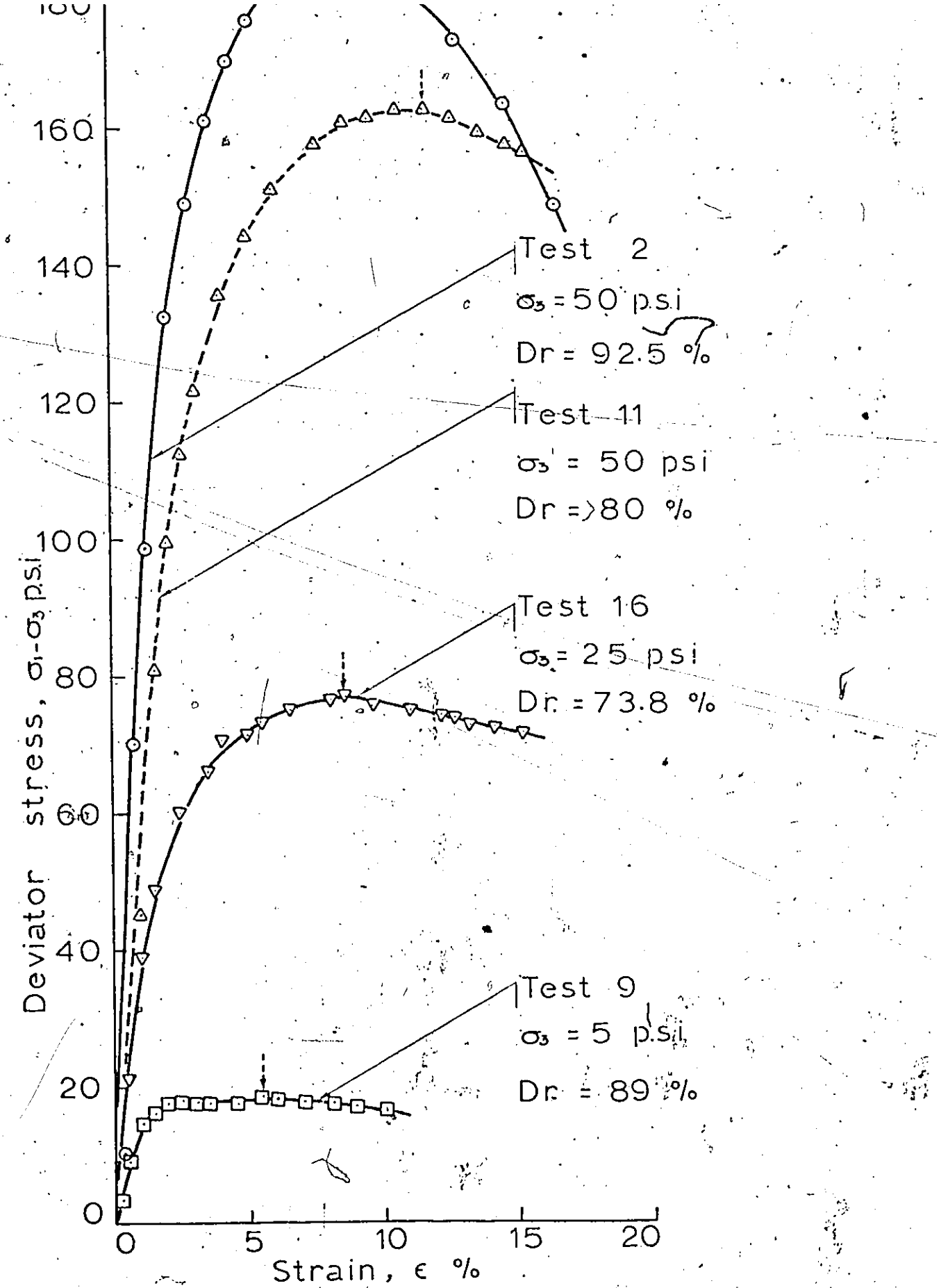

FIG. 4.2.13 STRESS-STRAIN CURVES FOR TRIAXIAL COMPRESSION TESTS

Test #	Method of sample Propara.	D_r %	σ_3 psi	$\sigma_1-\sigma_3$ psi	σ_1 psi	σ_1/σ_3	ϵ_f %	e_o	n	$(\frac{\Delta v}{v})_f$ %	ϕ Degrees	σ_n psi	τ_f psi	Remarks
1	SR*	93.0	22.2	83.5	105.7	4.78	4.7	0.65	0.39	+1.3	40.8	36.7	31.6	Test I conducted
2	SR	92.5	50	184.7	234.7	4.70	7.8	0.65	0.39	+1.7	40.5	83.5	70.1	at constant p=50
3	HM**	88.9	50	163.4	213.4	4.27	6.3				38.3			$\sigma_n=\frac{\sigma_1+\sigma_3}{2}$
4	HM	92.7	50	174.2	224.2	4.48	8.3				39.4			$-(\frac{\sigma_1-\sigma_3}{2})\sin\phi$
5	HM	92.0	50	174.4	224.4	4.49	7.0				39.4			$\tau_f=(\frac{\sigma_1-\sigma_3}{2})\cos\phi$
6	SR	92.9	50	180.4	230.4	4.61	9.6	0.65	0.39	+2.1	40.0	82.2	69.1	
7	SR	94.7	80	271.6	351.6	4.40	9.6	0.64	0.39	+1.4	39.0	130.4	105.6	
8	SR	92.6	25	95.3	120.3	4.81	7.0	0.65	0.39	+3.5	41.0	41.3	35.2	
9	SR	89.0	5	18.3	23.3	4.66	5.5	0.67	0.40	+3.4	40.3	9.0	7.0	
10	SR	92.4	5	19.6	24.6	4.92	5.5	0.65	0.39	+4.2	41.5	8.3	7.3	

*SR = Sand raining method

**HM = Hand-compacted method

(Continued)

TABLE 4.2.1

SUMMARY OF RESULTS OF THE DRAINED TRIAXIAL COMPRESSION TEST.

Test #	Method of sample Prepara.	D_r %	σ_3 psi	$\sigma_1-\sigma_3$ psi	σ_1 psi	σ_1/σ_3	ε_f %	e_o	n	$(\frac{\Delta v}{V})_f$ %	ϕ Degrees	σ_n psi	τ_f psi	Remarks
11	SR	79.8	50	162.7	212.7	4.26	11.6	0.72	0.417	+1.84	38.2	81.2	64.0	dense
12	SR	73.2	50	149.1	199.1	3.98	10.8	0.75	0.429	+0.67	36.8	79.2	59.0	sand
13	SR	75.3	80	230.1	310.1	3.88	14.7	0.75	0.428	-0.56	36.2	127.1	93.0	
14	SR	70.4	25	76.7	101.7	4.06	7.6	0.77	0.433	+1.13	37.3	40.2	30.5	
15	SR	70.7	5	15.3	20.3	4.06	7.6	0.76	0.432	+3.19	37.3	8.0	6.1	
16	SR	73.8	25	76.9	101.9	4.08	8.6	0.75	0.428	+1.42	37.3	40.2	30.6	
17	SR	61.9	50	135.1	185.1	3.70	16.3	0.81	0.448	-1.6	35.1	78.7	55.3	medium
18	SR	64.5	80	209.8	289.8	3.62	19.3	0.80	0.443	-2.2	34.5	125.5	86.4	dense sand
20	SR	66.3	5	13.75	18.7	3.76	11.1	0.80	0.444	+2.79	35.5	7.9	5.7	
21	SR	57.0	25	67.9	92.9	3.72	13.2	0.84	0.455	+0.37	35.2	39.4	27.8	
23	SR	54.7	5	13.40	18.4	3.68	14.7	0.85	0.459	+2.07	34.9	7.9	5.5	

TABLE 4.2.1 (contd. from previous page)

4.3 Direct Shear Box Tests

Direct shear box tests were conducted on 2 inch by 2 inch by approximately 1.5 inch high samples. The rate of shear displacement was chosen as 0.016 inch per minute. This rate of strain was compatible with the rate for the triaxial tests.

Figures 4.3.1 to 4.3.4 represent plots of shear displacement in inches versus shear stress, ratio of shear to normal stress and volumetric strain per cent for the direct shear box tests carried out on very dense sand samples.

These tests were run at normal stresses of 8, 40, 80 and 109.5 psi. The corresponding void ratios were 0.64, 0.67, 0.65 and 0.65 respectively.

Figures 4.3.5 to 4.3.8 represent similar graphs for the direct shear box tests carried out on dense sand specimens.

These tests were carried out at normal stresses of 8, 40, 80 and 109.5 psi. The corresponding void ratios were 0.70, 0.74, 0.72 and 0.75.

Tests for medium dense sand samples are given in Figs. 4.3.9 to 4.3.12.

These tests were also carried out at normal stresses of 8, 40, 80 and 109.5 psi. The corresponding void ratios were 0.78, 0.81, 0.79 and 0.79.

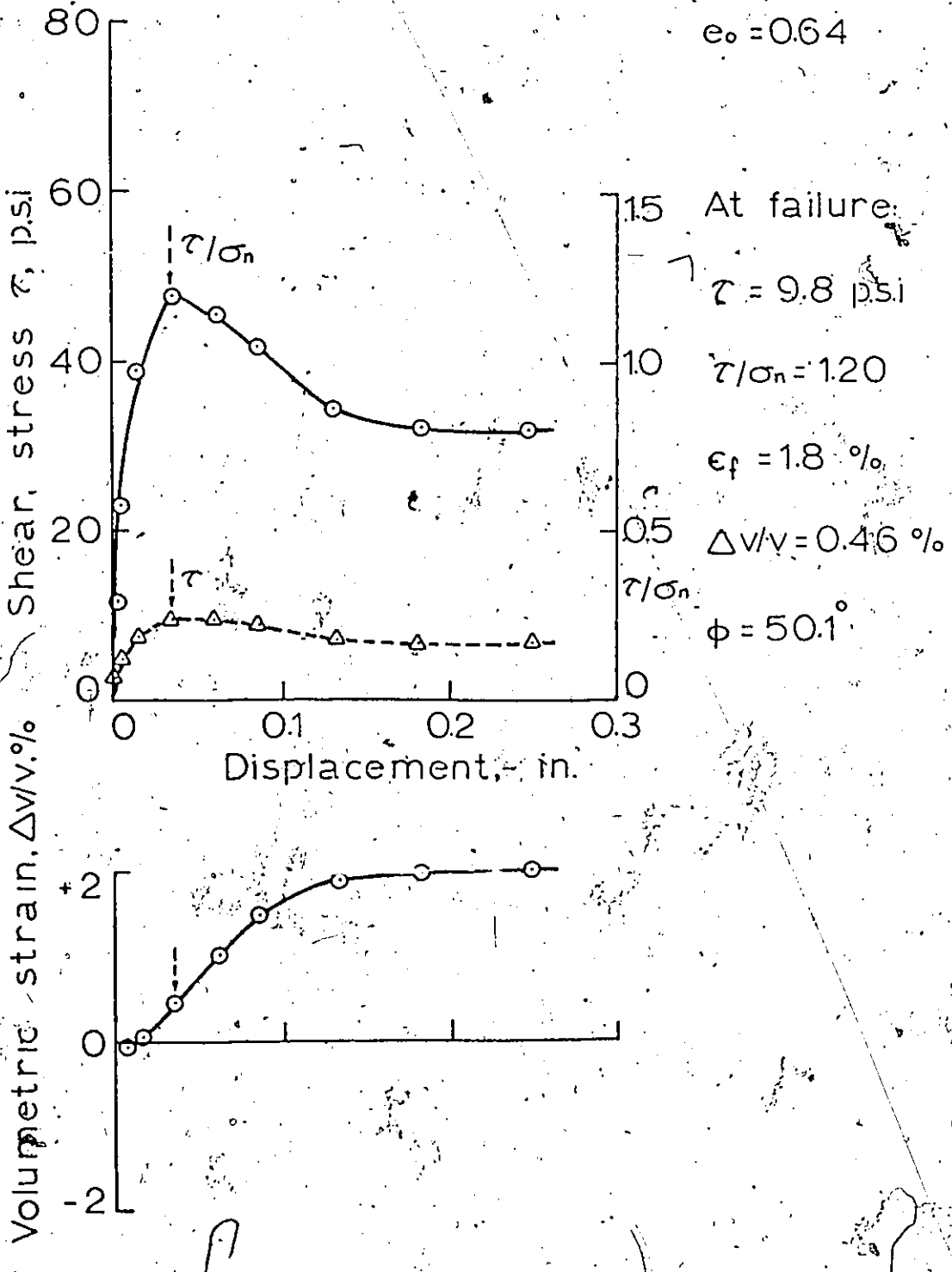

FIG. 4.1.1 RELATIONSHIP BETWEEN STRESS AND SHEAR DISPLACEMENT FOR VERY DENSE SAND IN DIRECT SHEAR FOR AN APPLIED NORMAL STRESS OF 8 p.s.i.

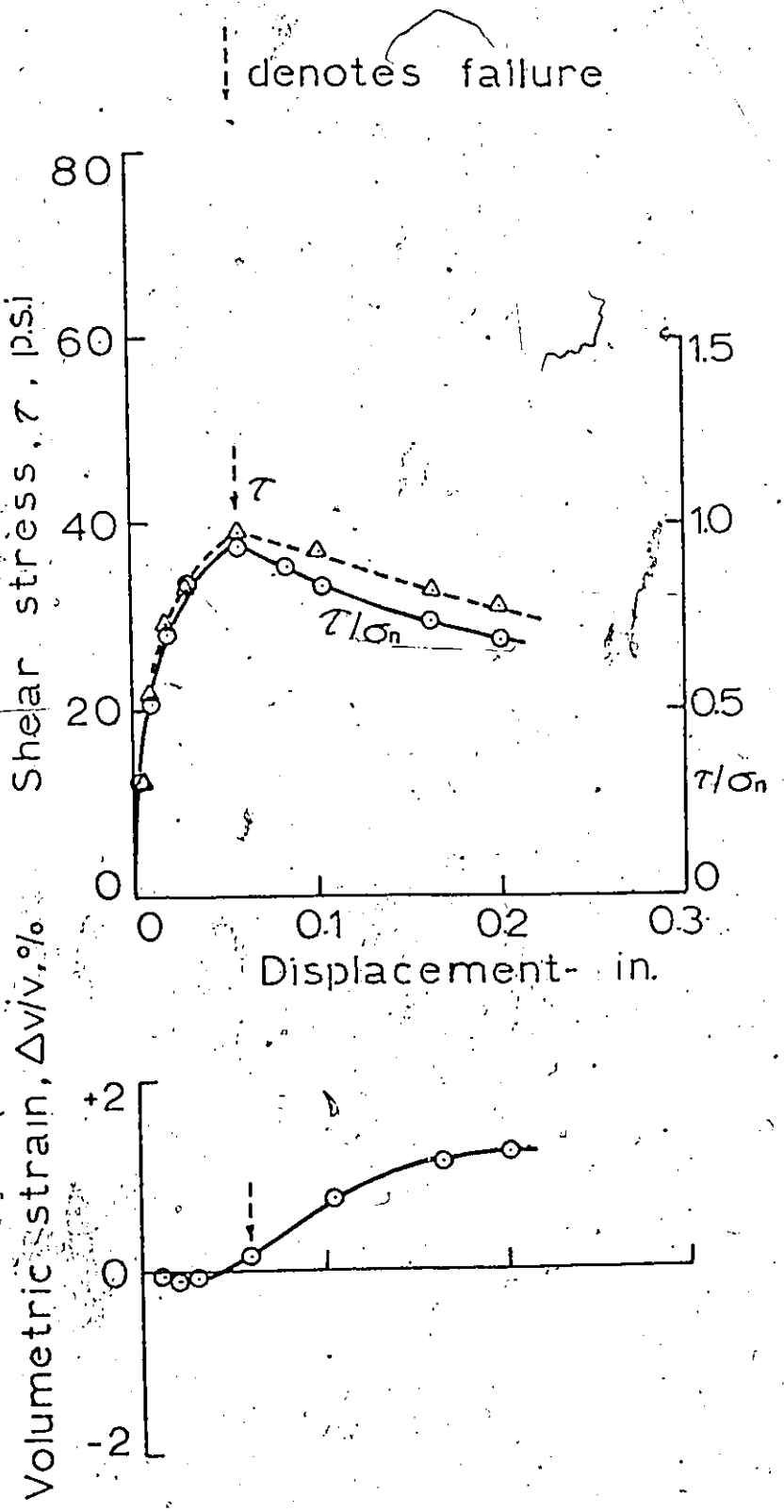

FIG. 4.3.2 STRESS-VERSUS SHEAR DISPLACEMENT FOR VERY DENSE SAND IN DIRECT SHEAR FOR AN APPLIED NORMAL STRESS OF 40 p.s.i.

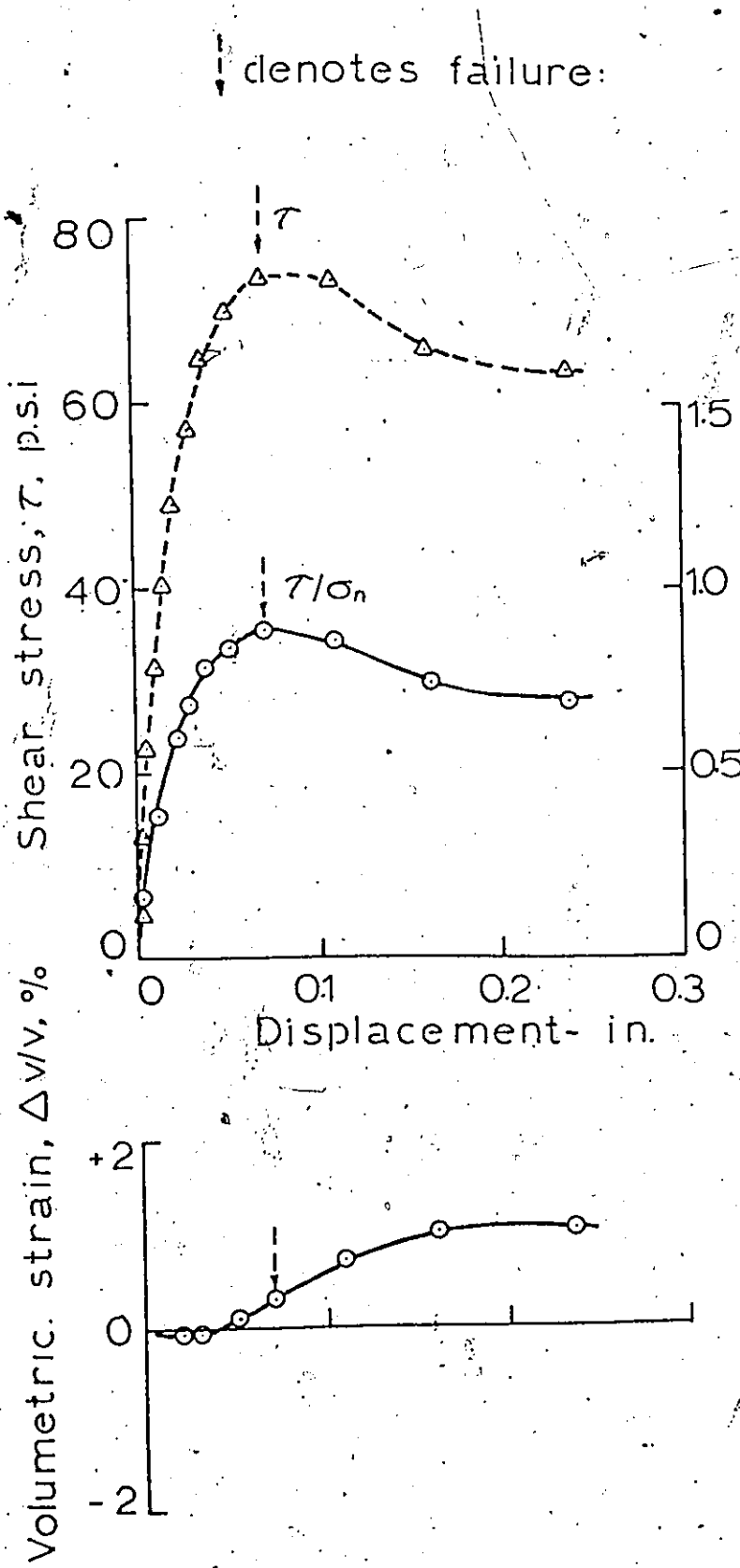

FIG. 4.3.3 STRESS-SHEAR DISPLACEMENT FOR VERY DENSE SAND IN DIRECT SHEAR FOR AN APPLIED NORMAL STRESS OF 80 p.s.i.

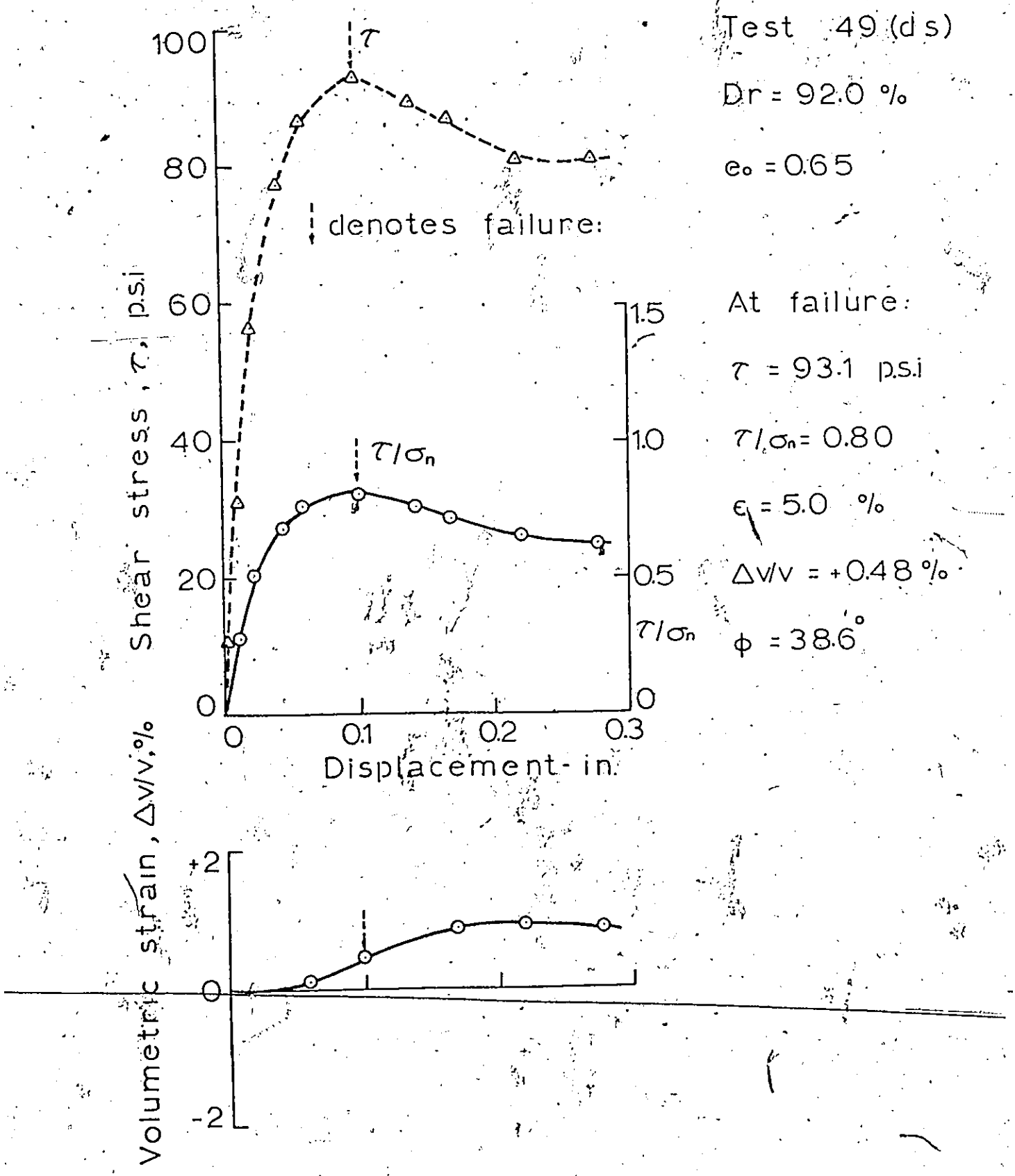

FIG. 4.3.4 STRESS-SHEAR DISPLACEMENT RELATIONSHIP FOR VERY DENSE SAND IN DIRECT SHEAR FOR AN APPLIED NORMAL STRESS OF 109.5 p.s.i.

Test 39(d,s)

Dr. = 83.2 %

e_o = 0.70

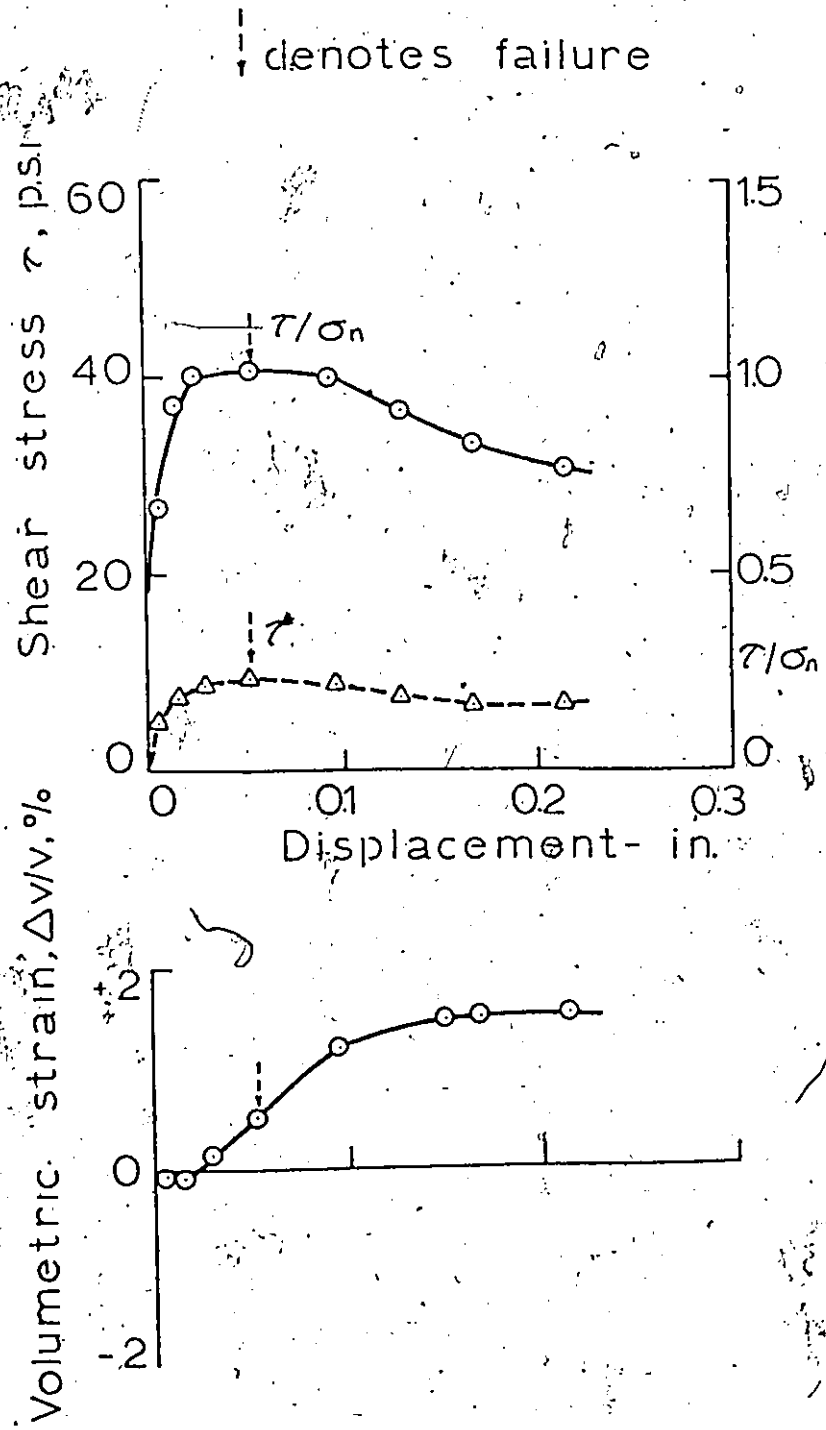

At failure:

τ = 9.4 p.s.i

τ/σ_n = 1.14

ϵ = 2.65 %

$\Delta v/v$ = +0.56

ϕ = 48.7°

FIG. 4.3.5 STRESS-DISPLACEMENT RELATIONSHIP FOR DENSE SAND IN DIRECT SHEAR AT AN APPLIED NORMAL STRESS OF 8 p.s.i.

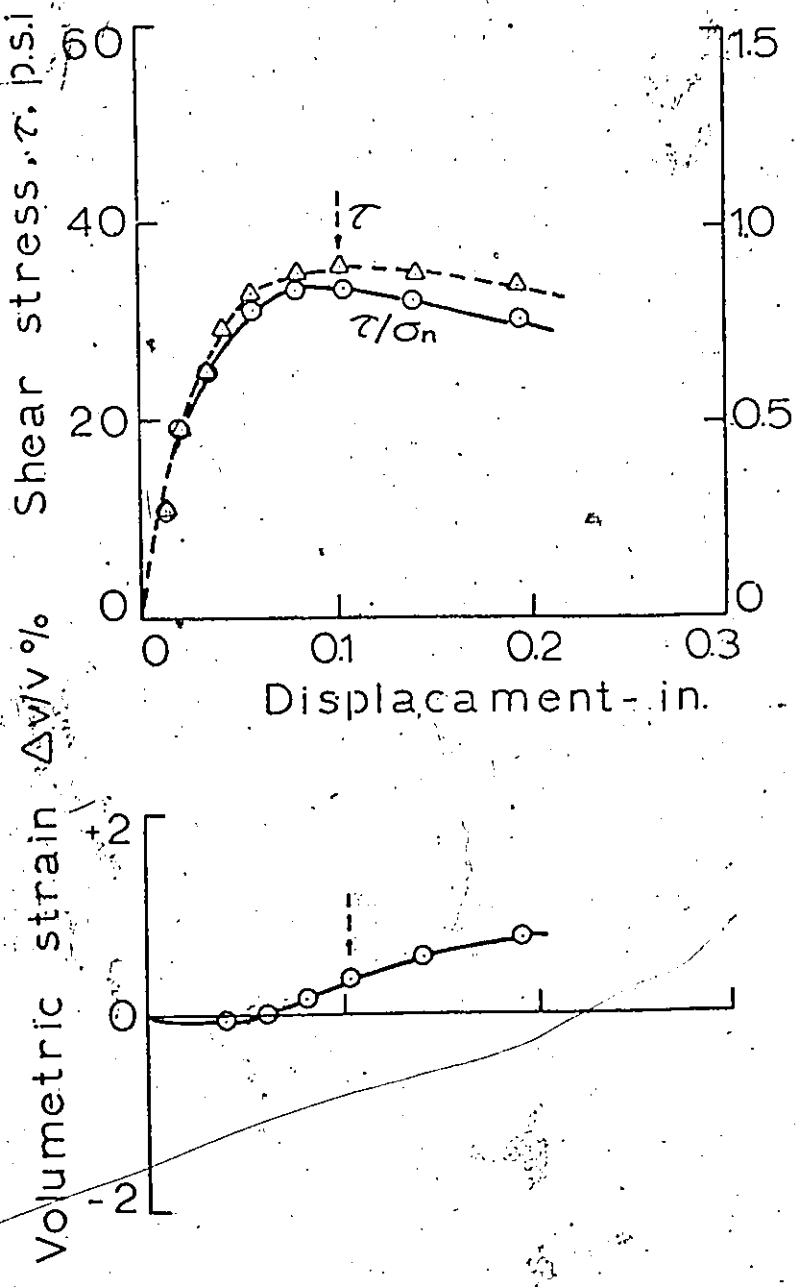

FIG. 4.3.6 STRESS-DISPLACEMENT RELATIONSHIP FOR DENSE SAND IN DIRECT SHEAR AT AN APPLIED NORMAL STRESS OF 40 p.s.i.

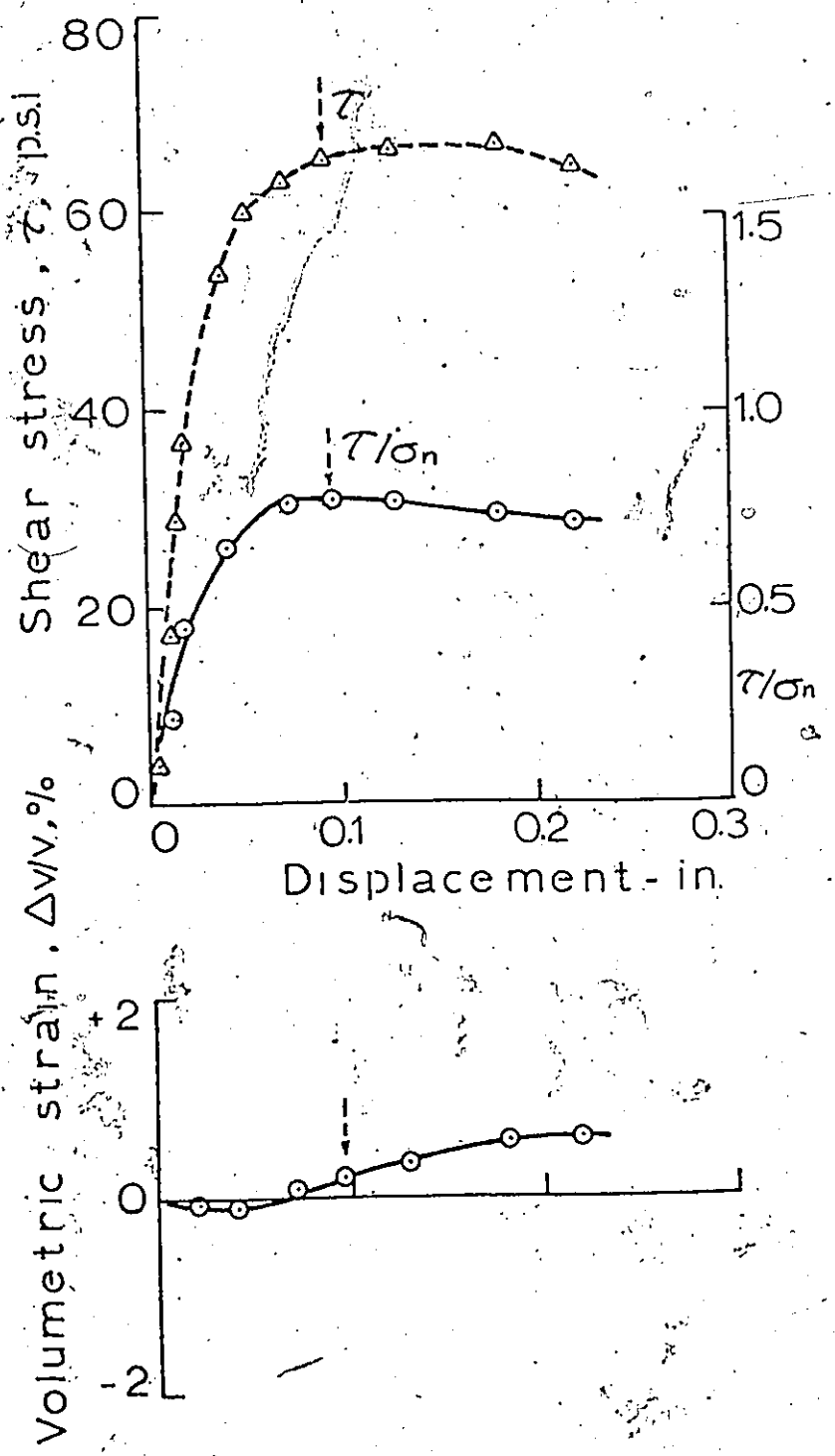

FIG. 4.3.7 STRESS-DISPLACEMENT RELATIONSHIP FOR DENSE SAND IN DIRECT SHEAR AT AN APPLIED NORMAL STRESS OF 80 p.s.i.

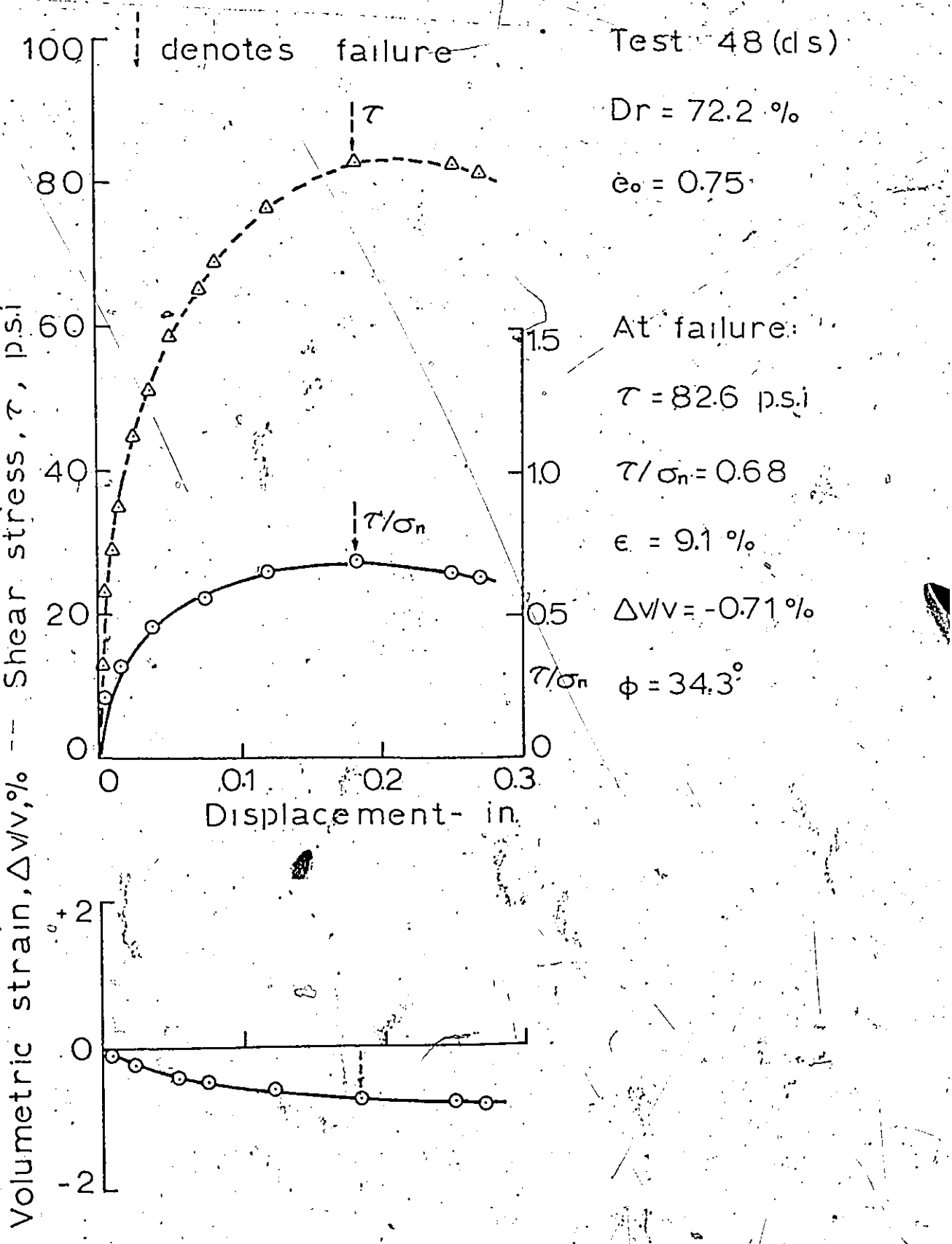

FIG. 4.3.8 STRESS-DISPLACEMENT RELATIONSHIP FOR DENSE SAND IN DIRECT SHEAR AT AN APPLIED NORMAL STRESS OF 109.5 p.s.i.

Test 25 (d s)

Dr = 67.9 %

e_o = 0.78

denotes failure

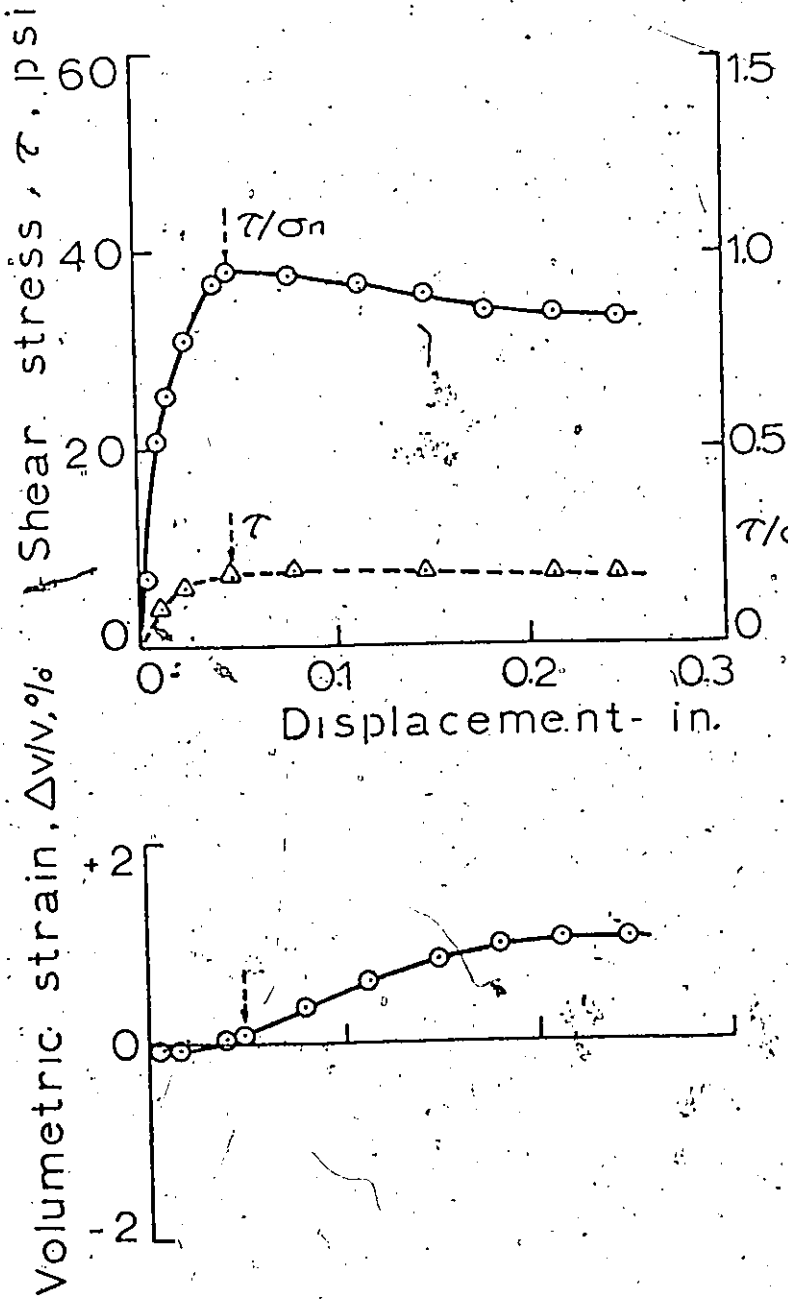

At failure:

τ = 7.8 psi

τ/σ_n = 0.95

ϵ = 2.4 %

$\Delta v/v$ = +0.1 %

ϕ = 43.5°

FIG. 4.3.9 RELATIONSHIP BETWEEN STRESS AND DISPLACEMENT FOR MEDIUM DENSE SAND IN DIRECT SHEAR AT AN APPLIED NORMAL STRESS OF 8 p.s.i.

Test 2.6 (d s)

Dr = 62.1 %

e_o = 0.81

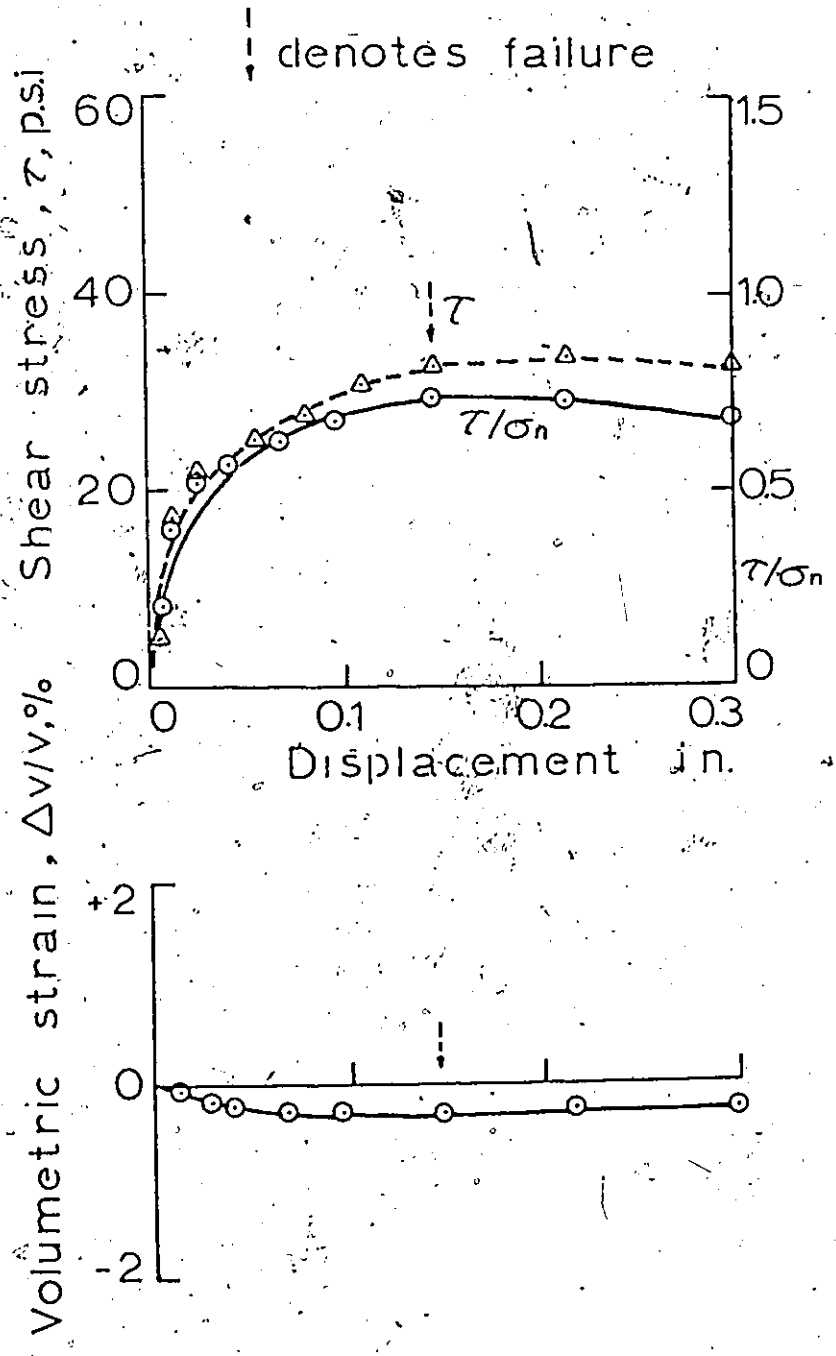

At failure:

τ = 32.9 p.s.i

τ/σ_n = 0.75

ϵ = 7.4 %

$\Delta v/v$ = -0.32 %

ϕ = 36.9°

FIG. 4.3.10 STRESS-DISPLACEMENT RELATIONSHIP FOR MEDIUM DENSE SAND IN DIRECT SHEAR AT AN APPLIED NORMAL STRESS OF 40 p.s.i.

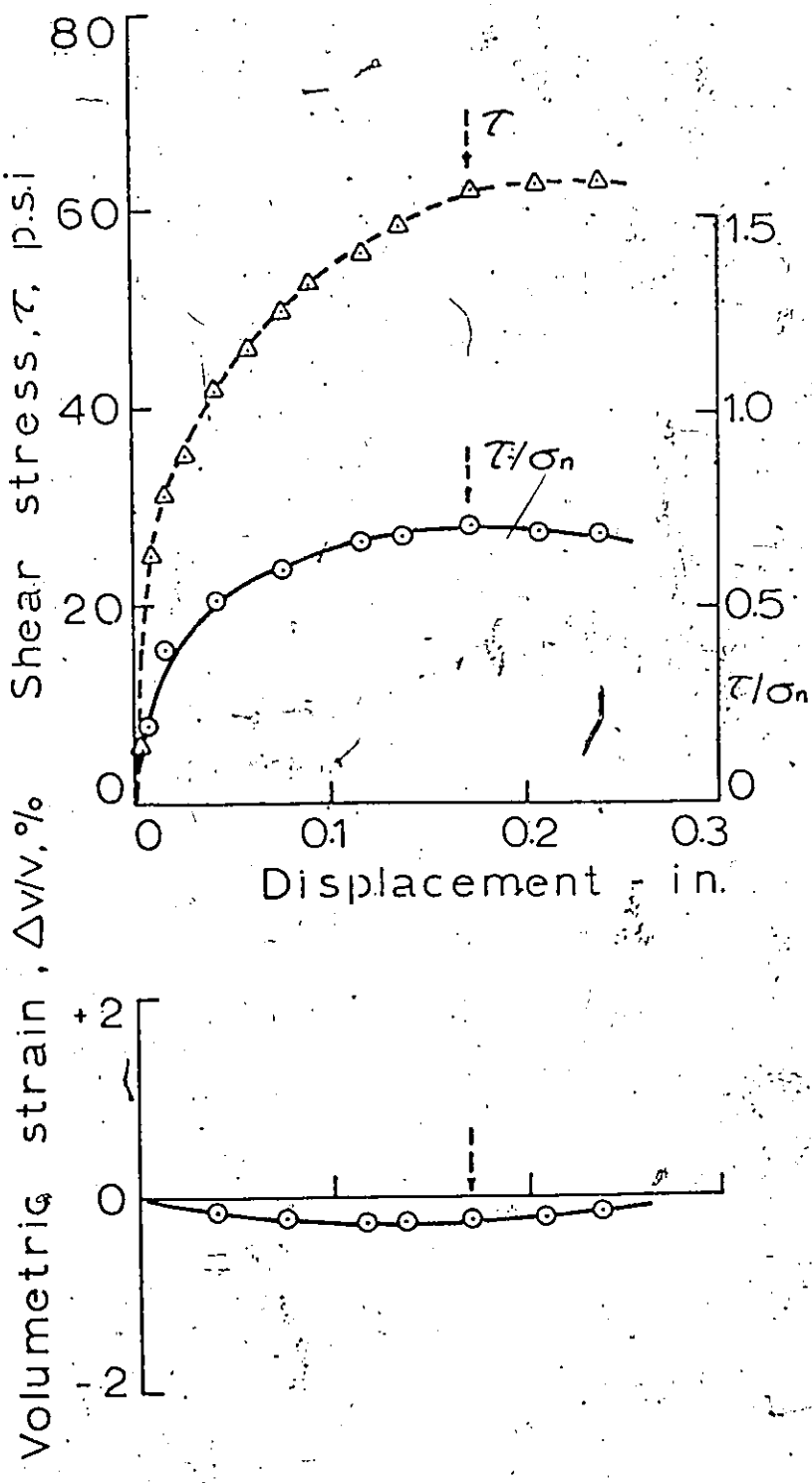

FIG. 4.3.11 STRESS-DISPLACEMENT RELATIONSHIP FOR MEDIUM DENSE SAND IN DIRECT SHEAR AT AN APPLIED NORMAL STRESS OF 80 p.s.i.

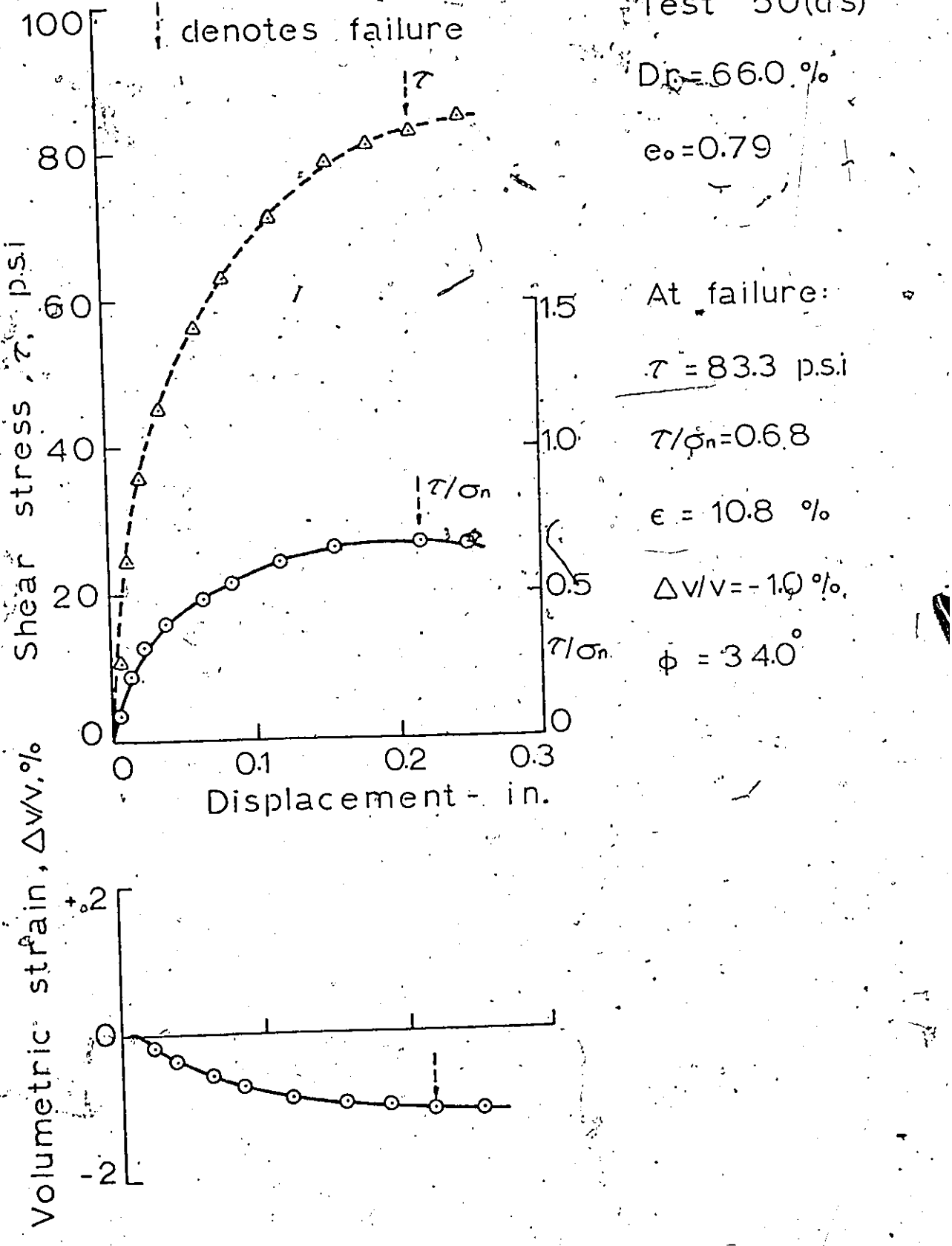

FIG. 4.3.12 STRESS-DISPLACEMENT RELATIONSHIP FOR MEDIUM DENSE SAND IN DIRECT SHEAR AT AN APPLIED NORMAL STRESS OF 109.5 p.s.i.

In Table 4.3.1 the results from direct shear box tests are given.

4.4 Ko-Tests

Coefficient of earth pressures at rest tests were performed at relative densities of 90, 73, 62, and 58 per cent. The values of Ko obtained were 0.39, 0.40, 0.41 and 0.44 respectively as shown in Figs. 4.4.1 to 4.4.4.

Summaries of these results have been presented in Fig. 5.1.11 where the Ko-values are plotted against relative density.

Values of Poissons ratio have been plotted in Fig. 5.1.11.

Test #	Unit Weight pcf	D_r %	e/n	σ_n psi	Corrected σ_n at failure psi	Max shear force lbs	τ psi	τ/σ_{nmax}	Shear Displacement inches	$(\frac{\Delta v}{v})\varepsilon/\gamma$	ϕ Degrees	Remarks
25	93.5	67.9	0.78/0.44	8	8.2	30.4	7.8	0.95	0.08	+0.10	43.6	Medium
26	91.8	62.1	0.81/0.45	40	43.4	120.0	32.5	0.75	0.148	-0.32	36.9	dense
27	96.4	68.0	0.78/0.44	40	41.6	129.0	33.4	0.81	0.068	+0.19	38.9	+ increase
29	95.8	76.2	0.73/0.42	80	86.4	235.2	63.0	0.73	0.136	+0.09	36.3	in volume
30	92.6	65.0	0.79/0.44	80	88.1	226.0	62.1	0.71	0.172	-0.21	35.2	i.e. dilating
34	95.6	75.5	0.74/0.42	40	42.2	133.8	35.2	0.84	0.086	-0.10	39.9	Dense
35	95.5	75.0	0.74/0.43	40	42.5	135.4	35.9	0.85	0.104	+0.34	40.3	sand
36	96.5	78.0	0.72/0.42	80	84.5	247.4	65.2	0.77	0.094	+0.20	37.7	
39	97.9	83.2	0.70/0.41	8.0	8.3	36.4	9.4	1.138	0.054	+0.56	48.7	
40	98.4	84.8	0.69/0.41	8.0	8.2	35.9	9.2	1.121	0.046	+0.44	48.3	Very dense
41	99.4	88.3	0.67/0.40	40.0	41.5	151.0	39.1	0.944	0.058	+0.18	43.4	sand
42	98.6	85.5	0.68/0.41	40.0	42.0	151.6	39.7	0.947	0.080	+0.23	43.4	
43	100.8	92.6	0.65/0.39	80.0	83.3	277.2	72.0	0.866	0.068	+0.46	40.9	
44	100.6	92.0	0.65/0.39	80.0	83.5	282.6	73.7	0.883	0.072	+0.31	41.4	
46	91.7	61.7	0.81/0.45	8.0	9.0	26.7	7.5	0.833	0.214	+0.08	39.8	
47	89.4	52.0	0.86/0.46	25.0	27.2	72.3	19.6	0.723	0.150	-0.38	35.9	
48	94.6	72.2	0.75/0.43	109.5	121.2	298.8	82.8	0.682	0.182	-0.71	34.3	
49	100.6	92.0	0.65/0.39	109.5	115.9	351.9	93.0	0.803	0.100	+0.48	38.6	
50	93.0	66.0	0.79/0.44	109.5	123.4	295.6	83.3	0.675	0.216	-1.04	34.0	
51	101.6	95.0	0.64/0.39	8.0	8.2	38.3	9.8	1.196	0.036	+0.46	50.1	

TABLE 4.3.1

SUMMARY OF RESULTS OF THE DIRECT SHEAR BOX TEST

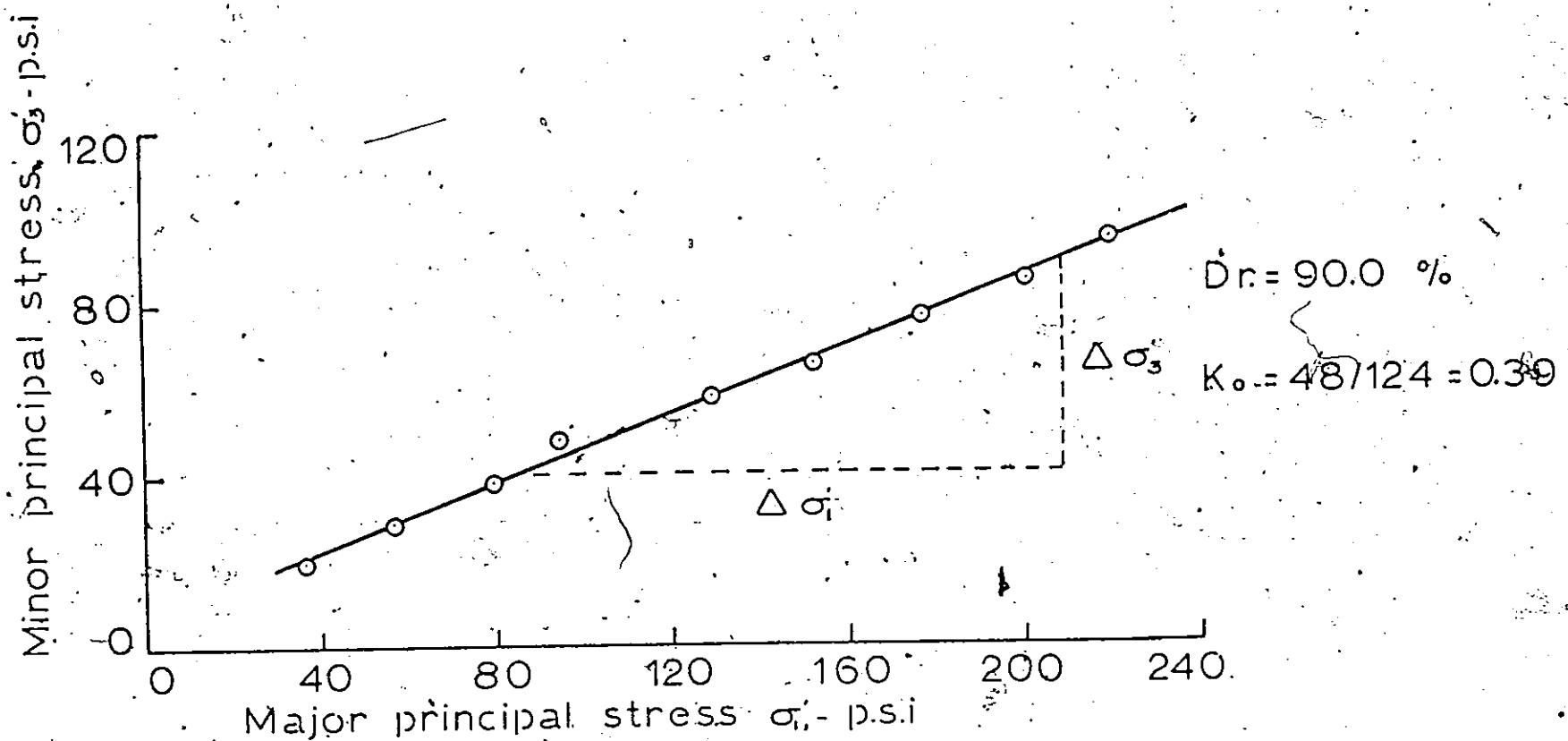

FIG. 4.4.1 MAJOR PRINCIPAL STRESS VERSUS MINOR PRINCIPAL STRESS FOR KO TEST 38.

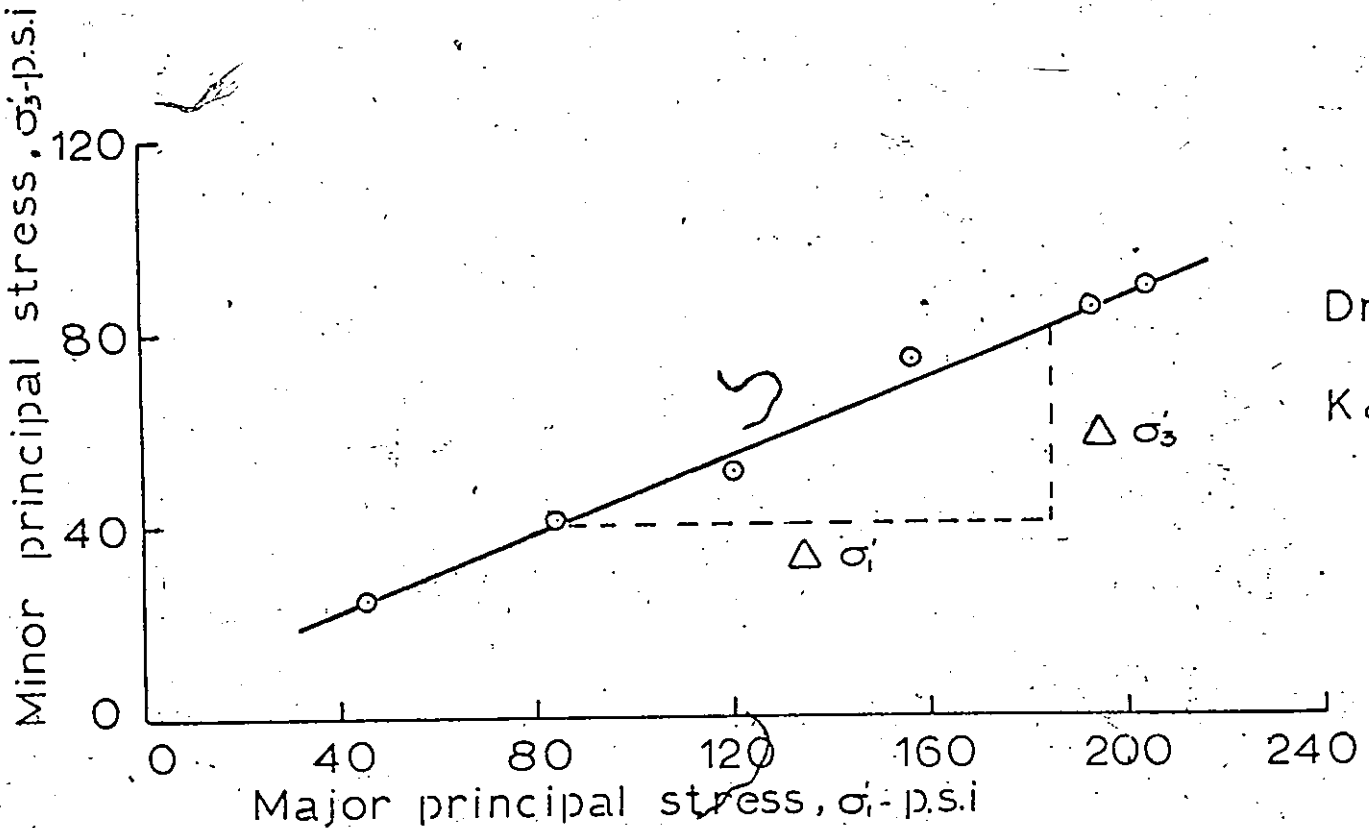

FIG. 4.4.2 MAJOR AND MINOR PRINCIPAL STRESS RELATIONSHIP FOR KO TEST 31.

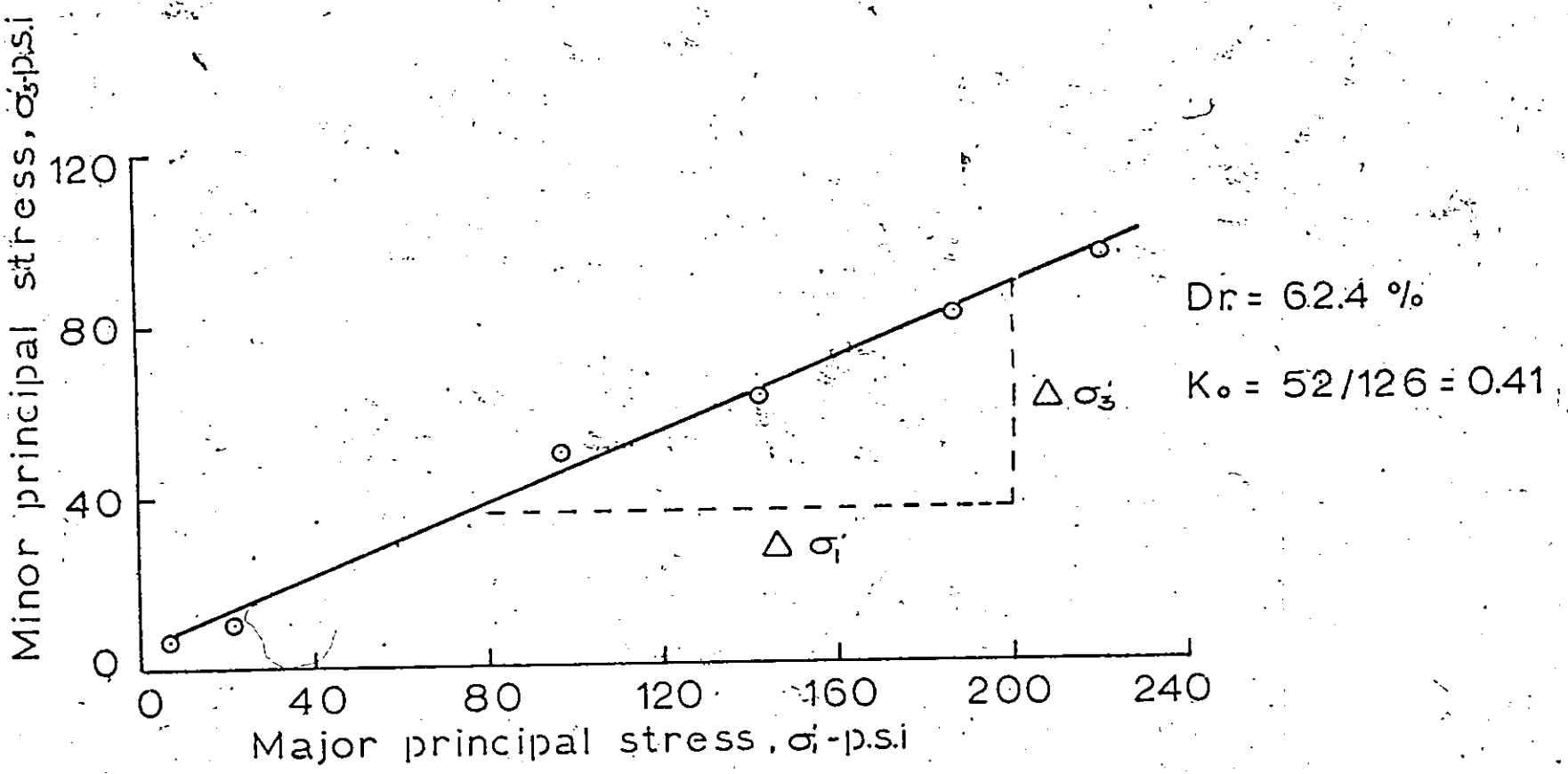

FIG. 4.4.3 RELATIONSHIP BETWEEN MAJOR AND MINOR PRINCIPAL STRESS FOR KO TEST 22.

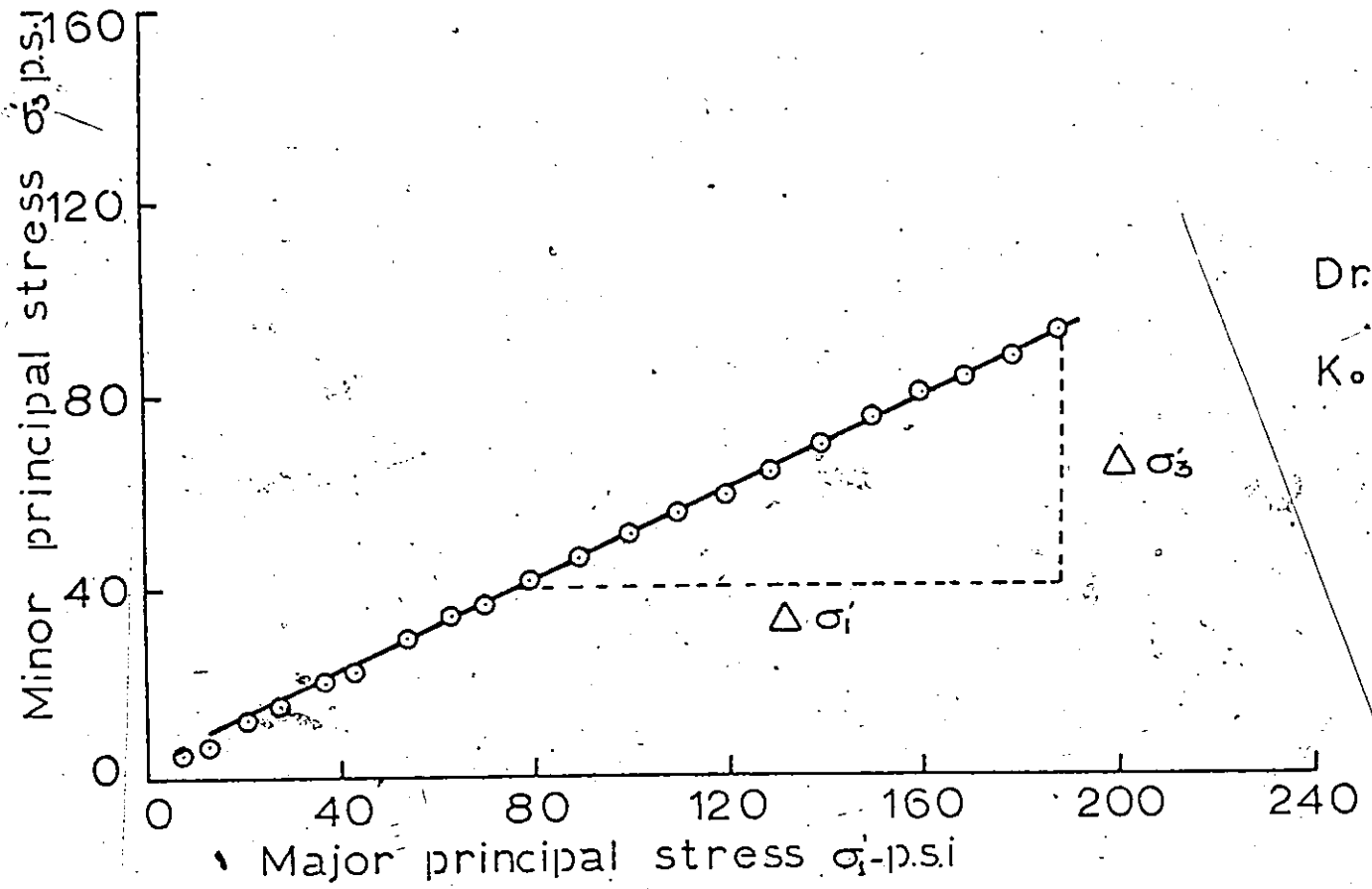

FIG. 4.4.4 MAJOR PRINCIPAL STRESS VERSUS MINOR PRINCIPAL STRESS FOR KO TEST 45.

CHAPTER 5

ANALYSIS AND DISCUSSION OF TEST RESULTS

In this Chapter the results of tests as reported in Chapter 4 are analyzed and discussed. The analysis and discussion have been split into the following main parts:

1. General discussion
2. Analysis of data
3. Factors influencing test results
4. Comparison of test results with other work.

5.1 General discussion

In this section the general behaviour of the sand during drained triaxial compression and direct shear is discussed. The coefficient of earth pressure at rest of the sand is also considered.

5.1.1 Consolidated-Drained Triaxial Compression Tests

These tests were carried out on isotropically consolidated samples at the required confining pressure. After the sample was allowed to consolidate at the required confining pressure, the deviator stress was applied until the sample failed. All the tests were drained tests. Either the maximum deviator stress or the maximum stress ratio could be considered as the failure criterion because they yielded the same results.

In Figs. 4.2.1 to 4.2.4 typical results are shown from triaxial tests for very dense sand samples. In Fig. 4.2.1 the sand sample had an initial relative density of 92.4 per cent and a corresponding initial void ratio of 0.65. The samples, the results of which are shown in Figs. 4.2.2 to 4.2.4, had relative densities of 92.6 per cent, 92.9 per cent, and 94.7 per cent respectively. The corresponding void ratios were 0.65, 0.65 and 0.64. The confining pressures were 5, 25, 50 and 80 p.s.i. respectively.

Certain trends are immediately noticeable from the plots. With an increase in confining pressure the axial strain at failure increased, and the stress ratios σ_1/σ_3 decreased. The corresponding value of the friction angle decreased. The volumetric strain (in this case +ve when dilating) decreased as the confining pressure was increased. The difference in the value of ϕ is 2.5 degrees; a result of the difference in the value of confining pressure alone and is associated with a nonlinear failure envelope.

As the strain increased the stress also increased and in general reached a clearly defined peak for the dense sand samples. The stresses then decreased with strain. The sample tested under a confining pressure of 5 p.s.i. did not exhibit a marked decrease of stress after the peak value was reached.

At very small strains even the dense samples showed a decrease in volume; this decrease being smallest for the

samples tested under a confining pressure of 5 p.s.i. Gradually as the confining pressure was increased, there was a larger volume decrease, as could be expected. Consequently, the net volumetric strain at failure was smallest for the highest confining pressure and greatest for the smallest confining pressure.

Figures 4.2.5 to 4.2.8 show the stress strain curves for dense sand specimens. The relative density was 70.7 per cent, 70.4 per cent, 73.3 per cent and 75.3 per cent respectively. The corresponding void ratios were 0.76, 0.77, 0.75 and 0.74. The tests were run at 5, 25, 50 and 80 p.s.i. respectively. The stress-strain curves of these samples were similar to the curves of the very dense sand samples. However the peak values were not as distinct, and the slope of the stress-strain curves became almost horizontal after the maximum stress had been reached for low confining pressures. The axial strains at failure were larger and the stress ratios were less compared to the corresponding values for the very dense sand. The corresponding values of ϕ were also less. The difference in the value of ϕ due to the variation in the confining pressure alone was 1.2 degrees as compared to 2.5 degrees for the very dense samples. The extent of the nonlinearity of the failure envelope was lower as compared to the very dense samples of sand. This decrease in the value of ϕ can be attributed to a smaller amount of particle crushing at lower densities.

The extent of volume change at failure had also decreased as is evident from Table 5.1.1 for very dense sand.

From Figs. 4.2.9 to 4.2.12 for medium dense sands it will be noticed that the strain to failure had increased further and was 19.2 per cent for 80 p.s.i. of confining pressure. The rate of volume change had also decreased as is evident from Table 5.1.1.

The decrease in the rate of the volume change indicates that the densities of the sample tested were approaching the density corresponding to the ϕ_{cv} value. This is evident from Fig. 5.1.1(a). This figure was drawn to find ϕ_{cv} as suggested by Lee and Seed (1967). Fig. 5.1.1(b) is drawn for very dense sand samples.

The value of ϕ_{cv} as found from tests 12, 13, 14 and 15 was 36.5 degrees for a confining pressure of 68.3 p.s.i. and a void ratio equal to 0.75. For a confining pressure of 31 p.s.i. the ϕ_{cv} value was found to be equal to 35.4 degrees; and the corresponding void ratio was equal to 0.82, as determined from tests 17, 18, 20 and 21. This resulted in an average ϕ_{cv} equal to 36 degrees. It should be noted that the definition of ϕ_{cv} as used by Lee and Seed differs from the definition considered by Casagrande and Rowe.

Figures 5.1.2 to 5.1.4 show the Mohr-Coulomb plots for the different densities investigated. It is evident from these figures that for the range of relative densities investigated, the Mohr-Coulomb envelope was not a straight line but became gradually flatter as the normal stresses increased.

Fig.	Dr Percent	σ_3 p.s.i.	σ_1/σ_3	ε_f %	ϕ^o	$(\frac{\Delta v}{v})_f$	Remarks
4.2(1)	92.4	5	4.9	5.50	41.5	.042	Very
(2)	92.6	25	4.8	7.00	41.0	.035	Dense
(3)	92.9	50	4.6	9.00	40.0	.021	Sand
(4)	94.7	80	4.4	9.60	39.0	.014	
(5)	70.7	5	4.1	7.60	37.3	.032	Dense
(6)	70.4	25	4.1	7.61	37.25	.011	Sand
(7)	73.3	50	4.0	10.80	36.80	.007	
(8)	75.3	80	3.9	14.70	36.15	.006	
(9)	66.3	5	3.8	11.10	35.45	.028	Medium
(10)	57.0	25	3.7	13.20	35.15	.004	Dense
(11)	61.9	50	3.7	16.30	35.05	-.011	Sand
(12)	64.5	80	3.6	19.20	34.50	-.022	

TABLE 5.1.1

SUMMARY OF TYPICAL TRIAXIAL COMPRESSION

TEST RESULTS

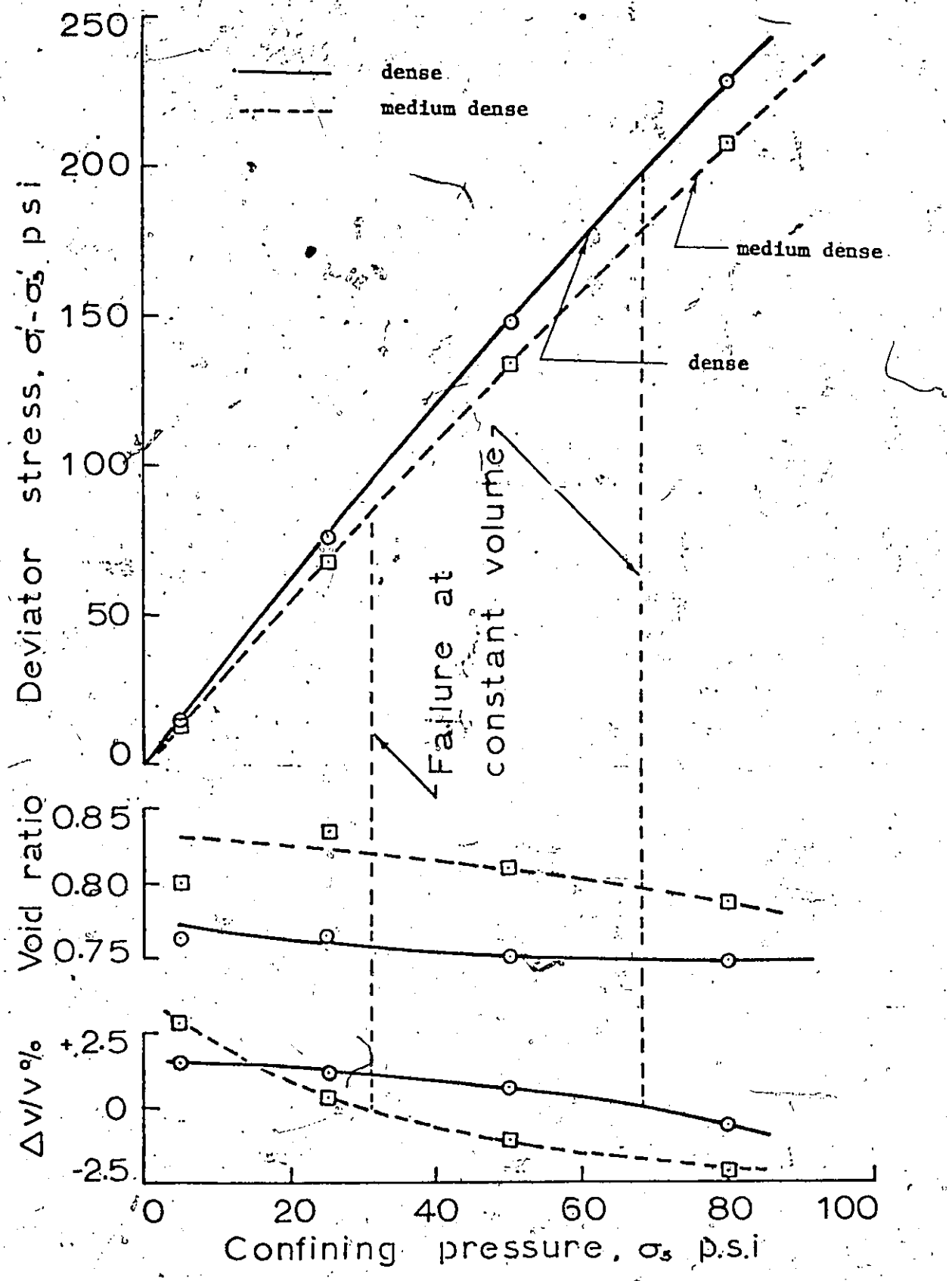

FIG. 5.1.1a CONDITIONS AT FAILURE FOR DENSE AND MEDIUM DENSE SAND IN TRIAXIAL COMPRESSION.

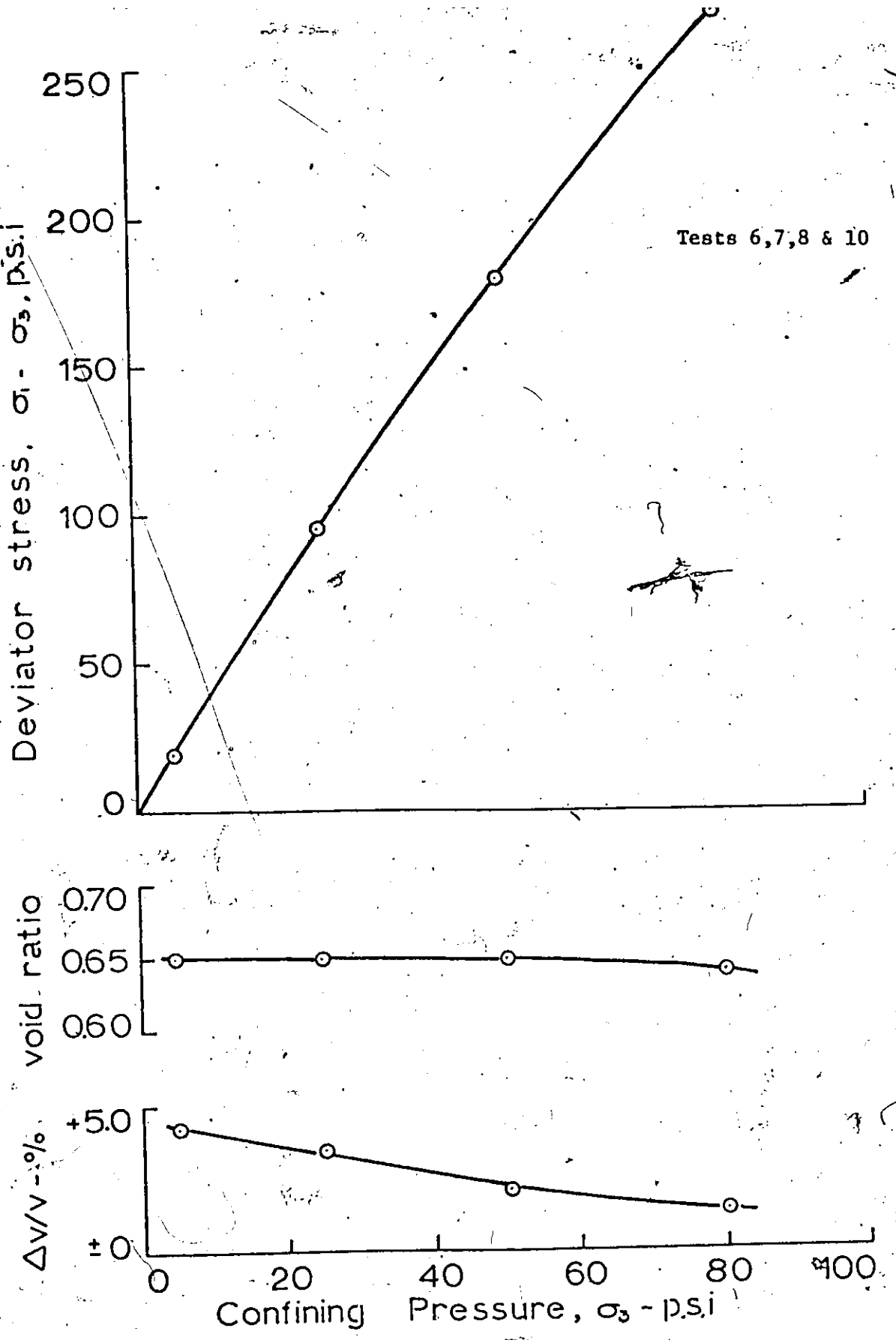

FIG. 5.1.1b CONDITIONS AT FAILURE FOR VERY DENSE SAND IN TRIAXIAL COMPRESSION

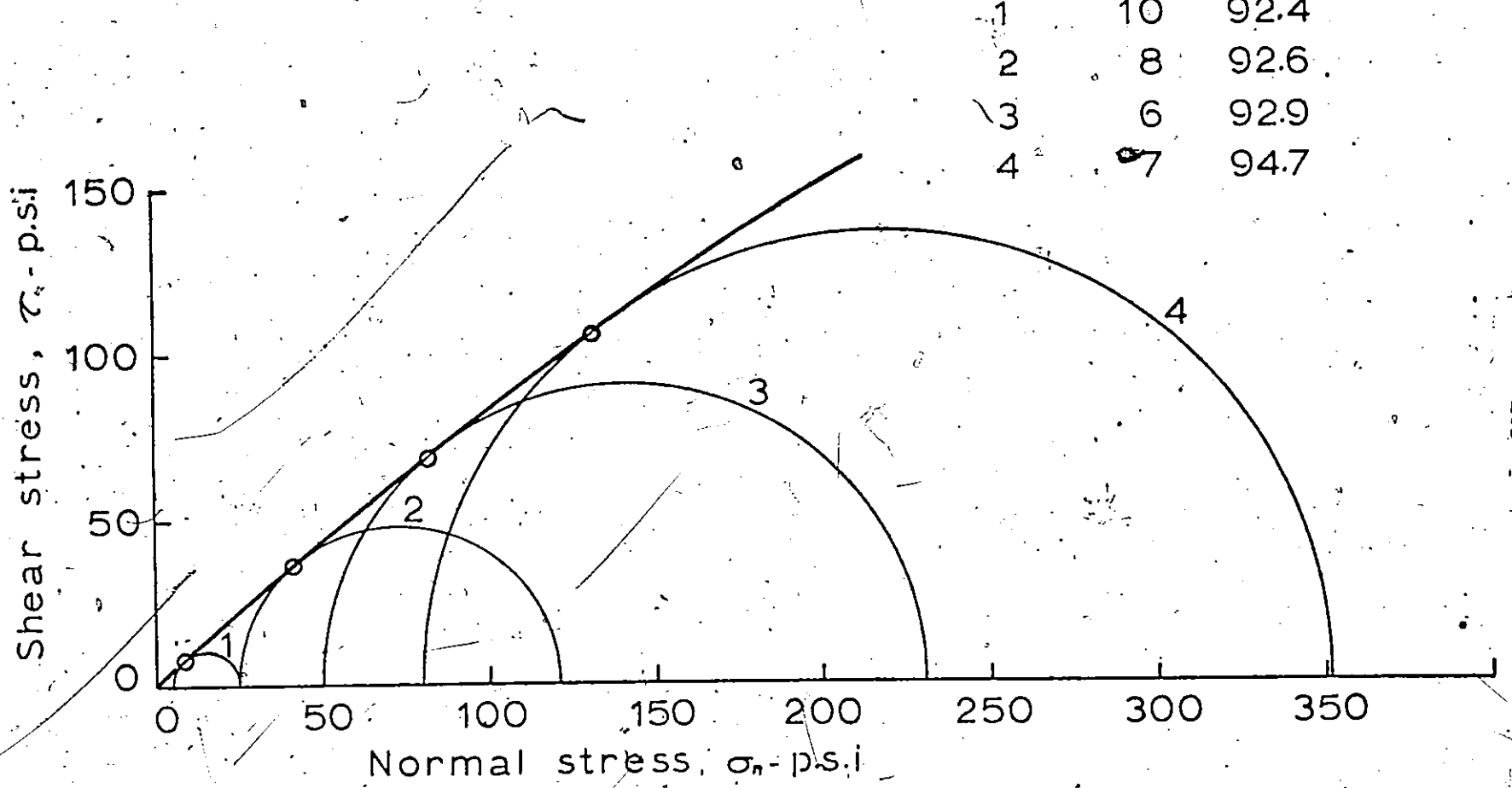

FIG. 5.1.2 MOHR-COULOMB'S ENVELOPE FOR VERY DENSE SAND IN TRIAXIAL COMPRESSION.

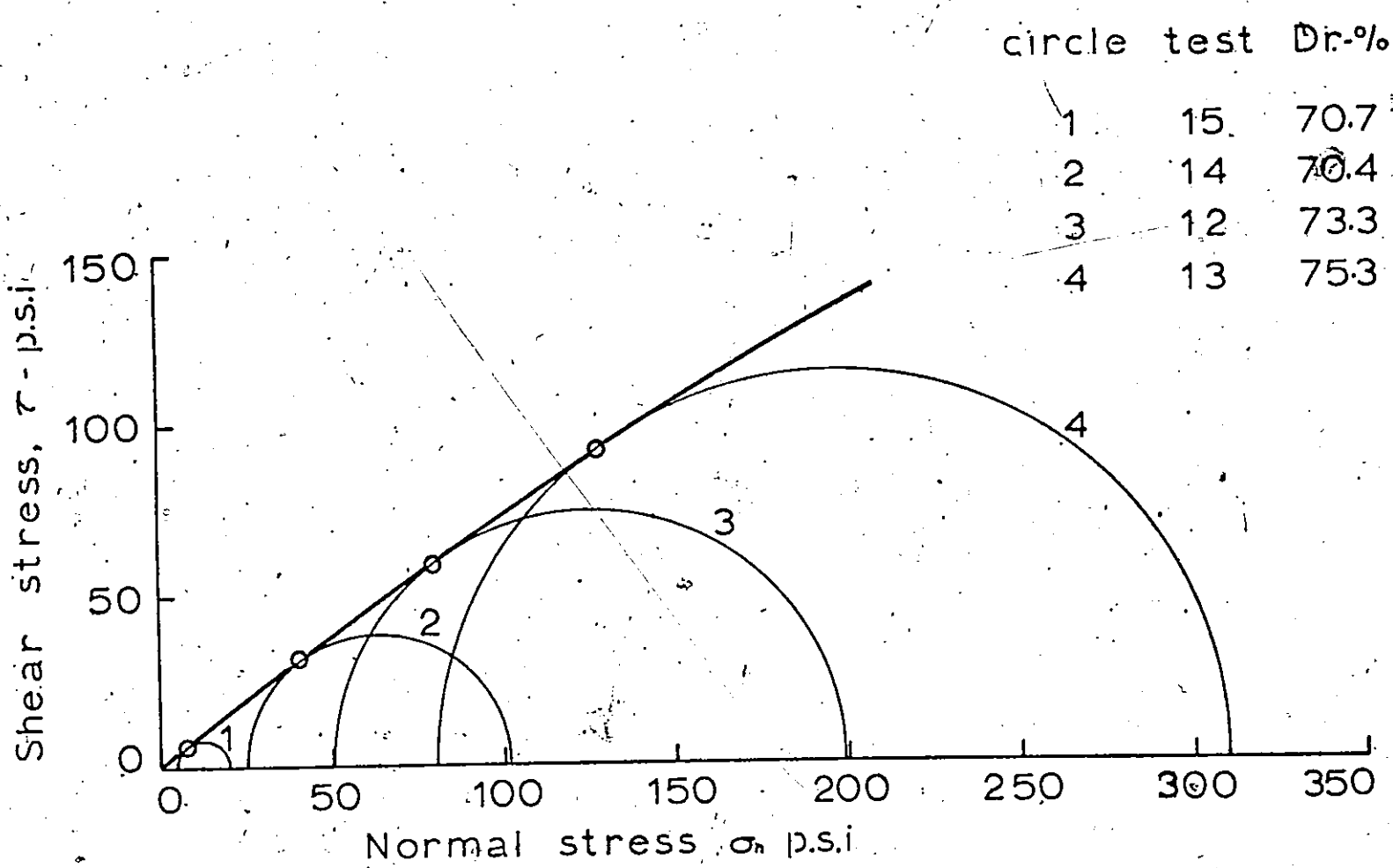

FIG. 5.1.3 MOHR-COULOMB'S ENVELQPE FOR DENSE SAND IN TRIAXIAL COMPRESSION.

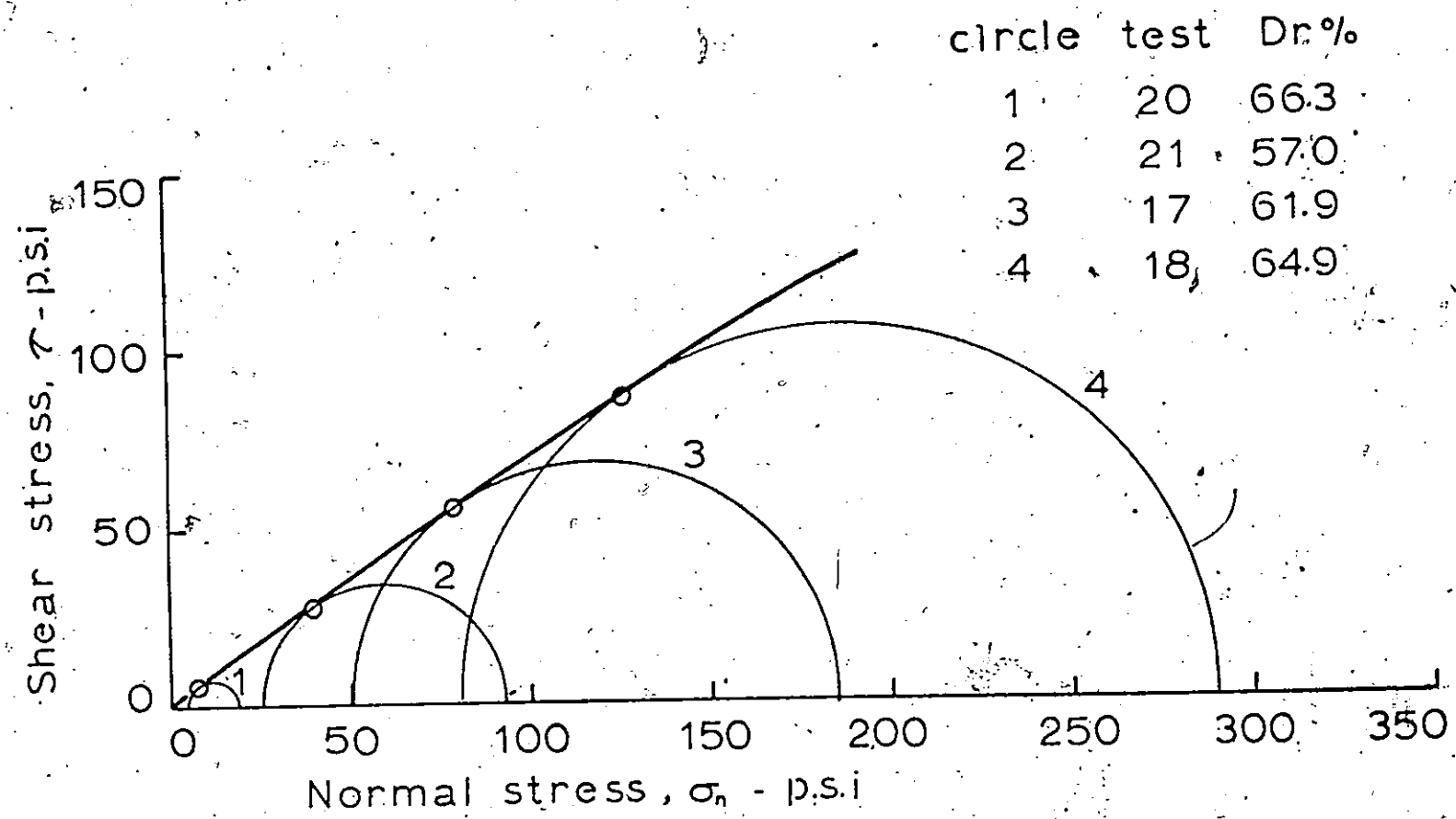

FIG. 5.1.4 MOHR-COULOMB'S ENVELOPE FOR MEDIUM DENSE SAND IN TRIAXIAL COMPRESSION.

For the very dense samples, the envelope was almost linear up to about 40 p.s.i. of the applied normal stress. For the dense sand linear behaviour was observed up to about 50 p.s.i. and for the medium dense sand it was about 60 p.s.i. of normal stress before a deviation from linearity occurred. These values suggest that the Mohr-Coulomb envelope will be a straight line for lower relative densities up to a certain range of normal stress.

Figure 5.1.5 is a plot of normal stress versus ϕ for various relative densities. The three curves for relative densities of 90, 75 and 60 per cent were interpolated. The relative densities were those at the end of consolidation. It should be noted that beyond 60 p.s.i. of normal stress the plots became more curved downwards, suggesting crushing of sand grains. This was confirmed by grain size analyses after tests at 80 p.s.i. of confining pressure as given in the grain size distribution curve in Fig. 3.1.

Figure 5.1.6 gives a plot of the porosity versus ϕ for each of the range of confining pressures investigated.

Figure 5.1.7 depicts a plot of porosity versus volumetric strain (positive indicates an increase in volume, whereas negative indicates a decrease in volume).

It should be noted that the range of volumetric strain was smallest for 5 p.s.i. confining pressure and largest for 80 p.s.i. confining pressure considering the entire range of porosities.

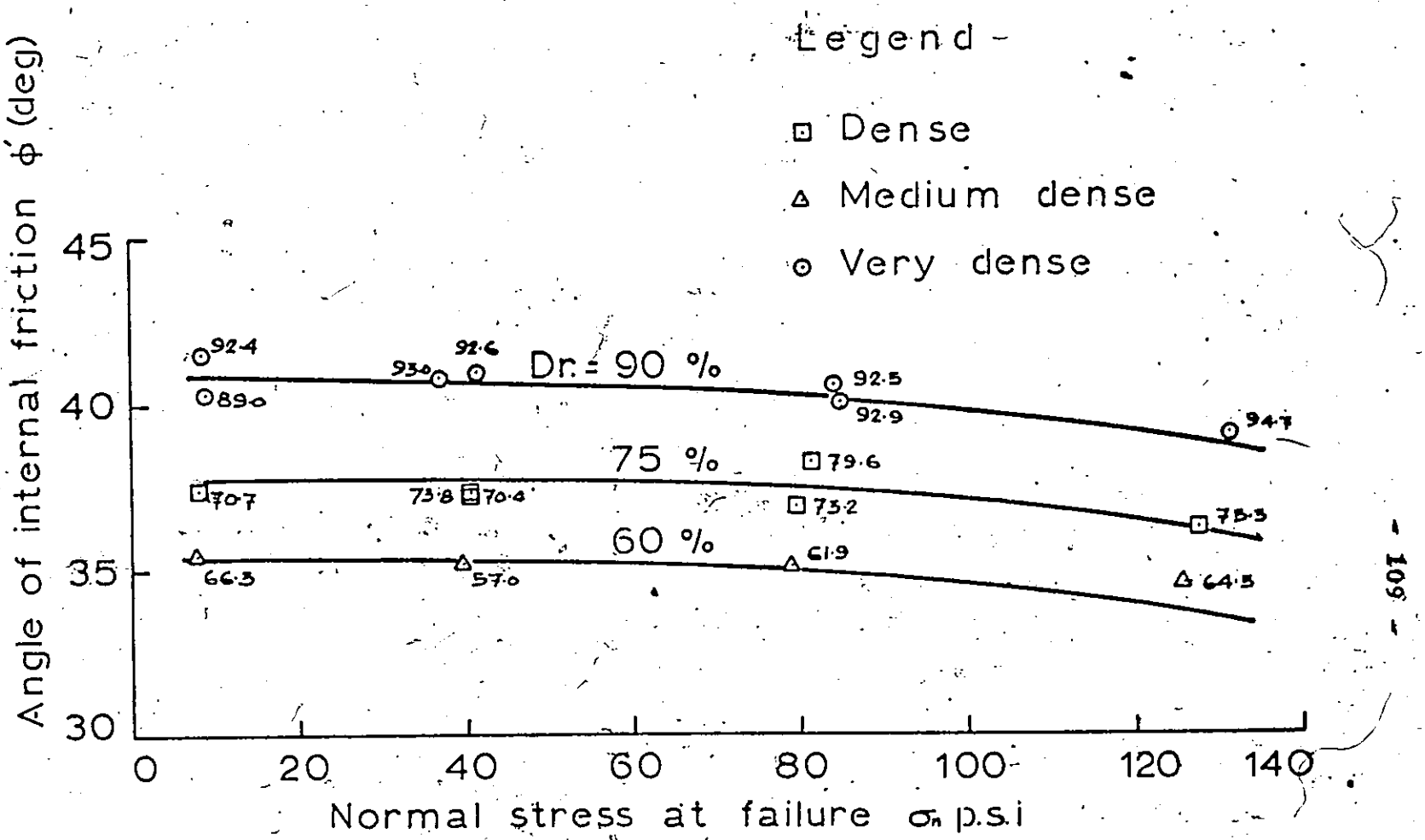

FIG. 5.1.5 NORMAL STRESS AT FAILURE VERSUS ANGLE OF INTERNAL FRICTION FROM DRAINED TRIAXIAL COMPRESSION TESTS AT VARIOUS DENSITIES.

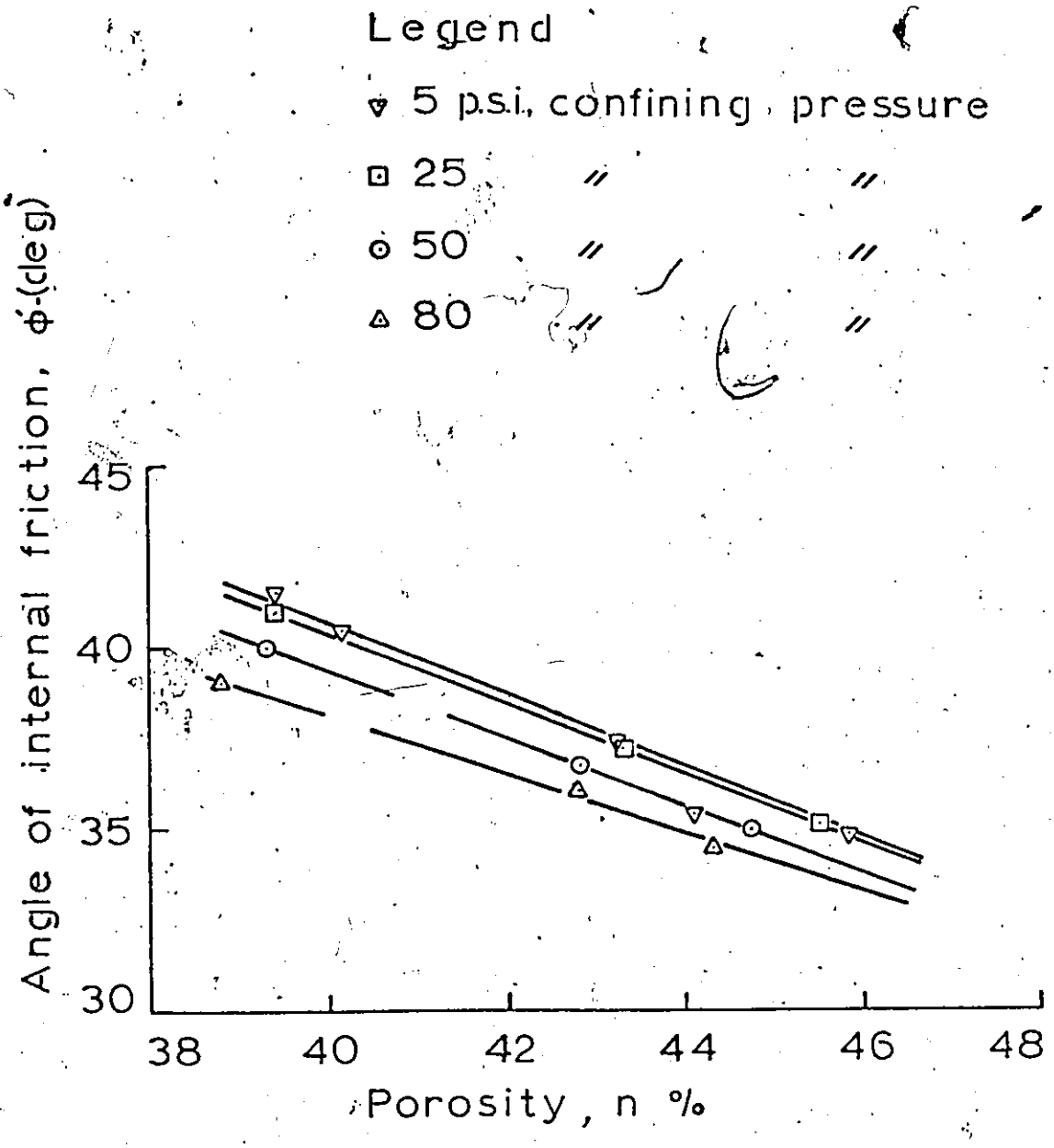

FIG. 5.1.6 CHANGE OF ANGLE OF INTERNAL FRICTION WITH POROSITY FOR DRAINED TRIAXIAL COMPRESSION TESTS AT VARIOUS CONFINING PRESSURES.

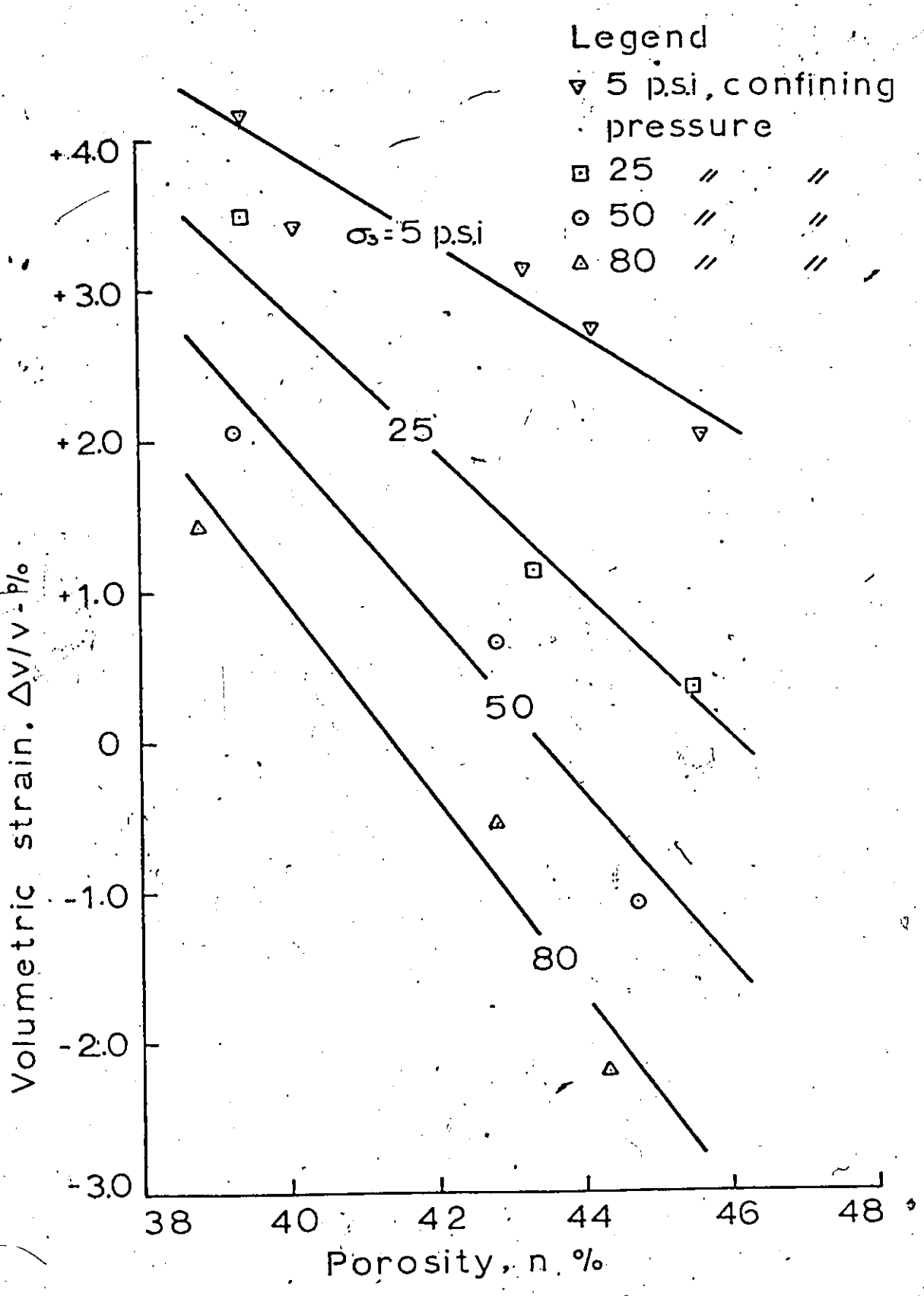

FIG. 5.1.7 POROSITY VERSUS VOLUMETRIC STRAIN AT FAILURE IN DRAINED TRIAXIAL COMPRESSION TESTS FOR SAND AT VARIOUS CONFINING PRESSURES.

5.1.2 Direct Shear Box Test

Direct shear box tests were conducted on 2 inch by 2 inch by approximately 1.5 inch high samples. The rate of shear displacement was chosen to be 0.016 inches per minute.

Figures 4.3.1 to 4.3.4 represent plots of shear displacement (inches) versus shear stress, ratio of shear to normal stress and volumetric strain per cent for the direct shear box tests carried out on very dense sand samples.

These tests were carried out at normal stresses of 8, 40, 80 and 109.5 p.s.i. The corresponding void ratios were 0.64, 0.67, 0.65 and 0.65 respectively.

It is noted from the plots that for a given density the value of ϕ was highest at 8 p.s.i. normal stress and lowest for 109.5 p.s.i. normal stress. For a normal stress of 8 p.s.i. the stress ratio; i.e., τ/σ_n was highest at 0.035 inches of shear displacement. For a normal stress of 109.5 p.s.i., however, the stress ratio was highest for a shear displacement of 0.1 inches.

For normal stresses of 40 and 80 p.s.i. the maximum stress ratios were attained at 0.058 and 0.072 inches of shear displacement respectively. That is to say that the displacement at failure increased steadily with an increase in applied normal stress. The stress ratio and shear stress versus displacement graphs had well defined peaks. The stress ratio gradually dropped after they had passed the peak reaching constant values under large displacements.

For applied normal stresses of 8, 40 and 80 p.s.i. some decrease in volume was noted in the initial stage of the test. This decrease in volume was completely absent for the sample tested at an applied normal stress of 109.5 p.s.i.

The overall volume change was highest for the sample tested at a normal stress of 8 p.s.i. and smallest for the sand specimen subjected to a normal stress of 109.5 p.s.i.

Figures 4.3.5 to 4.3.8 represent similar graphs for the direct shear box tests carried out on dense sand specimens.

These tests were carried out at normal stresses of 8, 40, 80 and 109.5 p.s.i. The corresponding void ratios were 0.70, 0.74, 0.72 and 0.75 respectively.

The τ/σ_n versus shear displacement curves had well-defined peaks but the overall stress-strain curves had become flatter. The volumetric strain decreased as the normal stresses were increased and became actually negative for a applied normal stress of 109.5 p.s.i. The displacement at the peak also increased gradually as the normal stresses were increased. This meant that as the density decreased, the displacement at failure increased correspondingly.

The test results for the medium dense sand samples are given in Figs. 4.3.9 to 4.3.12.

These tests were also carried out at normal stresses of 8, 40, 80 and 109.5 p.s.i. The corresponding void ratios were 0.78, 0.81, 0.79 and 0.79 respectively.

The same comments as given for Figs. 4.3.5 to 4.3.8 apply in these cases, except that the values of stress ratios and shear stresses had correspondingly reduced. The displacement to failure had increased accordingly. Positive volumetric strains had become smaller and negative volumetric strains had become larger, again suggesting, lower ϕ values.

Figure 5.1.8 shows the graphs of normal stress versus shear stress at failure for various ranges of densities for direct shear box test. The curves for relative densities of 65, 75 and 92 per cent were interpolated from the different test results.

The relationship of normal stress to angle of internal friction for various densities is given in Fig. 5.1.9. Figure 5.1.10 shows the plot for the porosity versus ϕ for different normal stresses. From the two figures it can be seen that the value of ϕ increases as the normal stress decreases. The normal stresses shown in Fig. 5.1.10 are the initial applied normal stresses rather than the corrected normal stress at failure. This was done for the sake of comparison. However, the corrected normal stresses at failure are given in Fig. 5.1.9 based on a corrected specimen area obtained by deducting the displacement times the width of the samples from the area of the sample at the start of the test. It is seen from Fig. 5.1.9 that the normal stress at failure was not markedly different from the initial normal stress for the smaller normal stresses. The difference increased gradually as the normal stress was

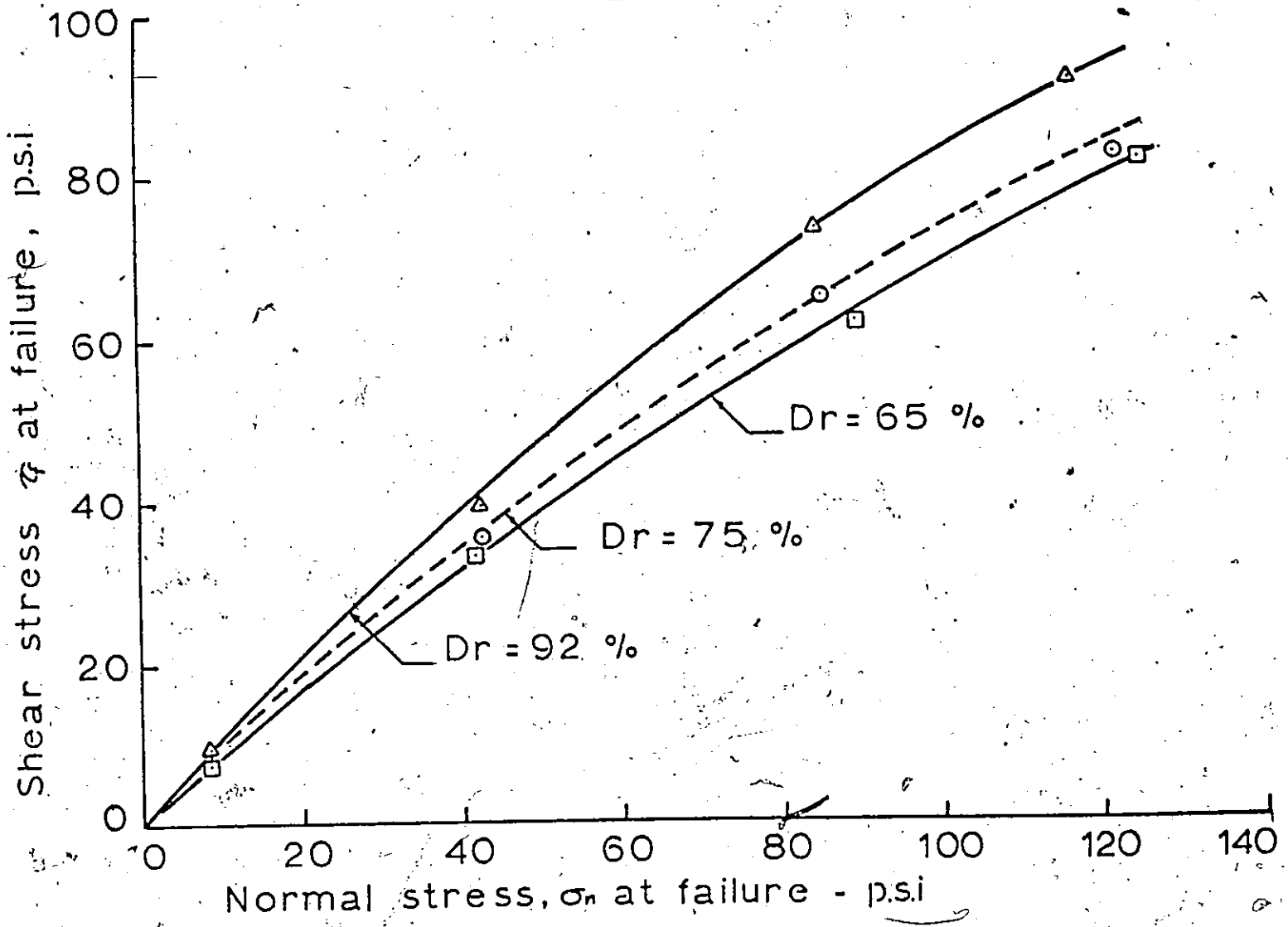

FIG. 5.1.8 RELATIONSHIP BETWEEN NORMAL STRESS AND SHEAR STRESS AT FAILURE FOR DIRECT SHEAR TESTS.

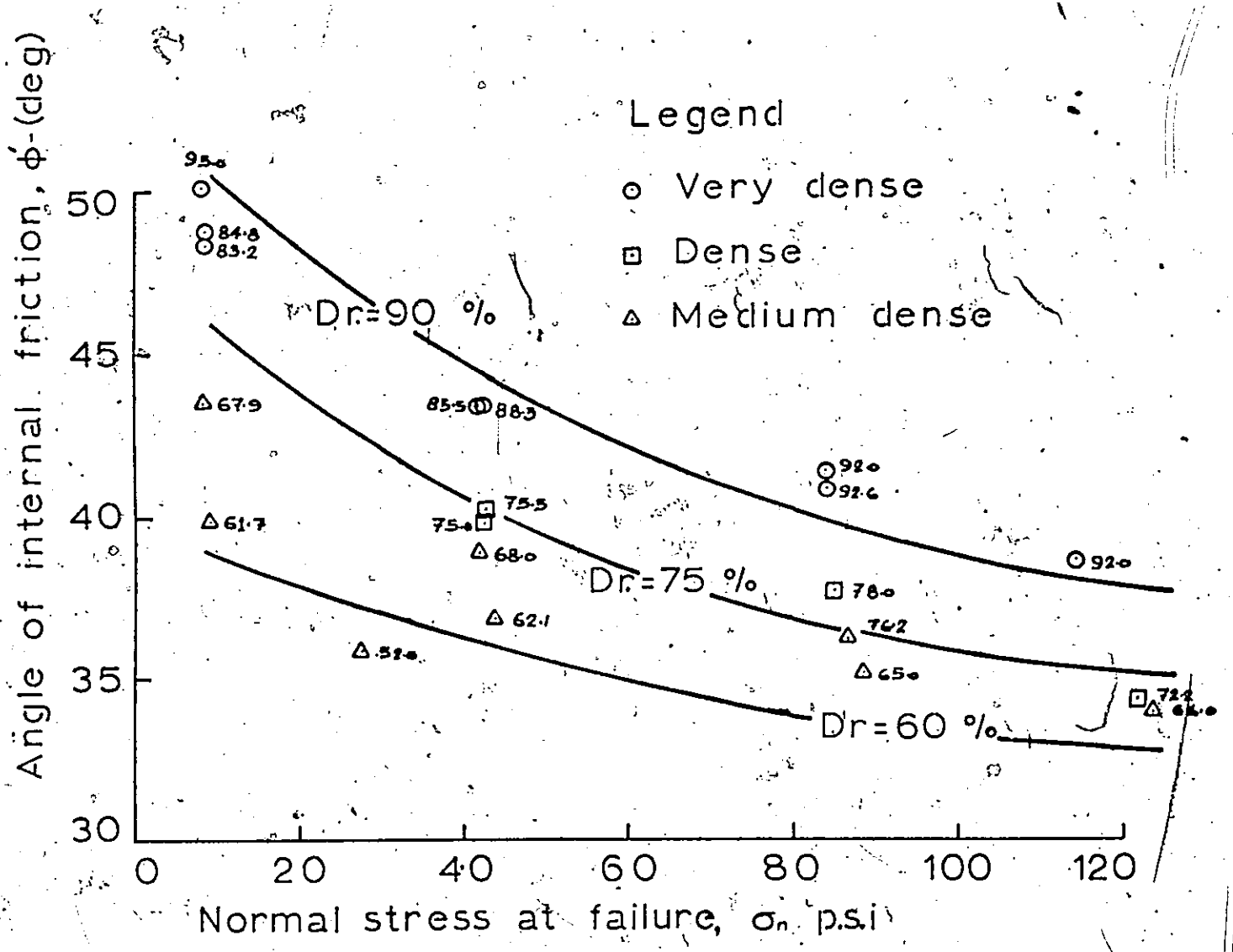

FIG. 5.1.9 RELATIONSHIP BETWEEN NORMAL STRESS (CORRECTED) AND ANGLE OF SHEARING RESISTANCE FOR DIRECT SHEAR TESTS.

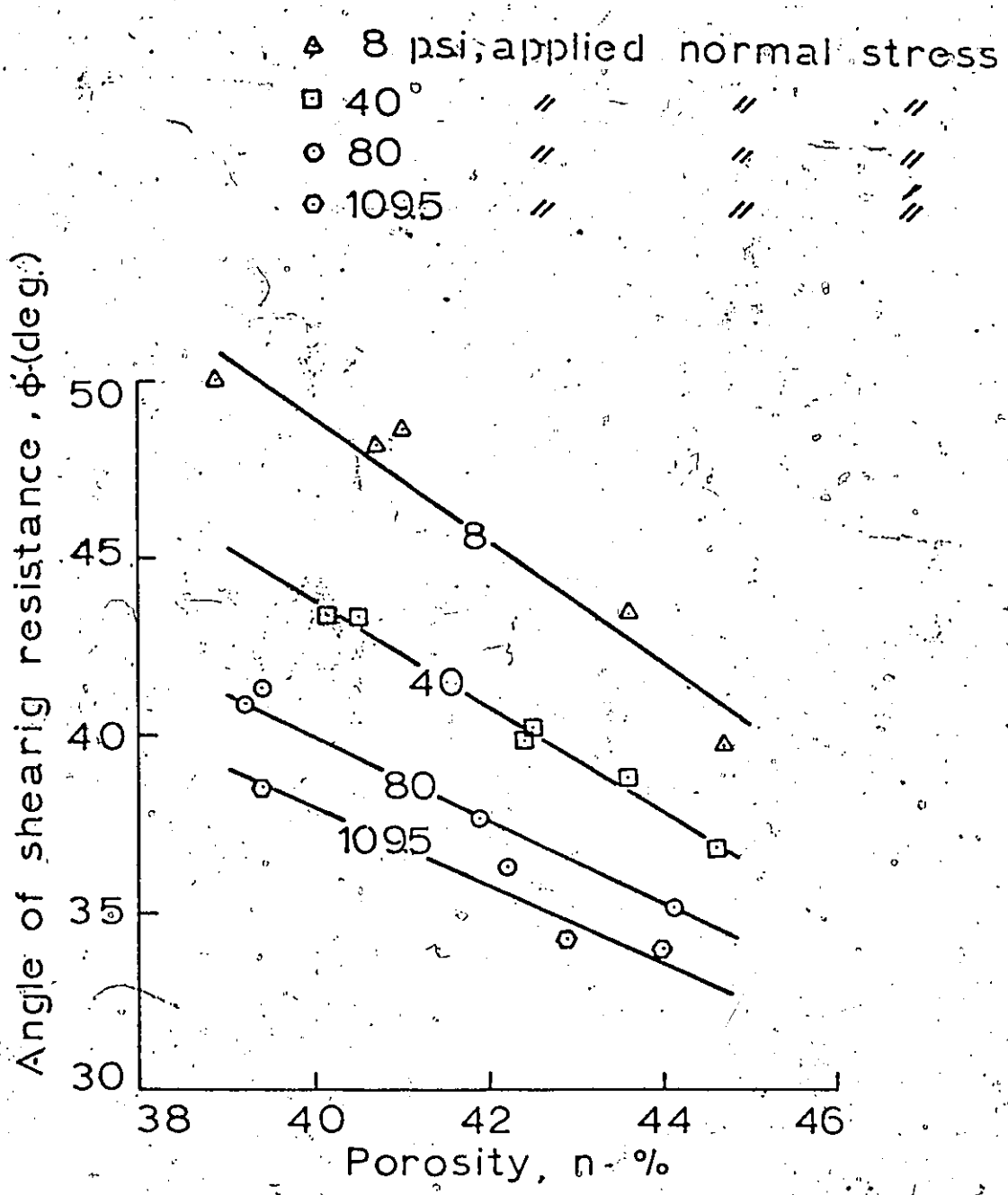

FIG. 5.1.10 POROSITY VERSUS ANGLE OF SHEARING RESISTANCE FOR VARIOUS APPLIED NORMAL STRESS FROM DIRECT SHEAR TESTS.

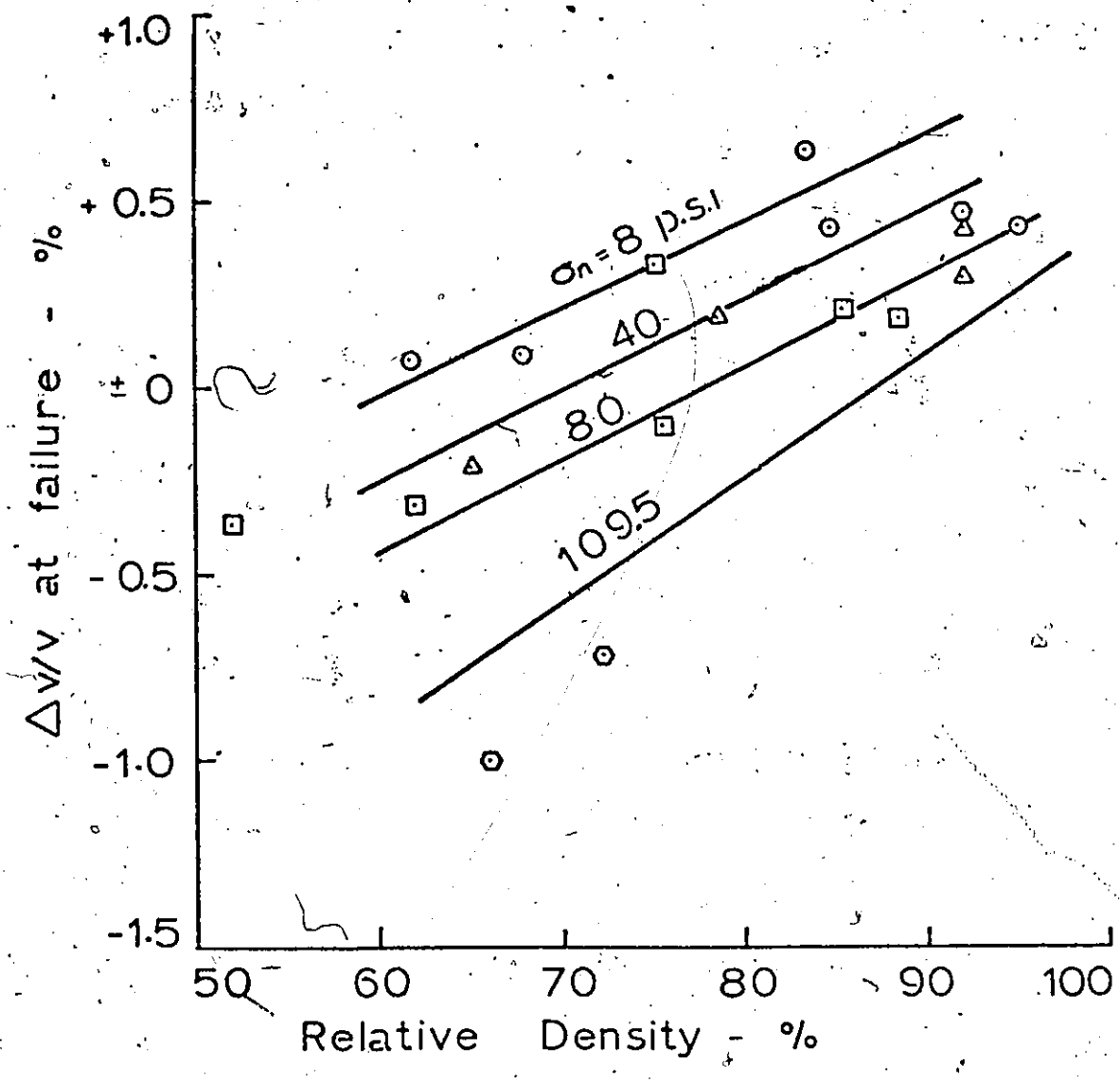

FIG. 5.1.11 RELATIONSHIP BETWEEN VOLUMETRIC STRAIN AT FAILURE AND RELATIVE DENSITY FOR VARIOUS NORMAL STRESSES IN DIRECT SHEAR TESTS

increased. This is because shear displacement at failure was smallest for the lowest normal stresses and largest for the highest normal stresses. At an applied normal stress of 8 p.s.i., the stress at failure was 8.2 p.s.i. For applied normal stresses of 40, 80 and 109.5 p.s.i., the normal stresses at failure was around 42, 84 and 120 p.s.i. respectively. These results suggest that the displacement to failure increases with increase in applied normal stress. Fig. 5.1.11 relates the volumetric strain to relative density at various applied normal stresses.

5.1.3 Ko-tests

Four Ko-tests were performed at relative densities of 90, 73, 62 and 58 per cent. The values of Ko obtained were 0.39, 0.40, 0.41 and 0.44 respectively as shown in Figs. 4.4.1 to 4.4.4.

These results are summarized in Fig. 5.1.12 where the Ko-values are plotted against relative density. The value of the Poisson's ratio has been calculated using the formula suggested by Timoshenko (1934).

$$\mu = \frac{Ko}{1 + Ko} \qquad (5.1)$$

The calculated values of Poisson's ratio have also been plotted in Fig. 5.1.12.

From Fig. 5.1.12 it will be noted that the value of Ko and μ vary linearly between relative densities of 65 and 90 per cent. This variation in values of Ko is very small in the above range. The value of Ko increases as the

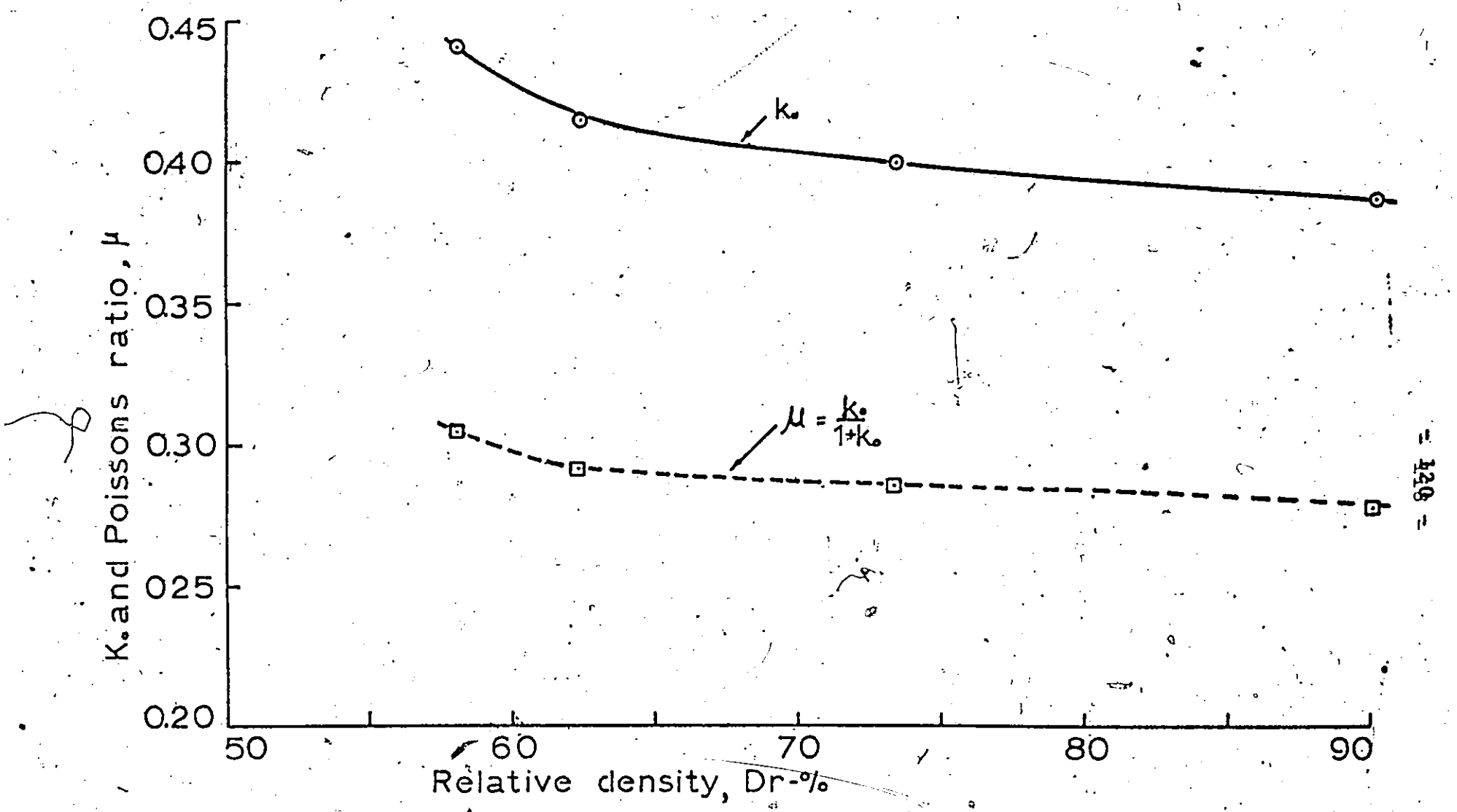

FIG. 5.1.12 COEFFICIENTS OF EARTH PRESSURE AT REST, KO, AND CORRESPONDING POISSON'S RATIOS, μ, VERSUS RELATIVE DRY DENSITY, D_r.

densities are decreased. However, in the dense and very dense range the value of Ko may be considered constant.

There was a fairly good agreement between the Ko-values obtained in the laboratory with the theory proposed by Jaky and illustrated by Bauer (1969) for predicting the coefficient of earth pressure at rest. This comparison is made in Fig. 5.1.13. The value of was taken for 5 p.s.i. confining pressure in the triaxial tests. Value of ϕ at relative densities of 90, 73, 62 and 58 per cent were equal to 40.7, 37.3, 35.5 and 34.9 degrees respectively.

5.2 Analysis of Test Data

In this section the triaxial test data are analyzed with the help of the theory of elasticity. Values of shear displacements are calculated from the theory of elasticity as well as conventional methods for determining the shear displacements. No attempts have been made to show the derivation of the expressions involved.

For the direct shear box test, shear displacement and shear stress have been obtained directly from the test data.

5.2.1 Triaxial Tests

In the triaxial tests all the samples failed by increasing in diameter, more or less uniformly from top to bottom. In the conventional method of analysis, it is assumed that throughout the test of the sample, the shear displacement takes place along a plane inclined at an angle of $(45+\phi/2)$ with the plane of the major principal stress. The shear displacement along this plane is obtained by dividing the vertical deformation by Sin $(45+\phi/2)$. The value of shear

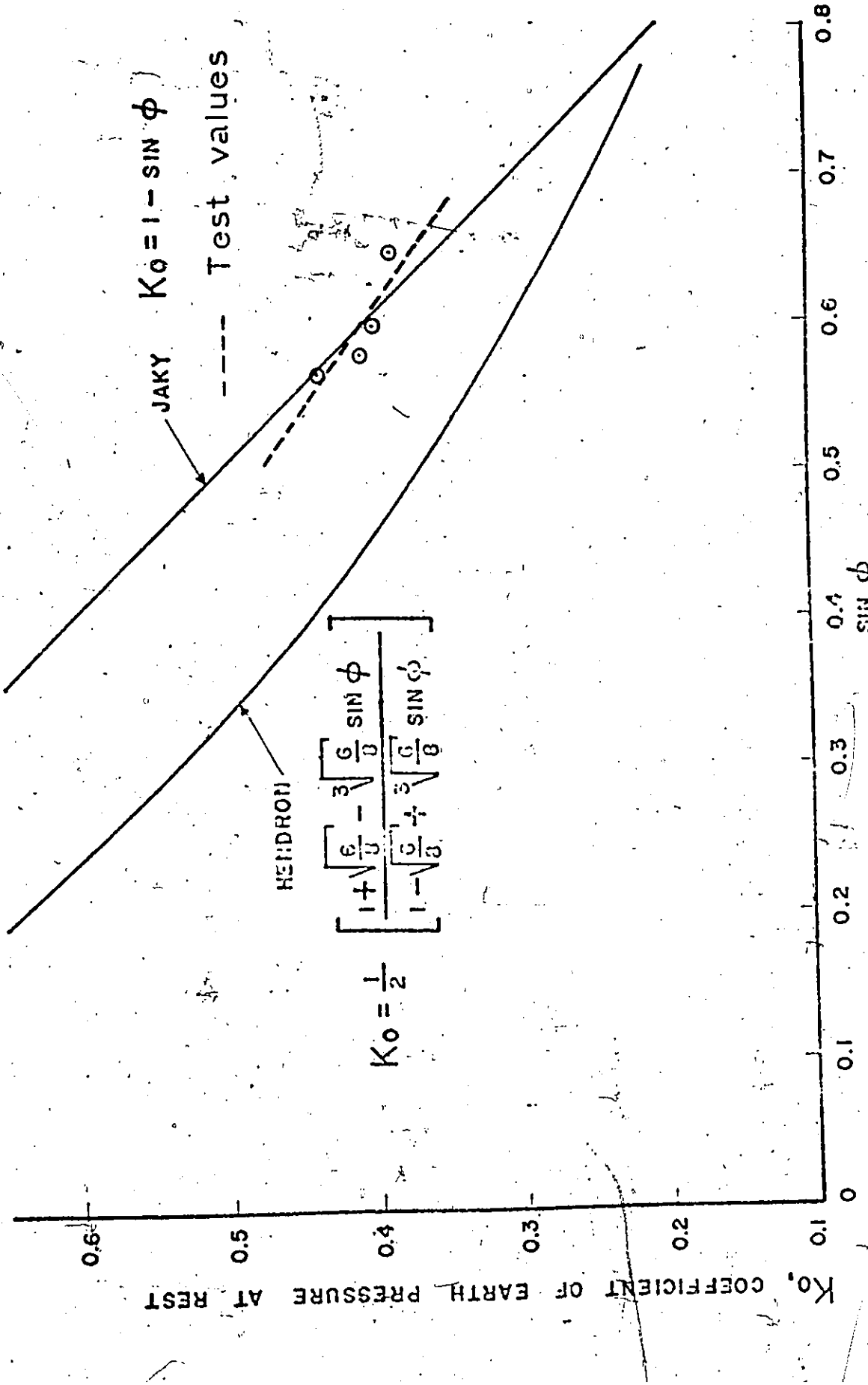

FIG. 5.1.13 VARIATION OF KO WITH Sin ϕ

stress is obtained by the expression $(\frac{\sigma_1-\sigma_3}{2})$ Cos ϕ, where $\sigma_1-\sigma_3$ is the deviator stress.

If an approach based on the theory of elasticity is followed, it can be said that

$$\varepsilon_1 + \varepsilon_2 + \varepsilon_3 = \Delta v/v \qquad (5.2)$$

since $\varepsilon_2 = \varepsilon_3$ in a triaxial test then

$$\varepsilon_1 + 2\varepsilon_3 = \Delta v/v \qquad (5.3)$$

Where the compression is negative while expansion is positive. The increase in volume is considered to be positive.

The shear strain based on a unit length is given by the expression

$$\gamma xy = [(\varepsilon_1 + \varepsilon_3) \text{ Sin } (90^o + \phi)] \qquad (5.4)$$

Here ε_1 and ε_3 both will be positive for a maximum value.

The change in the length of the diagonal at any instant is given by the expression

$$\text{CHANGE IN DIAGONAL} = \frac{1}{\sqrt{2}} \text{Cos}(\pi/2+\gamma xy) = -\frac{1}{\sqrt{2}} \text{Sin } \gamma xy \qquad (5.5)$$

where γxy is in radians. This has to be multiplied by 57.3 to get the value of the angle in degrees. In order to determine the total deformation the change in length given by Equation 5.4 has to be multiplied by the length of the failure plane.

Two approaches can be adopted for determining the length of the failure plane. For the sake of easy comparison

the original length of the sample is taken. The length of the failure plane shall be equal to the diameter divided by Sin $(45-\phi/2)$ or the height divided by Sin $(45+\phi/2)$. The smaller of the two values has been taken. Results obtained for shear displacement are the same using Mohr's circle of strain.

Tables 5.2.1 to 5.2.3 show the shear deformation following the conventional approach as well as the approach based on the theory of elasticity. It can be seen that for test 10 the difference between the two shear deformations at failure is +0.02 inches. This difference for tests 8 and 14 is +0.05 inches and +0.07 inches respectively. The positive sign indicates that the conventional shear deformation is greater than the shear deformation based on the elastic approach.

The conventional approach is adopted because this is straightforward and simple to use. Figures 5.2.1 to 5.2.3 show the shear deformation versus shear stress plots for triaxial tests, for very dense, dense and medium dense sand.

In Fig. 5.2.1 for very dense sand sample, test 10 has been carried out at 5 p.s.i. confining pressure, whereas test 8, 6 and 7 have been carried out at 25, 50 and 80 p.s.i. confining pressure respectively. It may be noted that the shear displacement to failure and the shear stress to failure increases as the confining pressures are increased. The shear stress decreases considerably after reaching the

Test 10 (T.C.)
ϕ= 41.5°, Cos (45-ϕ/2) = 0.9118, Cos ϕ = 0.7490, D_r = 92.4%, σ_3 = 5 psi, Sin(90+ϕ) x 57.3 = Cos ϕx57.3 = .749x57.3 = 43
Length of failure plane = 3.9/Sin (45-ϕ/2) = 9.5 or 7.9/Sin (45+ϕ/2) = 8.6 inches

ε_1	$\Delta v/v$	Deformation x - inch (10^{-3})	ε_3	$\varepsilon_1+\varepsilon_3$	$\frac{x}{0.9118}$	[Sin(90+ϕ)x57.3] x($\varepsilon_1+\varepsilon_3$) = γ_{xy}	Change/ Unit Length = $\frac{1}{\sqrt{2}}$ Sinγ_{xy}	$\tau=(\frac{\sigma_1-\sigma_3}{2})Cos\phi$	Shear Def. 8.6x$\frac{1}{\sqrt{2}}$Sinγ_{xy}	Remarks
0.005	.000	40	0.002	0.007	0.04	0.3	0.004	3.98	0.03	Difference in shear deformation at failure = 0.02"
0.015	+.007	120	0.011	0.026	0.13	1.12	0.013	6.41	0.11	
0.025	+.015	200	0.020	0.045	0.22	1.93	0.023	7.34	0.20	
0.035	+.024	280	0.030	0.065	0.31	2.8	0.034	6.81	0.29	
0.055	+.042	440	0.048	0.103	0.48	4.4	0.054	7.30	0.46	Failure
0.075	+.056	600	0.066	0.141	0.66	6.1	0.075	7.10	0.64	
0.085	+.064	680	0.074	0.159	0.75	6.8	0.084	7.10	0.72	
0.10	+.074	800	0.087	0.187	0.88	8.0	0.098	6.00	0.84	

TABLE 5.2.1

CALCULATION OF SHEAR DISPLACEMENTS

Test 8
$\phi = 41.0^{\circ}$, $\cos(45-\phi/2) = 0.9100$, $\cos\phi = 0.7547$, $D_r = 92.6\%$, $\sigma_3 = 5$ p.s.i., $\varepsilon_3 = (\varepsilon_1 + \Delta v/v)/2$
$\sin(90+\phi)$ 57.3 = 43.3, Length of failure plane = 7.9/$\sin(45+\phi/2)$ = 8.6 inches.

ε_1	$\Delta v/v$	Deformation x - inch (10^{-3})	ε_3	$\varepsilon_1+\varepsilon_3$	$\frac{x}{0.9100}$	$[\sin(90+\phi)\times 57.3]$ $(\varepsilon_1+\varepsilon_3) = \gamma_{xy}$ degrees	Change/ Unit Length $= \frac{1}{\sqrt{2}}\sin\gamma_{xy}$	$\tau=(\frac{\sigma_1-\sigma_3}{2})\cos\phi$ = p.s.i.	Shear Def. $8.6\times\frac{1}{2}\sin\gamma_{xy}$	Remarks
.01	-.002	80	.004	.014	0.08	0.60	.007	23.0	.06	Difference in shear deformation at failure = +.05"
.02	+.003	160	.011	.031	0.17	1.34	.016	30.3	.14	
.03	+.008	240	.019	.049	0.26	2.12	.026	33.3	.22	
.04	+.015	320	.028	.068	0.35	2.94	.035	34.3	.30	
.06	+.029	480	.044	.104	0.52	4.50	.055	35.7	.47	
.07	+.034	560	.052	.122	0.61	5.30	.065	35.9	.56	Failure
.08	+.041	640	.060	.140	0.70	6.06	.075	35.6	.64	
.09	+.048	720	.069	.159	0.79	6.90	.085	35.2	.73	
.12	+.060	960	.090	.21	1.05	9.10	.112	33.3	.96	

TABLE 5.2.2

CALCULATION OF SHEAR DISPLACEMENT

Test 14

ϕ = 37.3, Cos(45-ϕ/2) = 0.8960, Cosϕ = 0.7955, D_r = 70.4%, σ_3 = 25 p.s.i.,
Sin(90+ϕ) x 57.3 = 45.5
Length = 7.9/Sin(45+ϕ/2) = 8.8 inches

ϵ_1	$\Delta v/v$	Deformation x - inch $(10)^{-3}$	ϵ_3	$\epsilon_1+\epsilon_3$	$\frac{x}{.896}$	$[\text{Sin}(90+\phi)\times 57.3] = (\epsilon_1+\epsilon_3) = \gamma xy$	Change/ Unit Length $= \frac{1}{\sqrt{2}} \text{Sin}\gamma xy$	$\tau = (\frac{\sigma_1-\sigma_3}{2})\text{Cos}\phi$ p.s.i.	Shear Def. $8.8 \times \frac{1}{\sqrt{2}} \text{Sin}\gamma xy$	Remarks
.01	-.003	80	.003	.013	.089	0.59	.0074	18.1	.065	Difference in shear deformation equals 0.07 inches at failure
.025	-.002	200	.011	.036	.223	1.64	.0198	25.5	.174	
.04	+.001	320	.02	.06	.36	2.73	.033	28.3	.29	
.056	+.005	440	.03	.086	.49	3.91	.048	29.7	.43	
.076	+.011	600	.044	.120	.67	5.5	.068	30.5	.60	Failure
.086	+.014	680	.050	.136	.76	6.2	.076	30.5	.67	
.106	+.018	800	.062	.168	.89	7.65	.093	29.7	.82	
.116	+.022	920	.069	.185	1.02	8.42	.103	29.2	.91	
.122	+.023	960	.072	.195	1.07	8.84	.108	28.9	.95	

TABLE 5.2.3

CALCULATION OF SHEAR DISPLACEMENT

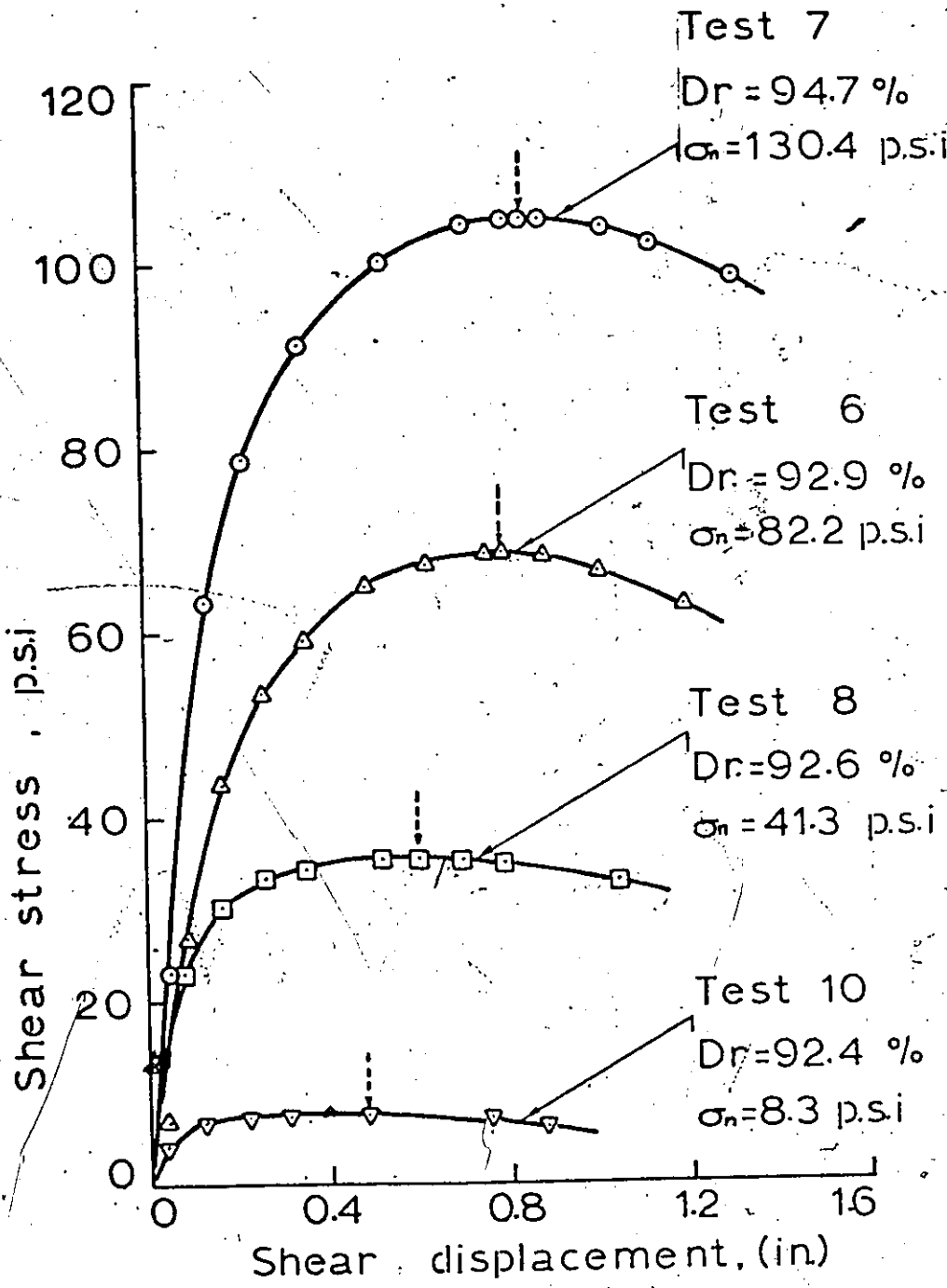

FIG. 5.2.1 SHEAR STRESS VERSUS SHEAR DISPLACEMENT CURVES (TRIAXIAL COMPRESSION)

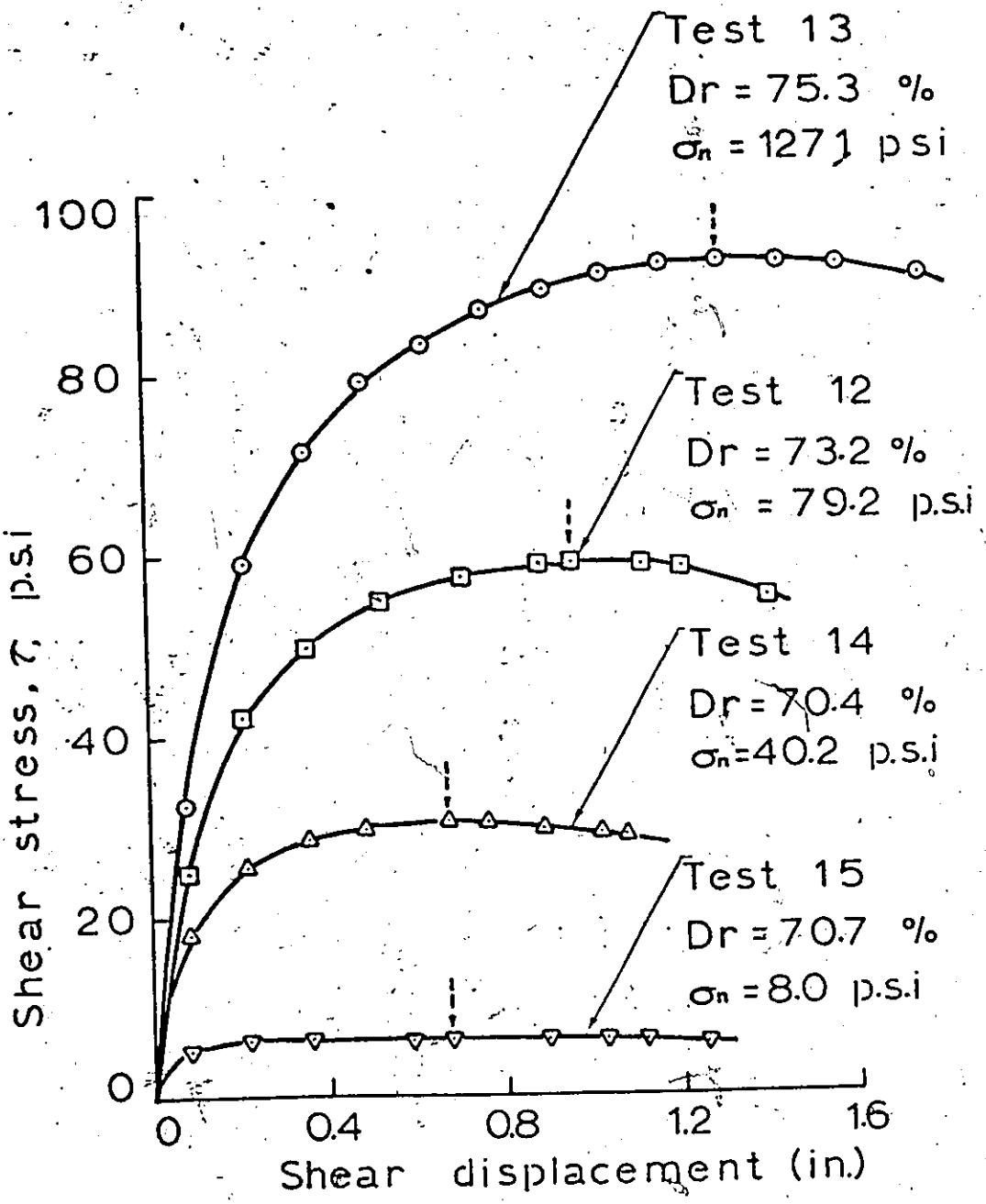

FIG. 5.2.2 SHEAR STRESS VERSUS SHEAR DISPLACEMENT CURVES (TRIAXIAL COMPRESSION)

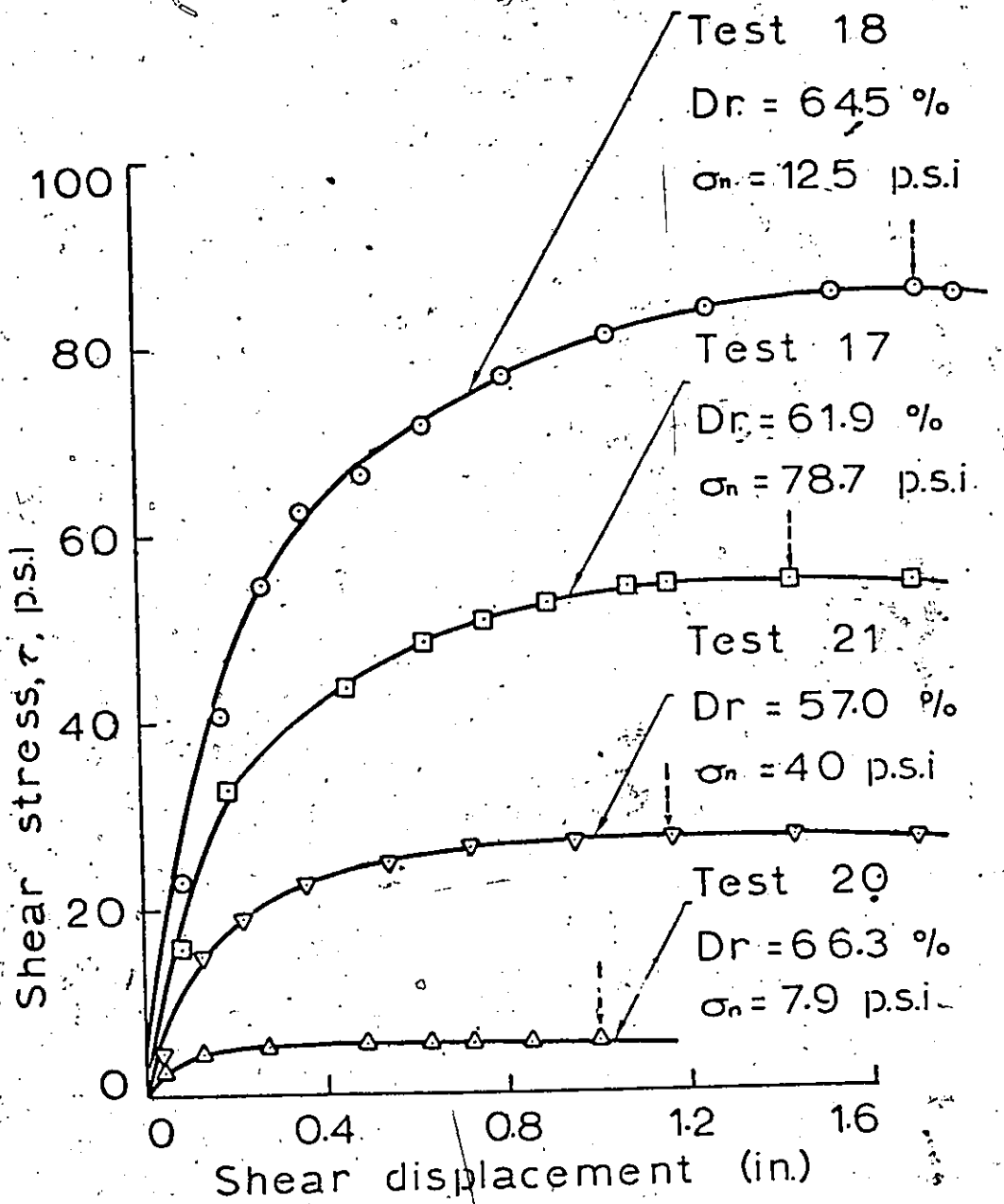

FIG. 5.2.3 SHEAR STRESS VERSUS SHEAR DISPLACEMENT (TRIAXIAL COMPRESSION)

peak as the shear deformation continues to increase. The trends in Fig. 5.2.2 for dense sands are similar. Only the extent of shear deformation corresponding to the shear stress at failure has increased and the extent of the drop in the value of the shear stress after reaching the peak value has decreased. Fig. 5.2.3 for medium dense sand indicates increased shear displacement for the shear stress to reach a maximum value. There is hardly any discernable drop in the value of the shear stress past the peak value. Here also the shear stress to failure and shear displacements to failure increase as the confining pressures are increased.

These phenomena can be explained from the concept of shear strength at constant volume. If a triaxial test is run in such a way that the volume remains constant and the volume of the sample is monitored and the confining pressure is adjusted to hold this volume constant then for a dense sand the confining pressure will have to be increased considerably. This means that a dense sand which has been held under a constant volume can sustain a much greater axial stress than a specimen which has been held under a constant confining pressure and is allowed to expand during shear. In the case of a very loose specimen under constant volume, the confining pressure may have to be decreased as the test progresses, and consequently the compressive strength is decreased.

Hence in a triaxial test, if a dense sand has to fail in shear, the high degree of interlocking must somehow be overcome. This can be accomplished either (a) by shearing and fracturing of the particles or (b) by increasing the volume. If the soil is free to dilate, the path of least resistance is to expand and overcome interlocking before failure takes place.

In a conventional triaxial test during continuous straining both the deviator stress and the void ratio achieve values that are independent of the initial void ratio. At this condition the sand strains without further volume change and with constant deviator stress.

Taking now a look at Fig. 5.2.3 for test 20, 21, 17 and 18 for medium dense sand and corresponding stress-studies plots of Figs. 4.2.9 to 4.2.12 it is observed that the rate of volume change for these tests was very small as the shear displacements were increased. This phenomena suggests that the value of ϕ in the above cases had reached close to ϕ_{cv} as defined by Casagrande. Hence the Fig. 5.2.3 for medium dense sand indicates an almost constant value of shear stress past the peak value. In the above tests the value of ϕ ranged from 35.5 to 34.5 degrees. These values were close to the ϕ_{cv} value of 36 degrees as defined by Lee and Seed.

For dense sand the ratio of volume change is highest for 5 p.s.i. confining pressure, because of a small mean normal stress. Hence for a small shear displacement the

entire shear stress is mobilized. As the confining pressure is increased the mean normal stress increases, the rate of volume change decreases, and it takes large amounts of shear displacement before the sample fails. This is evident from Fig. 5.2.1 for very dense sand giving the relationship between shear stress and shear displacement.

At large confining pressures the interlocking decreases as a result of crushing of the partitles. Decrease in interlocking again means greater shear displacement before the failure occurs, where interlocking is negligible shear displacement almost amounts to sliding on a plane surface. Large displacements precede failure in such cases. The reverse is true for cases where interlocking is highest.

5.2.1.1 Secant Modulus

In the series of triaxial tests, the secant modulus at half the deviator stress at failure was determined for each stress-strain curve.

Table 5.2.4 indicates the variation of E_s with relative density and confining pressure. In the first set of values for very dense sands it will be seen that E_s at one half of the peak strength is 0.45 for a confining pressure of 5 p.s.i. The values of E_s being equal to 2180 p.s.i. As the confining pressure is increased, the strain at one half of the peak also increases. The value of E_s, the modulus

Test	Relative Density D_r %	σ_3 p.s.i.	Axial Strain ε at 1/2 peak %	Deviator Stress $(\sigma_1-\sigma_3)$ p.s.i. 1/2 peak	Secant Modulus E_s p.s.i.
10	92.4	5	0.45	9.8	$\frac{9.8}{.45}$ x100 - 2180 psi
8	92.6	25	0.80	47.6	$\frac{47.6}{.80}$ x 100 = 5950
6	92.9	50	1.3	90.2	$\frac{90.2}{1.3}$ x 100 = 6950
7	94.7	80	1.3	135.8	$\frac{135.8}{1.3}$ x 100 = 10450
15	70.7	5	0.4	7.65	$\frac{7.65}{0.4}$ x 100 = 1910
14	70.4	25	0.8	38.35	$\frac{38.35}{0.8}$ x 100 = 4800
12	73.3	50	1.3	74.5	$\frac{74.5}{1.3}$ x 100 = 5720
13	75.3	80	1.7	115.0	$\frac{115.0}{1.7}$ x 100 = 6760
20	66.3	5	0.75	6.9	$\frac{6.9}{0.75}$ x 100 = 9201
21	57.0	25	1.40	33.95	$\frac{33.95}{1.40}$ x 100 = 2420
17	61.9	50	1.8	67.55	$\frac{67.55}{1.8}$ x 100 = 3750
18	64.5	80	2.3	104.9	$\frac{104.9}{2.3}$ x 100 = 4560

TABLE 5.2.4

CALCULATION OF SECANT MODULUS E_s, AT ONE-HALF THE PEAK STRESS

also increases. However, for test 7 where the relative density is a bit high ε at half the peak has not increased too much but the secant modulus has increased considerably. The value of E_s at 80 p.s.i. of confining pressure is almost five times the value at 5 p.s.i. confining pressure for the same density.

Considering the second set of values of E_s, it can be noted that E at half the peak has generally increased, and the corresponding value of the deviator stress has also decreased. The third set of results for the medium dense sand samples also shows the same trend.

This suggests that the value of the secant modulus is highest for the largest relative density and maximum confining pressure within the range investigated.

The value of E_s decreases as the relative density decreases. Figure 5.2.4 shows the variation of Secant Modulus with relative density and confining pressure.

5.2.1.2 Strain Contours

The stress points of the stress paths were drawn for the different triaxial tests, at various relative densities. Figures 5.2.5 to 5.2.7 represent the stress paths for the very dense, dense and medium dense sands, respectively. Strains were indicated on the plots for different tests at approximately the same relative density. Lines were then drawn to join the points on the stress paths having the same strain.

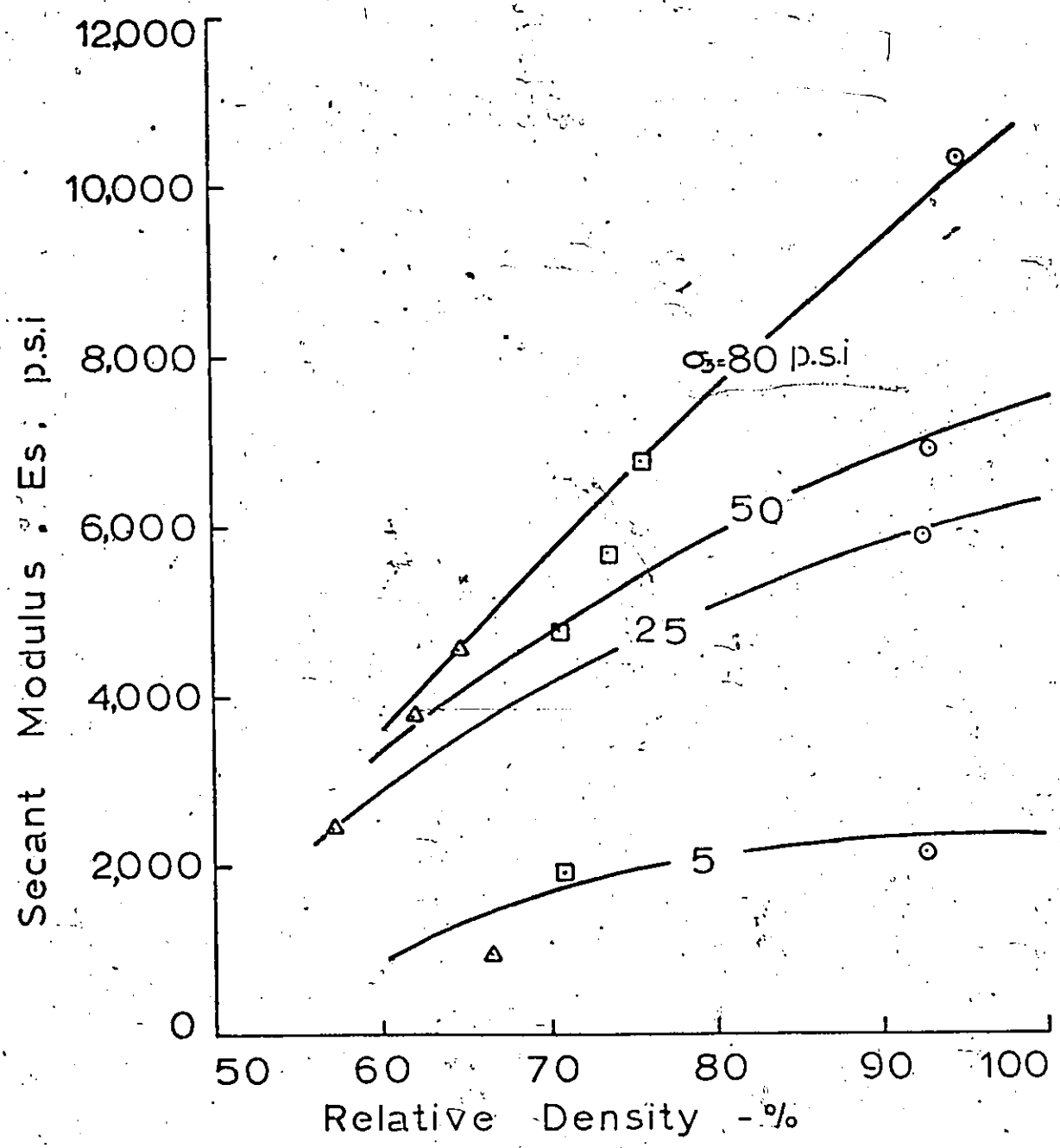

FIG. 5.2.4 VARIATION OF SECANT MODULUS AT 1/2 PEAK WITH RELATIVE DENSITY AND CONFINING PRESSURE

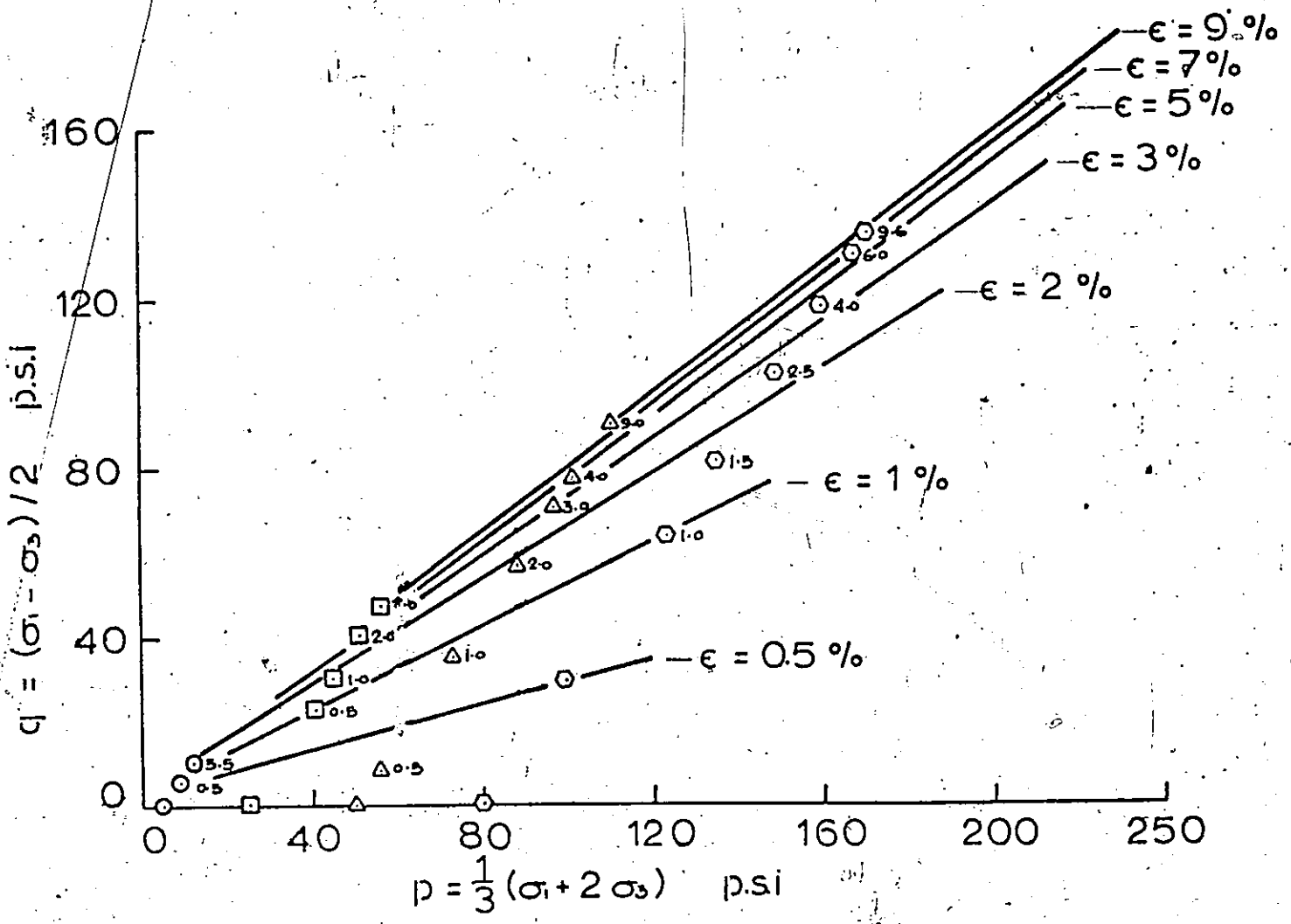

FIG. 5.2.5 AXIAL STRAIN CONTOURS FOR VERY DENSE SAND - AV. REL. DENSITY 92 PER CENT

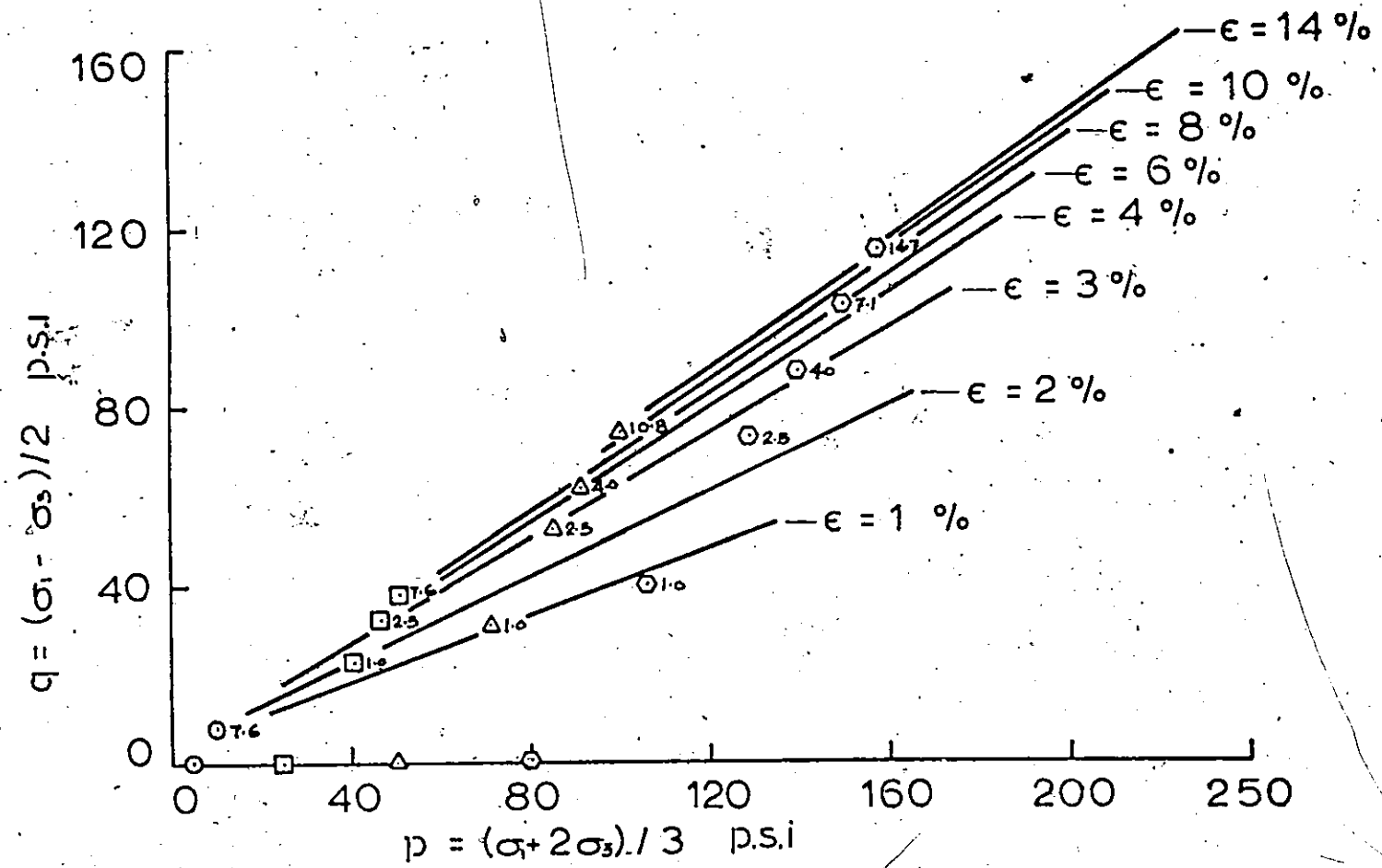

FIG. 5.2.6 AXIAL STRAIN CONTOURS FOR DENSE SAND
RELATIVE DENSITY 72%

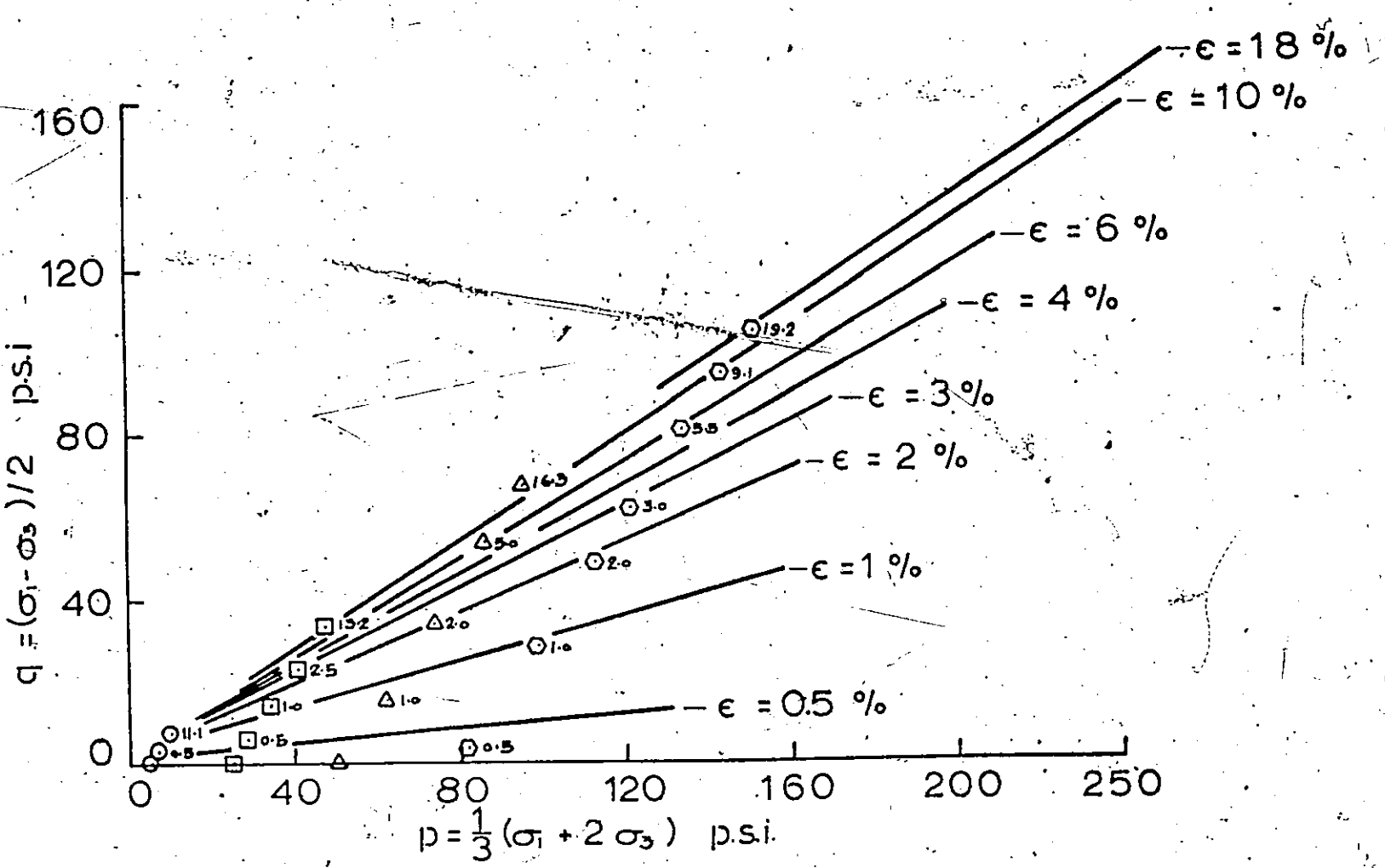

FIG. 5.2.7 AXIAL STRAIN CONTOURS FOR MEDIUM DENSE SAND
AV. REL. DENSITY 62 PER CENT

As can be seen, the last line joining the points at failure (peak stress) for each stress path will represent the strains at failure which can be called the failure line.

From the graphs it is evident that for the same relative density the strain at failure is smallest for the smallest mean stress and highest for the highest mean stress.

The strain contours tend to converge at the origin.

As the relative density decreases the strain to failure increases as evidenced from Figs. 5.2.6 to 5.2.7. The maximum peak strain for a relative density of 92 per cent is 9.6 per cent, at 80 p.s.i. of confining pressure. The corresponding strains at failure for relative densities of 72 and 62 per cent are 14.7 and 19.2 respectively.

The stress path can also be used to predict strains if the relative density of the sand and the stress range are known.

5.2.1.3. Relationship between Shear Stress and Shear Displacement for Triaxial Tests

It was desired to determine and predict the shear stress with shear displacement for a range of relative densities and normal stresses. In Fig. 5.2.8 the shear stresses versus the shear strains have been plotted for different normal stresses and relative densities for the triaxial compression test data.

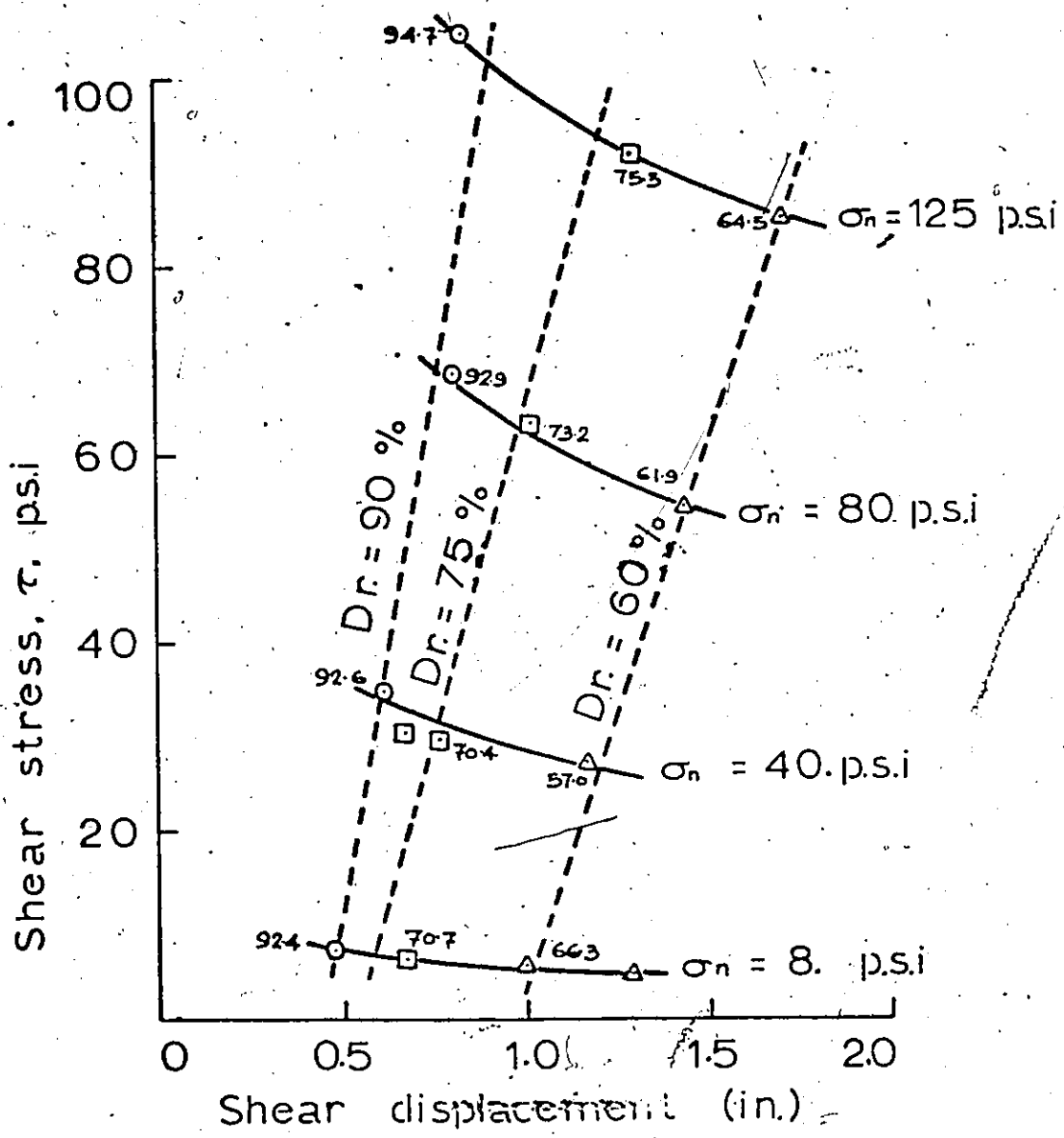

FIG. 5.2.8 VARIATION OF SHEAR STRESS AND SHEAR DISPLACEMENT WITH RELATIVE DENSITY AND NORMAL STRESS IN TRIAXIAL COMPRESSION

As can be expected for a given relative density the shear stress is lowest for the lowest normal stress and increases as the normal stress is increased. The shear displacement however, also increases as the normal stresses are increased. The difference in the shear stress is not very marked at low normal stresses as the relative density is varied.

The difference in the shear stress for the same range of relative density however increases as the normal stress is increased. These findings are a corollary to the observations illustrated in the stress path plots in the foregoing section. Figure 5.2.8 can therefore be used to predict the shear stress developed in the soil for a given shear displacement, relative density and normal stress.

5.2.2 Shear Stress versus Shear Displacement for Direct Shear Box Tests

In order to relate the shear displacement with the shear stress in direct shear, Figs. 5.2.9 to 5.2.11 were drawn for very dense, dense and medium dense sand samples respectively. It should be noted from Fig. 5.2.9 that the shear displacement and shear stress to failure increase as the normal stresses acting on the samples are increased. There is a sharp drop in the value of shear stress past the peak. From Fig. 5.2.10 for dense sand samples it will be seen that the shear displacement to failure increases

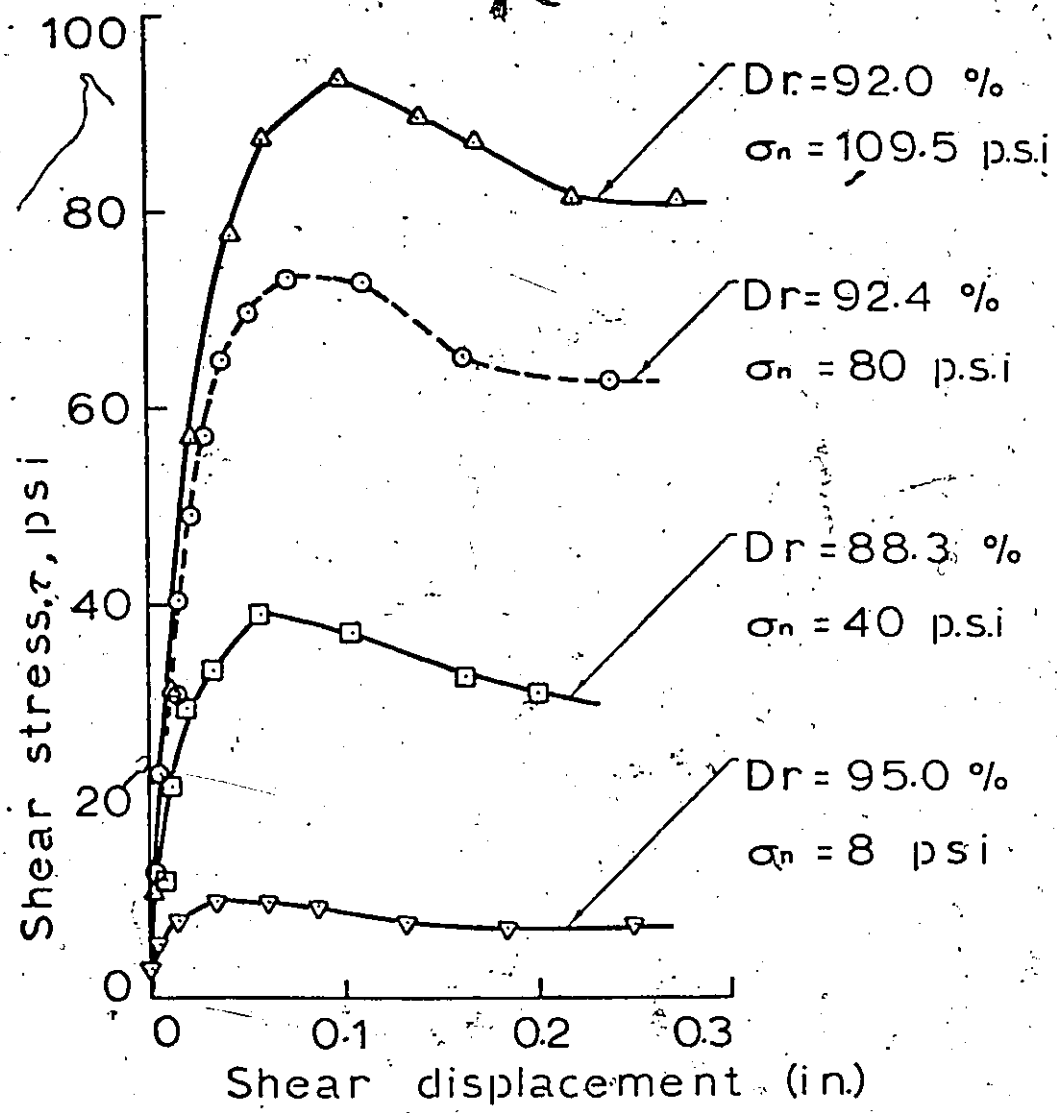

FIG. 5.2.9 SHEAR STRESS VERSUS SHEAR DISPLACEMENT (DIRECT SHEAR)

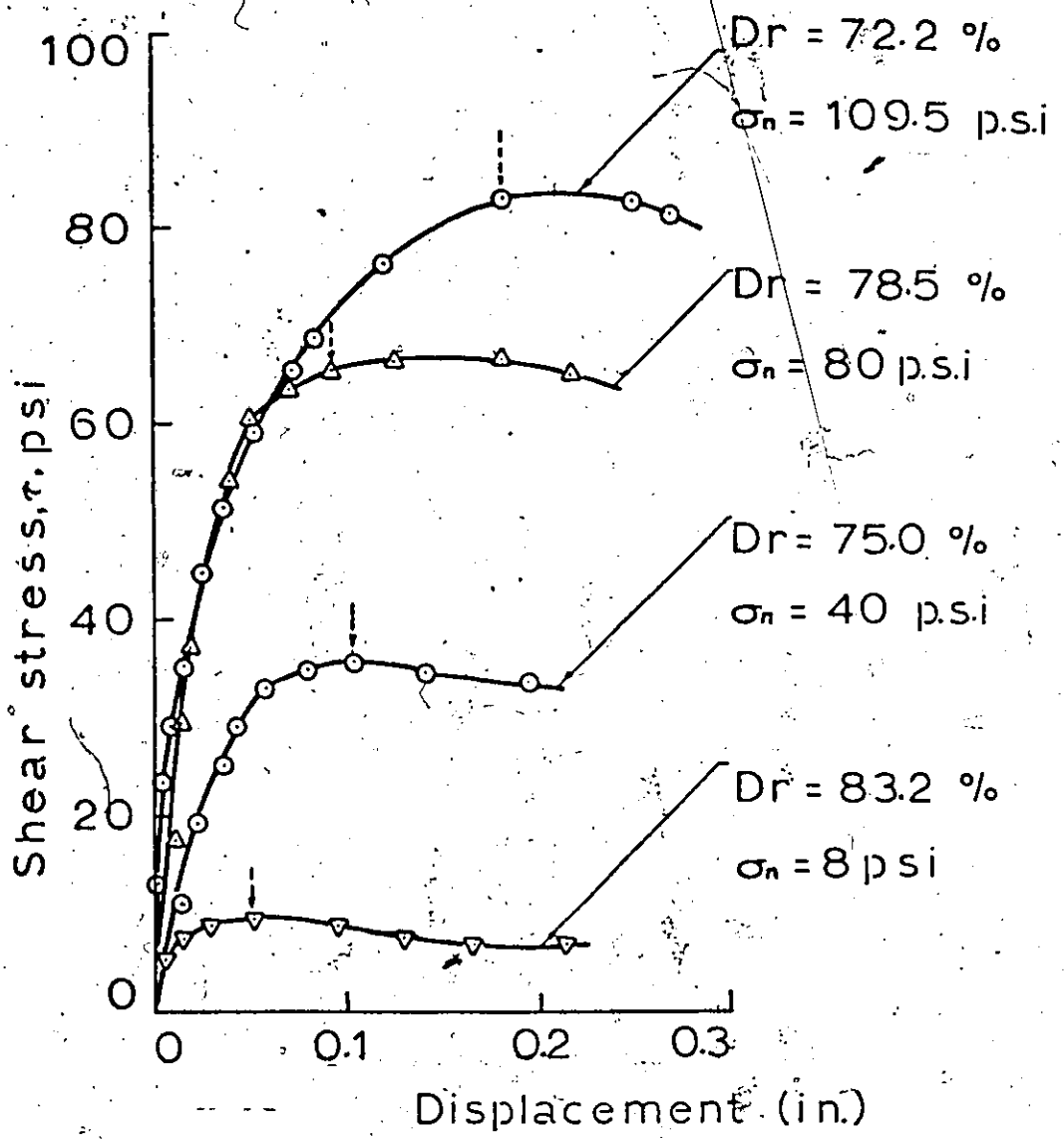

FIG. 5.2.10 SHEAR STRESS VERSUS SHEAR DISPLACEMENT (DIRECT SHEAR)

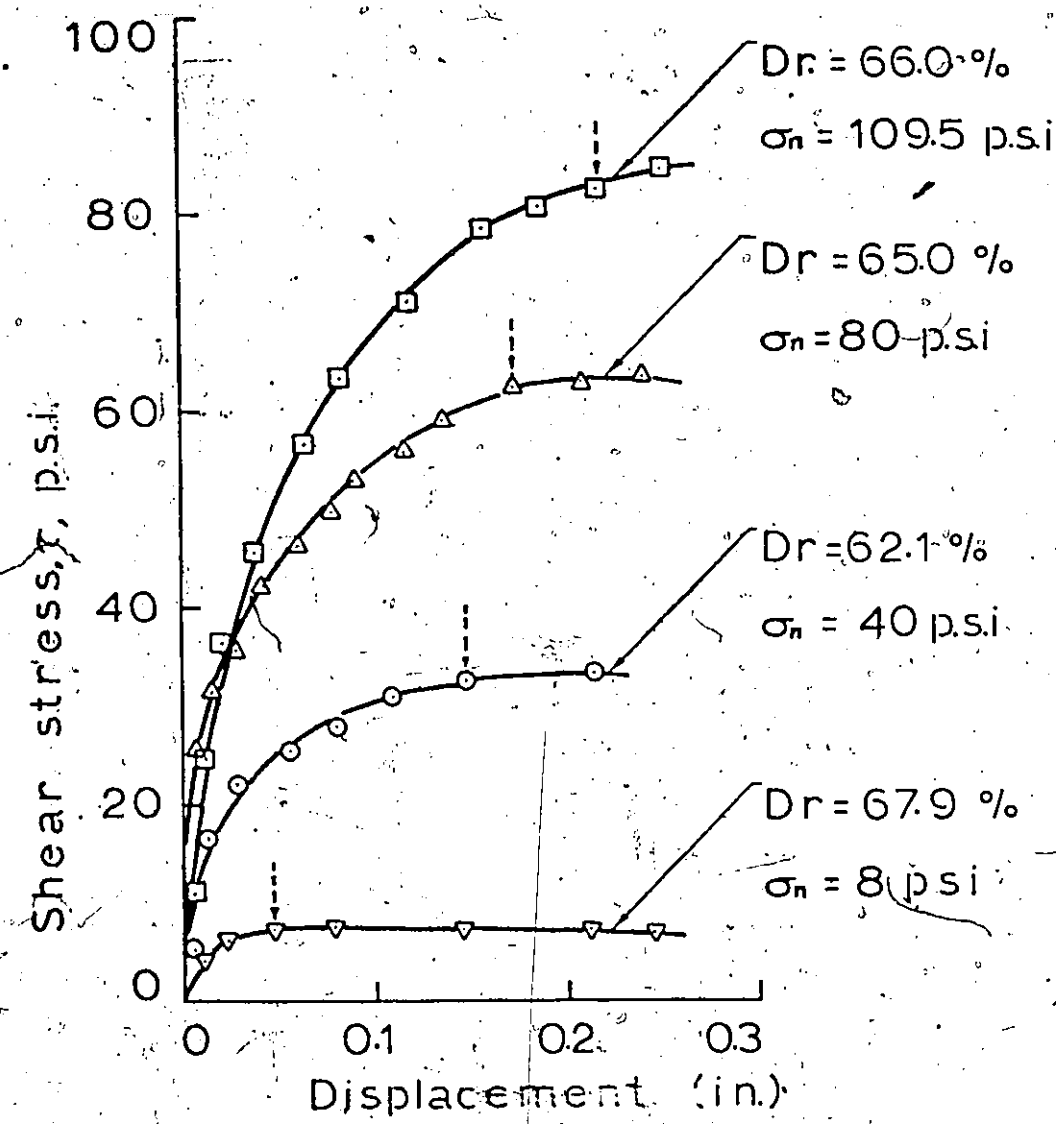

FIG. 5.2.11 SHEAR STRESS VERSUS SHEAR DISPLACEMENT (DIRECT SHEAR)

in proportion to the value of the applied normal stress for very dense sand samples. The drop in the value of shear stress past the peak varies inversely with the level of the applied normal stress. For medium dense sand samples represented in Fig. 5.2.11 the displacements to failure have increased further compared to corresponding normal stresses for dense and very dense sand samples. However, for low normal stress of about 8 p.s.i. there does not appear to be any appreciable change in the value of shear displacement to failure with increasing normal stress. For medium dense sand samples the shear stress continues to increase past the peak as defined earlier for determining the value of ϕ for direct shear box tests.

In order to predict the shear stress with shear displacement under various conditions to normal stress and relative density, Fig. 5.2.12 was drawn for the sand undergoing direct shear. This figure is very similar to Fig. 5.2. for triaxial compression.

A comparison with Fig. 5.2.8 reveals that for comparable shear stress the shear displacements are much smaller in direct shear. This difference is due to different strain conditions existing in the two types of tests.

5.3 Factors Influencing the Test Results

The discussion of the factors influencing the test results will be divided into the following subsections.

1. Triaxial consolidated-drained compression test results, and

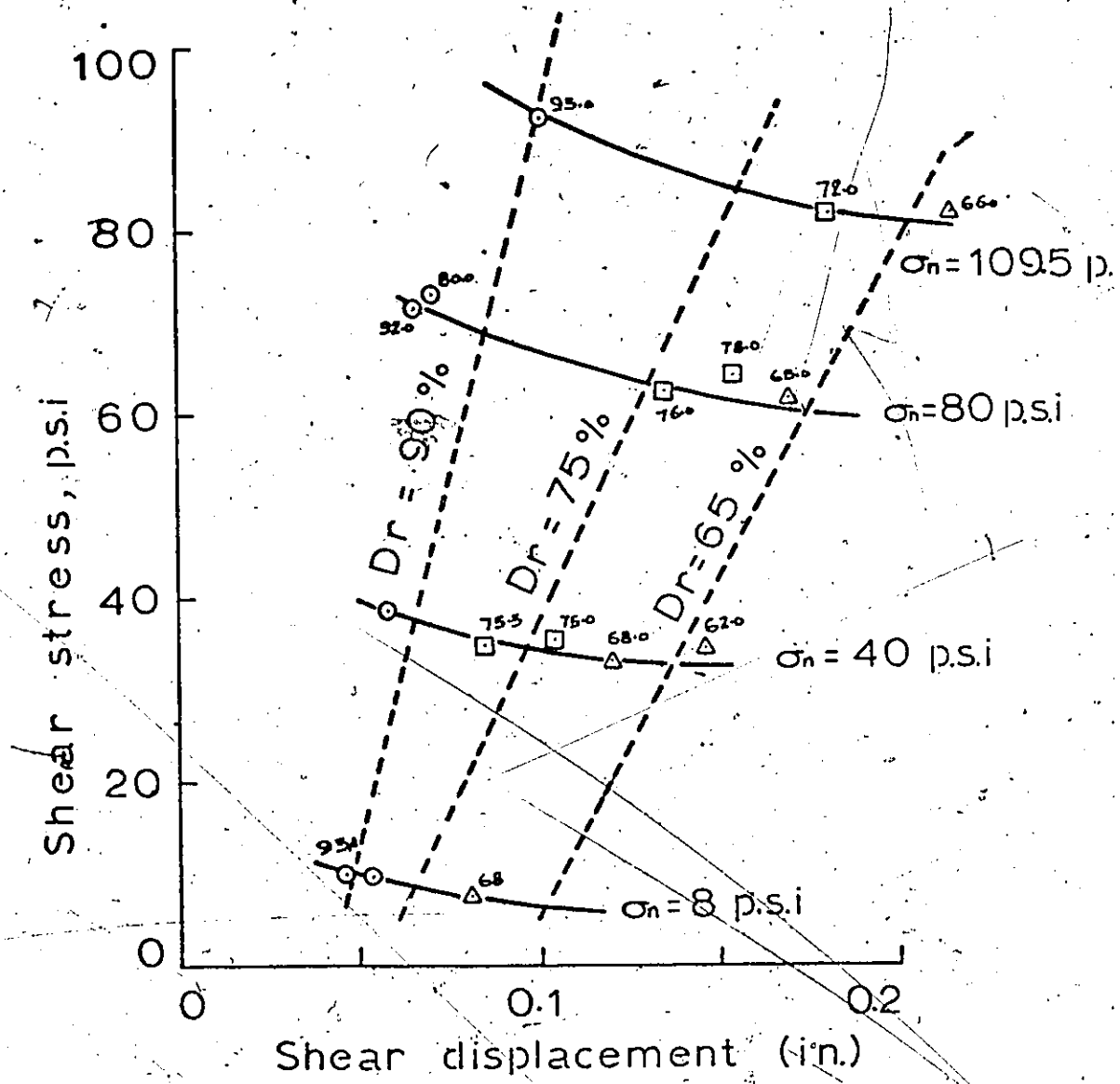

FIG. 5.2.12 VARIATION OF SHEAR STRESS AND SHEAR DISPLACEMENT WITH RELATIVE DENSITY AND NORMAL STRESS IN DIRECT SHEAR

2. Direct shear box test results.

5.3.1 Triaxial Consolidated-Drained Compression Tests

Effect of density

In Figs. 4.2.3, 4.2.7 and 4.2.11, the results from typical triaxial compression tests at a constant cell pressure of 50 p.s.i. were shown as deviator stress, stress ratio and volumetric strain versus axial strain plots. These three figures represent the results of tests on very dense, dense and medium dense sand samples with void ratios of 0.65, 0.75 and 0.81 respectively. As can be seen from the curves the densest sample shows the largest maximum stress ratio which occurs at the smallest axial strain and the greatest dilation and therefore exhibiting a net volume increase; while the loosest sample showed the lowest stress ratio occurring at the largest axial strain and showing a net volume decrease. Thus the densest sample gives the highest ϕ value and loosest sample gives the lowest angle of internal friction ϕ under a constant cell pressure.

Effect of confining pressure

The results from typical triaxial compression test at varying confining pressures were given in Figs. 4.2.1 to 4.2.4 for deviator stress, stress ratio and volumetric strain versus axial strain graphs. The tests were carried out at a constant relative density of about 92 per cent and varying confining pressures of 5, 25, 50 and 80 p.s.i. with void

ratios of 0.65, 0.65, 0.65 and 0.64 respectively. It should be noted that the stress ratios were greatest for 5 p.s.i. confining pressure and smallest for 80 p.s.i. confining pressure. The axial strain at failure were lowest for 5 p.s.i. and highest for 80 p.s.i.; even though the void ratio of 0.64 for 80 p.s.i. confining pressure was lower than the other void ratio in the series.

Effect of grain size

The average grain size D_{50} in this test series was about 0.6 mm. For quartz the value of ϕ_μ would be 24 degrees according to Rowe (1962). The value of ϕ_{cv} as found from the triaxial tests was about 36 degrees as is evident from Fig. 5.1.1(a).

Using Bishop's empirical formula

$$\text{Sin}\phi_{cv} = \frac{15 \tan \phi_\mu}{10 + 3 \tan \phi_\mu} \qquad (2.30)$$

$$\therefore \quad \text{Sin } 36^\circ = \frac{15 \tan \phi_\mu}{10 + 3 \tan \phi_\mu} = 0.587$$

$$\therefore \quad \phi_\mu = 23.9^\circ$$

Hence we can say that the value of ϕ_μ for the sand used in the test series was 24 degrees, in agreement with Rowe.

It has been shown by Leslie (1963) that the value of ϕ increases with decrease in average particle size for the same value of uniformity coefficient. For small variations in particle size these differences were not marked.

Since the present test series was conducted on the same sand; this effect could not be ascertained.

Effect of angularity and grading

Table 5.3.1 (after Sowers and Sowers, 1970) gives the values of ϕ for sands in loose and dense states, based on particle shape and grading.

From this table it can be seen that well graded and angular particles would interlock more thoroughly amongst themselves and would give a rise to higher friction angles.

In the present case the sand was angular and uniform and the table for the value of ϕ fits very closely to the values of ϕ obtained from the triaxial tests. Using Sowers table, the value of ϕ should lie between 35 and 43 degrees.

Mineral composition

The sand used in the test series and in the sand box is basically crushed quartz with a ϕ_μ of 24 degrees and ϕ_{cv} equal to 36 degrees. There was good interlocking between the sand particles which gave high ϕ values.

The chemical analysis of the sand was carried out by the Department of Geology at the University of Ottawa and is given below.

"99.5 per cent of the sample of sand consisted of angular particles of quartz. Most of them were single crystals, others were aggregates of two or more crystals. Most were pure quartz. Some contained tiny inclusions of black magnetite.

Shape and Grading	Loose	Dense
Rounded; Uniform	30	37
Rounded; Well graded	34	40
Angular; Uniform	35	43
Angular; Well graded	39	45

TABLE 5.3.1

EFFECT OF SHAPE AND GRADING ON THE VALUE OF ϕ (AFTER SOWERS AND SOWERS, 1970)

0.5 per cent of the particles consisted of various rock and minerals including:

a) Muscovite mica.

b) Black magnetite together with small amounts of quartz or other minerals.

c) Powdery white rounded particles consisting of a very fine aggregate or serpentine (not confirmed).

d) Greenish rounded particles of rock, crystals of plagioclase feldspar, hornblende or some other iron magnesium minerals and magnetite.

e) Yellowish brown to red brown particles which are aggregate of rutile (not confirmed).

f) Foreign particles including wood, and a small disc shaped particle of plastic or other synthetic material."

From the engineering point of view it can be concluded that the sand consisted of crushed, angular, uniformly graded quartz particles.

Interlocking

It has been shown by Rowe (1962) that

$$\sigma_1'/\sigma_3' = \tan \alpha \tan (45^\circ + \tfrac{1}{2} \phi f) \qquad (5.1)$$

where $$\tan \alpha = \left| \frac{\sigma_1'}{\sigma_3'} \left(1 + \frac{dv}{d\varepsilon_1}\right) \right|^{1/2} \qquad (2.25)$$

Here dv is positive for an increase in volumetric strain; that is the soil is dilating; and α is the packing parameter.

From the test result presented it can be seen that an increase in confining pressure decreased the interlocking effect due to grain crushing at contact points. This resulted in a lower friction angle.

A sample calculation for α for the tests represented in Figs. 4.2.1 to 4.2.4 is given below. The value of α varies continuously throughout the test. Here the value of α at failure were calculated from the data presented in Fig. 4.2.1 for a confining pressure of 5 p.s.i.

$$\tan \alpha = [4.92 \ (1 + \frac{D_{.D42}}{0.055})]^{1/2}$$

$$= [4.92 \ (1.76)]^{1/2}$$

$$= 2.94$$

Therefore α = 71.2 degrees.

Similarly for a confining pressure of 25 p.s.i. (Fig. 4.2.2), the value of α was found to be 69.5 degrees. In Figs. 4.2.3 and 4.2.4 tests carried out at confining pressure of 50 and 80 p.s.i. the values of α were calculated to be equal to 67.2 and 66.1 degrees respectively.

Therefore the difference between the values of α for confining pressure of 5 p.s.i. and confining pressure of 80 p.s.i. is 5 degrees. Fig. 5.2.13 shows the variation of the Packing Parameter, α with relative density and confining pressure.

Effect of Structure

From Table 4.2.1 it can be noticed that tests 4 and 5 were performed on hand-made samples with relative

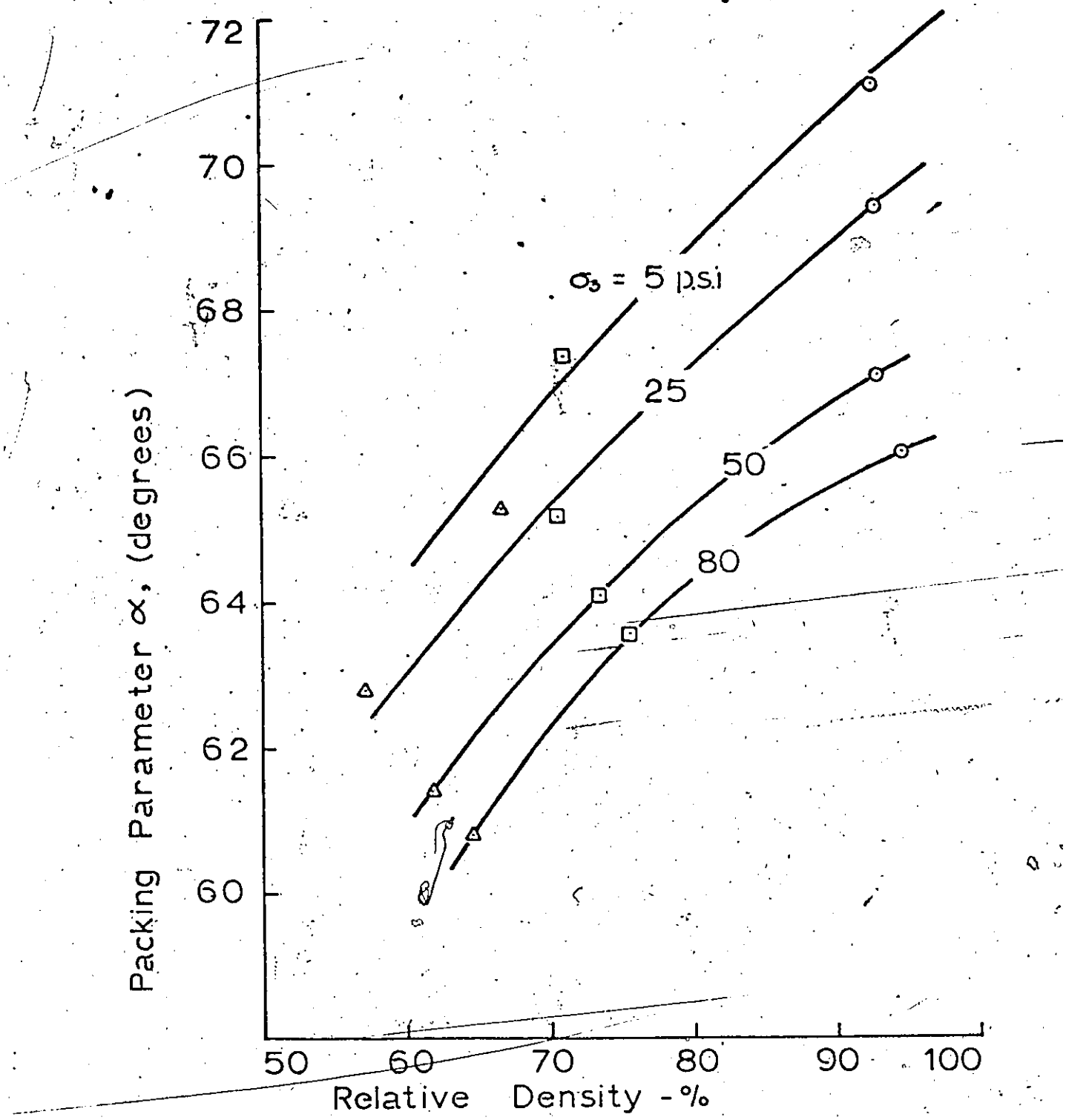

FIG. 5.2.13 VARIATION OF PACKING PARAMETER, α WITH RELATIVE DENSITY AND CONFINING PRESSURE

densities of 92 and 93 per cent respectively. With a confining pressure of 50 p.s.i. both the tests gave a value of ϕ equal to 39.4 degrees.

Test 2 was performed on a sample made with the sand raining device having a relative density of 93 per cent and a confining pressure of 50 p.s.i. The value of ϕ found was equal to 40.5 degrees. The only difference between the two samples was in the manner of their preparation. This resulted in a difference of 1.1 degrees in the value of ϕ in the aforesaid density and pressure range. These tests thus indicated the influence of structure on the strength of sand. The different structure was due to the different type of compaction or deposition of the sand.

5.3.2 Direct Shear Box Tests

Effect of normal stress

The effect of normal stress on the value of ϕ are comparable to the effect of confining pressure in the case of triaxial tests.

Figures 4.3.1 to 4.3.4 represent typical results from the direct shear box tests conducted at 8, 40, 80 and 109.5 p.s.i. applied normal stress and initial consolidation void ratios equal to 0.64, 0.67, 0.65 and 0.65 respectively. The corresponding maximum τ/σ_n values were 1.20, 0.94, 0.88 and 0.80; which clearly indicates the influence of applied stress on the value of ϕ. It should

also be noted that the shear displacement at failure was smallest for the smallest applied normal stress and highest for the highest normal stress. The volumetric strains were greatest for the smallest normal stress and smallest for the highest applied normal stress.

Effect of strain condition

It was assumed that in the conventional direct shear box test most of the distortion occurred in a thin zone of unknown thickness. The volumetric strain in this zone is quite different from the average overall volumetric strain of the entire sand sample. Therefore the average volumetric strain as determined for the entire sample does not provide a complete picture of what was going on in the sample. Therefore it is difficult to get other than qualitative volumetric strain data from the usual direct shear box test.

The phenomenon that the volume change occurs only on the failure plane will result in very small average volumetric strains. This is indirectly responsible for the higher values of ϕ in the dense range, and lower values of ϕ in the low densities and high applied normal pressure range.

This very phenomenon can also be due to the effect of wall friction inside the box as well as the fact that particle sliding is not uniform throughout the body of the

specimen. That is to say that non-uniform strain conditions in the direct shear box with consequent increased volumetric strain at high densities resulted in high ϕ values. In loose samples the smaller negative volumetric strains (decreasing volumetric strains being negative) gave a still smaller value of ϕ.

Effect of sample size

The size of the sample in the direct shear box test was 2 inch by 2 inch by 1.5 inch high. The extent of error in measuring the volume of the sample affected the relative density in the order of 3 to 4 per cent. A small correction of 0.115 cubic inch^3 due to the volume of the teeth in the serrated plates alone alters the relative density of the sample by 4 to 7 per cent, depending on the volume of the specimen.

5.4 Comparison of Test Results

Two simple approaches for comparison of the values obtained from the direct shear tests and consolidated drained triaxial compression tests could be followed.

One approach would be to compare the ϕ values obtained from the direct shear and triaxial compression tests for different relative densities against normal stress as shown in Fig. 5.3.1.

The other approach would be to plot ϕ values against porosity for direct shear tests and triaxial compression tests for different normal stresses.

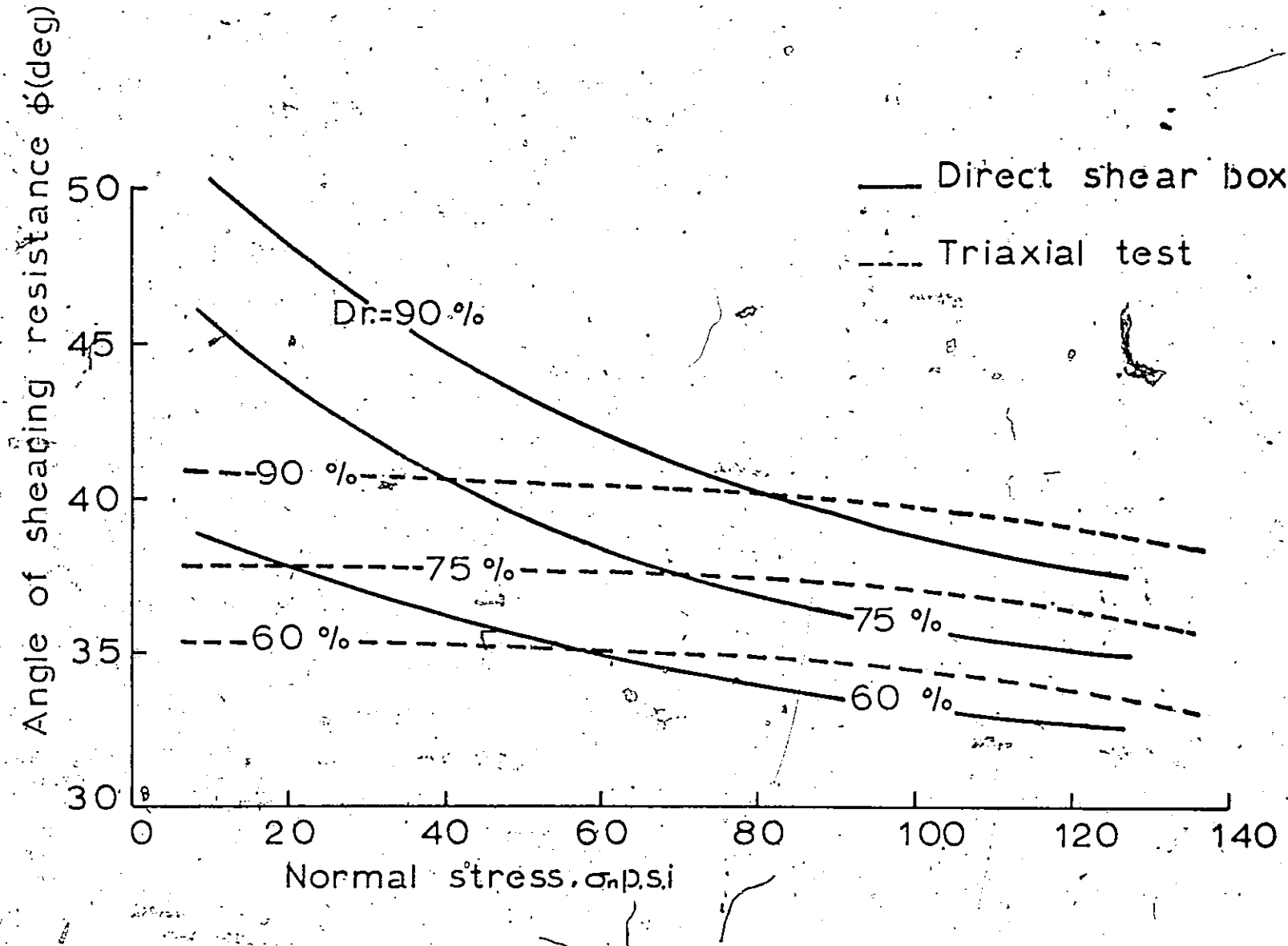

FIG. 5.3.1 RELATIONSHIP BETWEEN NORMAL STRESS AND ANGLE OF INTERNAL FRICTION. FOR DIRECT SHEAR AND TRIAXIAL COMPRESSION.

The second approach has been used by Cornforth (1964) for the comparison between triaxial and plane strain tests as given in Fig. 5.3.3.

Nash (1953) plotted porosity against angle of shearing resistance for direct shear and triaxial compression tests as given in Fig. 5.3.4.

Figure 5.3.1 has been redrawn from Fig. 5.1.5 and Fig. 5.1.9; whereas Fig. 5.3.2 has been reproduced from Fig. 5.1.6 and 5.1.10.

An inspection of Fig. 5.3.1 reveals that the curves of the direct shear tests are concave upward and those for the triaxial tests are concave downwards.

At small normal stresses the value of ϕ for direct shear test at a relative density of 90 per cent is higher by about 9 degrees than the value of ϕ for the triaxial tests. At 75 per cent relative density the direct shear ϕ-value is higher by about 8 degrees. At 60 per cent relative densi the ϕ-value for direct shear tests is higher by about 3.5 degrees. Hence it could be expected that at still smaller densities and small normal stress at failure, there would be no difference between the ϕ values obtained from the two tes

The same inference could be drawn from the fact that the difference in the value of ϕ for the two types of tests became zero at σ_n = 80 p.s.i. for 90 per cent relative density; at σ_n = 70 p.s.i. for 75 per cent relative density

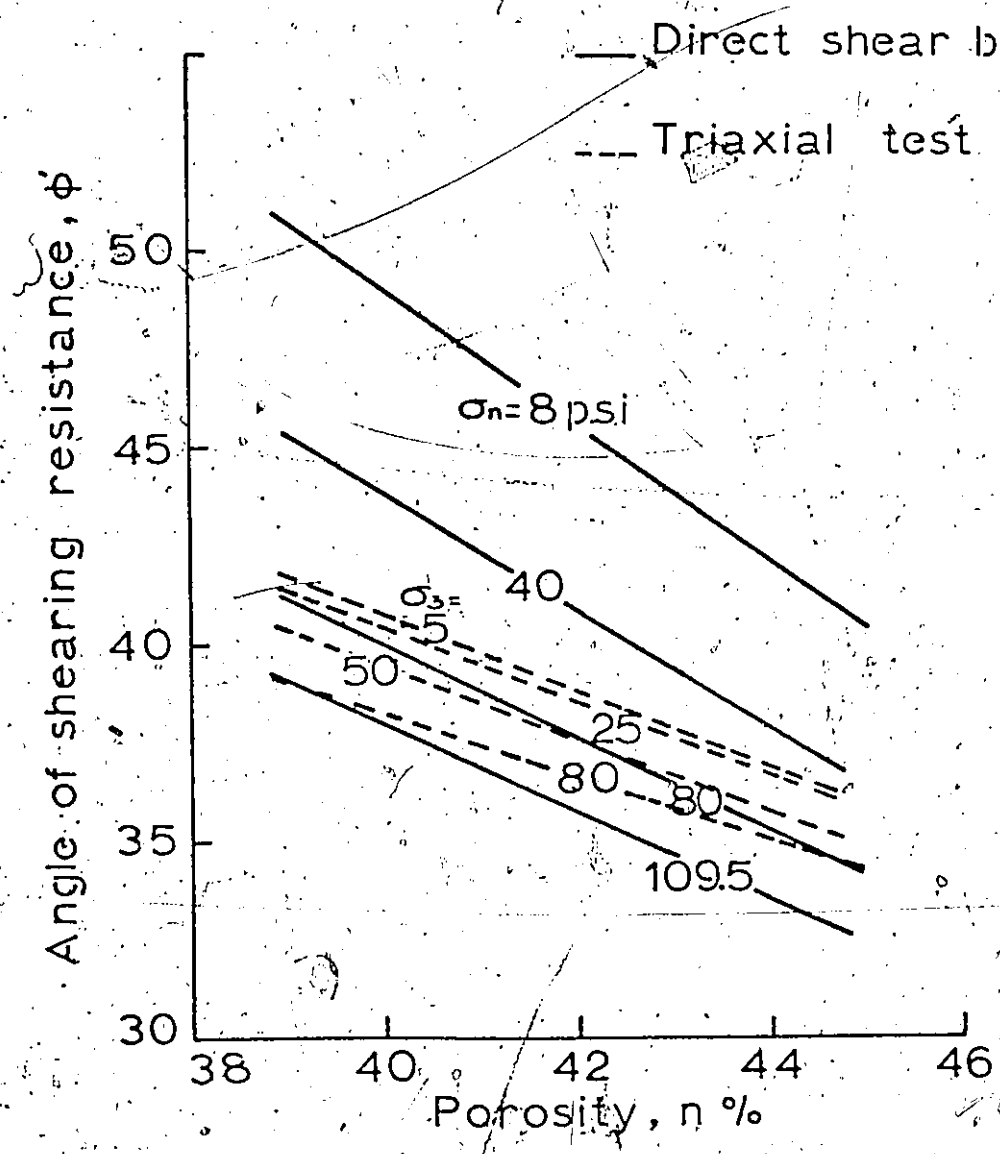

FIG. 5.3.2. POROSITY VERSUS ANGLE OF SHEARING RESISTANCE FOR DIRECT SHEAR TESTS AND TRIAXIAL COMPRESSION TEST.

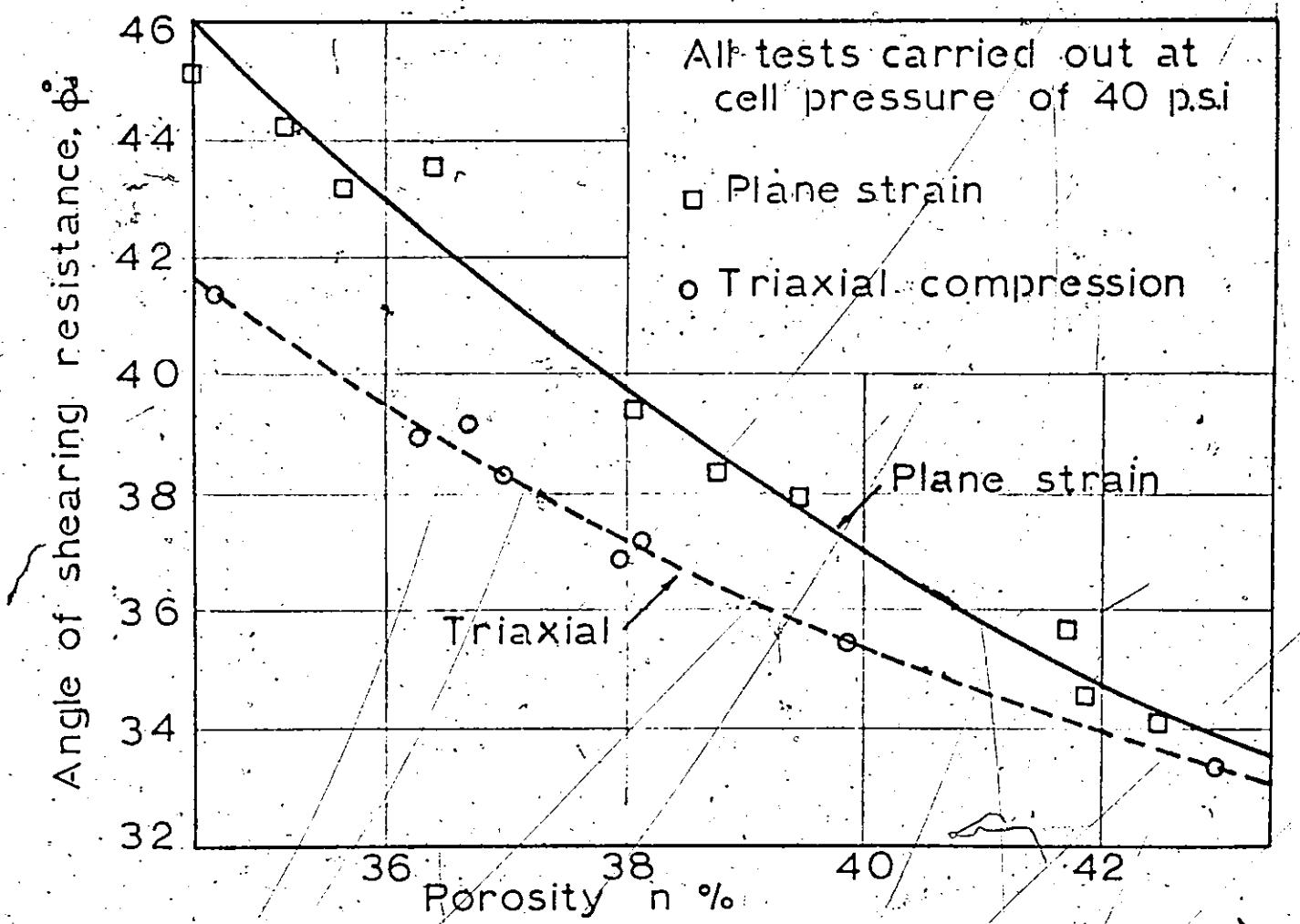

FIG. 5.3,3 COMPRESSION BETWEEN PLANE STRAIN AND TRIAXIAL COMPRESSION TESTS (AFTER CORNFORTH, 1964).

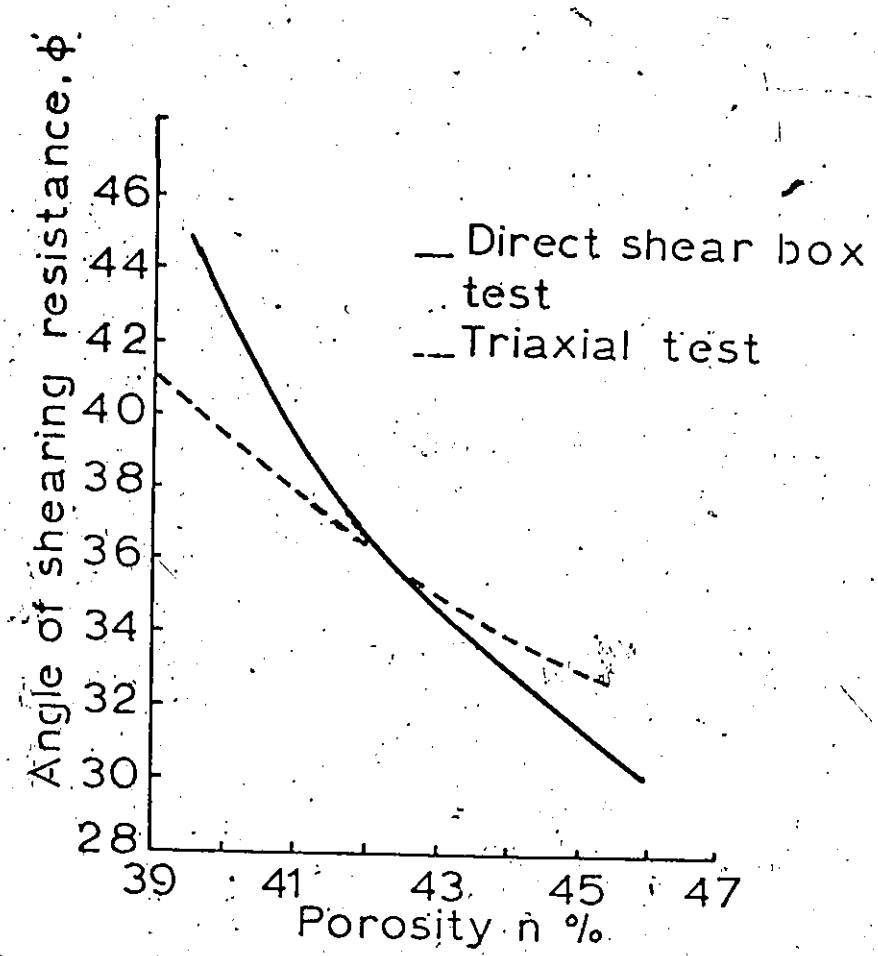

FIG. 5.3.4 COMPARISON BETWEEN DIRECT SHEAR TEST AND TRIAXIAL TEST (AFTER NASH, 1953)

and at σ_n = 60 p.s.i. for a relative density of 60 per cent.

At about 120 p.s.i. normal stress, the ϕ values for triaxial tests are higher by about one degree as compared to the direct shear box test values for relative densities varying from 90 per cent to 60 per cent.

These findings compare with the findings of Nash (1953), Fig. 5.3.4.

Nash has shown that at smaller porosities, triaxial values for ϕ are lower as compared to direct shear values, whereas at higher porosities triaxial test values are higher than direct shear values.

Figure 5.3.2 again, compares with Fig. 5.3.4 (reproduced from Nash, 1953). For the sake of clarity the individual test points have not been shown.

The sand used by Nash was a fine closely graded sand. At lower porosities the value of ϕ obtained by Nash in direct shear tests was higher by about 10 per cent and at higher porosities the value of ϕ was lower by about 5 per cent.

Comparison of plane strain and triaxial tests on sand

In many practical cases the shear deformation occurs in one plane, and the intermediate principal stress comes into play. Failure of soil beneath a strip footing and failure of a retaining wall are both cases of plain strain.

In view of the popularity of the triaxial test many investigators have tried to establish a relationship between ϕ from a triaxial test to the ϕ value obtained from a plane strain test. Lee (1970) summarizes the investigation of many researchers and it appears that in general the value of ϕ obtained from plane strain tests is larger by 3 to 5 degrees at higher relative densities. This difference is almost negligible at low relative densities. Figure 5.3.3 from Cornforth (1964) also leads to the same conclusions. According to Lee (1970) the values of ϕ for the plane strain tests as obtained by Bishop for dense sand was higher by 4 degrees.

CHAPTER 6

SUMMARY AND CONCLUSIONS

6.1 Summary

An investigation has been conducted on the shear strength properties of crushed quartz sand in the laboratory using drained triaxial compression tests and conventional direct shear box tests. The tests have been carried out at different relative densities and different normal stresses. Ko tests have been performed for various densities.

Some of the results have been presented in the form of stress paths for triaxial tests for very dense, dense and medium dense sand samples for varying stress range. Strain contours have been drawn to predict strains for given stress conditions.

Plots have been drawn relating shear stress and shear displacement with relative density and normal stress for triaxial tests and direct shear box tests.

For Ko tests comparisons have been made with solution proposed by Jaky and Hendron as reported by Bauer (1969).

The experimental investigation served several purposes. Firstly, the physical properties of sand grains like grain size distribution, roundness and sphericity were determined. The mineralogical contents were also established.

The angle of internal friction for various densities were determined. The variation of ϕ with normal stress for a given relative density was evaluated. Relationships between shear stress and shear displacement were given.

6.2 Conclusions

The following conclusions are based on the experimental test results and the preceding discussions and interpretation of the data presented.

1. The main object of this study was to determine accurately the values of the angle of internal friction for different void ratios and densities under different normal stresses; this objective was achieved.

2. It is concluded that the value of ϕ is largest for the highest density and smallest for the lowest density. In the triaxial tests the densest sample showed the largest maximum stress ratio occurring at the smallest axial strains and the greatest dilation; resulting in a net volume increase. The loosest sample showed the lowest stress ratio occurring at the largest axial strain exhibiting a net volume decrease. In the direct shear box tests, under a constant normal stress similar behaviour was noted. The densest sample failed at smallest displacement and greatest dilation with a net volume increase; whereas the loosest sample failed at large displacement and net volume decrease.

Thus in both triaxial compression and direct shear the densest specimen yielded the highest ϕ-values and the loosest specimen gave the smallest ϕ-values.

3. The value of the angle of internal friction depended on the confining pressure in the case of triaxial tests and on the normal stress in the case of direct shear box tests.

For a given relative density the value of ϕ is highest for the smallest normal stress and lowest for the largest normal stress. The axial strains at failure are also lowest for smallest normal stress.

4. Over a given range of porosity the overall volumetric strain in the triaxial test was smallest for smallest confining pressure and highest for highest confining pressure, with the result that the angle of internal friction was highest for smallest confining pressure and lowest for highest confining pressure over the entire range.

5. The extent of grain crushing during shear was dependent on the level of stress and the relative density of the sand. It appeared that crushing of the very dense sand occurred at 40 p.s.i. of normal stress. For dense and medium dense sand crushing occurred at 50 and 60 p.s.i. of normal stress respectively. That is to say that the extent of grain crushing is highest in the densest range and smallest in the loosest range. This crushing is the result of the increased mean normal stress at failure.

6. The phenomena of interlocking among the particles was found to be dependent on density. The greater the density, the greater was the interlocking effect. The interlocking decreased as the confining stress on the sample increased. The extent of decrease of interlocking was highest for densest specimen tested at constant confining pressure.

7. The Mohr-Coulomb plot was not a straight line for very dense, dense or medium dense sand; but became more and more flat as the stress levels were increased. However, the Mohr-Coulomb plot tended towards a straight line as the relative density decreased.

8. From the comparison of the direct shear results with triaxial test results it can be concluded that -

(a) at a relative density of 90 per cent and a normal stress of 80 p.s.i. both the tests gave a value of ϕ equal to 40 degrees. At a relative density of 75 per cent and a normal stress of 70 p.s.i. ~~both tests~~ yielded a value of ϕ equal to 37.5 degrees. The value of ϕ was equal to 35 degrees at a relative density of 60 per cent and a normal stress of 60 p.s.i.

(b) At a relative density of 90 per cent the maximum direct shear value of ϕ was equal to 50 degrees and the corresponding triaxial compression value of ϕ was 41 degrees. At 75 and 60 per cent relative densities, the direct shear value of ϕ was 46 and 39 degrees respectively. The value of ϕ in triaxial

compression at relative density of 75 and 60 per cent was 39 and 35.5 degress respectively.

9. The extent of shear displacement and shear stress was related to the strain condition. In the direct shear test where the particles are not quite free to move with respect to each other, a small amount of shear displacement was necessary to mobilize the shear stress. The value of ϕ was also higher, because the volumetric strains in direct shear were small and hence the interlocking effect gave rise to high ϕ values.

In the triaxial test the strain conditions were very different. The sample was free to expand. Hence in order to mobilize the same shear stress large shear displacements were necessary.

The difference in the values of ϕ for the two types of test was a maximum for densest specimen, because the interlocking effect was greater in the denser specimen.

10. There was a fairly good agreement between the Ko-values obtained in the laboratory with the theory proposed by Jaky (1944) for predicting the coefficient of earth pressure at rest.

compression at relative density of 75 and 60 per cent was 39 and 35.5 degress respectively.

9. The extent of shear displacement and shear stress was related to the strain condition. In the direct shear test where the particles are not quite free to move with respect to each other, a small amount of shear displacement was necessary to mobilize the shear stress. The value of ϕ was also higher, because the volumetric strains in direct shear were small and hence the interlocking effect gave rise to high ϕ values.

In the triaxial test the strain conditions were very different. The sample was free to expand. Hence in order to mobilize the same shear stress large shear displacements were necessary.

The difference in the values of ϕ for the two types of test was a maximum for densest specimen, because the interlocking effect was greater in the denser specimen.

10. There was a fairly good agreement between the Ko-values obtained in the laboratory with the theory proposed by Jaky (1944) for predicting the coefficient of earth pressure at rest.

6.3 Suggestion for Further Research

It was felt that the studies presented do not quite simulate deformation and shear stress behaviour that would be encountered in the sand box. Hence tests should be conducted on plane strain devices so as to predict and relate the shear stress and shear deformation along the failure plane in the prototype sand box.

APPENDIX A

BIBLIOGRAPHY

Ashtakala, B. 1968, Successive yield Theory of Earth Pressure, Ph.D. Thesis, University of Waterloo, pp. A-8 to A-9.

Barden, L. and McDermott, R.J.W. 1965. Use of free ends in triaxial testing of clays. Journal, S.M. and F.L. ASCE, SM6, Vol. 1, p.4535.

Bauer, G.E.A. 1969. Stresses and Deformation in Braced Cuts in Sand, Ph.D. Thesis, University of Ottawa.

Bishop, A.W. 1954. Correspondence on Shear Characteristics of a Saturated Silt, Measured in Triaxial Compression. Geotechnique, Vol. IV, pp.43-45.

Bishop, A.W. and Green, G.E. 1965. The influence of end restraint on the compression strength of cohesionless soils, Geotechnique XV, No. 3, pp.243-266.

Bishop, A.W. and Henkel, D.J. 1962. The measurement of soil properties in the triaxial test. Edward Arnold (Publishers) Ltd., reprinted 1969.

Bowles, J.E. 1968. Foundation analysis and design, McGraw-Hill Book Company, New York.

Casagrande, A. 1940. Characteristics of cohesionless soils affecting the stability of slopes and earth fills. Contributions to Soil Mechanics, 1925-1940, Boston Society of Civil Engineers, October 1940.

Cornforth, D.H. 1964. Some experiments on the influence of strain conditions on the strength of sand. Geotechnique, Vol. XIV, pp.143-166.

Feda, J. 1969. Effect of structure on the shearing strength of sand. 7th Intl. Conf. SM and FE, Mexico, Vol. 1, pp.121-126.

Frydman, S., Zeitlen, J.G., and Alpan, I. 1973. The membrane effect in triaxial testing of granular soils, Journal of Testing and Evaluation, Vol. 1, No. 1, January, pp.37-41.

Holubec, I. 1966. The yielding of cohesionless soils. Ph.D. Thesis, University of Waterloo, February, pp.48-49.

Holubec, I. and Scott, J.D. 1965. A triaxial piston load transducer. University of Waterloo, Department of Civil Engineering. April.

Kolbuszewski, J.J. 1948. An experimental study of maximum and minimum porosities of sand. Proc. 2nd Intl. Conf. Soil Mechanics and Foundation Engineering, Vol. 1, pp.158-165.

Kolbuszewski, J. 1958. Fundamental factors affecting experimental procedures dealing with pressure distribution in sands. Proc. Brussels Conf. on Earth Pressure Problems, Vol. 1, pp.71-83.

Krumbein, W.C. 1941. Measurement and geological significance of shape and roundness of sedimentary particles. Journal Sedim. Petrol., Vol. 11, No. 2, pp.64-72.

Lambe, T.W., and Whitman, R.V. 1969. Soil Mechanics. John Wiley and Sons, Inc., New York.

Lee, L.K. and Seed, H.B. 1964. Discussion of Rowe and Barden Importance of free ends in triaxial testing. Journal, SM and FE, ASCE, 90, SM6, pp.173.

Lee, L.K. and Seed, H.B. 1967. Drained strength characteristics of sand. Journal, SM and FE, ASCE, SM6, November, pp.117-141.

Lee, I.K. 1968. Soil Mechanics Selected Topics. Butterworths, London, pp.236-237.

Lee, I.K. 1966. Stress-dilatancy performance of Feldspar. Journal SM and FE, ASCE, SM2, March, pp.79-102.

Leslie, D.D. 1963. Large scale triaxial tests on gravelly soils. Proc. 2nd Pan. Am. Conf. Soil Mech. and Foundation Engineering (Brazil), Vol. 1, pp.181-222.

Leussink, H. and Wittke, W. 1963. Difference in triaxial and plane strain shear strength. Symposium on Laboratory Shear Testing of Soils, ASTM, STP 361, pp.77-89.

Meyerhof, G.G. 1963. Some recent research on the bearing capacity of foundations. Canadian Geotechnical Journal, Vol. 1, No. 1, pp.16-26.

Mitchell, R.J. 1973. An apparatus for plane strain and true triaxial testing of undisturbed soil samples, Canadian Geotechnical Journal, Vol. 10, No. 3, August, pp.520-527.

Nash, K.L. 1953. The shearing resistance of a fine closely graded sand. Proc. 3rd Intl. Conf. Soil Mech. Vol. 1, pp.160-164.

Powers, M.C. 1953. A new roundness scale for sedimentary particles. Journal Sedim. Petrol., Vol. 23, No. 2, pp.117-119.

Rowe, P.W. 1962. The stress-dilatancy relation for static equilibrium of an assembly of particles in contact. Proc. Royal Society, A, Vol. 269, pp.500-527.

Rowe, P.W., Barden, L. and Lee, I.K. 1964. Energy components during the triaxial cell and direct shear tests. Geotechnique, Vol. XIV, No. 3, September, pp.247-261.

Rowe, P.W. and Barden, L. 1964. Importance of free ends in triaxial testing. Journal SM and FE, ASCE 90, SM1, Vol. 1, p.3753.

Rowe, P.W. 1969. The relation between the shear strengths of sand in triaxial compression, plane strain and direct shear. Geotechnique, Vol. 19, No. 1, pp.75-86.

Rittenhouse, G. 1943. A visual method of estimating two dimensional sphericity. Journal Sedim. Petrol. Vol. 13, No. 2, pp.79-81.

Sowers, G.B. and Sowers, B.F. 1970. Introductory soil mechanics and foundations. Macmillan, New York.

Taylor, D.W. 1948. Fundamentals of soil mechanics, John Wiley and Sons, Inc., New York, pp.345-346.

Timoshenko, S. 1934. Theory of elasticity. McGraw-Hill, p.8.

Walker, B.P. and Whitaker, T. 1967. An apparatus for forming uniform beds of sand for model foundation tests. Geotechnique, Vol. 17, No. 2, pp.161-167.

APPENDIX B

FRICTIONLESS END PLATENS AND SAMPLE FORMER

B.1 Introduction

The common barrelling of an initially cylindrical sample tested by conventional triaxial techniques, and using porous stones as end platens, is the most obvious indication of non-uniform strain conditions resulting from the restricted lateral deformation adjacent to the surfaces near the ends of the specimen.

This leads to a departure from the condition of uniform stress and strain.

In order to have uniform strain conditions throughout the body of the sample, Rowe and Barden (1964) used polished end platens which were covered with a thin layer of silicone grease and a latex rubber disc of 0.010 inch thickness. With this technique the friction at the surface of the platens were largely eliminated.

B.2 Frictionless End Platens

Based on the principles outlined by Rowe and Barden (1964), frictionless end platens were designed for 4 inch diameter by 8 inch high samples to accommodate an axial strain of 30 per cent. The platens were 0.75 inch thick and were made of ordinary mild steel. The faces

of the platens were ground smooth and polished and then were chrome plated. The sides were also ground smooth and chrome plated.

In order to prevent sidesway buckling during tests, small cylindrical dowels were provided at the centre of the two platens as suggested by Rowe and Barden (1964). These details can be seen in Fig. B.1.1.

Plate B.1 shows the bottom plate in place on the base of the triaxial cell, the bottom part of the sample former is shown assembled and the two upper halves are depicted separately. Before the preparation of a sample a thin film of silicone grease was applied to the bottom platen and was then covered with a rubber disc of 0.014 inch thickness.

Similarly, after the sample was prepared, the top platen was placed on the sample after it was covered with a thin film of silicone grease and a latex disc.

Arrangement for drainage of the base was provided by a 1/2 inch x 1/8 inch thick porous plate recessed in the centre of the bottom platen.

The base of the triaxial cell had its drainage connection somewhat off centre, therefore an inclined hole had to be provided through the bottom platen as shown in Fig. B.1.1. Necessary rubber O-rings were provided for sealing purposes.

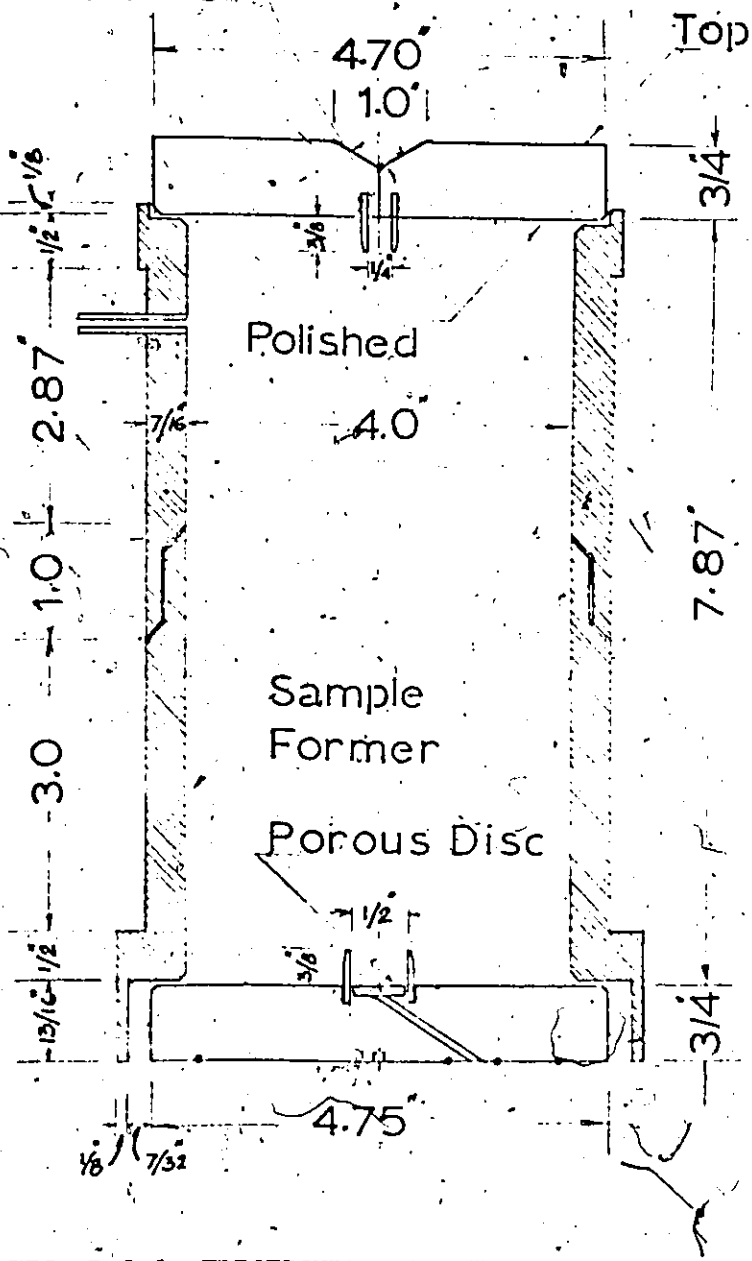

FIG. B.1.1 FRICTIONLESS PLATENS AND SPLIT SAMPLE FORMER.

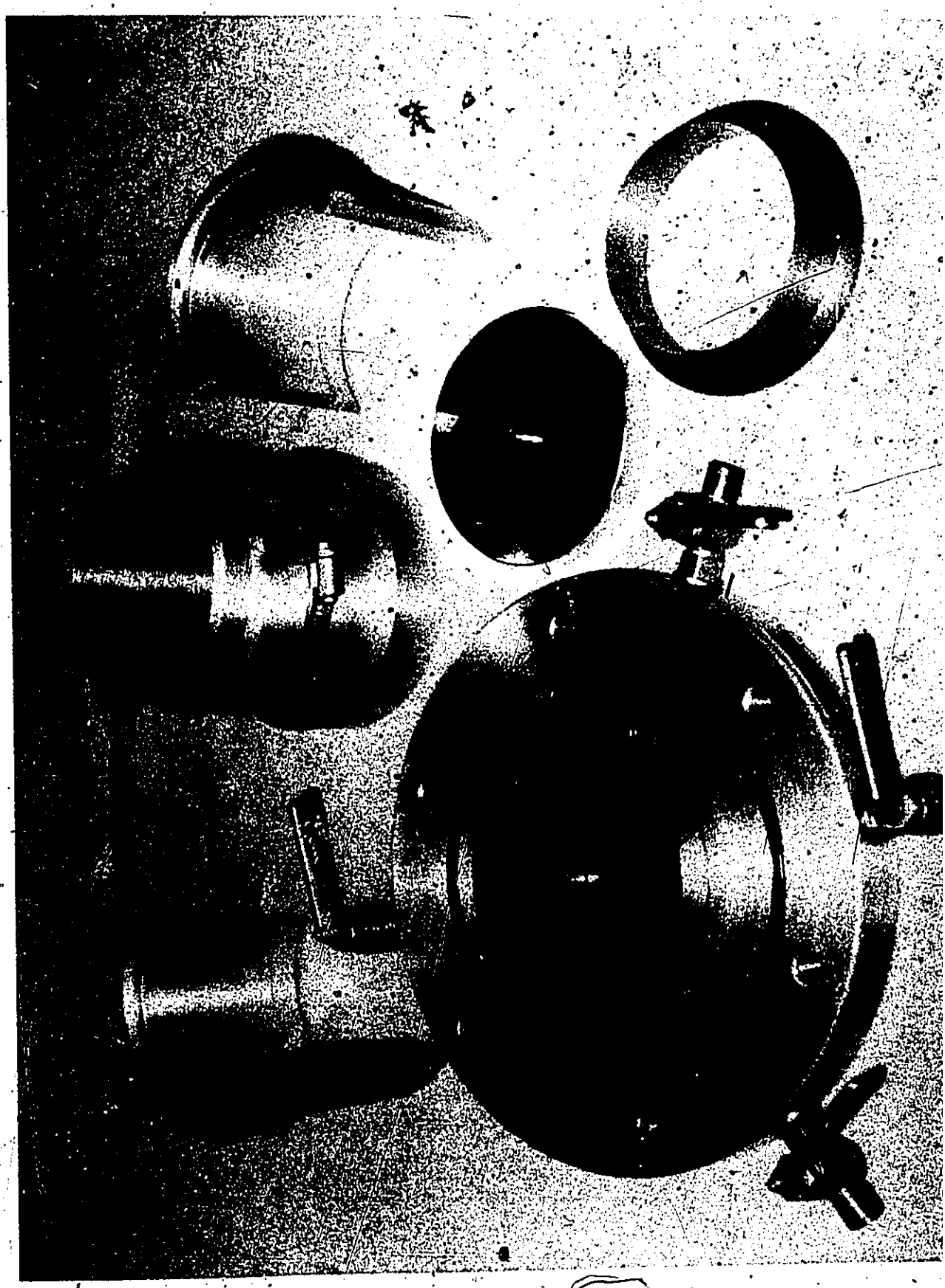

PLATE B.1 TOP AND BOTTOM PLATEN, SAMPLE FORMER AND KNIFE EDGE COLL

B.3 The Sample Former

A specially made sample former was required to accommodate the enlarged platens. This was achieved by designing a sample former in four pieces. The former had two top pieces and two bottom pieces. It could be assembled with the help of ordinary hose clips. A small clearance of 0.05 inch was provided at the top between the top platen and the former so that there was enough space for the rubber membranes with some allowance for rotating the top platens to ensure proper seating.

The former was made from chrome plated aluminum.

The sample former can also be seen in Fig. B.1.1 and Plate B.1.

APPENDIX C

TRIAXIAL PISTON LOAD TRANSDUCER

C.1 Introduction

The problem of the magnitude of piston friction in the bushings of a triaxial cell has been realized by many researchers. Several methods, such as rotating bushings, or measurement of the load inside the triaxial cell were used to eliminate this problem. It was felt that a load transducer at the bottom of the loading piston inside the triaxial cell could provide a satisfactory solution. The design chosen necessitated as little modification as possible to the existing triaxial cell piston and still allowed the cell to be used in the normal manner with a proving ring.

The load transducer was comprised of a load cell enclosed by housing mounted on a modified triaxial cell piston. The load cell consisted of strain gauges mounted in a full bridge arrangement on a 17-4PH stainless steel cylinder.

C.2 Material

The material suitable for the design of a load cell should be linearly elastic, it should have a high yield stress, a low modulus of elasticity for high sensitivity, show no hysteresis effect, show no creep under load, be corrosion resistant and have a good machinability.

Considering the above criteria, stainless steel 17-4PH with yield strength of 110,000 p.s.i. in the annealed state was finally selected. A comparatively high modulus of elasticity of 28×10^6 p.s.i. was considered acceptable in the light of the large load of 10,000 pounds that the cell was to be designed for. The components of the load cell were to be heat treated before final assembly.

As can be seen from Fig. C.1 the transducer consisted of a push rod A, which was in compression when measuring loads in compression. The member B had strain gauges fixed on the outside and was under tension when measuring loads in compression. The member C served as a housing for the cell and was connected to the piston through a rubber O-ring for a seal. Member B was connected to member C by means of 6 - #4/40 socket head cap screws through a sealing gasket. Member A can be screwed on to member B and is in intimate contact with member B when screwed on. There is a gap of 0.04 inches between member A and B.

Foil type, temperature compensating strain gauges were used, each with a resistance of 350 ohms.

C.3 Design

Design of compression member A

A working stress of 75,000 p.s.i. was assumed. Further, in order to provide connection between member A and B, the member A was tapped to provide threads equivalent

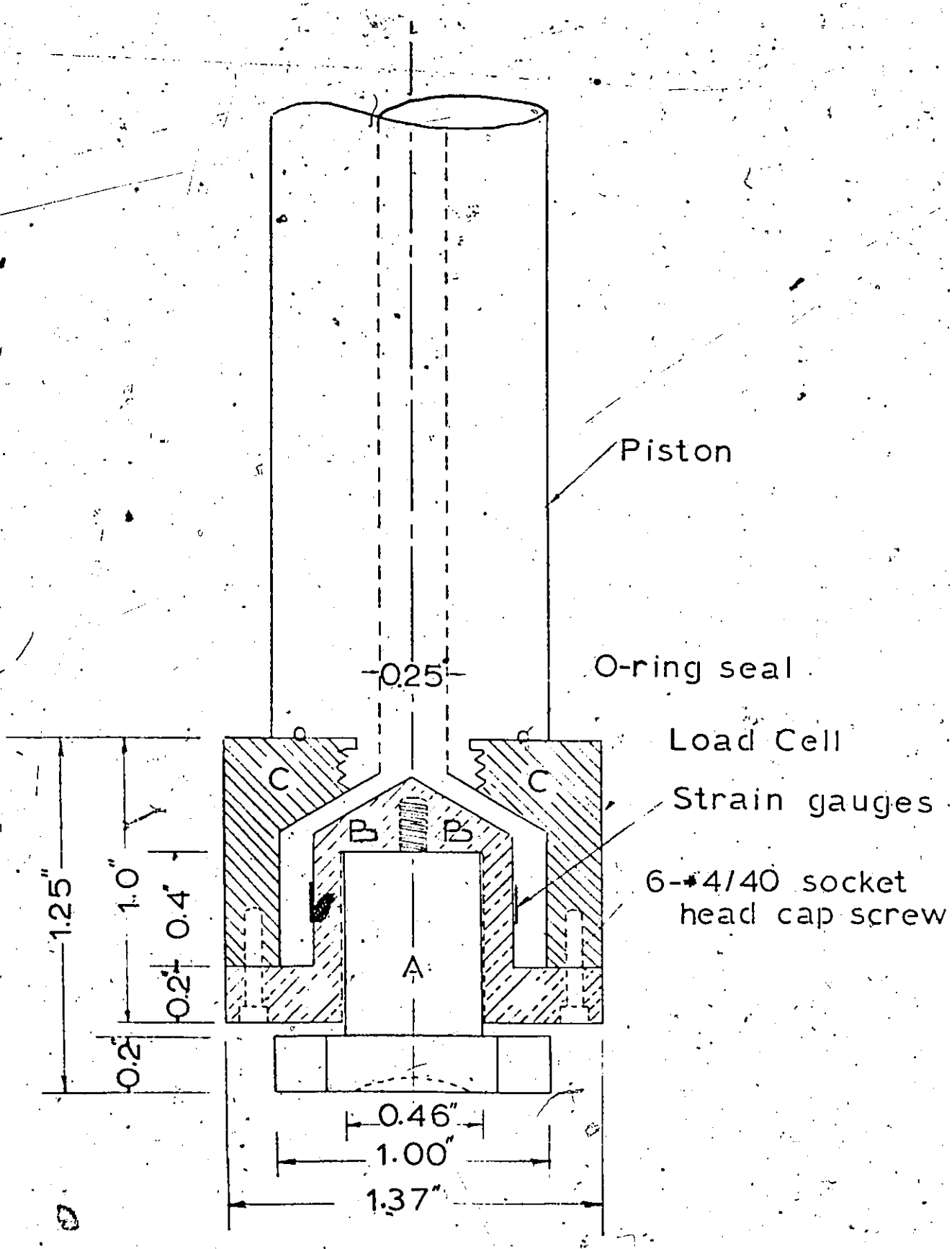

FIG. C.1 .TRIAXIAL PISTON AND LOAD CELL ASSEMBLY.

to #4 'UNBRAKO' with U.N.C. threads of 40 per inch, having an outside diameter of 0.112 inches, and an area of 0.01 sq. inches.

For a load of 10,000 pounds, this resulted in a diameter of 0.43 inches. A diameter of 0.46 inches was used.

Design of tension member B

Allowing a clearance of 0.02 inches on either side of member A yielded an inside diameter of 0.50 inches for member B. Stress consideration yielded an outside diameter of 0.70 inches, and a wall thickness of 0.1 inches.

The flange of member B was taken as 0.2 inches which was on the safe side.

The thickness of the housing member C was also taken as 0.2 inches.

A full bridge strain gauge arrangement and the manufacturer's gauge factor gave a strain gauge indicator reading of $2(1-\mu)1834 = 4770$ micro inches/in. During the calibration of the load cell a bridge constant of approximately one was established which yielded a relation of 1 lbs = 1 micro in/in.

C.4 Modification of the Triaxial Cell Piston

A standard Wykeham-Farrance piston was modified by replacing the loading cap at the bottom of the piston with the load cell and its housing, and drilling a hole up

through the piston for the lead wires. In addition, a slot was made at the top of the piston to take out the lead wires for connecting to the Budd Strain Indicator. A detachable collar at the top prevented the piston from falling into the cell when not in use. Plate C.1 shows the load transducer with the lead wires coming out from the slot. The top collar has been shown separately.

C.5 Calibration of the Load Cell

A calibration process was used to obtain a convenient bridge constant which would give direct load readings.

Since large loads were involved, the calibration was done using a 10,000 pound proving ring against a steel dummy sample placed inside the cell filled with water.

Calibration of the transducer was also carried out by running long duration tests with a dead load of 1000 lbs.

It was observed that the load cell had a hysteresis effect and that the hysteresis effect would not be considered negligible. The load cell was also found to be extremely temperature sensitive under large loads.

A typical calibration curve for the loading cycle has been shown in Fig. C,2. From the curve it will be noted the extent of correction to be applied in order to get the loads directly in pound was not a constant quantity. This correction did not vary linearly with increase of load.

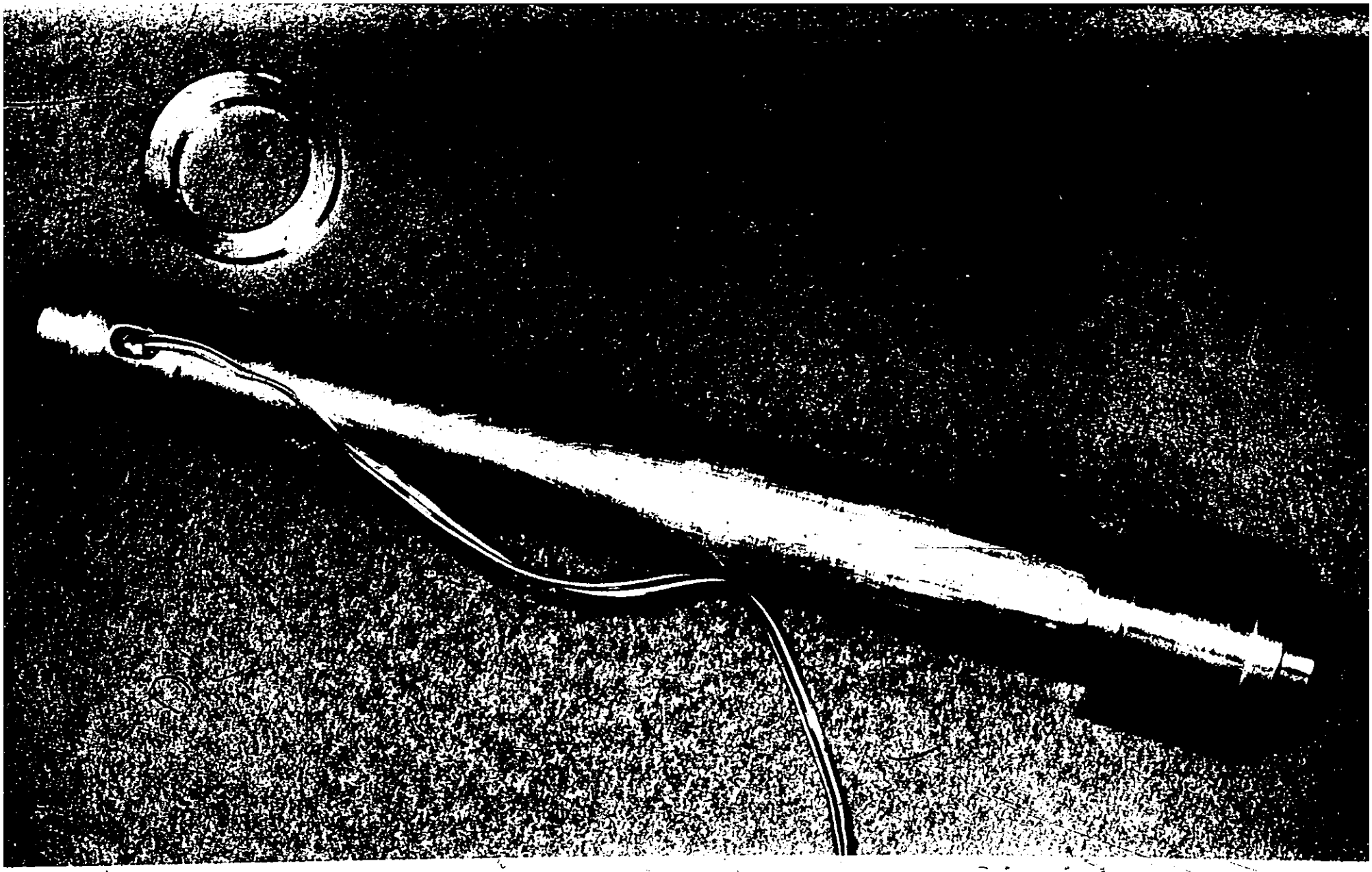

PLATE C.1 LOAD TRANSDUCER WITH TRIAXIAL PISTON, LEAD WIRES AND COLLAR.

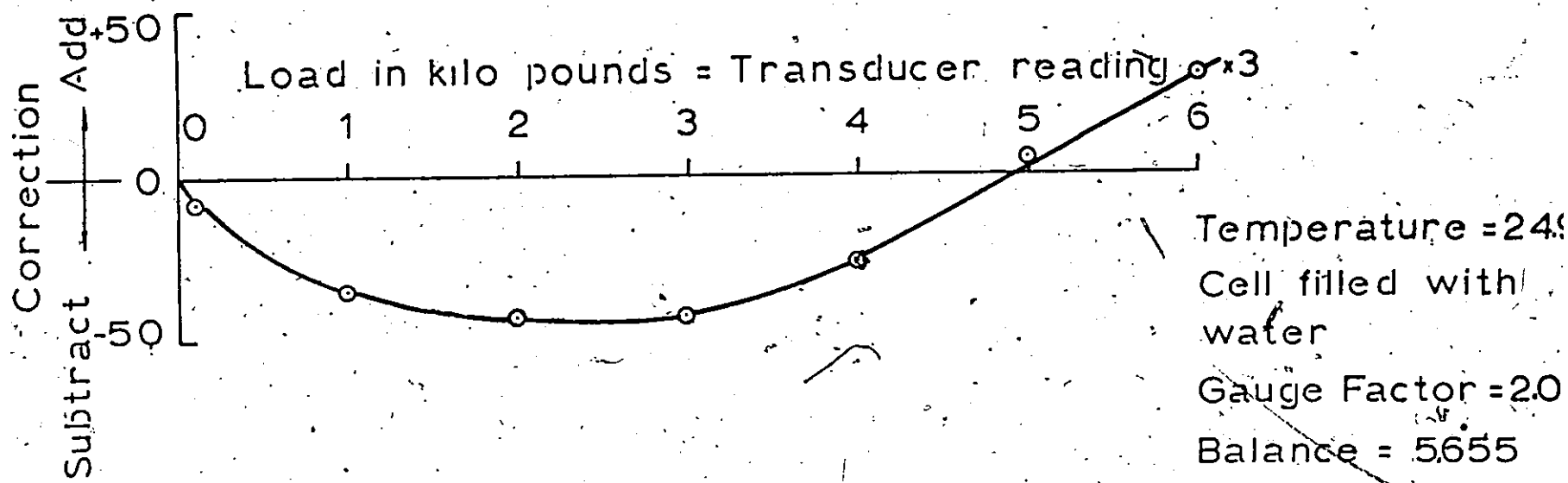

FIG. C.2 TRANSDUCER READING VERSUS LOAD CORRECTION

From the many calibration tests run the calibration curves were not the same for any two tests carried out in the same manner and under the same conditions as shown in Fig. C.1.

There were two likely reasons for such a behaviour of the load cell. Firstly, the gauges were erratic under load. Secondly, there existed a possibility of stress concentration and stress relief which was picked up by the strain gauges.

An attempt to correct these defects would have meant a change in the design of the transducer. It was therefore decided to run the triaxial test using rotating bushings to minimize piston friction. This method has been used by other researchers.

APPENDIX D

EFFECT OF FRICTION BETWEEN THE UPPER AND LOWER BOXES OF THE DIRECT SHEAR APPARATUS

D.1 Introduction

The magnitude of the friction developed between the upper and lower boxes during a conventional direct shear test is an unknown quantity. Hence an attempt was made to evaluate quantitatively the influence of this friction on the test results. The tests presented in this thesis were carried out with the separating screws turned down so that the two boxes were separated from each other throughout the entire test. It was thought that this would limit the magnitude of friction due to metal to metal contact. The friction developing from a thin layer of sand between the two boxes could thereby be eliminated, since the upper box would rest on the tips of the two screws rather than on the sand particles. This procedure, followed in this test series, was contrary to common practice. Hence a series of tests was conducted at various densities and normal stresses with the screws turned down on the one hand and with the screws retracted after being turned down on the other.

D.2 Magnitude of Friction

Figure D.1 shows the magnitude of the frictional force developed on application of normal loads of 95.5 lbs. and 320.5 lbs applied on the upper box. Load was applied after the screws were turned down and left down. The two boxes were then made to move with respect to each other. The frictional force developed with increasing displacement was measured. For the smaller normal load, the coefficient of friction was 0.08. The coefficient of friction was 0.12 for the higher normal load. Thus an average value of the coefficient of friction of 0.10 can be assumed to have developed as a result of friction between the screws and the lower box. It can be visualized that not all of the normal load applied in the direct shear test will be transmitted through the screws to the bottom box. The normal loads are applied directly to the sand sample and the force transmitted through the screws will depend on the magnitude of the horizontal load applied to the inside of the upper box by friction. The vertical component of this frictional force will be very small and may be 2 to 3 per cent of the entire vertical load applied to the sample. Hence for practical cases the friction that results can be neglected.

D.3 Typical Test Results

Figures D.2 and D.3 represent typical test results from sixteen direct shear tests carried out with (a) the

⊙ Test # 9: 320.5 lb Load with screws down

⊡ Test #10: 95.5 lb Load with screws down

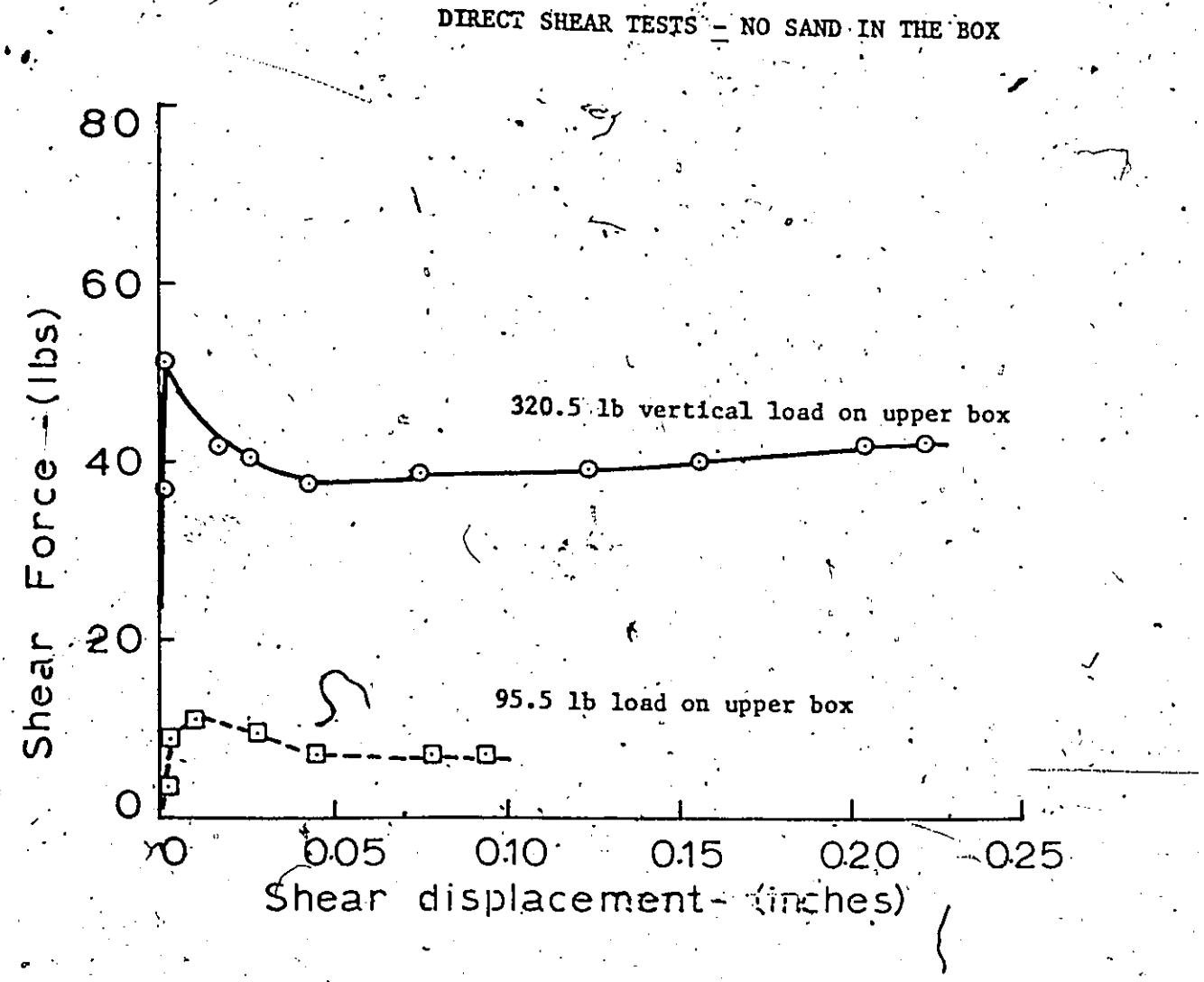

FIG. D.1 DISPLACEMENT VERSUS FRICTIONAL FORCE FOR APPLIED NORMAL LOADS OF 95.5 AND 320.5 lbs WITH SCREWS TURNED DOWN

⊙ Test #5: Screws down, D_r = 77.5%, σ_n = 24 p.s.i., ϕ = 39.2°

⊡ Test #6: Screwed down and then retracted, D_r = 78.0%, σ_n = 24.0 p.s.i., ϕ = 40.4°

DIRECT SHEAR TESTS BOX FILLED WITH SAND

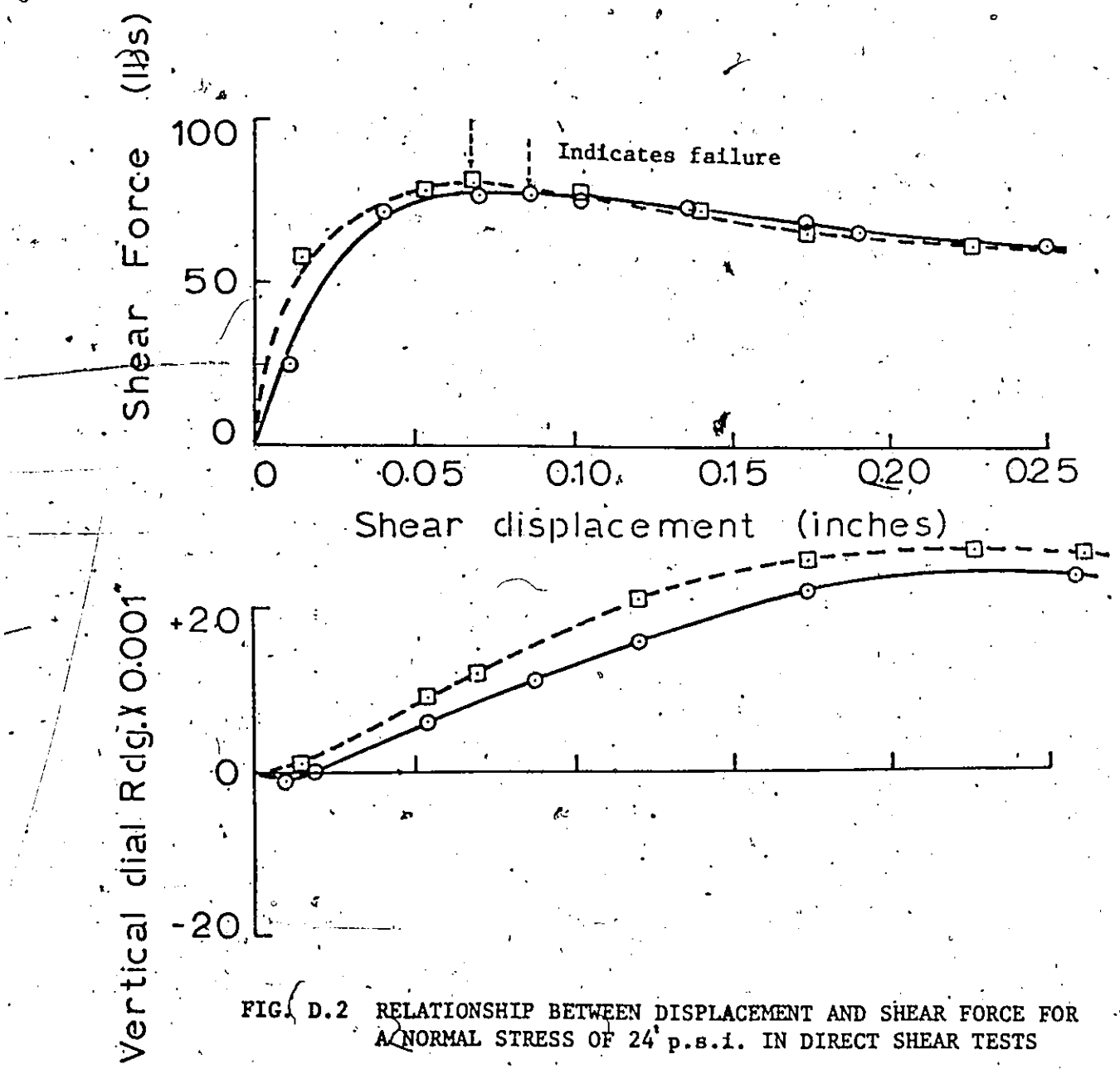

FIG. D.2 RELATIONSHIP BETWEEN DISPLACEMENT AND SHEAR FORCE FOR A NORMAL STRESS OF 24 p.s.i. IN DIRECT SHEAR TESTS

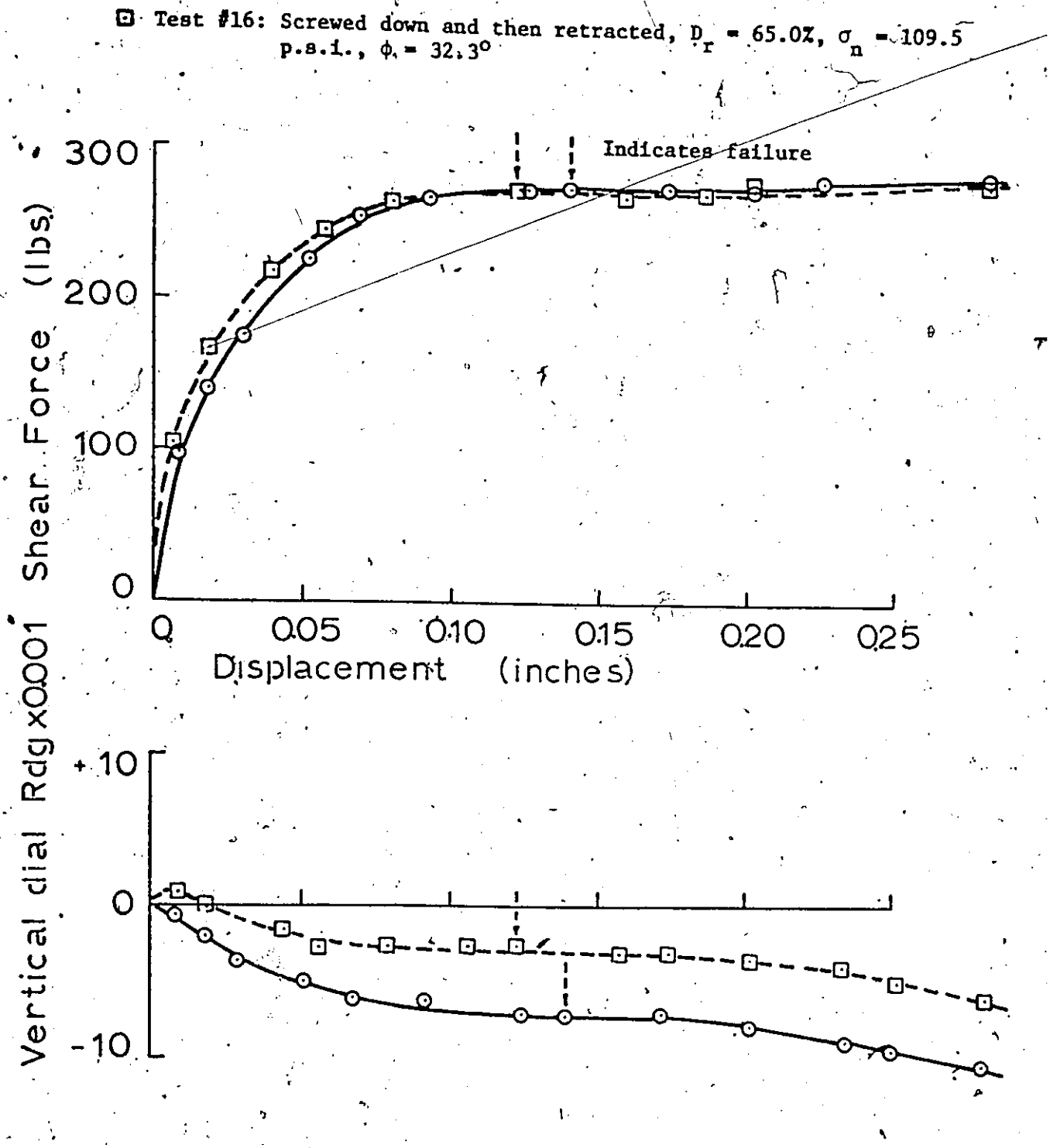

FIG. D.3 RELATIONSHIP BETWEEN DISPLACEMENT AND SHEAR FORCE FOR A NORMAL STRESS OF 109.5 p.s.i. IN DIRECT SHEAR TESTS

screws turned down and (b) the screws turned down and then retracted.

From the curves it will be noted that any two plots are almost coincident throughout the test.

This indicates that the magnitude of the friction with the screws turned down and with the screws retracted is the same. This indirectly proves that the friction developed with a thin layer of sand between the two boxes is the same as that between the screws and the lower boxe .